An Investigation of Mechanical, Thermal and Wear properties of Marble Dust/Calcium Oxide Filled Metal Alloy Composites for Ball Bearing

A THESIS SUBMITTED IN PARTIAL FULFILLMENT OF THE REQUIREMENT FOR THE AWARD OF THE DEGREE OF

Doctor of Philosophy
In
Mechanical Engineering

Submitted to
Malaviya National Institute of Technology, Jaipur, Rajasthan

By

Swati Gangwar

Student ID: – 2012RME9544

Department of Mechanical Engineering
Malaviya National Institute of Technology
Jaipur-302017, Rajasthan, INDIA

November, 2016

An Investigation of Mechanical, Thermal and Wear properties of Marble Dust/Calcium Oxide Filled Metal Alloy Composites for Ball Bearing

A THESIS SUBMITTED IN PARTIAL FULFILLMENT OF THE REQUIREMENT FOR THE AWARD OF THE DEGREE OF

Doctor of Philosophy

In

Mechanical Engineering

Submitted to

Malaviya National Institute of Technology, Jaipur

By

Swati Gangwar

Student ID:–2012RME9544

Under the supervision of

Dr. Amar Patnaik

and

Prof. I.K. Bhat

Department of Mechanical Engineering

Malaviya National Institute of Technology

Jaipur-302017, Rajasthan, INDIA

November, 2016

Dedicated to
My Parents

ACKNOWLEDGEMENT

Encouragement motivates a person towards one's aim while guidance helps one to achieve it. This thesis owes its existence to the help, support and inspirations of many people. In the succession firstly I would like to extend my heartfelt thanks to my supervisor's **Dr. Amar Patnaik and Prof. I.K. Bhat** for their virtuoso enlighten and constant support throughout the research work, without their guidance patience and constant encouragement, completion of the thesis would not have been possible.

Secondly I am highly grateful to **Prof. Udaykumar Yaragatti** Director MNIT Jaipur for drizzling his consecutive support throughout the research work and I am also oblige to **Prof. G.S. Dhangayach** Head of the Department of Mechanical Engineering for his constant guidance and heartening other faculty members from this Department towards the research work.

I am also applaud Centre for development of stone Rajasthan (CDOS), Advanced Research Centre for Tribology and Material Research Centre, MNIT Jaipur for providing funds as well as their continuous support to compile my research work victoriously.

I am owe to my Parents, husband, sisters, brother and my near and dear one's for their stupendous encouragement and make my strength during this beautiful journey of my life without any complaints and expectations.

Also I want to thank my fellow research scholars, Mr. Shiv Ranjan Kumar, Mr. Manoj Janardan Pawar and Mr. Vikash Gautam who offered a lot of help during my PhD study. I also thank to all other technical staffs that helped me directly and indirectly in my thesis work.

Finally, but most importantly, I thank God Almighty my Lord for giving me the will power and strength to make it this far when I didn't a see a light.

Date:
M.N.I.T. Jaipur *Swati Gangwar*

ABSTRACT

For the different industrial applications wear phenomenon play a major cause in the wastage of materials that affects the performance as well as on cost factors. The tribology comes in existence from the past many years as a saviour that significantly work for materials reliability and wear reduction. The introduction of reinforcement into a metal matrix metal alloy produces a composite material with a charismatic amalgamation of physical, mechanical and tribological properties and that cannot be obtained with monolithic alloys so far. The major purpose for producing metal matrix composites (MMCs) is to attain lightweight materials with high specific strength and stiffness. The new aspects regarding filler materials in metal alloy composites were prioritized in this research work. Innumerable analysis were perceived in this research work to encapsulate the physical, mechanical and tribological analysis that summarized in this research work from mechanical analysis to tribological analysis for environmental waste like marble dust and CaO particulates filled metal alloy composites for bearing applications.

This research work is done into two parts for fabricated particulate filled metal alloy composite materials. The first part of the thesis comprises the description about the experimental analysis for physical, mechanical, fracture and thermal analysis of particulate filled metal alloy composites; the later or second part of the thesis has been reported about the effect of different particulates on the sliding wear behaviour of metal alloy composite materials. In this research work two materials (Marble dust (industrial wastes) and Calcium oxide) has been used as filler materials at five different weight percentages (0 wt.-%, 2.5 wt.-%, 5wt.-%, 7.5wt.-% and 10wt.-% and two alloy materials (ZA-27, SiBr alloy) used as matrix materials for the fabrication of composite materials. The fabrication of composites were held in high-temperature vertical vacuum furnace that consisting of one heating unit including one graphite crucible, plunger through a narrow 8 mm diameter tip and temperature measuring instrument (Infrared temperature measuring sensor) respectively.

The mechanical properties compressive strength and impact strength have positive effect (665MPa and 6J respectively) up to 7.5 wt.-% MD filled ZA-27 alloy composites, but the flexural strength shows the increasing effect (684.38 MPa) up to 10 wt.-% MD reinforcement. Similarly, the magnitude of stress intensity factor (SIF) for varying crack length (1, 2, 3 and 4 mm) of MD filled ZA-27 alloy composites increases and the highest value of SIF occurs, 1.899 MPa.m^1/2 for 4mm crack

length. This may be due to strong bonding in between the interface of reinforcement and matrix phases. Similar results of hardness and flexural strength is found for CaO filled ZA-27 metal alloy composites while impact strength and stress intensity factor (SIF) of the calcium oxide (CaO) filled ZA-27 alloy composites show positive impact up to 10 wt.-% reinforcement content (Impact strength: 5J and SIF: 2.0127 MPa.m^1/2; for 4mm crack length) respectively except the compressive strength that shows an increasing effect on composite materials only up to 5 wt.-% reinforced contents (i.e. 723 MPa). The MD and CaO filled SiBr alloy composite materials also shows the increasing effects up to 7.5 wt.-% particulates for hardness, compressive strength, flexural strength and impact strength. The maximum amount of SIF is found for 10 wt.-% (i.e. 2.5391MPa.m^1/2, 1.91338 MPa.m^1/2 for 4mm crack length) of MD and CaO filled SiBr alloy composites for 4 mm crack length respectively. Similarly based on the above said suggested materials for a single row deep groove ball bearing has been modelled through FEM analysis for unfilled as well as particulates filled metal alloy composites and also analysed the effect of hardness, contact stress and displacement in between the inner races, outer race and ball of the specific ball bearing application at specific loading condition (i.e. load 500N). And then finally, the obtained simulated results through FEM analysis were compared with Hertzian contact stress equations for validation purposes.

The thermo-mechanical properties such as dynamic mechanical analysis (DMA) and thermo-gravimetric analysis (TGA) of SiBr and ZA-27 alloy were also examined to observe the thermal characteristics of the composites at a higher temperature range of (25-900°C) and (25-250 °C) respectively, for unfilled and particulates filled metal alloy composites. The storage and loss modulus (used to measure the stored energy and dissipated energy as heat for materials) of marble dust filled ZA-27 alloy composites, that shows the variation in the order of E'2.5%> E'7.5%> E'10% > E'0% > E'5% and the decrement of storage modulus is found from 130 ºC approximately, and it goes diminish up to 250ºC while for loss modulus different wt.-% of MD filled were E"2.5%> E"7.5%> E"10% > E"0% > E"5% respectively. Tan δ graph shows the increasing values with the increase in temperature. The value for steady state specific wear rate and the coefficient of friction were calculated for different boundary conditions and then Taguchi design of experiment methodology is taken care to compute the experimental specific wear rate

of the proposed alloy composites and then analysis of variance (ANOVA) is performed to get the most prominent effective factor in comparison to other factors.

The surface morphology of the worn and unworn samples is performed using the field emission scanning electron microscope (FESEM) to understand the wear mechanism prevailed at rubbing surfaces and then Atomic Force Microscopy (AFM) analysis is studied to evaluate the surface profile of the worn sample. At the end, Energy Dispersive X-ray analysis (EDAX) is also performed to find out the elemental compositions of the worn alloy composites. Finally, the calculation of ranking order for different physical, mechanical, fracture and wear behaviour of particulate filled metal alloy composites has been done by using a preference selection index (PSI) method. The sequencing of ranking is ZA-5> ZA-0> ZA-6 >ZA-1> ZA-3 >ZA-4 >ZA-2> SiBr-7> ZA-7 SiBr-2> SiBr-6> SiBr-3> SiBr-1> SiBr-5> ZA-8 >SiBr-0> SiBr-8> SiBr-4 for physical and mechanical properties and SiBr-7> ZA-4 >ZA-8> ZA-7 >ZA-3 >SiBr-4 >ZA-6 >ZA-2 >SiBr-3> SiBr-8> SiBr-1> ZA-5> ZA-1> SiBr-0> SiBr-2> ZA-0> SiBr-6> SiBr-5 for wear behaviour is found that shows ZA-5 (2.5wt.-% CaO filled ZA-27 metal alloy) has the optimal performance for physical and mechanical properties among all other particulate filled metal alloy composites similarly, SiBr-7 (7.5wt.-% CaO filled SiBr metal alloy) shows optimal performance for wear behaviour among all other particulates filled metal alloy composites considered in this study.

******

Table of Contents

******

List of Figures

******

List of Tables

******

List of Abbreviations

MMC	: Metal Matrix Composite
REB	: Rolling Element Bearing
MD	: Marble Dust
CaO	: Calcium Oxide
ZAMD	: Marble Dust Filled Zinc Alloy Composites
ZAC	: Calcium Oxide Filled Zinc Alloy Composites
SiBrMD	: Marble Dust Filled Silicon Bronze Alloy Composites
SiBrCaO	: Calcium Oxide Filled Silicon Bronze Alloy Composites
VHN	: Vickers Hardness Number
FS	: Flexural Strength
FEM	: Finite Element Method
SIF	: Stress Intensity Factor
SENT	: Single Edge Notched Tension
LB	: Lower is Better
Ws	: Specific Wear Rate
TGA	: Thermo-Gravimetric Analysis
DMA	: Dynamic Mechanical Analysis
E'	: Storage Modulus
E"	: Loss Modulus
Tan δ	: Damping Factor
ANOVA	: Analysis of Variance
FESEM	: Field Emission Scanning Electron Microscopy
AFM	: Atomic Force Microscopy
EDAX	: Energy Dispersive X-Ray
PSI	: Preference Selection Index

******

Chapter 1
Introduction

Chapter 1

INTRODUCTION

1.1. Background and motivation

In ancient civilization, humans had very limited resources in terms of materials, so the use of natural resources: stone, muds, woods, and so on were widely accepted by humans, at that time for different uses. By the passing time they contrive numerous techniques to developed materials that have superior properties in terms of natural ones concluded various metals [1]. The enhancement of materials becomes improved and the advance materials come into existence like smart materials, bio-materials, composite materials and many more who are exiting or yet to come. With the span of time, the properties of materials become improved some of them like the light in weight, lower cost, and higher strength. In the mid of twentieth century, the processes used for fabrication of parts made from different composite materials evolved from operations that relying on manual labor to manufacture by automated equipment controlled from sophisticated microprocessor systems. Consequently, it importantly used to study about the polished surfaces of such materials in industrial laboratories by optical microscopes and scanning electron microscopes [2].

In the middle of the twentieth century, the processes used for fabrication of parts made from composite materials evolved from operations that relying on manual labor to manufacture by automated equipment controlled from sophisticated microprocessor systems. Consequently, it becomes increasingly important to study the micro-structural behavior of a polished surface of materials in different industrial laboratories using scanning electron microscopes or some other high magnified microscopes. The materials that have remarkable properties such as higher strength, stiffness, wear and corrosion resistance, density etc. not easy to find them by only monolithic or conventional metals, ceramics or polymers, so as to get such enhanced material properties researchers needs to develop advanced materials, in this regard high strength composite materials one of them.

The development, design, and manufacturing technologies of composite materials one of the most advance and important research in material's history. Composites come into existence due to its unprecedented physical and mechanical properties, which can enhance the features or fulfill the requirements of a particular application. Composites have great resistance to secure the application by high-

temperature corrosion, oxidation, and wear, which could not possible with conventional monolithic materials. Composites technology also entitled the solid materials and ceramics technology in those applications, where conventional materials were inefficient due to lower strength and poor resistance to thermal and mechanical shock. Hence, kind of fabrication techniques adapted for large and complex structures, which consolidate the complex parts and also reduced the manufacturing cost of structures. Therefore, now-a-days composites are widely used for house hold purposes to high hand aerospace applications so far i.e. aerospace industry or in structural engineering or machine parts, automobile, train, sports equipment's, brakes, pressure vessels, marine structures and biomedical services [3].

In the past five decades, considerable attention has been devoted to composite materials. Numerous expressions were suggested for micro-structural study when different factors such as geometry, material properties and the volume concentrations of the selected materials that known. The mechanical behavior of materials describes the response of materials to mechanical loads or deformation, which can perceive the effect of applied load, atomic behavior, and defects. The composite materials defined as the material that consisting of two or more distinct phases (such as matrix phase and Reinforcement phase), which have bulk properties in each of its individual constituents. Composites classified according to matrix and fillers or reinforcements. According to a matrix, it's classified as Metal matrix composites (MMCs), Organic matrix composites (OMCs) and Ceramic matrix composites (CMCs) and according to reinforcement classified as continuously and discontinuously reinforced composites. With the advancement of the composites day by day, its uses increased widely in many areas like automobiles, aircraft, bio-medical, armor vehicles and many more [4].

Metal matrix composites (MMCs) now-a-days have received increasing attention in the recent decades as an engineering material for industrial applications. The immersion of reinforcement particulates into a metal matrix / metal alloy fabricate a composite material with the combination of appealing physical, mechanical and wear properties in comparison of a base or monolithic alloys. Hence, MMCs widely accepted in many applications such as aerospace, automotive and power utility industries due to its prominent characteristics. However, their mechanical and tribological properties such as strength, toughness, corrosion and wear resistant shows the great effect with the dependency of some factors. The major purpose of producing metal matrix composites (MMCs) was to achieve lightweight materials with high

specific strength and stiffness. Majorly it focuses on increases the mechanical properties of Particle reinforced metal matrix composites (PRMMCs) while adding particulates; it affects most of the properties of PRMMCs so far. The parameters related to the particles are volume fraction, size, shape and distribution of particles and among the selected parameters, the most important parameter being the volume fraction. The mechanical properties of metal matrix composites depending on the type and volume fraction of the reinforcement, dislocation strength and the defects introduced during the fabrication of MMCs. Most widely considered properties in MMCs have its tensile strength, compressive and bending strength, ductility and dynamic hardness and fracture strength respectively.

In recent years, metal matrix composites (MMC) widely used over monolithic metals due to its superior properties such as higher specific strength and modulus, lower coefficient of thermal expansion and better material properties at elevated temperatures. It also becomes prime choice of industrialists for critical structural applications due to an amalgam of surpassing mechanical properties like better elastic modulus, material strength, the stability of materials at high temperature and wear resistance as a comparison of monolithic alloys [5]. In MMCs, ceramic particulates become very widely considered now-a-days as reinforced particulates to enrich the strength, stiffness and different material properties by the selection of different parameters such as weight/volume percentage, reinforced particle shape and size, distribution of particles in matrix materials, etc. [6].

Metal composite materials widely used in many areas of day to day life. Similarly with other composites, Metal matrix composites (MMCs) consist two or more than two distinct phases, which gives the enhanced property that would not be possible by individual phases. MMCs are widely used now a day's due to its admirable properties as compared to other composites that prompt as [7];

- Extensive weight savings because of higher strength-to-weight ratio.
- Exceptional dimensional stability.
- Higher elevated temperature.
- Higher strength and stiffness.
- Higher thermal and electrical conductivity.
- Better transverse properties

The metal matrix composites have reinforcement that used in metals for different objectives like it used to reduce the weight of the application which become

a priority nowadays in every structural application. The objectives for the development of light metal composite materials as [8].

- To increase the tensile and yield strength at room temperature and above are maintained ductility or rather toughness
- To Increase the creep resistance at higher temperatures as compared to other conventional alloys
- To improve the fatigue strength, thermal shock, and corrosion resistance
- To increase in Young's modulus and reduced the thermal elongation.

The efficient and reliable working of any machine has highly dependent on the efficient function of its various components. Bearings in machines serve as a vital element in this regards [9]. The bearings a load carrying element and subjected to the intense tribological environment; any damage to them, results were a loss of productivity and financial aspects [10]. Therefore, scholars in these researches focused on their efficient working either by designing them or by the development of effective material that gives win-win results across all working parametric conditions [9, 10]. Traditionally monolithic alloys used for bearing applications in most of the cases. The material research over the decade reported the development of tailored alloy composite materials that exhibits enhanced and enriched properties like high specific strength, stiffness, better wear resistance, dimensional stability, etc. most suitable for tribological applications [11]. It has been reported from the literature review that ceramic particulate filled alloy composites serve as an excellent material substitute for monolithic materials in bearing applications [11-17].

Recent developments, for example, dual phase steel, which evolved in the 1970s have connected or brought closer the metal matrix composites to engineering practice [18]. Mechanical behavior referred as a response of materials when the force applied to them. On loading condition, a material may either deform or break. The strength may refer as when the stress required to deform a material or stress required to cause fracture; therefore, in both cases care should be taken with the term strength and other failure properties [19]. Therefore, then fails due to a fracture in structure, that's to break the structure in one or more than one piece under the action of variable loading. However, fracture occurred unexpected, sudden, and unfortunately, so it's natural to us to focus or give attention on the fractures that minimize these undesired consequences when designing any modern-day structural applications. Fracture

mechanics, all about the study of crack behavior, fracture of materials and their preventions [20].

In the engineering practices, wear was the major cause for wastage of material and loss of mechanical performance. By the reduction of wear, considerable savings happened to the materials and performances. Friction considered as a primary cause for wear and energy dissipation. From the research, it's estimated that in the present one-third of the world's energy resources needed to overcome friction in one form or another. In reducing friction, lubrication plays an effective and important role. Tribology, used to overcome the problems of great economic significance i.e. reliability, maintenance, and wear that occurred in technical equipment ranging from household appliances to spacecraft.

Tribology term focuses on friction, wear and lubrication of interacting surfaces in relative motion, which came into existence by a committee of the Organization for Economic Cooperation and Development in 1967. 'Tribology' comes from the Greek word 'tribos' which means rubbing or sliding [21]. After Second World War most of the knowledge about the Tribology being gained as a very new area of science. In comparison to many other basic engineering subjects like thermodynamics, mechanics and plasticity, tribology was relatively old and established. After innumerable experiments and theories about the tribology, general observation compresses about the study as;

- Study about the characteristics of films that develop between intervening materials when bodies were in contact.
- Study about the consequence which occurs by film failure or absence of a film that were usually manifested by severe friction and wear.

The rolling element bearing (REB) used in any machinery one of the most critical parts that defines the efficiency and lifespan of a particular component of machinery which degrade with respect to time due to the cause of wear [22]. REB's mostly emphases on reduce wears that can occur by improving material properties. The study about the defects like high stress and strain induced at a certain position of components, influence of surface contact geometry, applied load magnitude and defect location, etc. can be occurred as studied by many researchers[23]. Most of time materials used for the bearing i.e. steels such as high carbon chromium bearing steel; induction hardened steel, high/mid carbon alloy steel, rather than these steel bearings also made by Si_3N_4 [24]. Now-a-days mostly bearings emphasized on particulate filled

composites, or polymeric materials to prepare it. Although it's not only material property, but also a system response such as sliding velocity, applied pressure, and environmental conditions, etc. [25]. In bearing, industries use different grades of materials for the production of various bearing components. The materials were processed to maximize bearing performance and its life period was kept in view the design criteria, handling process, installation, lubrication condition and system cleanliness. As we know that the classical rolling-element fatigue failure are taking place in the subsurface origin and has been considered the prime life-limiting factor for rolling element in bearings [26]. Therefore, it was also observed that less than 10% of the bearings displaced from equipment's service was failing due to high wear rate, improper lubrication, life subsurface fatigue and many more and the other remaining 90% bearings fails due to like manufacturing defects, material defect, lubricant improper flow, contamination of lubricant, excessive dirt ingestion, improper installation of bearing, misalignment of bearing cages axis and corrosion etc. [27]. Mostly these failures for bearing were unpredictable; it can happen anytime either installation or performance such as physical, mechanical and wear characteristics respectively. Therefore, most of the researchers focused on the development of metal matrix composites along with inclusion of hard ceramic or filler materials in the composites to improve the wear resistance and friction properties, because the wear and friction properties of the composites depend on the quantity of reinforcing material, size, shape as well as the distribution of particles/ fiber inside the material [28; 29].

Numerous bearing materials extended propitious properties individually, such as light in weight and low friction to fulfill the required service by the particular application, but the cast bearing bronzes alloys for bearings tender an extensive range of applicability. These bearing materials have a glowing amalgamation of physical and mechanical properties that allow the researcher or fabricator to fabricate the optimum design of bearing without accommodating the required characteristics unnecessarily [30]. During dry sliding wear test condition, pin sample, and rotating disc were generated high operating temperature at sliding zone that leads towards materials wear and tear condition that further required component replacement. Therefore, wear can be assumed as a major problem for the enhancement of life-span of any component subjected to wear zone. Hence, particulate filled metal alloy

composite showed a major alteration in the place of pure alloys, especially in dry lubricating conditions.

The Zinc-aluminum alloy (ZA-27) widely used as a substitute of brass and cast malleable iron for making wear resistance machinery parts. The zinc, aluminum alloy ZA27 has a numerous or a wide range of working applications. It is most widely used as bearing materials due to its excellent fluidity, high damping capacity, good cast-ability, low friction coefficient, high wear resistance in both dry and lubrication conditions and the lower production cost [12; 13]. The service life of bearings depends upon it tribology performance i.e. Sliding wear and friction across the contact zone have a direct influence on its fatigue life [15-17; 31; 32]. The zinc, aluminum alloy has the capability to replace the cast aluminum alloy, cast iron, plastics or even steels and some other such type of materials for the casting of Tribo-elements for the operation that performed under moderate exploitation temperatures. Despite its many superior characteristics that performed at room temperature, it shows the degradation of material's tensile strength and creep resistance phenomenon when the operating temperature goes above 100°C, which respectively lowers its area for the particular applications. So to overcome by its different degrading properties at high-temperature zones, researcher starts to use different ceramic materials to reinforce with the alloys since the mid-1980s.

The zinc alloy (ZA-27) has excellent bearing properties that make it suitable for different wear resistant applications generally for industrial area applications. Such alloy work as good wear resistant materials under higher applied load conditions, slow to a medium range of rpm and indigent lubricating conditions. The ZA-alloys have dendritic structure during solidification condition, whereas the size and inter dendritic spacing depends on casting parameters. The cooling effect of material processing imposes a strong effect on the grain size of the dendritic structure of the fabricated materials. The repercussion of dendritic structure induced lower in ductility as well as the higher heterogeneity of cast alloy’s mechanical properties. Some other issues related to ZA-alloys refer to dimensional uncertainty, caused by the existence of Meta stable phases. Copper and copper based alloy materials acceptable by industries on worldwide level due to their distinctive material properties such as good wear and corrosion resistance, strength, self- lubrication mechanism and machinability of the components respectively [33]. The major working application area of silicon bronze (SiBr) based alloy for engineering parts tribology analysis [34] such as bearing

materials, because of its high thermal conductivity and magnificent workability [35]. The bronze materials used as the most versatile class of bearing materials because of its extensive mechanical as well as wear resistance properties. Similarly, the superior corrosion resistance properties of bronze alloy for bearing materials can also be used for different operating conditions. As we know that the bearing material should be cost effective and can be easily available, bronze alloys consummate all these requirements because its having economical so as low-cost manufacturing, and also having better machinability that cannot be challenged by other bearing materials and due to this reason it has two steps ahead position in comparison of other bearing materials, that can be selected to fulfil the requirement of any bearing applications. By that bronze, materials can fit the needs of a particular design with its extensive range of material properties [36, 37].

1.2. Thesis outline

The prompt of the thesis were catalogued as below:

Chapter 1: The introduction like a backbone, that concluded all the data related to the thesis that we have to go through, throughout the report. This chapter has the entire summary that would be necessary to complete the picture.

Chapter 2: The background information about the issues that we have to cover in the thesis concluded by chapter two i.e. literature review. It bonded the research works on the physical, mechanical; fracture toughness, thermo-mechanical, sliding wear and optimization properties of various types of particulate filled metal alloy composites, that has been discovered by various investigators previously.

Chapter 3: The materials (matrix and fillers), methods and different test procedure followed by this chapter. It included details about the fabrication and characterization of the composites under investigation and also explained optimization technique for wear behavior (Taguchi experimental design) and PSI (Preference Selection Index) method for overall optimized values.

Chapter 4: Presents the physical, mechanical and fracture toughness analysis of the metal alloy composites of experimental technique and compared with FEM for validation of simulated results. Study about Fractographs of a fractured surface after the tensile test shown, also entitled the optimum mechanical properties for particulates filled metal alloy composites by the PSI optimization method.

Chapter 5: Covered the thermo-mechanical analysis of unfilled and particulate filled metal alloy composites by dynamic mechanical analysis (DMA) and thermo-gravimetric analysis (TGA) methods.

Chapter 6: Includes the Sliding wear behavior of particulate filled metal alloy composites. It presents a detailed study on the effect of particulate fillers on the sliding wear behavior of ZA-27 and SiBr alloy composites, micro-structural examination by FE-SEM/EDAX and AFM techniques. Finally, the outcomes of sliding wear behavior optimized by Taguchi experimental design and the best optimize the value of overall Tribology aspects determined by the PSI optimization method.

Chapter 7: Put the light of the findings of this research work, specific conclusions have been drawn from the experimental and analytical outputs.

The next chapter briefly presents/discuss the literature review of various research papers on physical, mechanical, thermo-mechanical, tribological analysis of a series of experimental bearing materials. The specific objectives of this work are clearly outlined in the next chapter.

******

Chapter 2
Review of Literature

CHAPTER 2
LITERATURE REVIEW

2.1 Introduction

The main purpose of the literature review was to provide background information about the research work that's going to consider in this thesis and the relevance of those points should be emphasized during the study. This chapter summaries, various issues available over a decade on physical, mechanical, thermo-mechanical, fracture toughness and wear behavior of metal and metal alloy composites. The topics briefly reviewed all the relevant literature and still needs further research to improve the above said properties for industrial, automotive, and structural applications respectively. Also, there were several important parameters have been overlooked by the previous research literature among which the types of reinforcements, geometry and size of the reinforcement, etc.

The following points were discussed keeping given our research works as:

2.1.1 On physical and mechanical properties of particulate filled metal alloy composites.

2.1.2 On fracture toughness of particulate filled metal alloy composites.

2.1.3 On thermo-mechanical properties of particulate filled metal alloy composites.

2.1.4 On sliding wear and friction behavior of particulate filled metal alloy composites.

2.1.5 An implementation of Design of Experiments (DOE) and Optimization techniques particulate filled

Summary of the literature survey and the research gap

2.1.1 On physical and mechanical properties of particulate filled metal alloy composites

Composite materials have been in attention for the last five decades. Some expressions or methods have been given by many researchers, by which macroscopic properties can be found out when the properties, geometry and volume fraction of the constituent components are known [38]. The mechanical behavior of materials defined the response of that material to mechanical loads or deformation. The outcomes can be

understood in terms of the initial effects of mechanical loads on defects or atomic motion [39].

The metal matrix composites (MMCs) own improved mechanical, thermal and other properties as compared to monolithic alloys, such improved properties as; high specific strength, modulus, damping capacity, wear and corrosion resistance, etc. The metallic composite defined as the combinations of two or more than two distinct phases of metal, that has the bulk phase as matrix and another phase as reinforcement. Such materials were produced by controlling the structural phenomenon to get the optimum material properties. The properties of composite materials depended upon the individual properties of its phases, their size, shape and orientation etc. [40]. The primary function of MMC's was to distribute the applied load to the position of reinforcement. The wetting phenomenon in MMC's fabrication plays an important role, because of wettability the bonding in between matrix and reinforcement shows strong behaviour and also distribute the load from matrix to reinforcement without failure of materials [41]

From the literature review, it was proposed that the mechanical properties of metal matrix composites were dependent on the type and volume fraction of the reinforcement, dislocation strength and the defects introduced during the fabrication of MMCs. Most widely considered property in MMCs were its tensile strength, compressive and bending strength, ductility and dynamic hardness and fracture strength respectively. The composites have higher elastic moduli as compared to monolithic alloy. The amount of elastic modulus increased with an increased in weight. -% of particulates but at a progressively decreasing rate. The composites have better tensile and yield strengths than the unreinforced alloy and also lowered ductility than the monolithic alloy [41]. The ductility of materials was decreased linearly with the increased inwt. -% of particles. Similarly, Poza and Llorca [42] studied the microstructure and tensile properties of an 8090 Al-Li alloy reinforced with 15 vol. % SiC particles, together with those of the monolithic alloy processed following the same route and they found that the inclusion of SiC particles improved the grain structure during extrusion process that inhibited the precipitation of Al_3Li at ambient temperature. The factors that determined the different properties of particulate filled composite materials were strongly influenced by volume fraction, microstructure behavior, homogeneity effect and isotropy of materials. The particulate reinforcements such as SiC, Al_2O_3 and aluminide were generally preferred to impart

higher hardness. The coating of reinforcements with Ni and Cu also leads to good quality interface characteristics and hence contribute in improving the hardness of the particulate filled alloy composites. Whereas, TiC dispersed in Al matrix composites, increases the hardness to weight ratio gradually. Louis et al. [43] concluded that the increased in hardness property of composites, depends upon not only the hardened ceramic particles and on the size of the ceramic particles although on the structure of the composite and good interface bonding.

The strength of SiC, Al_2O_3, TiC and TiB_2 particulate reinforced Al-MMCs was observed an increment at the cost of decreased amount of ductility; this was found because of increasing wt.-% and reduced size of ceramic particulates in the composite. The SiC reinforcement in the Al-MMCs was more fracture resistant compared to Al_2O_3 and Si. The SiC particulates show harder in nature in comparison to other reinforced particles that shows the most effective barrier to subsurface shear at the counter surface when two body were in contact during motion, and this result was likely due to differences in particles shape [44]. However, by the incorporation of TiO_2 particles resulted in the wear of disc and the TiO_2 particle used to reduce both plastic flow and metal transfer to the pin in the matrix material [45]. But TiC-reinforced Al356alloy was the hardest and exhibited the lowest wear rate and while the amount of load increases the transition from low wear rate to high wear rate occurs [43]. Similarly, Aldas and Mat [46] were used SiC as reinforcement with Pb 20%Sn alloy was studied in both experimental and numerical method and found that the particle fraction decreases along the axis of the mould. Therefore, for a particular cross-section, the particle fraction was found to increase towards the wall due to the increased drag force exerted on the particles near the wall. In another study, Singla et al. [47] were used SiC as filler in the metal matrix composites and concluded that with increased in percentages of SiC particle, an increase in hardness, impact strength and normalized the displacement have been observed. The best results have been obtained at 25% weight fraction of 320 grit size SiC particles, and the maximum hardness was lies in 45.5 BHN with a maximum impact strength of 36 N-m respectively. The detail of selected particulate filled metal and metal alloy composites mechanical properties are presented in Table 2.1 based on their applications in industrial use.

Bobic et al. [48] studied microstructure and mechanical properties of $Zn_{25}Al_3Cu/Al_2O_3$ particulate composites and concluded that the large Al_2O_3 particles were uniformly distributed in the matrix $Zn_{25}Al_3Cu$ alloy regardless of the amount of

reinforcing particles. Also, the hardness of $Zn_{25}Al_3Cu/Al_2O_3$ particulate composites increases with the increased in the amount of reinforcing particles, whereas, unfilled Zn25Al3Cu alloy (as-cast) exhibited higher compressive strength with respect to that of $Zn_{25}Al_3Cu/Al_2O_3$ composites at ambient temperature. Whereas, ZA-alloy matrix composites reinforced with different hard ceramic particles and short fibers showed excellent wear resistance, superior hardness, modulus and greatly reduced the creep rate compared with that of parent matrix alloy material. As ZA-27 alloy has shown good wear resistance and tensile strength substantially higher than that of ordinary cast aluminium alloys [49]. They described the mechanical properties like UTS, yield strength, Young's modulus, and hardness of ZA-27 alloy that increased significantly but at the cost of ductility and toughness. Zinc-aluminium (ZA) alloys have emerged as potential engineering materials for a variety of applications, especially in automobile sectors. Sharma [50] studied about the Short Glass Fiber-Reinforced ZA-27 alloy Metal Matrix Composites in his research work and found, that the modulus of elasticity and ultimate tensile strength of the composite gradually increased with the increasing volume fraction of the fiber, although the ductility decreased with an increased in volume fraction of the fibers.

Sharma and Girish [51] reported that the mechanical properties of discontinuously reinforced composites are strongly dependent on many variables, including the distribution of the particles in the matrix, the mechanical properties of the matrix and the reinforcing particles and the interfacial bond between the matrix and reinforcement. There was a decrease in the inter particle distance between the hard hematite particles, which causes increased resistance to dislocation motion as the hematite content is increased. They found in the presence of hard hematite particulates the ultimate tensile strength and young's modulus become increasing while ductility decreases. Similarly, results were observed by Humphreys et al. [52] and Stone et al. [53] in which the strength of the particle reinforced composite was most strongly dependent on the volume fraction of reinforcement with somewhat weaker dependence on particle size. This was because reinforced particles act as barriers to dislocations in the microstructure.

From 1990's it has been seen that the metal matrix composites replaces conventional materials in many applications like commercial and industrial applications. Initially, they show the disadvantages for various mechanical properties like tensile strength, ductility, fracture toughness and fatigue performance of

automobile applications as compared to those of the constituent matrix materials by Hemanth [54]. In his report, he was discussed about the mechanical properties of chilled aluminium quartz cast able particulate composites and found that the value of ultimate tensile strength of chilled composites was increased by increasing the addition of dispersoids up to 6wt.-%. Poddar et al. [55] observed that the presence of particulate increases the yield strength and young's modulus because smaller particle reinforcement leads to better improvement in elastic modulus and yield strength. The basic mechanism of composite deformation is the load transfer from the matrix to reinforcement and a good bonding between matrix and reinforcement gives rise to better load transfer and improved properties. As the effect of particle size on mechanical properties of SiCp/5210 Al metal matrix composite studied by Dong et al. [56] explained with the decreasing in particle size, the bending strength of the composites increases. Similarly, Sharma et al. [12] reported the presence of hard zirconium particulate with ZA-27 matrix composite imparting more resistance to composites against the applied tensile load. In the case of particle-reinforced composites, there was a restriction to the plastic flow as a result of the dispersion of the hard particles in the matrix, thereby providing enhanced tensile strength in the composite. Regarding ductility, from their studies the ductility decreases as the zircon content increases, this was due to the embrittlement effect because of the presence of hard zircon particles that resist the passage of dislocations either by creating stress fields or by including large differences in the elastic behavior between matrix and dispersed.

Ceschini et al. [57] found that microstructure modification in forged composites increases the tensile property of materials, both at room and high temperature and the formation of inter metallic compound both in the cast and forged form. In forging inter metallic compounds were mainly observed, which enhances the stability of Al2618 at high temperature. Kleis and Hussainova [58] reported that alumina fiber reinforcement significantly enhances the tensile as well as compression properties both at elevated temperature, but at the cost of ductility and toughness, this was due to the presence brittle of SiO_2 layer at the fiber/matrix interface resulting in de-cohesion of fiber/matrix and impairing the performance of reinforcing material. Kevorkijan [59] studied the quality of aluminium dross particles and cost-effective reinforcement for structural aluminium-based composites and report that a minor improvement was found in the strength of materials with the inclusion of fine dross

particles (particle size less than 10 mm), but for the composites where larger dross particles being used, no strengthening effect was observed. Sharma et al. [60] studied that by the addition of Quartz particles have a positive effect on a lead alloy as it increases the hardness, ultimate tensile strength, impact strength but at the cost of ductility. The Increase in hardness was due to lead soft alloy and hard quartz particle dispersoid, and these particles act as barriers for the movement of dislocations and hence increased the hardness of the composites.

The different mechanical properties of ZA-27 alloy composites which reinforced with TiO_2 particles investigated by Ranganath et al. [61]. In their report, they found that with the increment of reinforcement from 2-6%, the different mechanical properties like ultimate tensile strength, hardness, yield strength also increases simultaneously except ductility and toughness. Therefore, it was a disadvantage of composite which scarifies too much of its ductility and toughness property with the increasing in wt.-% of reinforcement in the composites. Kok [62] found that the mechanical properties such as tensile strength, hardness increases with the decreasing in elongation may be due to the decreasing in size of the particles and increasing in volume fraction. Similarly, the hardness values for quartz particulate that reinforced by LM6 alloy composites were measured by Hamouda et al. [63]. They found the tensile strength of the composites decreases with the increases in wt.-% of quartz particulate. Xiandong et al. [64] studied about Cast aluminium alloy and zinc alloy matrix composites that were reinforced by ceramic particles and graphite flakes respectively. They demonstrated that the particle reinforced composites showed good tribological properties with more uniform wear rate. They also show the wear rate and friction coefficient decreases, which should be appreciable and the seizure resistance increases similarly. Kennedy [65] found that during the preparation of composites a Ti-B-C reaction layer was formed on the surface of the particle, but during the heat treatment process the layer was intact and stable and acts as a protective layer thereby reduces the degradation of the particle and increases the stiffness with the increased in volume fraction. Hence, the reaction layer improves the adhesion between the matrix and reinforcing particle respectively.

Similarly, another group was studied the aluminium/TiC metal matrix composites [66] and studied about the effect of different mechanical properties and interfacial strength of the composites. They used both cast and powder metallurgy techniques for the casting of composites and found that the stiffness and ductility were

similar for both the process. However, when the material was melted by PM it signifies both reduction in strength and ductility of the material. In both the cases ductility was improved by the extrusion through the porosity reductions and the break-up of particle clusters. Hossein et al. [67] reported about the mechanical behavior of zircon particulate filled metal alloy composites which show with an increase in zircon content, sintering temperature the hardness of the composite increases. Also to increase in zircon content the distance between the particle decreases and dislocation pileups and hence reduction in elongation occurred. Ganesh and Chawla [68] were studied about the particle orientation anisotropy effect on mechanical properties of metal matrix composites. In their study, they found that with the increasing in the amount of SiC reinforcement the extent of anisotropic behavior was also increased. As ceramic, metal alloy (Titanium matrix composites) have been widely used now-a-days in different applications like the exhaust valves in automotive engines in the advanced military, biomedical engineering sectors and sporting goods respectively [69]. Similarly, Kaataih and Girish [70] found that by the addition of TiO_2 particles the mechanical properties of the composites such as ultimate tensile strength, yield strength and hardness has a significant effect but the ductility of the composite decreases. A study about the tensile property of titanium matrix composites reinforced with TiB and Nd_2O_3 were studied by Geng et al. [71]. They reported that the tensile strength of the composites has an increment at elevated temperatures as compared to titanium matrix, and the ductility of composites was also increased with the increment of reinforcement particles. Aqida et al. [72] explained that porosity also one of the major defects that affecting the different mechanical properties such as hardness, ultimate tensile strength, and yield strength, modulus of elasticity and poison's ratio of the particulate reinforced metal matrix composites. It was formed because of gas entrapment, water vapor on the surface of the particle, shrinkage during solidification and air bubbles entering the matrix material, etc.

Ramesh et al. [73] compare the mechanical properties of Al6061 matrix reinforced with graphite and about particles and found that both the particles have different effects on mechanical properties of MMCs. Therefore, for graphite filled composites the properties such as ultimate tensile strength, compressive strength, modulus of elasticity and ductility increases with volume fraction whereas, hardness decreases due to soft graphite particles. However, by the addition of about particle the UTS, hardness, yield strength and modulus of elasticity increases, but decreased in

ductility due to about particles were heard and acted as barriers to the movement of dislocations. Hence, concluded that compromise was necessary for deciding the volume fraction of graphite as well as about particles to enhance the mechanical properties of aluminum matrix composites. Similarly, Mizuuchi et al. [74] found that with the low-pressure casting/combustion process the near-net shaped tri aluminide composites were produced without any cavities and the tensile strength of the aluminum composites containing Ti increased with the increased in Ti content. The different mechanical properties like tensile, hardness and compression tests, etc. for nano and micro-composites (A356/Al_2O_3) with different weight percentage of particles was studied by Sajjadi et al. [75]. They observed from their investigation that the mechanical properties (such as yield strength, ultimate tensile strength, compression strength and hardness) show the increment with the addition of alumina (micro and nano) led. Silva et al. [76] studied about the micro structural and mechanical characterization of a Ti_6Al_4V/TiC/10p composite that was processed by the hot isostatic pressing (BE-CHIP) method. They reported that proper distribution of particles and size of particles highly affects the damage mechanisms of the composite. Lee et al. [77] considered two different composites (AZ91 matrix reinforced with kaowool alumina silicate fibers and saffil alumina short fibers) fabricated by squeeze casting with variation in pressure and reported that as the applied pressure increases the fiber breakage occurs. Whereas, the composites with saffil reinforcement the micro-cracks occurred at the fiber/matrix interface and there was no degradation of the fiber noticed that indicates that higher applied pressure with saffil reinforcement leads to improvement in mechanical properties. Ozben et al. [78] explained that as the volume fraction of reinforcement increases the hardness and tensile strength increases continuously but the impact toughness decreases due to the rigid inter-metallic compound formation between matrix and reinforcement interface due to the size, shape of the particle and also dendrite air gap formed due to slow cooling is also a reason for reduced impact toughness. Similarly, the tensile strength of continuous molybdenum fiber reinforced aluminium matrix composites was studied by Chen et al. [79] and they presented that with the increased in fiber content the strengths of 0°/90° dual-directional composites also increases. The different mechanical properties like hardness, tensile strength, compression strength, and impact strength were increased with the addition of fly ash content in composites, except the value of density. This study was done by Mahendra and Radhakrishna [80] for Al–4.5% Cu alloy reinforced

with fly ash content. Zohangguang et al. [81] reported that the fatigue behavior of the matrix composites was superior then that of the alloy composites. The key to controlling the properties of metal matrix composites and the interaction between the crack and the interface was essential for determining the critical conditions of fatigue failure as the metal matrix composite body with heterogeneous structure was necessary to introduce micromechanics and statistical concepts for better understanding of mechanical properties and fracture process. Bekheet et al. [82] reported that the addition of SiC particles refines the matrix by reducing the grain size of the matrix and also peak hardness of the composite was higher than the alloy. The addition of SiC particles and the artificial aging significantly improves the fatigue behavior of the composite. Similarly, Milan et al. [83] shown that the particle volume fraction and particle size enhances the fatigue crack growth resistance. However, Seah et al. [84] reported that with the increase in SiC particulates the hardness of the composites increases, which was due to SiC being very hard dispersed and also act as barriers to the movement of atoms which dislocates within the matrix and the dispersion strengthening effect was retained at high temperatures because of SiC particles did not react with matrix even at high temperatures.

Sharma and Ramesh [85] found that the UTS, compressive strength and hardness of the composite were higher than the matrix alloy and a marginal improvement in UTS, hardness and compressive strength due to heat treatment process. The addition of reinforcement noticeably enhances the dislocation density due to variation in the co-efficient of thermal expansion and with the increased in volume fraction of reinforcement the ductility decreases automatically. Similarly, Pradeep et al. [86] predicted that by the addition of graphite particles and nitriding improves the mechanical properties such as, tensile strength, hardness, % elongation and modulus of elasticity as the nitriding less distortion then either conventional carburizing or hardening. Similarly, Seah et al. [84] observed that as hardness increases monotonically with aging time and the role of particulates are negligible because of artificial aging enables the precipitation of different phases of composites and expected to improve the hardness of the material. During this process, the conversion of BCC phase to FCC and HCP phase takes place which results in precipitation hardening. Al alloys (Al2124-T1 and Al6061-T1) which was mixed with SiC particles was studied by Milan and Bowen [83] for the finding of different mechanical properties of the long fatigue crack growth. They found the fatigue crack

growth resistance was increased near the threshold and the paris regimens with the increased particle volume fraction and particle size of the composites, with the marginal effect of matrix strength. Eshani and Reihani [87] reported that addition of SiC particles to Al6061 alloy increase the hardness, yield strength, elastic modulus, and tensile strength, but the elongation decreases due to the more thermal mismatch between the matrix and reinforcement. The increased in dislocation density, the fracture surfaces of the composite show brittle fracture, voids and dimples due to decohesion of SiC particle and ductile fracture of the matrix material was observed. Kashyap et al. [88] found that the strengthening of PMMCs was associated with dislocation density in the matrix alloy by considering commercial Aluminium alloy which has a lower work hardening rate but exhibited the highest strength due to the prismatic punching of dislocations. Bauri and Surappa [89] reported that with the increased in volume fraction of SiCp, the ultimate tensile strength, compressive strength and hardness increases as the volume fraction increases to 18% and beyond that the strength decreases due to the particle clustering and also the fracture surface of the composite shows the mixed mode bimodal distribution of dimple. Similarly, Basavarajappa et al. [90] showed the mechanical properties such as ultimate tensile strength, yield strength, hardness and compressive strength increases with the increased in volume fraction but the density of the composite decreases gradually. The increased in UTS, YS, and compressive strength may be due to SiC particles acts as barriers to the dislocation and also as the volume fraction increases the inter particle distance between the reinforcement particles decreases and causes increased resistance to dislocation movement and the dislocation piles up and restricts the plastic flow and hence increase the strength. But with the deceased in ductility with increased in volume fraction was due to the presence of hard particle SiC and embrittlement effect of SiC and graphite particles restricts the passage of dislocations. However, Das et al. [91] found that by the addition of SiC particle the hardness increases but it reduces the forgebility of the composite due to the uniform distribution of hard SiC particle in the soft alloy matrix. Similarly, Long et al. [92] reported by the addition of SiC particle accelerates the age hardening response of the matrix alloy and improves the stiffness, flexural strength, hardness and fatigue strength along with significant reductions in toughness and ductility respectively. The precipitate hardening can be attributed to the thermal mismatch between the matrix and the reinforcement. Deng and Chawla [93] used two-dimensional finite element methods (FEM) simulation to quantify the effect

of clustering on local and macroscopic stress–strain behavior of Al–SiCp composites. The models explicitly incorporate cracking of the particles for two levels of particle clustering and concluded that particle clustering has a significant effect on the ductility of the composites; if particle clustering was included in the simulation and the particle fracture was not considered due to the particle clustering has very little effect on the tensile behavior of the composites.

Table 2.1 Physical and mechanical properties of particulate filled metal alloy composites.

Sl. No.	Metal matrix	Particulate	Physical / mechanical properties	Ref.
1	Pb 20%Sn alloy	SiCp	The particle fraction was found to decrease along the axis of the mold. The distribution of particles estimated from the trajectories of representative particles with the Lagrangian point of view. The numerical results are reasonably suited to experimental data.	10
2	Aluminum alloy, Zinc alloy	Graphite flakes, SiC, Al_2O_3, B_4C	The particle reinforced composites show good tribological properties, with the wear becoming more uniform, the wear rate and friction coefficient, Decreasing appreciable and the relative seizure resistance Increasing.	64
3	Aluminum alloy	SiC	The composite exhibited a higher Young modulus and tensile strength along, then the longitudinal direction (Parallel to the extrusion axis) than in the transverse direction.	68
4	Aluminum LM6Alloy	SiO_2	The hardness value of the silicon dioxide reinforced LM6 alloy matrix composites increased with the Increased addition of quartz particulate in the matrix and it well supported.	63
5	Aluminum alloy (A356)	Al_2O_3	The yield, ultimate and compression strength of the composite increase with increasing Al_2O_3 content because of increase in load stress.	75

6	Aluminum	Molybdenum	The strengths of 0°/90° dual-directional composite fiber increased with fiber content.	79
7	ZA -27 alloy	Short glass Fiber (2, 7, 12, 17%Vf)	The Young's modulus and UTS of the composite material increase with an increase in the fiber volume fraction.	50
8	Titanium	TiB and Nd_2O_3	Compared with titanium matrix, the tensile strength of the composites has a significant improvement at elevated temperatures. The ductility of the composites improves with the content of neodymium and the test temperatures.	71
9	Al6061-T1, Al2124-T1	SiC particles	An increase in particle volume fraction and particle size increases the fatigue crack growth resistance at near threshold and in the Paris regimens, with matrix strength having the smaller effect.	83
10	ZA-27	TiO_2	It was found that with an increase in percentage of titanium dioxide reinforcement from 2-6%, mechanical properties such as UTS, yield strength, and hardness increased significantly but at the cost of ductility and toughness	61
11	AZ91D	SiC	The presence of SiC particulate leads to significant improvement in hardness, elastic modulus and yield strength, and decrease in ultimate tensile strength and ductility	94
12	Al–4.5% Cu	Fly ash 5, 10, 15 wt. %)	The fluidity and density of the composites decrease whereas the hardness increases with an increasing percentage of fly ash particulates. The tensile strength and impact strength increase with an increasing percentage of fly ash particulates.	80

13	Al 5210	SiCp	The bending strength of SiCp/5210 Al composite with a high volume fraction (50%) increases with decreasing particle size	56
14	Aluminum	Glass	Addition of glass particles into the aluminum matrix improves the strength of aluminum alloy at the expense of ductility, impact energy and fatigue life.	95
15	Chilled Aluminum	Quartz Particles	The UTS values of the chilled composites were increased by increasing the addition of dispersoids up to 6wt. %	54
16	Aluminum	hematite (Iron Oxide)	The ultimate tensile strength and Young's modulus of the composite increased while the liquid fluidity and solid ductility decreased with the increase in hematite content in the composite specimens. The fluidity of the liquid was greater in a metal mold than in a sand mold, and it decreased with an increase in reinforcing particle size and increased with pouring temperature.	14
17	AA 6061	MICRAL-20TM (A mixture of alumina and mullite)	The composites had higher elastic moduli than the unreinforced alloy. The composites had better tensile and yield strengths than the unreinforced alloy. The composites had lower ductility than the unreinforced alloy. The ductility decreased linearly with increasing particle volume fraction.	96
18	A356	Dross particles	Tensile properties of composite materials showed that a slight improvement in strength over the unreinforced matrix.	59
19	Titanium	TiCp/Ti–6Al–4V and TiBw/Ti	The TMCs (titanium matrix composites) reinforced with in situ TiB whiskers exhibit high strength and stiffness as well as good creep and fatigue resistances.	69

20	Aluminum	TiCp	Severe particle clustering and significant losses in both strength and ductility. Composite ductility enhanced by extrusion through the removal of porosity and the break-up of particle clusters. Enhanced interfacial bonding in cast Al/TiC composites was in turn attributed to the use of a flux, which cleans the particle and matrix surfaces, enabling intimate contact and the formation of strong chemical bonds.	66
21	Ti6Al4V	TiC particles	The damage mechanisms of both tensile and fracture toughness specimens of the composite material were strongly influenced by the poor distribution of the reinforcement (particle clustering and large particulate size). The failure of the composite was controlled by fracture of the reinforcement followed by ductile failure of the titanium matrix.	76
22	ZA-27 alloy	-	Mechanical deformation increases the tensile strength of the fractionally melted alloy twice that of the as cast alloy. Zinc and copper leave the dendrite phase during the test at holding temperature and the alloying elements become lower in the fractionally melted specimens. Porosity of the as-cast alloy decreases.	97
23	$Zn_{25}Al_3Cu$ alloy	Al_2O_3	Cracks in large Al_2O_3 particles could be induced by thermal stress. Hardness of $Zn_{25}Al_3Cu/Al_2O_3$ particulate composites increases with increase of amount of reinforcing particles. $Zn_{25}Al_3Cu$ alloy (as-cast) exhibit higher compressive yield strength with respect to $Zn_{25}Al_3Cu/Al_2O_3$ composites at room temperature.	11

24	ZA27	-	Al and Cu elements are homogeneously distributed in the matrix of squeeze cast ZA27 alloy. Hardness, tensile strength and ductility of ZA27 was greatly affected by applying pressure.	98

2.1.2 On fracture toughness of particulate filled metal alloy composites

Fracture used very widely property of materials due to which different structural failures occur in different applications. When such failure occurs, they were unexpected, sudden, and unfortunate, and it was obvious for us to give attention on that failure, to find the way of minimizing them. The study about the crack behavior, prevention and analysis of fracture of materials was known as fracture mechanics [20].

Advanced near term high-temperature composite materials are the essential key to the successful development of the next generation of aerospace structures, propulsion and power generation system [99]. The fracture toughness measures the resistance of a material to the propagation of a crack. A growing interest and ever increasing need for improving fuel economy, reducing vehicle emission, increasing styling options, improving overall performance, while concurrently maintaining safety, quality, reliability and even ensuring profitability, considered as few of the challenges that should be addressed by materials used in a spectrum of applications in both the aerospace and ground transportation systems. These requirements led to the development and emergence of the new metallic materials, namely, metal matrix composites (MMCs) [100].

Tjong and Ma [101] studied Al-Cu alloy composite reinforced with SiC, TiB_2 and Al_2O_3 particles and concluded that the creep resistance behaviour of Al-Cu composites were higher than the Aluminium composites this is attributed to dispersion strengthening of Al_2Cu precipitates. Similarly, a study has been made to understand the role of composite microstructure of failure through the mechanism governing the quasi-static and cyclic fracture behavior of different metal alloy composites by Srivatsan et al. [99, 100, 102, and 103]. Jhu et al. [104] found that the creep resistances of TiCp/Ti-6Al-4V composites were higher than the matrix alloy due to the incorporation of TiC particulates which decreases the creep rate. Similarly, Oh, and Han [105] explained that with the increased in particle volume fraction the fracture toughness increases as TiC particle was effective to reduce the void formation

and coalescence because of low aspect ratio. Whereas, short-fiber/particle hybrid composites can provide better control of damage tolerance properties over conventional discontinuously reinforced composites. The fracture mechanism for two different composites (Cu/Al_2O_3 and Al/Al_2O_3) and metal–matrix composite (Al/SiC) was investigated by Agrawal and Sun [106] and they found different fracture mechanisms for different composites. The crack propagation was found in the Cu phase and at the interface when a high tensile stress was found in Cu phase and at Cu-Al_2O_3 through three points bending test, whereas, for Al/Al_2O_3 composite the crack propagation was found inside the ceramic phase only. Park et al. [107] compared the fatigue life of composites processed by two routes firstly from liquid metallurgy route and secondly by powder metallurgy route and finally concluded that the composites processed in powder metallurgy route show enhanced fatigue life with no significant change in fatigue strength by increasing the volume fraction of reinforcement. Mukherjee et al. [108] were studied the effect of residual fracture behavior stresses on the interface of metal-matrix composites. They used the j integral method for finding the strain-energy release rates for cracks along bimaterial interfaces in the presence of friction. Hua et al. [109] compared the flexural and fracture behavior of the composites and concluded that flexural strength and fracture toughness of SiCw/SiC composites are higher than that of SiCp/SiC. Similarly, Reddy and Zitoun [110] found that the mechanical properties such as yield strength, flexural strength decreases with the increased in volume fraction beyond 20%, which was due to the reason that the matrix did not have enough internal ductility and could not overcome the internal stresses and clustering of particles. A study about the fracture that was based on numerical analysis for SiC fiber reinforced titanium composites studied by Rajesh et al. [111] and they reported graceful failure in their study when the composite materials become failed after initial debonding of atoms under applied stress. As different numerical studies were also being done by many researchers for fracture toughness of metal alloy composites. Kolednik and Unterweger [112] found that cracks were initiated by particle fracture and also by the matrix/particle de-cohesion effect, whereas the crack tip opening displacement (COD) were found along with the matrix material. As COD matrix depends on the particle fracture strain and the local deformation pattern, i.e. to which degree the plastic deformation was confined to the region in front of the crack. Similarly, crack tip damage development and crack growth resistance in particulate reinforced metal matrix composites (Aluminium

359/20%Vr SiC and aluminium 6061/20%Vf Micral) reported by Leggoe et al. [113]. Finally, they concluded that under plane strain conditions, both composite materials have decreased the crack growth resistance due to the effect of 'anti –shielding' on damage accumulated near the crack tip in the effective process zone. Oezdemir et al. [114] reported that with the increased in SiC particles the ultimate tensile strength, yield strength increases, but the ductility decreases, whereas, in forging the UTS, YS also increased but there was a significant improvement in ductility of the composites. Mazen and Ahmed [115] found that the composites manufactured via hot pressing followed by hot extrusion shows improved elongation to fracture that indicates good ductility as compared to MMCs manufactured by other techniques and the strength of the composite were function of volume reinforcement as the reinforcement increases the strength decreases because under tensile loading voids opened by de-cohesion between matrix and reinforcement. Pandey et al. [116] studied the deformation and fracture of particle-reinforced alloy composites and observed that the damage modes in the composites were due to particle fracture, interface de-bonding and matrix rupture respectively. However, in over aged condition the interface de-bonding dominates and also the toughness has strong inverse dependences and good positive correlation to work hardening. Ochaiai et al. [117] were studied about the residual stresses in YAG (Yttrium aluminium garnet) composites phase of the melt growth of Al_2O_3/YAG eutectic composite at room temperature by using the indentation test for fracture and also finite element stress analysis (FEA) method. They found from their investigation that the fracture toughness of YAG in the composites was higher than that of the bare YAG taken out from the composite. Azrami [118] investigated the creep properties of nickel aluminide composite material, reinforced with SiC particles and reported that from microstructure characterization the porosity increases with the increased in volume fraction of the SiC particle and strain rate was lowered compared to the unreinforced alloy. The microstructure and fracture toughness properties of Mg–Al–Zn–Si_3N_4 composites were studied by Wang et al. [119]. They found that with the increased in volume fraction of reinforcement up to >6%, the amount of fracture toughness was decreased initially very slow but after that it shows the drastic decrement. Poza and Llorca [120] studied the effect of 8090 Al alloy that was reinforced with SiC particles. They used 15 vol. % SiC particles in the composites and found that the monolithic alloy was failing due to the presence of transgranular shear effect with the slip bands during the monotonic deformation condition, whereas, the

fracture was not affected by these problems during cyclic deformation. Konopka et al. [121] studied the effect of metal particles on the fracture toughness of ceramic matrix composites, and they concluded that the fracture toughness was totally controlled by the volume fraction of the metallic phase and size of metal particles. They also found that if there was no proper distribution of particles in composites, the influence of crack propagation may occur. Similarly, Mica flakes were used as reinforcement in a composite that came from the source of micro cracks and showed the good command for controlling ductility of the composite material [122]. Singh and Prasad [123] studied the tensile and fracture behavior of metal matrix composites and reported that there was decreased in tensile strength of the composite due to the loss of Mg during the fabrication of composite in stir casting method. Reddy and Zitoun [124] compared the mechanical property of different Al alloys for matrix materials and summarized that the alloying elements played a major role in improving the mechanical properties of the metal matrix composites. The simulation was also an important factor in the study of fracture behavior of different metal alloy composites. Kim et al. [125] studied about the simulation of fracture behavior in particle dispersed ceramic composites that reinforced with SiCp and Al_2O_3 particulates and found that with the decreased of volume fraction, fracture toughness will also decrease. Similarly, observation of fracture toughness by using finite element method was viewed by Pendola et al. [126], Gastaldi et al. [127], Pires et al. [128], Ural et al. [129] and Warner and Molinari [130] in their studies. However, to examine the enhancing damage tolerance of conventional discontinuously reinforced aluminium composites, the dynamic crack propagation characteristics of the composites were strongly dependent on the volume fraction; yield stress, the arrangement of ductile phases of reinforcement with to the notch and the impact velocity employed in a particular experiment [131]. Table 2.2 shows the fracture toughness properties of particulate filled alloy composites.

Table 2.2 Fracture toughness properties of particulate filled metal alloy composites

Sl.No.	Material	Fracture toughness properties	Applications	Ref.
1	Ti_6Al_4V /TiB alloy	High-cycle fatigue fracture revealed similar morphology at the ambient and elevated temperatures. The fracture surface was microscopically rough and revealed features reminiscent of classic ductile	Aerospace structural, propulsion and power generation systems.	99

		failure. The fracture surface comprised of microscopic cracks, tear ridges, shallow dimples and voids of varying size.		
2	Ti_6Al_4V/SCS-0 SiC and Ti-6Al-4V/SCS-6 SiC **(**Silicon carbide fiber (SCS-6) reinforced-reaction-formed silicon carbide matrix composites**)**	The SCS-0 interface has a much higher fracture strength than the SCS-6 interface, although both these interfaces exhibit similar apparent debonding stresses.	To find out interfacial properties and their influence on the properties of MMCs	132
3	Mg–Al–Zn–Si_3N_4 composites	Mg–Al–Zn–6%Si_3N_4 composites had an improvement of fracture toughness owing to relatively homogeneous Si_3N_4 particle distribution encircled by metal matrix, the occurrence of interface reaction product as $MgAlO_2$ spinel phase. With the increases of volume fraction of reinforcement (>6%), the bending strength and fracture toughness decreases slowly at initial stages and then decreases rapidly at the end.	Automotive, highway, aerospace and electronics industries	119
4	2009 aluminum alloy reinforced with SiC particulates	The intrinsic brittleness of the reinforcing SiC particulates coupled with the propensity for it to fracture due to localized inhomogeneous deformation and local stress concentration results in particulate cracking and interfacial failure through	Aircraft structures, gas turbine engines, automobiles, electronics, spacecraft and even	133

		debonding being the dominant damage modes.	recreational goods	
5	Al 2080 reinforced with SiC particulates	Fracture of the matrix between the dispersed particulates and particulate clusters coupled with particle cracking and decohesion at the interface, allows the microscopic cracks to grow rapidly and coalesce by fracture through ductile metal matrix resulting in macroscopic failure and low tensile ductility.	Automotive and selected aerospace products	100
6	SiC fiber (SCS-6) reinforced titanium (Ti-15V-3Cr-3Al-3Sn) composite	The composite retains sufficient load bearing capability upon initial debonding to allow a graceful failure. The residual stresses due to the coefficient of thermal expansion (CTE) mismatches between the fiber and the matrix with single or multilayered interphases were also compared with the help of axisymmetric analysis of the composite.	For high-performance structural materials because of their high strength and stiffness	111
7	Fiber reinforced cementitious composites (FRCC)	Assuming that stronger matrix will result in stronger material may be proved wrong in the case of FRCC. The weakening of the matrix allows easier development of concurrent cracks, and consequently, more energy consumption. The results presented here show that the weakening of the matrix resulted in certain cases, even a little increase in the peak-load value, as well as considerably higher fracture energy and ductility. In the case of FRCC. The weakening of the matrix allows easier development of concurrent	In concrete technology	122

		cracks, and consequently, more energy consumption. The results presented here show that the weakening of the matrix resulted in certain cases, even a little increase in the peak-load value, as well as considerably higher fracture energy and ductility.		
8	Alumina matrix composites with molybdenum particles	The change of the fracture toughness of a ceramic–metal composite can be controlled by the volume fraction of the metallic phase and size of metal particles. It was also evident, that the metal particle distribution in the matrix will influence the crack propagation. Given a defined volume fraction of metal particles in the matrix and size of these particles, a different level of uniformity of their distribution will result in a different number of metal particles encountered by the propagating crack.	For advantageous properties like Hardness, Rigidity, Abrasive Toughness and low Density.	121
9	7093/SiC/15p composite,	The dynamic crack propagation characteristics of the composites observed to be strongly dependent on the volume fraction of the ductile phase reinforcement in the composite, the yield stress of the ductile phase reinforcement, the arrangement of the ductile phase reinforcements with respect to the notch, and the impact velocity employed in a particular experiment.	Structural applications. And to increase high specific stiffness, high specific strength, high thermal conductivity, good oxidation and wear resistance,	131
10	Cu/Al_2O_3 and Al/Al_2O_3	From three point bend test it was found that high tensile stresses in Cu phase, and at the	For better toughness and structural	106

	and a composite Al/SiC	Cu-Al_2O_3 interfaces lead to crack propagation inside Cu phase and at the interface. Whereas, for Al/Al_2O_3 composite the crack propagated inside the ceramic phase. In contrast, the fracture characteristics of metal–matrix composite (Al/SiC composite) were dominated by the metal matrix.	integrity	
11	Fiber/matrix interface	It found that crack initiation switches from the support to the loading end with the reduction in residual stresses with increase in plastic strain. Evaluation of strain-energy release rates through the use of J integral for cracks along bimaterial interfaces in the presence of friction was still a 'mathematical problem' and care needs to be exercised in the interpretation of the numerical predictions.	Advanced propulsion systems of twenty-first century aircraft,	108
12	2014 aluminum alloy reinforced with Al_2O_3 particulates	With an increase in Al_2O_3 reinforcement content fracture of the composite was dominated by particulate cracking and decohesion at the particulate matrix interface.The events leading to void growth and eventual coalescence were rapid following the initiation of micro cracks, through cracked particles, decohesion at the interface and voids.	Structural applications	102
13	Al/Al_2O_3 multilayered composites.	Measurements of elastic and plastic strain distributions around cracks in ductile/brittle multilayer's were made with high- resolution by moiré interferometry and compared	Electronics industry such as in thermistors, electronic packaging applications,	134

		with the predictions of numerical models. The models are then applied to a stochastic analysis of the mode of fracture of multilayer's with variable layer thickness ratios. Key micro structural parameters that were shown to be important include the parameters describing the distribution of flaws in the brittle layers, the yield stress of the metal and the relative layer thicknesses.	structural applications such as in armour	
14	Aluminum alloy 7034 reinforced with SiC particulates	For a given volume fraction of the SiC particle reinforcing phase in the 7034 aluminum alloy metal-matrix, aging condition and load ratio, and fracture morphology was observed to be essentially similar at the different values of maximum stress. With a decrease in load ratio microscopic fracture events of the composite was dominated by failure of the reinforcing SiC particle both by cracking and decohesion at the particle–metal-matrix interfaces.	Military and space applications, automotive, aerospace products and even recreational goods	103
15	Aluminum 359/20%Vr SiC and Aluminum 6061/20%V f Micral	Under plane strain conditions, both materials were found to exhibit decreasing crack growth resistance as a crack extension proceeded, due to the 'anti –shielding' effect of damage accumulated in the process zone ahead of the crack tip.	Structural applications	113
16	Al_2O_3/YAG (Yttrium aluminum garnet) composites	The fracture toughness of YAG in the composite was higher than that of the bare YAG taken out from the composite. From the difference	To improve thermal efficiency in jet aircraft engines and high efficiency power	117

		in fracture toughness value, the residual stress of YAG in the composite was estimated to be around −170±100 and −220±130MPa. The residual stresses of YAG, estimated by the indentation fracture test, were in the ranges of around −400 to 0MPa and around −500 to 0MPa.	generation gas turbines.	
17	Fiber-reinforced composites	The mechanical response of the beams in three-point bending was computed using the finite element method, and the simulation results were in good agreement with the experimental data at both the microscopic and the macroscopic level, demonstrating the potential of this approach to simulate the fracture behavior of complex, heterogeneous materials. Finally, further applications of these multiscale applications are briefly noted.	Composite beam	135
18	Probabilistic methodology for nonlinear fracture analysis	The results show that the methodology (probabilistic methodology for nonlinear fracture analysis in order to get decisive help for the reparation and functioning optimally of general cracked structures) were able to give an accurate probabilistic characterization of the *J*-integral in elastic–plastic fracture mechanics without obviously time consuming. By introducing an "analysis re-using" technique, we show how the response surface method becomes cost attractive in the case of incremental finite element	For structural analysis and design	126

		analysis.		
19	A finite element study	The simulation results showed that bone's resistance against the propagation of a crack decreased sharply with increase in strain rates up to 1 s^{-1} and attained an almost constant value for strain rates larger than 1 s^{-1}. On the other hand, initiation fracture toughness exhibited a more gradual decrease throughout the strain rates. There was a significant positive correlation between the experimentally measured number of micro cracks and the fracture toughness found in the simulations. Also the amount of porosity did not affect the way initiation fracture toughness decreased with increasing strain rates, whereas it exacerbated the same strain rate effect when propagation fracture toughness was considered.	Human cortical bone	129
20	Alumina/Zirconia composites and ceramic coatings	An explicit approach has been adopted to detect the fracture onset at the grain boundary. This implies that the stress-free condition activated at a time step subsequent to the one in which the fracture criterion checked. The computational approach presented in this paper has shown the ability to determine the fracture pattern of brittle materials with grain microstructure and its evolution during loading.	The coating industry	127
21	Finitely deforming ductile	The effect of micro-crack closure, which may dramatically decrease the rate	In manufacturing industry such as bulk and sheet	128

	materials	of damage growth under compression, was incorporated and its computational implementation discussed. A simple technique to permit the use of simplex elements under finite strain near-incompressibility has been introduced in the context of transient explicit dynamic analysis. The method based on the enforcement of the volumetric constraint over patches of simplex elements. Hence, an error estimator based on the damage dissipation, which accounts for crack closure effects, has been proposed for use within an adaptive mesh refinement strategy.	forming, Cutting operations, like machining, slitting, guillotining etc.	
22	A numerical model	The proposed model procedure reaches a balance between accuracy and simplicity, and provides a helpful tool in predicting the fracture of large masonry structural elements when a single macro-crack, or finite number of them, was the main failure mechanism. The presented model does not include distributed cracking or damage to the structure and applies in the case of a macro-crack occurring, but this approximation can be relaxed if necessary. For engineering purposes, the averaging of the masonry properties provides sufficiently precise data for cohesive modeling. For small masonry elements, a more detailed analysis of fracture micro-mechanisms, especially	Brickwork masonry	136

		interface brick-mortar interaction, was required.		
23	8090 Al alloy reinforced with SiCp	The dispersion of the SiC particles restrained the formation of elongated grains during extrusion and inhibited the precipitation of Al_3Li. The unreinforced alloy failed by transgranular shear along the slip bands during monotonic deformation, whereas fracture was initiated by grain boundary delamination, promoted by the stress concentrations induced by the slip bands, during cyclic deformation. The fracture of the composite was precipitated by the progressive fracture of the SiC reinforcements during monotonic and cyclic deformation.	For improving the specific stiffness or strength.	120
24	Alumina ceramic	Fracture toughness was shown to be a strong function of micro crack coalescence, which points to grain boundary engineering as a promising direction for future research. Finally, the model suggested that the length of the longest micro crack cluster or the variance of micro crack length in a material could provide a criterion that, in association with nondestructive testing, may be useful for predicting impending catastrophic failure.	Demanding industrial applications	130
25	Al metal matrix composites reinforced with SiC short fibers and Al_2O_3p	In the SiC matrix composites dispersed with Al_2O_3 particles, the crack barely impinges on the particles .The related fracture resistance with crack extension decreases below the value of the matrix toughness	For crack propagation behavior	125

		due to the residual tensile stress in the radial direction. The estimated relative fracture toughness of the composite also decreases with the volume fraction of particles. Similarly when Al_2O_3 matrix dispersed with SiCp then the related fracture resistance shows pulse-like increases up to about 5 times the value of the matrix toughness when the crack propagates along interfaces, and an increasing R-curve behavior with crack extension predicted.		

2.1.3 On Thermo-mechanical properties of particulate filled metal alloy composites:

A material produces different chemical changes at a steady rate during heating, such as oxidation and degradation, and physical changes, the glass transition in polymers, conversions/inversions in ceramics and phase changes in metals. Thermal analysis was used to finding the X-ray diffraction analysis, optical and electron microscopy for the development of new materials and in production control. Sometimes it was also used to define the temperature and energy change that was associated with a structural change, and rest of the times it used qualitatively to provide a characteristic 'fingerprint' trace of a particular material. The various techniques of thermal analysis which are used to measure one or more physical properties of any material worked as a function of temperature [137].

The thermal properties of any material play an important role now-a-days. It was found at any part, at any time of material, but at some temperature which should be different from the fabrication temperature or if it was expected to perform some heat transfer function. The thermal property was used in many applications such as: heat sealing heads, heat exchangers, heat sinks, etc. Similarly the thermal expansion property plays an important role for dissimilar materials when they heated.

From the damping capacity, mechanical vibration can be converted into thermal energy; this was studied in Shastry et al. [16] research paper. They studied the

damping behaviour of aluminite particles that reinforced with ZA-27 alloy metal matrix composites .In their paper they found the value of damping capacity was increased with respect to increasing temperature whereas the value of dynamic modulus was decreased. The CTE (the coefficient of thermal expansion) become mismatch with the induced damping behaviour of metal alloy composites at a lower temperature. And for higher temperature the damping capacity shows the interface between the matrix-reinforcement and thermo elastic damping. Ren et al. [138] found that the addition of Si and Mg up to 6 and 4% resulted in poor thermo-physical properties due to higher porosity in the composites resulting from poor wettability between Al and Si. However, an increased in Si the elastic modulus, thermal dimensional stability and thermal conductivity of the composites increases and reduced the CTE. Huber et al. [139] reviewed on thermal expansion of Al matrix reinforced with different SiC particulates founds that CTE decreases with increase in reinforcement particles which is the result of thermal expansion of Al-Si matrix material. Similarly, Ren et al. [138] reported that for the lower content of Si and Mg the composites show poor thermo-physical properties because of higher porosity in composites. However, with the increase in Si content in Al enhances the elastic modulus, thermal dimensional stability and thermal conductivity of the composites and reduces the CTE of composites. The particle size of composite material plays an important role for finding the different properties. Study about the effect of SiCp/Al particle size on thermal expansion behaviour was studied by the Yan and Geng [140]. They used three different particle sizes of SiC i.e. 5, 20 and 56 μm for making composites. And found the CTE (coefficient of thermal expansion) of the composites totally dependent on the size of particles like the larger particle size composite (56 μm of SiC) have a larger value of CTEs. Zhang et al. [141] reported that the thermal conductivity of SiCp/Cu composites were low because of the lower low thermal conductivity of the matrix. The particle size plays an important role to find out the different properties for composites. The increment in the particle size improved the thermal expansion of composites, was found by Elomari et al. [142]. In their research work, They found the when 56 wt.-% of oxidized SiC particles mixed with aluminium matrix composites the value of CTE (co-efficient of thermal expansion) was decreased from25.2x 10^{-6} °C^{-1} to 12x 10^{-6} °C^{-1} .

Yue et al. [143] concluded that $ZnAl_2O_4$ coating increases the tensile properties of the composites and at higher temperature thermal stability of the

composites were improved. Ke et al. [144] reviewed the effect of particle size on the microstructure and thermal conductivity of Al/diamond composites prepared by spark plasma sintering and reported that larger size particles of diamond enhances the thermal conductivity of the composites this due to powerful interfacial bonding between diamond particle and Al matrix that was powerful than the toughness of Al matrix. Karthikeyan et al. [145] studied the CTE of composites and alloy that the composites exhibit lowers co-efficient of thermal expansion then the alloy materials. Similar results were also reported by Wang et al. [146] in which the wood-template based C/Al composites have lower CTE then Al alloy, which was because of the presence of porous carbon. Wu et al. [147] found that the addition of potassium whisker in composites have positive effect in improving the hardness of the composites but the ultimate tensile strength reduces due to the formation of a very thin interfacial layer between whisker and the matrix whereas the tensile strength has the positive effect with the formation of interfacial layer. Delannay et al. [148] found that the incorporation of long ductile fiber in place of ceramic fiber can significantly improve the fracture toughness and ductility of the composites and the thermal expansion for the ZA-8/aligned mild steel fibers was low compared to other ZA-8/Saffil, ZA-8/C and ZA-8/316L composites. Khalifa and Mahmoud [149] found that the tensile strength at room temperature with 10%SiCp increases the strength but reduces the ductility, both as cast and extruded composites exhibit high creep resistance than the alloy and at the elevated temperature results indicate that addition of SiCp decreases the strength as compared to matrix alloy but the extruded composites exhibit same pattern but slightly higher values of strength. Chawla et al. [150] studied about the thermal expansion behaviour for SiC reinforced 2080 Aluminum alloy composites and found the value of CTE was found lower for longitudinal orientation and higher for the short transverse direction. That means the value of CTEs is totally dependent on the orientation of SiC particles including extrusion axis in composites.

The presence of vibration suppression property in aerospace industry, semiconductors and automotive industries (passive damping) used as a critically important material property. This property's ultimate goal was to produce materials with high damping. Metals are chosen for such applications since they possess many mechanisms that contribute to the total damping e.g. point defect relaxation, dislocation motion, grain boundary sliding, inclusion-matrix friction, magneto elastic

effects and elasto-thermodynamic effects. To find out the damping capacities for the composites Wu et al. [151] used magnesium matrix that was reinforced by different volume fractions of graphite particles and fabricated by stir casting method. From their study, they found that with the increasing volume fraction from 0-10wt.-%, damping also increases and when volume fraction increases after 10 wt.-% damping almost keeps constant. Shastry et al. [152] observed that the damping property of MMCs depends on the weight percentage of the reinforcement and increases with increase in weight percentage of reinforcement, due to dislocation generation and motion as a result of plastic deformation at metal / reinforcement interface. Similarly Shastry et al. [152] studied about the thermal stresses on the thermal expansion and damping behavior for ZA-27 alloy metal matrix composites in his other research paper. Zhang et al. [153] was used SiC,that was reinforced with 1040 aluminium alloy composites to find out the internal friction and damping behaviour of the composites. They found the internal friction of Al/SiCp MMC was increased due to thermal cycling, and also the increment in dislocation during thermal cycling handles increasing damping capacity. The damping characteristics for carbon nano tube (CNT) studied by Deng et al. [154] in their research report. For find out the damping behaviour of composites they used different frequency at a different temperature from 25-400° C. From that they report that for high damping capacities, at an elevated temperature, CNT was a promising metal matrix without sacrificing the mechanical as well as stiffness properties. Similarly another investigation for damping behaviour studied by Girish et al. [32], for ZA-27 alloy composites that reinforced with graphite particles. They used compo casting method to prepare composite and with the use of dynamic mechanical analyzer evaluate damping properties. They report with respect to increasing temperature, the damping capacity of composite increases with increasing volume fraction of graphite particulates. Similarly same observation about the damping properties was found by Jian Ning et al. [155].

The thermal behaviour of ZA-27 alloy, reinforced with SiC, ZrO_2 or C was studied by El-khair et al. [156]. They found with increasing temperature the CTEs also increases for both ZA-alloy and composites, and also the drastic reduction of CTEs was found when adding the particles in composites as compared to unreinforced ZA-alloy. Jiejun et al. [157] reported that composites foams have better damping and sound absorption properties as compared to Al foams because of the presence of large amount of SiCp particles that interfaced with Al/SiCp great amount in the composite

foam which positively affects the vibration energy. Schaller [158] reported that metal matrix composites with long carbon or SiC are the smart choice for damping because these composites showed a high elastic modulus with Mg matrix. One of most important factors affecting the mechanical properties of MMCs is the heat treatment. Chaudhury et al. [159] studied the thermo-mechanical properties of $Al_2Mg_{11}TiO_2$ (rutile) composite. They were reported the preparation of composites was good. Pandey et al. [116] investigated the effect of aging conditions on mechanical properties of the PM-MMC Al7093-15%SiC. The yield strength increased with increasing aging time up to the peak-aged condition; further increase of aging time led to a slight decrease of the yield strength. The fracture strain and the strain hardening coefficient showed an opposite dependency on the aging time. A good correlation between the fracture strain and the strain hardening coefficient was found. As surface fracture inspection revealed the dominance of particle fracture for the solution annealed, under-aged, peak-aged and slightly over-aged conditions of the matrix, whereas interface debonding dominated in the highly over-aged condition. Suliaman et al. [160] found that the addition of SiO_2 to the matrix decreases the split tensile strength and modulus of elasticity due to increases in SiO_2 would create more sites for crack initiation and hence lower down the load bearing capacity of the composite but the increase in addition of quartz particles decreases the tensile strength because of the particle pull-out from the matrix due to the lack of bonding. Wu et al. [161] studied the damping capacity of Mg matrix composites and concluded that the damping increases as increased in volume fraction with a temperature range from room temperature to 125^0C and have no effect from 125-250^0C after that damping rapidly increases with increase in temperature from 250^0C-400^0C. Similarly, Shastry et al. [16] studied the damping behaviour alloy composites increases with the temperature and dynamic modulus found to decrease with the increase in temperature but at a lower temperature range the damping capacity changes may be because of CTE mismatch induced dislocations and at high temperature due to matrix-reinforcement interface. Different numerical studies were found for the damping capacity of composite materials. Yadollahpour et al. [162] studied in their study about the micro mechanical modelling approach for particulate filled composite materials, and they found by using Granato Lucke theory for damping capacity they observed the good agreement result.

Lu et al. [163] investigated the effect of cold rolling on a dynamic mechanical response of alloy composites and found that the damping capacities of the composites were dependent on volume fraction and the interfacial bond between particulate and matrix. Gu et al. [164] found that capacity at low temperature for pure Mg excels the composites at a temperature of 75^0C. The damping capacity of uncoated composites exceeds the pure Mg and at temperature 250^0C, superior damping capacity was shown by coated composites then the pure Mg. Similarly, they described the damping capacity for hybrid metal matrix composites in their second paper. They reported that the Mg matrix composite shows the lower damping capacity as compared to pure Mg. Zhang et al. [149] studied the effect of SiC and Graphite particles on the damping behavior of 6061Al metal matrix composites fabricated by Spray deposition method separately that the damping capacity of 6061 Al can be improved significantly by the addition of either SiC or graphite particles. Zhang et al. [165] studied the damping behavior of particulate reinforced 2519Al metal matrix composites in which the particulates are Al_2O_3, SiC and graphite. All the composites were fabricated by spray deposition method and concluded that the spray processed composites have exhibited significant damping gain. Cao et al. [166] studied the damping capacities of TiC reinforced magnesium matrix composites that the damping capacity increases with the increase in reinforcement volume percentage that was due to dislocation damping at room temperature and higher temperature due to interface damping. Mitra and Mahajan [167], Lavernia et al. [168], and Zhang et al. [169] studied the damping and interface of metal matrix composites that the damping behavior of metal matrix composites can be related to thermal mismatch-induced dislocation, interface damping, interaction damping behaviour. The enhanced dislocation damping due to thermal mismatch between reinforcement and matrix which increases the energy dissipation sources and the sliding of the interface between matrix and reinforcement dissipates energy under cyclic loading. The interaction between reinforcement and dislocations may be lead to changes in damping response and also the intrinsic damping of the reinforcement may be independent that of the matrix material. To control the vibration in many applications damping behaviour of materials plays an important role.

Rao et al. [170] investigate the thermal conductivity and thermal contact conductance properties for Al_2O_3/Al-AIN metal matrix composites for making heat sink for different electronic devices. And they found that the experimental results

were in good agreement as compared with theoretical models. Similarly, Chan and Liang [171] were also studied about thermal expansion and the bending angle for Al2024/15SiCp and Al2024/20SiCpmetal alloy composites. In their study they found for 15 wt.-% reinforcement composites, the larger bending angle was obtained. So with the lower amount of reinforcement, a high value of bending angle and low value of CTE (Coefficient of thermal expansion) was found. The damping properties for Mg-Cu based alloy were studied by Qing et al. [172]. By using the dynamic mechanical analyzer they reported that Mg-Cu alloys shows good damping capacities, but Cu have a significant effect on damping behavior individually. The increasing content of Cu decreases the damping capacities. Lu et al. [173] reviewed the various methods and proposed a new design method for processing high damping MMCs. The particles filled alloy possesses high strength, high damping, good mechanical property and flexibility. The existing materials still cannot meet the demands and design of available damping materials and Zhang et al. [174] reviewed the effect of secondary phases on damping behavior of metal, alloy and metal matrix composites and concluded that the rule of mixtures provides an approximate tool to estimate the overall damping capacity of the MMCs. Table 2.3 shows the **t**hermo-mechanical properties for particulate filled metal alloy composites

Table 2.3 Thermo-mechanical properties for particulate filled metal alloy composites

Sl. No.	Material	Thermo-mechanical properties	Applications	Ref.
1	Al alloys, Al-Cu alloys, Al-Si alloys, Al-Ag alloys, other Al alloys	The Kohen interface theory was more generally applicable to damping at elevated temperature where damping was intimately coupled to diffusion process.	In automobiles for mechanical vibrations	141
2	TiC reinforced magnesium matrix composite	The damping capacity of the magnesium alloy increased with the increase of reinforcement percentage. Improved damping capacities of composites can be attributed to dislocation damping mechanism at room temperature. At elevated temperatures, interface damping becomes a new contributor to the increase of damping	Vibration suppression, noise control and instrument stability enhancement in automotive industry, architectural industry and aerospace	138

		capacity.		
3	Mg-Cu based alloys	The as-cast hypoeutectic Mg-Cu binary alloys exhibit ultra-high damping capacities, while the eutectic Mg-Cu alloy exhibits low damping capacity. The more the content of Cu, the lower the damping capacities, which is due to the decrease of the α-Mg dendrite size and increase of volume fraction of eutectic phase.	In various fields of industry to vibration control	172
4	Magnesium matrix composites reinforced by graphite particles	The strain amplitude independent damping increases significantly as the graphite particle volume fraction increases from 0 to 10%, but almost keeps constant when the volume fraction exceeds 10%. Two damping peaks were found at 150 and 350°C, respectively.	In industry and transportation to noise control and instrument performance enhancement	161
5	Al 6061 with SiC and Gr Particulates	The damping capacity of 6061 Al could be significantly improved by the addition of SiC or Gr particulates through spray deposition processing.	To eliminate the need of special energy absorbers or dampers to attenuate undesirable noise and mechanical vibration	136
6	2519 Al alloy (Al-Cu-Mg-Mn) with SiC,Al_2O_3,Gr particulates	In the 30-250°C range, 2519 Al/Gr MMC shows a damping capacity that was two times higher than those of 2519 Al/SiC and Al/Al_2O_3 MMCs. In addition, the damping mechanism in 2519 Al/Gr MMCs was also attributed to high intrinsic damping of the graphite particulates.	To eliminate the need for special energy absorbers or dampers	137
7	ZA-27 with aluminite	The addition of aluminite particulate to the ZA-27 alloy	Good strength at high	16

	particulate	was found to provide a higher damping capacity and a greater dynamic modulus. The temperature dependence study of damping for all the samples showed an increase in damping capacity with increase in temperature accompanied by a decrease in dynamic modulus.	temperatures, good structural rigidity, dimensional stability, and lightness.	
8	14vol.%3.5μmSiCp:2024 Al and 18vol.%3.5μm SiCp:2048 Al	In the cold-rolled 14 vol.% SiCp:2024 Al composite, no apparent change of elastic modulus and damping capacity were observed, but in the 18 vol.% SiCp:2024 Al composite, as rolling reduction was increased from 0 to 20%, the elastic modulus decreased from 88 to 79 GPa and the damping capacity increased from 0.13 to 0.20.	Various demanding areas	134
9	Al/SiC/SiO_2	The effect of particle size was quite evident in the composites produced here: the larger the particles, the greater the thermal expansion of the composite. The observed behavior of these composites was discussed in terms of particle size, silica layer formed during oxidation, and thermal stresses developed as a result of the CTE mismatch between the reinforcement and the matrix.	Structural design, mechanical systems and electronic Packaging.	142
10	Magnesium matrix reinforced with Cu-coated and uncoated SiC particulates	The dynamic modulus of the coated SiC particulate reinforced composite improved strongly compared with that of the uncoated one, and that, the dynamic modulus of both uncoated and coated composites exceed that of pure Mg obviously. At low temperature, pure Mg exhibits the higher	To control of noise and the enhancement of vehicle and instrument stability.	135

		damping than the composites owing to its high intrinsic damping capacity; while at elevated temperature, the damping of both uncoated and coated composites will exceed that of pure Mg due to the contribution of interface damping.		
11	2080 aluminum with SiCp	The measured CTE of the Al/SiCp composites was anisotropic. The composite in the longitudinal orientation had the lowest CTE while the short transverse direction had the highest CTE. This was directly related to the orientation of the SiC particles along the extrusion axis in the composites. FEM simulations based on the microstructure of the composite showed that the state of internal stress determines the anisotropy of thermal behavior.	Electronic packaging	150
12	(SiCp+Al_2O_3·SiO_2f)/Mg hybrid metal matrix composite	The damping capacity of the Mg matrix composites was much lower than that of pure Mg. Dislocation damping and interface damping were the main damping mechanisms in Mg and its composites	Exhibiting good Mechanical properties and high damping.	175
13	1040 Al/SiCp	Thermal cycling causes the increase in internal friction of Al/SiCp MMC. The activation energy of samples after different cycles was calculated, yielding 1.02 eV and 1.09 eV for 50 and 500 cycles, respectively. Increase in dislocation during thermal cycling was responsible for the increase in peak temperature and activation energy.	Reduction in thermal stresses	153

14	2024Al reinforced with A multi-walled carbon nanotube (CNT)	The damping capacity of the composite with frequency of 0.5 Hz reaches 975×10−3, and the storage modulus was 82.3 GPa when the temperature is 400 °C, which shows that CNT was a promising reinforcement for metal matrix to obtain high damping capacities at an elevated temperature without sacrificing the mechanical strength and stiffness of the metal matrix.	Aerospace, mechanical, and civil systems	154
15	SiCp/Al	The composite containing small particle shows lower CTEs and lower increasing rate with temperature. The relative higher residual thermal stresses, generated within the composite containing the smaller particles, associated with high strain gradient, should be responsible for the observed difference in CTEs of the investigated composites under various particle sizes. At low temperature, the experimental CTEs of the composites show substantial deviation from the prediction of the rule of mixture (ROM) and Kerner's model, while the Kerner's model agrees relatively well at high temperature for the composite with the larger particle size.	For low coefficients of thermal expansion and high thermal conductivity.	140
16	ZA-27 alloy reinforced with SiC, ZrO_2 or C.	CTEs of both ZA-27 alloy and the composites increase with increasing temperature. The addition of particles results in a drastic reduction in the CTEs of the resultant composites in comparison to those of the	In critical structural applications (due to their superior mechanical properties such	156

		ZA27alloy. The solidification time of the ZA27–C composite was about 50% shorter than that of the ZA27 alloy, while for ZA27–ZrO_2 and ZA27–SiC composite about 25% longer than that of the ZA27 alloy.	as higher elastic modulus, tensile and fatigue strength, temperature stability and wear resistance in comparison to conventional alloys)	
17	Al–2Mg–11TiO_2	Electrical resistivity measurement showed a phase transformation at 360°C, which was consistent during DSC studies due to the precipitation of $TiAl_3$ phase. As-cast composite was both hot rolled and cold rolled successfully to 50 and 40% reduction, respectively. From fractographic analysis, it was clear that the crack had nucleated at the particle/matrix interface and propagated through the matrix by micro void coalescence.	Automotive and Aerospace	159
18	Zn-Al eutectoid alloy (Zn-Al) with graphite (Gr) particulates	The internal friction (IF), as well as the relative dynamic modulus, was measured at different frequencies over the temperature range of 20 to 400C. The damping capacity of the materials was shown to increase with increasing volume fraction of macroscopic graphite particulates	In structural application (To reduce noise and vibration)	155
19	ZA-27 alloy reinforced with aluminite particulate	Thermal expansion studies showed residual strains and maxima were obtained in the heating and cooling curves of the damping behavior of the	Electronic heat sinks and space structures	121

		composite. The thermal expansion study of thermal stresses leading to plastic deformation in the matrix and residual strain obtained was particularly useful in any application of the composite at elevated temperatures. The thermal stresses have been evaluated in both cases of thermal and damping studies and found to be in good agreement with each other		
20	Al2024/15SiCp and Al2024/20SiCp	A smaller value of CTE and a larger bending angle were found for the composite with lower amount of reinforcement. At high temperature, the Kerner model agrees relatively well With the experimental CTEs.	structural design, automotive and mechanical systems and electronic packaging	171
21	A356/SiCp	The particle reinforced Al matrix composite foams show better damping and sound absorption properties than Al foams due to the foam structure and the existence of large amount of SiC particles and SiC/Al interfaces. The loss factor of the particle reinforced Al matrix composite foam decreases with the increase of density.	aerospace, transportation, construction industries	176
22	ZA-27 alloy with graphite particles	Damping capacity increases with increase in reinforcement of graphite, particularly at ambient temperature. Also damping capacity (tan delta) increases with the increase in temperature for all the cases of graphite reinforcement and	Aerospace, structural and bearing applications	32

		there were no much variations in damping capacity (tan delta) up to 180°C temperatures.		
23	A numerical study	The metal matrix nano composites exhibit higher damping capacity than the unreinforced alloy. The influences of the grain size, boundary phase thickness and reinforcement size on the energy dissipation were calculated by the developed finite element model. Good agreement was observed between the G–L theory results and the data calculated from the finite element model.	To reduce high noise levels, stress fatigue failure, premature wear, operator discomfort, and unsafe operating conditions	162
24	SiCp/Cu composites	Thermal conductivity of SiCp/Cu composites was relatively low, mainly due to the intrinsically low thermal conductivity of the matrix. Elastic modulus was insensitive to alloying elements, while bending strength decreased dramatically when excessive alloying elements dissolved in the matrix	Electronic packaging and thermal management application	177
25	Al_2O_3/Al–AlN	The thermal contact conductance increases, as a function of contact pressure and it was a weak function of mean interface temperature. The theoretical models suggested for metallic contacts can be used for predicting the thermal contact conductance of Al_2O_3/Al–AIN metal matrix composites with reasonably good accuracy.	For thermal management applications	170

2.1.4 On sliding wear and friction behaviour of particulate filled metal alloy composites

Since 1980s various advanced materials were used by different material users for the different applications to fulfil the need of environment protection. The advanced materials were those who have enhanced properties and improved quality. For the development of high-performance vehicle many properties should be there in material like lighter, stronger, stiffer, and more temperature and wear resistant [178]. Wear can be defined as the gradual removal of material from solid surfaces as a result of mechanical action [179]. Due to the addition of reinforcement particles or fibres in the composite materials, sliding wear associated with deformation and dislocation in composite materials as compared to the pure alloy [180]. There were lots of metal alloy composites present in the advanced engineering materials, aluminium matrix composites was one of them, that have been widely used in weight-critical applications like aerospace, and due to its excellent properties i.e. high specific strength and better wear resistance, was recently used in automotive industries [181]. To control the tribological properties (friction and wear) for aluminium composites, done by controlling different factors that can be classified into two categories: one is mechanical and physical factors, and the other was the material factor [182]. Zhou et al. [178] studied aluminium alloy composites reinforced by SiC and Al_2O_3 particulates for finding the effect of different extrusion parameters on wear resistance of the composites by using the powder metallurgy (PM) casting method. They reported that with the addition of ceramic reinforcement with the alloy, wear resistance was increased. An aluminium alloy reinforced with SiC particulates that made by using conventional vortex casting technique was studied by Ramachandra and Radhakrishna [183] in their research study. They used different volume fraction (5%, 10%, and 15%) of SiC particulates to find out the sliding wear properties. They concluded that with the increasing in the amount of reinforcing particles the sliding wear also increases continuously.

The different tribological properties were widely used in the different applications as compared to mechanical properties. Many authors have investigated the friction and wear properties for aluminium alloy composites that influence the following factors as [184]:

- The composite matrix and counter part of material with their hardness.
- The type of reinforcement with its shape, size and volume percentage.

- Different testing conditions (load, speed, temperature, lubrication, environment conditions, etc.)

Different tribological properties of A356 reinforced with Al_2O_3 particulate was studied by Vencl et al. [184]. The use of different metal matrix composites was increasing rapidly day by day in automobile and industrial applications. Mostly used alloy A356 alloy for better tribological properties were studied by many authors. In the Vencle et al. paper they found with the use of pin-on-disc tribometer at different loads, sliding wear of composites found slightly higher comparing to the matrix material. Wu et al. [185] investigated the wear behaviour of Al/Si alloy reinforced with alumina silicate fibre by using squeeze casting process. The reinforcement particles directly affect the wear rate of composites. Ghosh et al. [186] used SiCp reinforced with aluminium alloy (6061 Al) (with from 8 to 37 mm size) for finding out the wear properties, made by plasma sprayed coating method. They investigated that the adhesion strength of composites was decreases with the increasing in SiC content with the decreasing in SiC particle size. Similarly, when the size of SiCp increasing, the abrasive strength of composites increases automatically. Asthana [187] studied the processing effect on different physical and mechanical properties of cast metal matrix composites by using kind of solidification and casting techniques. He found that to establish a rigorous protocol between both fabrication technique and properties of composites, we have to evaluate the composite performance in synergy with fabrication techniques.

Tribological behaviour of self-lubricating Al_2O_3–$20Ag_{20}CaF_2$ composites have been investigated by Jin et al. [188].They investigate in their report that during sliding condition plastic deformation plays an important role in the formation of lubricating film on the sliding surface. Similar, investigation about the wear behaviour of SiC reinforced with Si3N4- and Al_2O_3-matrix composites was reported by Dogan and Hawk [189]. They found that by the addition of SiCp in the aluminium matrix improved the tribological environment of the composites. Zinc base alloy was used in many applications due to its excessive properties like low initial cost; excellent foundry cast ability and fluidity, good mechanical properties as compared to other alloys. Ranganath et al. [30] were used ZA-27 alloy composites reinforced with garnet particles (30-50µm) in their investigation for finding out the sliding wear properties. They observed that by the addition of garnet particles in composites reduces the wear rate than the monolithic alloys. Therefore, with the increasing in garnet particles in

matrix wear rate goes decreases, but when we increased the applied load wear rate of composites also increases. Daoud et al. [190] studied the wear behaviour of Al_2O_3 and C particulates reinforced with Al5Mg alloy composites fabricated by vortex method. They found that there was no prominent effect on wear rate when the amount of C particulate increases. Although when the Al_2O_3 particulates reinforcement exhibited higher wear resistance as compared with monolithic alloy. Furthermore, by the addition of both particulates (C and Al_2O_3) in Al_5Mg matrix alloy did not significantly improve the wear rate of composites. Das [191] discussed the different wear behaviour (such as sliding wear, abrasive wear, erosion-corrosion, etc.) for Al-SiC composites in his research study. In his study, he was made a prototype that used for different industrial applications such as in brake drum, cylinder block, refrax apex insert, etc. and found that the ceramic phase and metallic matrix has good interface bonding when the proper distribution of particulates occurs in the matrix. Also found good wear resistance and seizure pressure properties for both dry and lubricating sliding wear as compared to monolithic alloys. These prototypes show encouraging results. Similarly Dinesh A. et al. [192] investigate the dry sliding wear behaviour for hybrid metal matrix composites by using the Taguchi technique. They want to establish a correlation between dry sliding wear behaviours of hybrid composites by using different wear parameters to analyse the wear problem of the metal matrix composites because dry sliding wear behaviour has a huge area of research for metal matrix composites. In their study, they found that the wear rate, load and sliding speed of the composites were highly influenced by wear factor i.e. sliding distance. Aluminium alloy which was reinforced by ceramic whiskers, fibres and particles now considered as tribo-materials. Roy et al. [193] used Al alloy reinforced with TixAly and Al_2O_3 particles for his study and find out the different tribological properties. Triboligical properties considered as a one of the major factor for controlling the performance in different structural applications. They found with the increasing reinforcement content (up to 20 vol %) the wear volume decreases and at 20 vol %reinforced Al composites have higher wear resistance.

The adhesive wear behaviour of 4147 Al alloy reinforced with SiC and B_4C particulates for the different wt.-% (10, 15 and 20 wt. %) was studied by Ipek [194]. In his study, he found that with the increasing amount of B_4C particulates in composites abrasive wear also increase. But because of good adhering properties SiC particle has more effect on wear resistance of composites as compared to B_4C

particulates. Similarly for dry sliding wear behaviour of metal matrix composites, one statistical approach was studied by Basavarajappa and Chandramohan [195]. In their study, they used Al alloy as matrix and SiCp as reinforcement for the composites which is produced by liquid metallurgy method of casting. They used Taguchi design of experiments that was successfully used for explaining the hybrid composites dry sliding behaviour. Now-a-days aluminium alloy composites the most attractive material in many applications like mechanical, automobile, and aerospace industries, due to its enhancing properties (light weight, thermal conductivity and recently wear resistance) over to other alloys. Bonollo et al. [196] Studied about the sliding wear behaviour of aluminium alloy reinforced with Al_2O_3 and SiC particulates. They found that the coefficient of friction increases up to a certain value about 8m of sliding for both composites when the flow properties of the third body are comparable.

Mahendra and Radhakrishna [197] studied about the fabrication and wear behaviour of Al–4.5% Cu alloy reinforced with fly ash content that was produced by using conventional foundry technique. Different wt.-% (5, 10 and 15 wt.-%) of fly ash content were used to added in molten metal. From the investigation, they found that the resistance to dry wear and slurry erosive wear increased with the increasing in the content of fly ash in composites also the corrosion resistance increases with increasing in fly ash content. The wear behaviour for ZA-27 alloy reinforced with garnet particles was studied by Kumar et al. [198]. The composites were made by using liquid metallurgy technique. The garnet particle varies from 0 % to 20 % by weight in steps of 5 % for making composites. The wear loss of the composites increased with the increasing in reinforcement, normal load and sliding speed. Shyu and Ho [199] were studied about wear behaviour of the aluminium alloy reinforced with TiC and fabricated by In situ process. They found the abrasive and sliding wear resistance increases with the increasing in TiC particles through In situ process.

Metal matrix composites become the large leading material in the composites and aluminium MMC received considerable attention due to its excellent engineering properties over to other materials. Kilickap et al. [200] studied the tool wear behaviour of SiCp reinforced with aluminium alloy. Tool wear mainly affected by cutting speed in dry turning condition. When coated tool was used than tool wear was lower as compares to uncoated one.

Pardo et al. [201] studied about the influence of reinforcement content and matrix composition on aluminium metal matrix oxidation resistance. They used four

composites (A360/SiC/10p, A360/SiC/20p, A380/ SiC/10p, A380/SiC/20p) for finding the composite influence on oxidation resistance. They found from their investigation that the degree of oxidation of composites increases with the SiCp concentration.

Table 2.4 shows the sliding wear and friction properties of particulates filled metal alloy composites.

Table 2.4 Sliding wear and friction properties of particulates filled metal alloy composites

Sl. No.	Metal matrix	Particulate	Wear and friction properties	Applications	Ref.
1	Al-20Si-5Fe-3Cu-1Mg	10 vol% SiC or Al_2O_3 particles	A further rise of this ratio leads to deterioration of local interfacial cohesion between the ceramic phase and the matrix dispersed with a high volume fraction of silicon crystals and intermetallic dispersoids, thus degrading the MMCs in tensile properties fretting wear tests at room and elevated temperatures and with dry and wet contacts show that the MMCs extruded at a higher reduction ratio has a higher mass loss and an increased the friction coefficient.	Aerospace, aircraft, automobile aerospace, aircraft, and automobile	178
2	Aluminum	Silicon carbide (SiC)	Sliding wear and slurry erosive wear resistance improved considerably with the addition of SiC particles, whereas corrosion resistance decreased. The bulk hardness increased with an increase in the	Automobile	183

			percentage of SiC particulates. There was not much change in the density of MMCs compared to the base metal.		
3	A356 (EN-Al Si7Mg0.3)	Al_2O_3	Improvement of wear resistance for the composite material with 3 wt. % Al_2O_3 reinforcement was significant for specific load up to 1 MPa. Adhesive wear was a predominant mechanism of wear followed by plastic deformation with increase of specific load. (dry sliding conditions)	In different industries	184
4	Al/Si alloy	Alumino silicate fiber	The additions of 3-7vol. % of fiber conferred a beneficial effect in reducing the wear rate of the alloy at room temperature. The MMC with 4.5% fiber exhibited the lowest value of the coefficient of friction.	Internal combustion engines as pistons, cylinder blocks and cylinder heads.'	185
5	Fe-C alloys	0.2 to 1.4 wt% Carbon	The erosion resistance increased as the micro structural features decreased in size, with the important micro structural variables being carbide spacing and ferrite grain size. (water as lubricant)	-	202
6	6061 Al alloy	SiC particles	The increase in the SiC content and decrease in particle size improved the erosive wear resistance of the	Cylinder blocks	186

			coatings. The abrasive wear resistance was found to improve with the increase in SiC particle size and with the SiC content in the composite coatings. Adhesion strength of the coatings to their substrates were found to decrease with increasing SiC content and with decreasing SiC particle sizes. (dry sliding condition)		
7	ZA-27 alloy	Zircon particles	It was found that with the increase in zircon content, the wear resistance increased monotonically. the wear rate of the composites was lesser than that of the matrix alloy and it further decreased with the increase in zircon content.(dry sliding condition)	Aerospace, aircraft, and particularly in automotive Industries.	159
8	Al_2O_3–20Ag20CaF2 disk	Al_2O_3 pin	Effective self-lubricating region (II) (continuous lubricating film) was almost independent of sliding speed, and mainly dependent on the load. In the low friction and wear region (II), the worn surface was found to be much softer than the original surface, and the distribution of Vickers hardness became more uniform.	Different Tribological applications	188

9	Si_3N_4 and Al_2O_3-matrix	SiC	The addition of SiC whiskers to a Si_3N_4 matrix sets up tensile stresses at the whisker-matrix interfaces, enhancing the bulk toughness of the composite, but degrading the abrasive wear properties by promoting easier whisker debonding and removal by the abrasive particles. The addition of SiC whiskers to an alumina matrix, on the other hand, results in the creation of compressive stresses at the whisker matrix interface, producing a relatively stronger bond that can better withstand the rigors of an abrasive wear environment.	Advanced structural applications, at elevated temperatures in severe environments	189
10	ZA-27 alloy	Garnet particles of size 30–50μm	The wear rates of the composites were lower than that of the matrix alloy and further decreased with the increase in garnet content. However, in both unreinforced alloy and reinforced composites, the wear rates increased with the increase in load and the sliding speed. The increase in garnet content, the wear resistance increased monotonically.	Requiring for good strength at high temperature, good structural rigidity, dimensional stability, and light weight	30
11	Al-alloy	SiC particle	Mechanical properties such as tensile strength,	Rotor, gas turbine blades	203

			modulus of elasticity, and hardness of composite are found to be greater than the matrix alloy. The strength and hardness of the as-cast composite are further improved by heat treatment. The ductility of the cast alloy improved by heat treatment.	of a helicopter engine, boiler, heat exchanger tubes, burner nozzles, pumps and valves, compressors, *etc*	
12	2024 and ADC12 aluminum alloys	SiC whiskers, Al_2O_3 fibers, SiC particles	The steady-state wear rate of MMCs decreased with increasing V_f. Whisker fragments formed in the wear process were small, resulting in little aggressive action on the counter face material. On the other hand, fiber and particle fragments were large in size and angular in shape, so that they promoted abrasion on the counter face at high V_f .(Dry sliding condition)	Pistons and cylinder liners in automotive engines	204
13	A360, A380 (A361 used as a reference)	SiCp	The degree of oxidation of the composite increases with the concentration of SiC particles. The hardness of the materials exposed at 350, 400, 450, and 500°C remains acceptable after 80 days of air exposure. This was because the reinforcement inhibits matrix creep at high temperatures (water as a lubricant)	Automobile-engine parts such as drive shafts, cylinders, pistons, and brake rotors, and in aerospace applications	201

14	Al5Mg alloy	Al_2O_3 (60 μm) or C (90 μm)	The addition of Al_2O_3 or C particulates increased the 0.2% proof stress and reduced both the tensile strength and ductility, compared with the monolithic alloy. The wear rate of the Al5Mg alloy decreased with the addition of C particulates. However, increasing the volume fraction of C particulates did not have a prominent effect on the wear rate.	Pistons and cylinder linear in car engines, automotive brake rotors, and other wear resistance parts	190
15	Al alloy-	SiC	Aluminum composite provides higher wear resistance than those of the base alloys in all tribo-conditions. As the erosive corrosive wear was dominated by erosive wear, the erosive-corrosive wear rate of the composite was noted to be less than that of alloy. Frictional heating and coefficient of friction are noted to be considerably less in composite as compared to that in the alloy. (SAE-40 lubricated oil)	Automobile and mineral processing industries such as brake drum, cylinder block, refrax apex insert etc.	191
16	Al2219	SiC	Sliding distance was the wear factor that has the highest physical as well as statistical influence on the wear of the composites (34.35%), the load (23.24), and sliding speed (21.5%). Out of the interactions the sliding speed and	Where light weight and energy saving was important design consideration	192

			load will contribute more (6.96%) ahead of sliding speed and distance (3.57) and other interactions will influence very less. The conformation tests showed that error associated with wear of the composite varies from 7.1% to 13.68%. (Dry sliding condition)		
17	99.9% pure aluminum	SiC particles	Cutting speed was the most influential machining parameter on tool wear. It increased tool wear with increasing. The tool wear doubled when cutting speed was 150 m/min compared to 50 m/min. Higher feed rates produced a higher tool wear. Higher feed rates produced poor surface quality. The influence of heat treatment of this material like homogenized process affected badly, it increased tool wear and surface roughness compared to not heat treatment application of the material.(Dry sliding condition)	Aerospace, automotive, electronics and medical industries	200
18	Aluminum	TixAly and Al_2O_3 particles	The reinforcement content should be optimized in order to obtain lower COF in in-situ reinforced Al composites. The wear data reveal that the wear	Automotive parts	193

			volume, estimated principally from the transverse wear scar diameter, decreases considerably with increase in reinforcement content (up to 20 vol %) under the investigated fretting condition.		
19	4147 Al, Al	B_4C, SiC	The wear resistance of Al/B_4C matrix increases considerably with increasing wt. % B_4C particle content in Al alloy matrix. When Al alloy matrix material was in severe adhesive-abrasive wear, the Al/B_4C composites are in light-mild adhesive wear stage at the same wear condition.	Different Tribological applications	194
20	AA2219	SiCp and SiCp-graphite	It was found that SiCp-Gr (graphite)-reinforced composites exhibit less volume loss when compared with SiCp-reinforced Composites. Sliding speed was the most significant factor affecting wear behavior followed by L (load) and D (sliding distance). The effect of interactions between the S and the L is more pronounced in SiCp-Gr composites.	Automobile industries	195
21	Aluminum	10 vol.% $A1_2O_3$ and Sic	Damage mechanisms of composites involve plastic deformation and	In mechanical, automotive	196

		particles	oxidation of the A1 matrix, with insertion of A1 fragments and $A1_2O_3$ particles (along with fragments of the reinforcing particles) in the third bodies. In this way, the abrasive power of the third-bodies increases considerably. For both composites, the friction coefficient against steel increases up to a steady-state value of 1.6 after about 8 m of sliding, when the flow properties of the third-bodies become comparable (dry sliding condition)	and aerospace industry, mainly for their light weight, thermal conductivity and energy efficiency, and more recently for their wear resistant, properties	
22	Al–4.5% Cu alloy	Fly ash	An increase in hardness, tensile strength, compression strength, and impact strength with increasing the fly ash content. The density decreases with increasing fly ash content. Resistance to dry wear and slurry erosive wear increases with increasing fly ash content. Corrosion increases with increasing fly ash content. (dry sliding condition)	Automobile and aerospace industry	197
23	ZA-27 alloy	Garnet particles	The wear loss of composites was less than that of the zinc-aluminum alloy, but increased with increase of reinforcement in load and sliding speed. Also	Tribological applications where demand for lightweight, stiff and strong	198

			the wear resistant will increase with increase in garnet content. (dry sliding condition)	materials	
24	Aluminum	Titanium carbide particles	The tensile and yield strength increased by up to 18% after the formation of TiC in the Al alloy matrix. The hardness increased by up to 20%. The abrasive and sliding wear resistance increased with the in situ formation of TiC particles.	Tribological applications, including plain bearings	199
25	Aluminum	37 vol% Al_2O_3 and 25 vol% SiC particles (contained up to 8 wt% Mg in their matrixes)	While matrix hardness and compression strength increased, amount of porosity and impact toughness decreased with increasing Mg content of the matrix. Metal–metal and metal–abrasive wear tests revealed that wear resistance of the composites increased with increasing Mg addition On the other hand, abrasive resistance decreased with increasing test temperature, especially above 200 8C. (dry sliding condition)	Aerospace and automotive industries due to their excellent combination of high specific strength and better wear resistance	205

2.1.5 On implementation of Design of Experiments (DOE) and Optimization Techniques for particulate filled metal alloy composites:

The optimization technique was one of the ancient and better ways to get the accurate solution of any problem. Different methods were used for getting the optimum values like Fuzzy Analytic Hierarchy Process (FAHP), Fuzzy Technique for Order

Preference by Similarity to an Ideal Solution (TOPSIS), balanced scorecard (BSC), etc. for different kind of applications. Lee et al. [206] used a Fuzzy AHP and BSC approach in his research paper to get the optimum results for the manufacturing industries IT department in Taiwan. In their study, they found by the use of FAHP, TOPSIS and BSC techniques the performance of IT department becomes improved. Similarly, some other optimization techniques were used by different authors in his research article like for personal selection, supply chain management, healthcare industries, etc. A Fuzzy AHP approach was used by Gungor et al. [207] to find out the personnel selection problem performance. They used FAHP to get the best adequate personnel dealing with the rating of qualitative as well as a quantitative criterion. For evaluating the environmental performance of suppliers Awasthi et.all [208] used a fuzzy multicriteria approach in his paper and they found that the proposed approach strength was its practical applicability and to provide outcome when there was a lack of quality information. Similar work was discussed in [209, 210, 211, and 212] other research papers.

Wear process in composites was a complex phenomenon involving some operating variables, and it was essential to understand how to wear characteristics of the composites were affected by different operating conditions. Although a large number of researchers have reported on properties, performance, and on wear characteristics of composites, neither the optimization of wear process nor the influence of process parameters on wear rate has adequately been studied yet. Selecting the correct operating conditions was always a major concern as traditional experiment design would require many experimental runs to achieve satisfactory results. In many processes, the desired testing parameters are either determined based on experience or by use of the handbook. However, it does not provide optimal testing parameters for particular situation. Thus several mathematical models based on statistical regression technique have been constructed to select the proper testing conditions [213-222]. The number of runs required for full factorial design increases geometrically whereas fractional factorial design is efficient and significantly reduces the time. Due to the simplicity, these methods were very popular, but this very simplicity has led to unreliable results and inadequate conclusions. The fractional design of experiment may not contain the best design point as the traditional multi-factorial experimental design can change one-factor-at-a-time. This method worked for the one factor at a time while the other remaining factors kept fixed at a specific

set of conditions. To overcome these problems, Taguchi and Konishi [223] advocated the use of orthogonal arrays and Taguchi [224] devised a new experiment design that applied signal-to-noise ratio with orthogonal arrays to the robust design of products and processes. In this procedure, the effect of a factor was measured by average results and therefore, the experimental results can be reproducible. Phadke [225], Wu and Moore [226] and other researchers [221-224] have subsequently applied the Taguchi method to design the products and process parameters. Basavarajappa and Chandramohan [227] used Taguchi method to study the influence of wear parameters on the wear rate and also found that the sliding distance was the parameter that has highest physical and statistical significance on the wear rate. Patnaik et al. [228] has demonstrated the use of Taguchi method for studying the effects of various parameters and their interactions in a number of engineering processes and successfully applied Taguchi design for parametric appraisal in wire electrical discharge machining process, drilling of metal matrix composites and erosion wear behaviour of metal matrix composites such as aluminium reinforced with fly ash, red mud, SiC, alumina, Titania and cement-by-pass-dust etc.

Joshi et al. [229] developed a benchmarking framework by using Delphi-AHP-TOPSIS methodology, to optimize the cold chain performance for a company that reveals its strengths / weaknesses and finally, identifies the potential alternatives for continuous improvement. In this method, whole benchmarking was divided into three stages. The first stage was the identification of suitable parameters, synthesis and prioritization of key performance factors and sub-factors were done, and a novel consistent measurement scale was developed. The second stage was Analytic Hierarchy Process (AHP) that was based on cold chain performance evaluation for an opted company against its competitors, and to optimize the cold chain performance for an individual factors as well as sub-factors, and lastly for an overall performance index. The third stage was Technique for Order Preference by Similarity to Ideal Solution (TOPSIS) based used for the continuous improvement of company's cold chain performance. Kelemenis and Askounis [230] were developed a method to develop the decision-making a process of an organization by using TOPSIS and incorporating a new concept for ranking of alternatives. This was based on veto threshold, a critical characteristic of the main out ranking methods. The ultimate decision criterion was not similar to off the accurate results but the gap in between alternatives to veto set by the decision makers. Rao [231] developed a decision-

making methodology for material selection using an improved compromise ranking method in which analytic hierarchy process(AHP) for assessing the weights of relative importance of attributes and by introducing a ranked value judgment in a fuzzy conversion scale for the qualitative values of attributes. They concluded that this method can consider any number of quantitative and qualitative attributes the material screening and choosing methods in which considered a variety of quantitative selection procedures and the systematic evolution and conclude that multi-criteria decision-making approach has the potential to improve greatly the material selection methodology. Jahan et al. [232] proposed a material selection procedure useful when material selection problem includes qualitative properties or user-interaction aspects. This procedure uses linear assignment method and multi criteria decision-making the process to rank the materials. Table 2.5 shows the optimization behaviour for particulate filled metal alloy composite.

Table 2.5 Optimization behaviour for particulate filled metal alloy composite

Sl.No.	Optimization Technique/Method	Results	Applications	Ref.
1	Fuzzy analytic hierarchy process (FAHP), balanced scorecard (BSC)	The constructed information system was suggested to be a good tool for solving other multiple-criteria decision-making problems.	Evaluating performance in IT department	206
2	Fuzzy Analytic Hierarchy Process (FAHP)	The result obtained by FAHP was compared with results produced by Yager's weighted goals method. In addition to abovementioned methods, a practical computer-based decision support system introduced to provide more information and help manager make better decisions under fuzzy circumstances.	For personnel selection	207
3	Fuzzy multicriteria approach (TOPSIS method)	The proposed approach can be practically applied in evaluating environmental performance of suppliers. Since the decision making process was sensitive to	Environmental performance of suppliers	208

		the number of participants involved and their expertise with the subject, their selection should be carefully done.		
4	Fuzzy Technique for Order Preference by Similarity to an Ideal Solution (TOPSIS)	The proposed approach has practical implications as the empirical test showed in the case of a CIO selection problem of a multinational firm, supporting a very sensitive decision in real time.	For personnel selection	209
5	TOPSIS and multi-choice goal programming (MCGP)	The proposed method may be useful for various MCDM (multiple criteria decision making) problems, such as management problems (e.g., project management and location selection) and marketing problems (e.g., new products development and promotion activities) when available data are inexact, vague, imprecise and uncertain by nature.	In supply chain management	210
6	AHP and Fuzzy TOPSIS	The work presented in this paper shows the applicability of the e-sq framework in explaining the complexity of aspects observed in the implementation of healthcare services via internet.	Electronic service quality in healthcare industry	211
7	Fuzzy AHP and Hierarchical Fuzzy TOPSIS	In the case of the vegetable oil manufacturer company provides the researchers and practitioners to understand in a better way the importance of developing organization strategy in channel management from a practical point of view.	In distribution channel management (For an edible-vegetable oils manufacturer firm)	212

2.2 Summary of literature survey

Proposal of new particulate filled metal alloy composites and their scientific principles effectively stimulated recent technology was a challenging task for present industrial revolution. The above reported literature survey reveals though much work on metal alloy composites, still we have possibilities to fill the gap of enhancement for metal alloy composites by the use of different kind of new environmental waste hard fillers i.e. marble dust and calcium oxide. The utilization of marble dust / CaO in construction applications like road filling, bricks, and ceramic tiles have already effectively used so far however, there were no such effective applications available till date as per availability of literature and personal experience in product making for industrial applications. Therefore, based on our present proposed research work related to fabrication of new materials for bearing materials especially utilization of marble dust as filler material in metal alloy composites to reduce the manufacturing cost keeping the properties remain constant. Hence, due to less studied area there are lots of chances for the further study of marble dust as filler in different areas. From the last quarter of a century, active research was going on in composites based on metals was now able to give a significant contribution towards industrial and engineering applications.

2.3 The knowledge gap in earlier investigations

From the literature review on particulate filled metal alloy composites reveals the following knowledge gap, through which the objectives of the present research work can be set.

- Though much work has been reported on various dry/wet sliding wear and friction characteristics of metals, alloys, and homogeneous materials, comparatively less has been reported on the sliding wear and friction performance of metal matrix composite and their alloy elements of dry lubricating conditions for bearing materials.
- A possibility that the incorporation of particles in MMC could provide a synergism in terms of improved wear resistance and friction characteristics have not been adequately addressed so far and there were not much data available about wear phenomena after addition of particulate or filler in the metal matrix composites with dry lubricating conditions.
- As far as wear and materials properties studies of metal matrix composites were concerned, many investigators have proposed some models to predict

materials wear/friction, mechanical, thermo-mechanical and other properties behavior of metal matrix composites, but only a few of them considered FEM/Simulation to predict the materials behavior analysis. As a result, a simulation/FEM model has been developed using less software.

- Studies carried out worldwide on wear behavior of composites have largely been experimental, and use of statistical techniques in analyzing wear characteristics was rare.
- Taguchi method, in spite of being a simple, efficient and systematic approach to optimizing designs for performance, quality and cost, was used only in a limited number of applications worldwide. Its implementation in parametric appraisal of wear processes has hardly been reported.

2.4 The objectives of this work outlined as follows

The project would deal with the following objectives such as;

- Fabrication of series of particulate filled series of metal alloy composites by stir casting techniques and also modeled through finite element simulation method.
- Evaluations of physical, mechanical, fracture and thermo-mechanical properties of the unfilled and particulate filled metal alloy composites
- Determination of fracture toughness of the proposed unfilled and particulate filled metal alloy composites and then conduct, fractography analysis for the fractured samples in tensile mode to examine the crack phenomenon at the composite surfaces.
- Characterization of thermal and thermo-mechanical properties such as thermo-gravimetric analysis (TGA) and dynamic mechanical analysis (DMA) respectively.
- Conducts sliding wear behavior of particulate filled metal alloy composites for estimation of wear rate under multiple operating conditions and a Taguchi optimization technique to validate the best results for particulate filled metal alloy composite materials. Also, characterize the micro structural behavior of material through FE-SEM/EDAX and AFM analysis.
- Finally, the optimization technique used to get the optimum results for physical, mechanical, fracture toughness and wear analysis of the particulate filled metal alloy composites by PSI (Preference Selection Index) optimization method.

Chapter Summary

This chapter was all about the different consideration that has been taken for the research purpose. The various aspects of metal and metal alloy composites reported as:

- The knowledge gap in earlier investigations
- The objectives of the present work

The next chapter materials and methods include a brief elaboration of used raw materials and test procedures in this research study. It presents the details of fabrication and characterization of the composites under investigation and also an explanation of the Taguchi experimental design.

******

Chapter 3
Materials and Methodology

CHAPTER 3
MATERIALS AND METHODS

This chapter describes the materials and methods used for the fabrication of particulate filled metal alloy composites and studied the physical properties (Density, void contents), mechanical characteristics (Hardness, compressive, flexural, impact, fracture toughness), thermo-mechanical properties such as Thermo gravimetric analysis and Dynamic mechanical analysis (TGA, DMA) and sliding wear characteristics of the alloy composites. It presents the detail fabrication process and the above properties experimental procedure in detailed in this chapter used for the research work. To distinguish the conspicuous factors for sliding wear analysis, the Taguchi experimental design (L_{25} orthogonal array) and analysis of variance (ANOVA) is used. Finally, the optimization technique is used to find the best combination of material properties for the fabricated metal alloy composites.

3.1. Properties of selected materials

3.1.1. Matrix Material (ZA-27 metal alloy)

ZA-27 is used as a matrix alloy due to superior and economical antifriction properties. It's an ideal bearing material for heavy and light load pressure with low and high surface speed. Zinalco or Zinc-Aluminum (ZA-27) alloy (Density 5 gm /cc^3, Hardness 119 BHN) supplied by ZORHAT Pvt. Ltd Baroda, India, used as the base matrix alloy. Applications in machine tools, heavy engineering industries, Power plants, Railways, Cement and Building industry,Transport industry, Aeronautics, Agricultural machinery, etc. The proposed matrix material chemical composition and detail mechanical properties are presented in Table 3.1 and Table 3.2 respectively. Due to its vital properties such as low energy requirement during casting materials, low melting point as compared to another metal alloy i.e. aluminum, iron, etc. and it's natural lubricity it's very conventionally used in the manufacturing of bearing and bushing applications.

Table 3.1. Chemical composition of ZA-27 alloy (In weight percent) [233]

Element	Aluminum	Magnesium	Copper	Zinc
Percentage composition (wt %)	25-28	0.01-0.02	2.0-2.5	Balance

Table3.2. Mechanical properties of ZA-27 alloy [234]

Mechanical Properties	Sand Cast
Ultimate tensile strength (MPa)	420-490
Yield strength-0.2% offset (MPa)	378
Elongation(%in 2")	2-8
Shear strength (MPa)	290-305
Hardness (Brinell)	90-120
Impact strength (J)	36.2
Modulus of elasticity(GPa)	77.9
Poisson's ratio	0.32
Density (gm./cc^3)	4.7-5.0
Thermal Conductivity (W/mK)	136

Figure 3.1. Cast ZA-27 metal alloys

3.1.2 Matrix Material (Silicon Bronze metal alloy)

Copper and copper- based alloy materials acceptable by industries on worldwide level due to their distinctive materials properties such as good wear and corrosion resistance, strength, self- lubrication mechanism and better machinability of the components respectively. Copper alloy (SiBr) (Density 8.49 gm. /cc^3, Hardness 115 BHN) supplied by Sohan Singh molding Pvt. Ltd., Faridabad, India is used as a base matrix alloy. The major working application area of silicon bronze (SiBr) based alloy is for engineering parts and tribology analysis such as bearing materials, because of its high thermal conductivity and magnificent workability.The proposed matrix material chemical compositions and detail mechanical properties for SiBr alloy is presented in Table 3.3 and Table 3.4 respectively.

Table 3.3. Chemical composition of SiBr alloy (In weight percent) [235]

Alloy	Si	Cu	Zn	Mg	Fe
Copper (Silicon Bronze)	2.4-4.0 (max)	90	1.5-4.0	1.0	1-2 (max)

Table3.4. Mechanicalproperties of SiBralloy [236]

Mechanical Properties	SiBr alloy
Ultimate tensile strength (MPa)	380
Yield strength-in comp. (MPa)	140
Elongation(%in 50 mm)	11
Melting point (ºC)	1060
Hardness (Brinell)	55-120
Modulus of elasticity(GPa)	117
Poisson's ratio	0.35
Density (gm./cc^3)	8.49
Thermal Conductivity (W/mK)	57.1

Figure 3.2. Silicon bronze metal alloys

3.1.3. Filler material (Marble dust)

Marble is a non-foliated metamorphic silicon bronze metal alloyrock resulting from the metamorphism of limestonethat mostly composed from calcite (i.e. a crystalline form of calcium carbonate ($CaCO_3$)). It is extensively used for sculpture, as a building material, and in many other applications. The marble dust (with 100 µm particles size) is used as a filler material and is collected from Centre for Development of Stones Jaipur, Rajasthan. The proposed filler materials chemical composition and detail mechanical properties of marble dust are presented in Table 3.5 and Table 3.6 respectively.

Table 3.5. Nominal chemical compositions of fillers (Marble Dust) [237]

	Constituents (in weight percent)							
Filler	SiO_2	Al_2O_3	Fe_2O_3	CaO	MgO	SO_3	K_2O	Loss on ignition
Marble Dust	4.67	-	0.03	**51.80**	0.4	-	-	**41.16**

Table 3.6. Mechanical properties of Marble Dust [238]

Sl.No.	Properties	Values
1	Melting point (°C)	1340
2	Density (gm/cc^3)	2.6-2.8
3	pH-value (100 g/l / 20°C)	8.5 - 9.5
4	Vapor pressure	insignificant
5	Solubility in water	< 0.03 % (20°C)

Figure 3.3. Marble Dust Particulates

3.1.4. Filler material (Calcium oxide)

The calcium oxide commonly known as quicklime or burnt lime is white crystalline solid has melting point around 2572°C. It is manufactured from coral, heating limestone, sea shells or chalk etc. The CaO (with 100 μm particles size) is used as fillermaterial for fabrication of particulate filled metal alloy composites and is supplied by Savita scientific and plastic products Jaipur, India. The mechanical properties of calcium oxide are

presented in Table 3.7, and the chemical compositions of the filler materials are shown in Table 3.8,

Table 3.7. Nominal chemical compositions of Fillers (Calcium Oxide) [239]

	Constituents (in weight percent)				
Filler	**CaO**	**SiO_2**	**MgO**	**$CaCO_3$**	**L.O.I.**
CaO	95.41	0.18	0.35	2.56	1.5

Table 3.8. Mechanical properties of Calcium Oxide [240]

Sl.No.	Properties	Values
1	Melting Point (°C)	2570
2	Boiling point (°C)	2870
3	Specific gravity	3.37
4	Density(g/cm^3)	3.35

Figure 3.4. Calcium Oxide particulates

3.2 High temperature vertical vacuum furnace

The high temperature vertical vacuum furnace is designed on the basis of cold wall principle as shown in Figure 3.5. This furnace is consisting of two major units, i.e. one heating section that consisting of bottom pouring graphite crucible connected with vertical graphite plunger and around the graphite crucible heating coils are wound. The periphery of the upper heating units one more layeris fixed where cooling water is uniformly circulated in order to protect the heating unit. The second major unit is casting

unit where cast iron mold is placed. Once the molten material is melted, the plunger is opened and the molten material will pour vertically into the cast iron mold. After cooling of the material the cast iron mold is removed from the furnace. This furnace has also provision for casting of the materials in vacuum environment in order to avoid evaporation of metal alloy or particulates or might be oxidized with external environment. Finally, temperature measuring instrument (Infrared temperature measuring sensor) is also placed at the top of the upper heating unit to measure the rise in temperature of the molten materials.

Figure 3.5. Image of High Temperature Vacuum Casting Machine

3.3. Fabrication of composites

The base material such as ZA-27 alloy / SiBr alloy and filler material (i.e. marble dust and calcium oxide) are pre-heated initially in a separate furnace up to 150^0C and after pre-heating initially the base material is poured in a graphite crucible. Once the base material is reached above its liquids temperature 500^0 C and 1100^0C respectively, a small quantity of magnesium (2wt. %) is added in the molten material to improve the

wettability of the composites. After uniform mixing of the base alloy and magnesium (Figures 3.5 and 3.6), the preheated filler particulates is poured into the molten metal alloy slowly as per desired quantity for 15 to 20mins at its melting temperature.

Once the mixture of filler particulates and matrix material reached its melting temperature the plunger is opened and the molten metal alloy is fallen vertically downward into a cast iron mold of size 140 × 90× 10 mm^3 and then allowed for cooling for half an hour. In this study, five different weight percentages (0, 2.5,5,7,5 and 10 wt.-%) of reinforced particulate filled metal alloy composites are fabricated for specific physical, mechanical, fracture, thermo-mechanical and wear analysis. The specimens are cut as per standard size for testing different material tests for different parametric conditions. The detail designation and compositions of the particulate filled metal alloy composites are presented in Table 3.9.

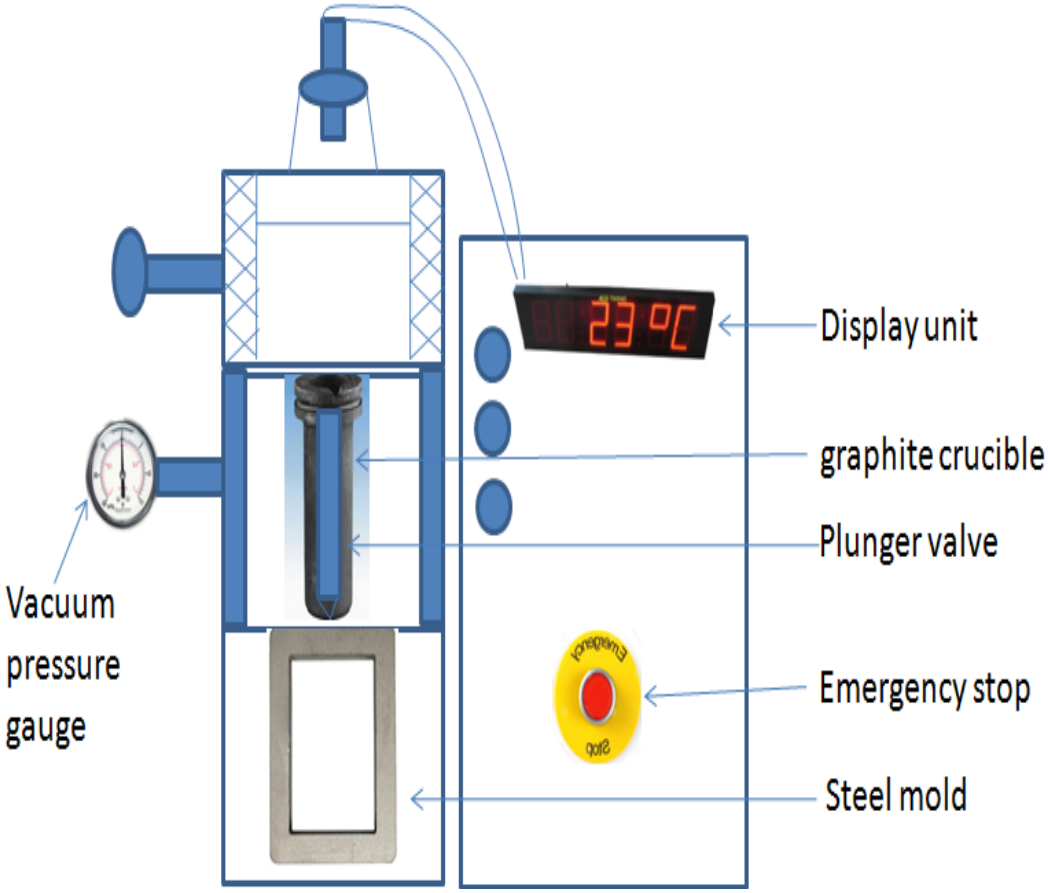

Figure 3.6. Schematic diagram of high temperature vacuum casting machine

Table 3.9. Designation and detailed composition of composites

Designation	Composition-1	Designation	Composition-2
ZAMD-1	ZA-27+0wt.% marble dust	ZACaO-1	ZA-27+0wt.% CaO
ZAMD-2	ZA-27+2.5wt.% marble dust	ZACaO-2	ZA-27+2.5wt.% CaO
ZAMD-3	ZA-27+5wt.% marble dust	ZACaO-3	ZA-27+5wt.% CaO
ZAMD-4	ZA-27+7.5wt.% marble dust	ZACaO-4	ZA-27+7.5wt.% CaO
ZAMD-5	ZA-27+10wt.% marble dust	ZACaO-5	ZA-27+10wt.% CaO
SiBrMD-1	AM-60+0wt.% marble dust	SiBrCaO-1	SiBr+0wt.% CaO
SiBrMD -2	AM-60+2.5wt.% marble dust	SiBrCaO -2	SiBr+2.5wt.% CaO
SiBrMD -3	AM-60+5wt.% marble dust	SiBrCaO -3	SiBr+5wt.% CaO
SiBrMD -4	AM-60+7.5wt.% marble dust	SiBrCaO -4	SiBr+7.5wt.% CaO
SiBrMD -5	AM-60+10wt.% marble dust	SiBrCaO -5	SiBr+10wt.% CaO

3.4. Simulation of particulate filled metal alloy composites by finite element method

3.4.1. Contact stress analysis of the particulate filled metal alloy composites using FEM element type and meshing procedure

FEM analysis for the spherical surface of balls and an elliptical surface of raceways in ball bearing is discretized by SOLID 185 elements. The SOLID185 elements are used for the 3-D modeling of solid structures and that shown by eight nodes with three degrees of freedom at each node: translations in the nodal x, y, and z directions (Figure 3.7). This element shows the presence of different materials properties such as plasticity, stress stiffening, hyper elasticity, creep, large deflection and large strain capabilities.

It also has haphazard formulation ability for simulating deformations of nearly incompressible elastoplasticity materials, and fully incompressible hyperplastic materials. For the meshing of inner and outer races of ball bearing sweep mesh command used by keeping element edge length 1mm and balls are meshed by set the global and keeping the smart mesh size as 2 mm and mesh is set to free mesh (Figure 3.8) [241].

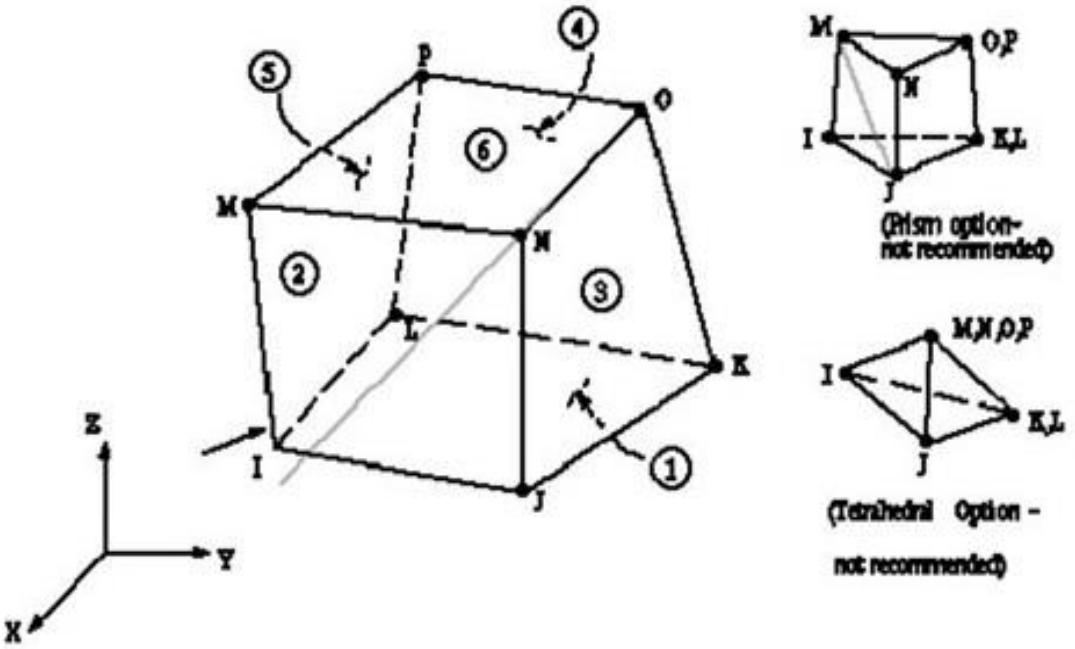

Figure 3.7. Geometry of Solid 185 elements for particulate filled metal alloy composites

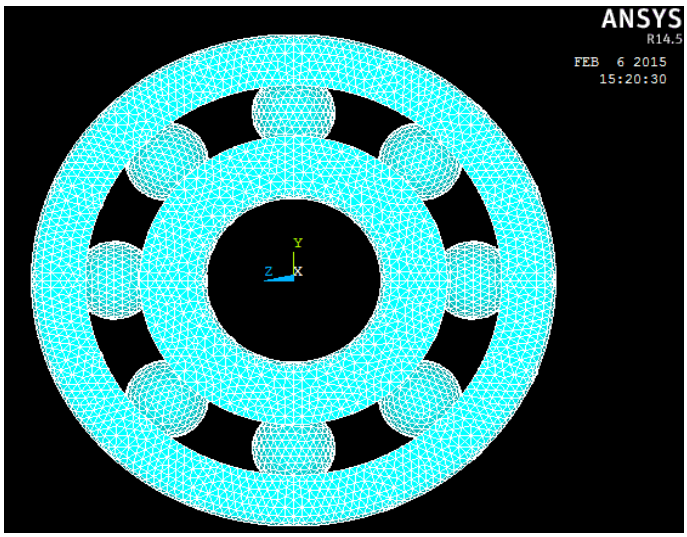

Figure 3.8. Meshed model of bearing for particulate filled metal alloy composites

3.4.2. Contact model

The contact problems between two surfaces are generally solved by two different techniques such as rigid-to-flexible bodies in contact and flexible-to-flexible bodies in contact. In this research work, flexible-to-flexible bodies in contact technique are followed due to ball bearing applications in which both the inner as well as outer races are

deformed according to loading conditions. The following elements are used for surface-to-surface contact that is TARGE169, TARGE170, CONTA171, CONTA172, CONTA173, and CONTA174 in this study. In the surface to surface contact concern one surface considered as a contact surface and another one considered as target surface. However, they must be chosen as a surface, and they should have similar material properties and the same real constant values. The convex surface is chosen as contact and concave surface as a target.

While designing the CAD model and during this applying the load in between the contact surface and target surface then one has to remember when we considered size of bodies that are in contact then the larger surface of the body considered as target surface with respect to a small surface. In this study which based on the ANSYS parametric modeling for three-dimensional finite element models of deep groove ball bearings are established to conclude the contact analysis numerically and also study the stress and strain distribution trend for ball bearing in the process of loading and the changes of bearing material under the different radial forces (Figures 3.9, 3.10). The contact and target surfaces can be invert and it works well. The chosen contact and target surface for ball bearing is shown in Figure 3.11.

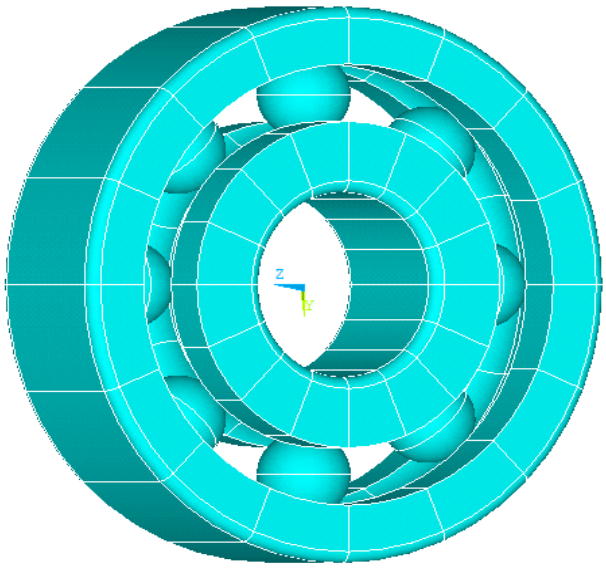

Figure 3.9. Geometric modeling of bearing for particulate filled metal alloy composites

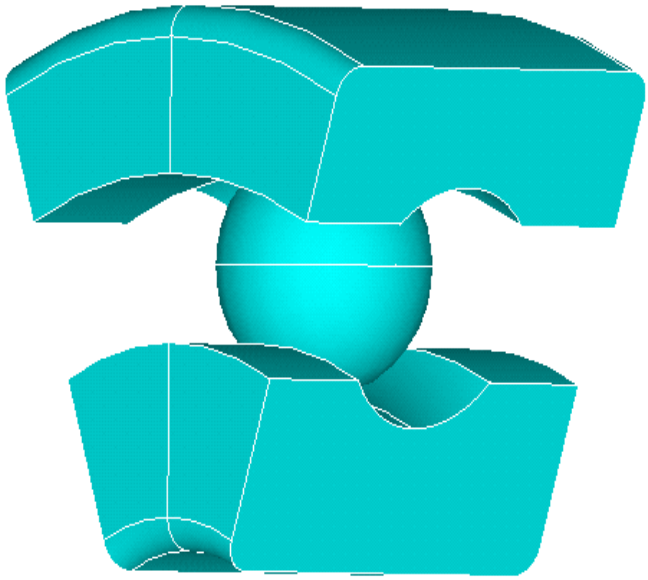

Figure 3.10. Three-dimension sub model of single row deep groove ball bearing for particulate filled metal alloy composites

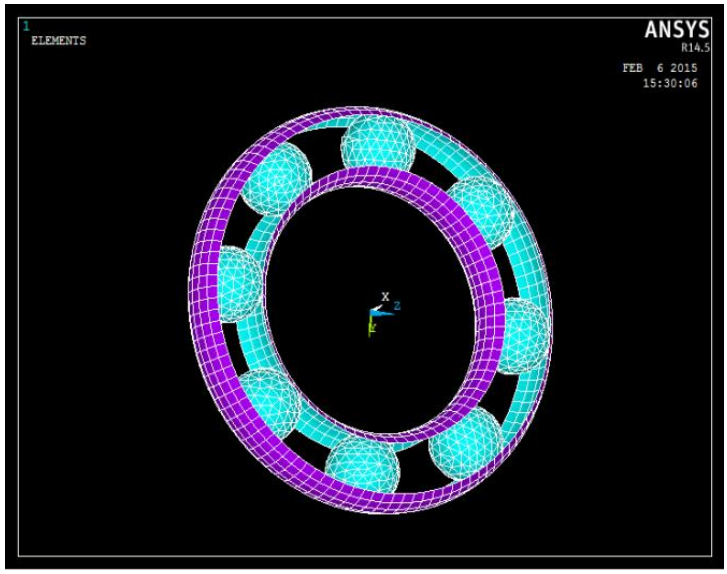

Figure 3.11. Contact and target elements for particulate filled metal alloy composites

3.4.3 Boundary condition and application of load

For the FEM analysis of single row deep groove ball bearing the following boundary conditions are considered as:-

- Constraint all the degrees of freedom for bearing outer ring's cylinder surface.

- Fixed the displacement of the axial direction (UX in Cartesian coordinate system) and circle direction (UZ in Cartesian coordinate system) of groove surfaces and bore surfaces of the outer ring, groove surface and cylinder surface of the inner ring and ball set.
- Added constraints of the radial direction (UY in Cartesian coordinate system)
- Applied radial load to the upper parts of outer raceway surface in negative Y-direction.

3.4.4. Structural analysis

For the simulation of ball bearing the flexible to flexible contacted model used for bearing raceways and balls. The model is shown in Figure 3.12. By the analysis the evaluated results founds as reaction force vs. displacement, stress, strain, stress intensity of ball and raceways. The chosen materials for the inner, outer ring as well as bearing balls is particulate filled metal alloy composites and the Young's modulus for different (0, 2.5, 5, 7.5, 10) wt. - % of particulates is different same for Poisson's ratio. In the ball bearing analysis, there is need to maintain the contact in between inner and outer raceways to transmit the accurate loads in between them [242].

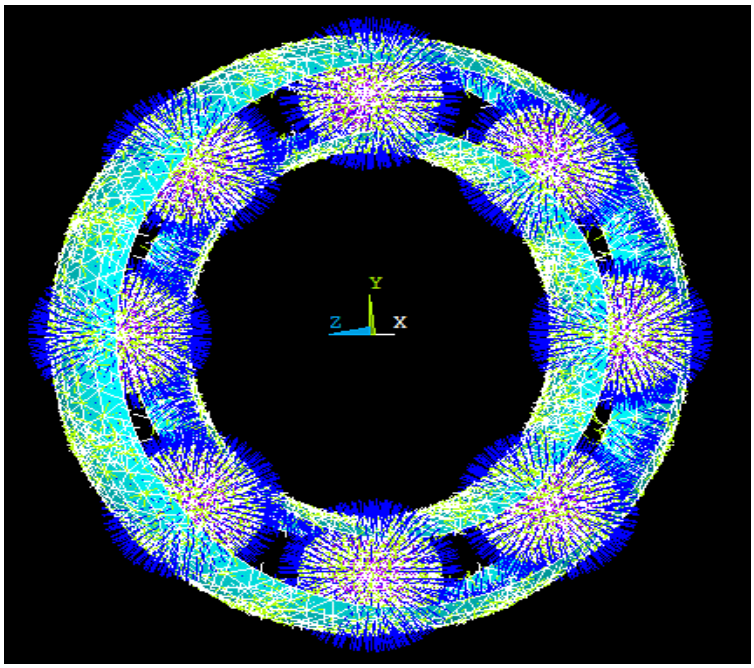

Figure 3.12. Contact models of ball and races for particulate filled metal alloy composites

3.4.5. Numerical modeling

A single row deep groove ball bearing with spare part number 6200 is used for this research work. The bearing geometry and bearing type for 6200 ball bearing are shown by Figure 3.13 and Table 3.10 respectively.

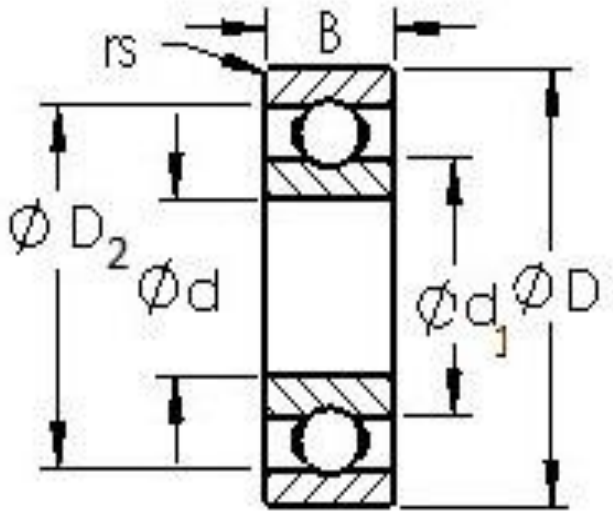

Figure 3.13. Geometry of ball bearing for particulate filled metal alloy composites

Table 3.10. Bearing's parameters [243]

Parameter Name	**Value (mm)**
Ball diameter	4.762
Bore diameter (d)	10.00
Inner raceway diameter (d_1)	15.738
Outer raceway diameter (D_2)	25.27
Outside diameter (D)	30
No. of balls	08
Inner raceway groove radius	2.44
Outer raceway groove radius	2.49
Width (B)	9.00
Radius ($r_{s)}$	0.60

3.4.6. Mathematical modeling

Theoretically the bearing contact stresses can be calculated by use of Hertz's equations, which are initially derived for contact in between two curved surfaces. With ellipsoidal-prism shape, pressure distribution is generated between the two contacts areas of bearings [244]. According to Hertz's theory, the equation of the radius of contact area is given by the following equation:

$$a=\sqrt[3]{3F\left[\frac{1-\upsilon 1^2}{E1}+\frac{1-\upsilon 2^2}{E2}\right]/4\left(\frac{1}{R1}+\frac{1}{R2}\right)} \quad (3.1)$$

The maximum pressure (or stress) at the center of an ellipsoidal contact area is given by the following Hertz equation.

$$P_{max} = 3\ W/\ 2\ \pi a^2 \quad (3.2)$$

In the analysis ball and race both have the same material, but the elastic modulus and Poisson's ratio are have different values for each material. In the FEM analysis bearing is stimulated with spherical radius R1 (2.381 mm) in contact with a spherical groove. During the application of the Hertzian theory, the spherical groove has been considered as a sphere with a negative radius R2 of -2.49 mm.

3.4.7. Hardness analysis of the particulate filled metal alloy composites using FEM

3.4.7.1 Finite element model

For the finite element analysis (FEA) of ball bearing contact problem, ANSYS 14.5 is used. The axis symmetry of ball indenter and the flat plate is taken to circumvent the computational intricacy of the spherical indentation that considered for the problem. So for that only cross sections of the ball indenter and test material are modeled. Figure 3.14 shows the hemisphere of the ball indenter which shown as a quarter of the circle and the material taken as a flat rectangle (Figure 3.14). And the contact region are created in between the rounded area of the indenter and the top most surface of the flat plate (Figure 3.15)

3.4.7.2. Element type and meshing

Element 183 are used for the contact analysis problem that has eight nodes and every node individually has two degrees of freedom respectively: translations in the nodal x and y directions. This used element may also use as a plane element or as an axisymmetric element.

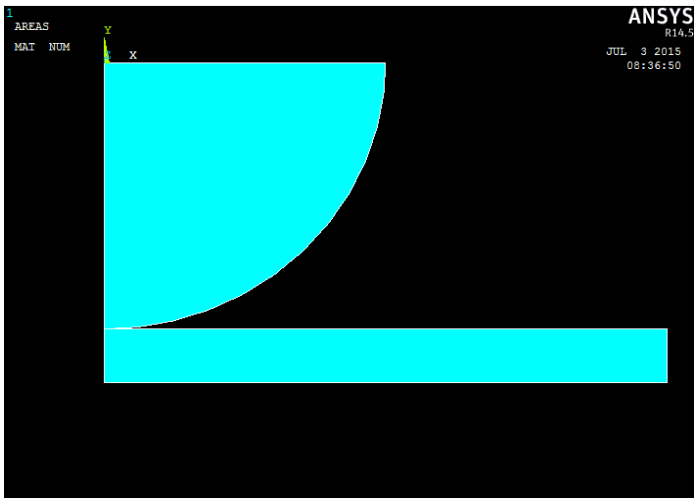

Figure 3.14. Geometrical modeling for particulate filled metal alloy composites

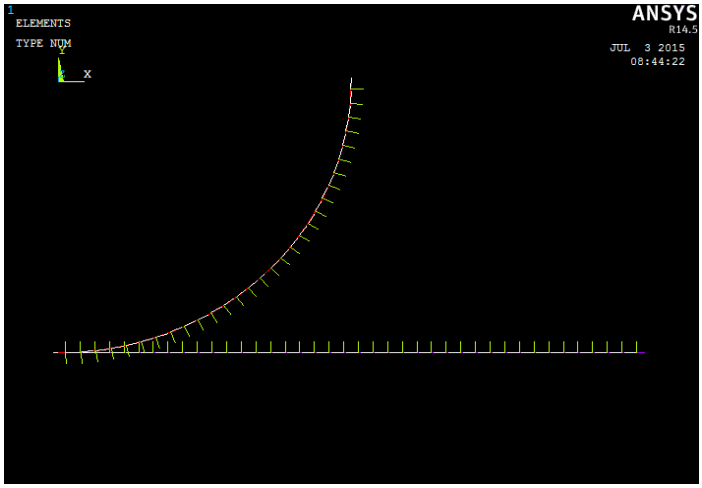

Figure 3.15. Contact models of indenter and plate for particulate filled metal alloy composites

The element 183 has different properties such as plasticity, creep, swelling, stress stiffening, large deflection, and large strain capabilities. The ball indenter and flat plate surface shows line contact and for flat plate contact 172 and target 169 elements are used. In the process indenter is defined as the contact region and specimen as the target for contact pair. The hemisphere and flat plate are meshed by free quad area mesh. Hemisphere has 30 element divisions on each line, and the plate has 40 elements division on each line (Figure 3.16). The finite elements mesh for flat surface material consists of 4108-node axisymmetric elements and 1206 total number of nodes.

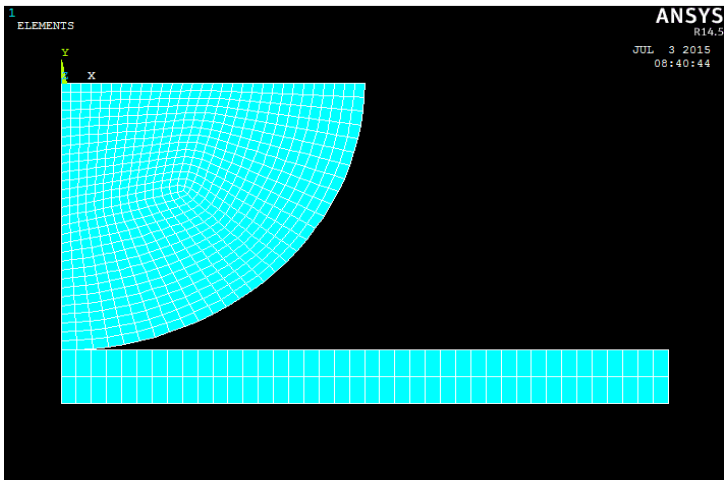

Figure 3.16. Meshed model of indenter for particulate filled metal alloy composites

3.4.7.3 Material properties and boundary condition

The quantity of nodes that lies on the symmetrical axis of the hemisphere and flat plat cannot proceed in a redial direction so far the existing nodes on symmetrical axis is constrained for the radial direction as well as the bottom nodes of the flat plat is coerce in all direction (Figure 3.17). An amount of 3000kgf load is applied on the center node of the top line of hemisphere.

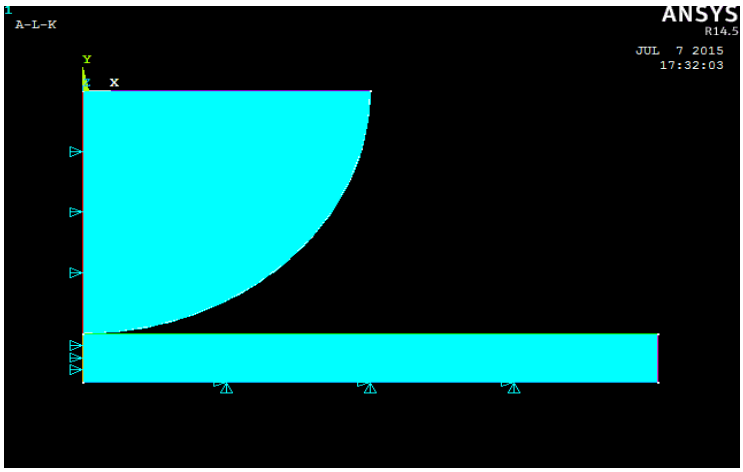

Figure3.17. Boundary conditions for particulate filled metal alloy composites

3.4.7.4. Mathematical modeling

For the measuring of hardness number, test been conducting in which a ball indenter of diameter D is penetrated in a flat plate surface of the specimen with an application of load W. With the effect of penetration a spherical cup indentation of diameter d and depth ω is

formed on the plate surface. The projected diameter d can be calculated by [245] the Eqs. (3.3) and (3.4):

$$d = 2\,[\omega\,(D-\omega)]^{1/2} \tag{3.3}$$

After measuring the penetrated diameter the hardness can be measure by the formula:

$$H = \frac{2W}{\pi d^2\left[1-\sqrt{1-\left(\frac{d}{D}\right)^2}\right]} \tag{3.4}$$

The finite element analysis of ball indenter with flat plat is examined for different composition of composite materials with their individual Young's Modulus, Poisson ratio and observed the hardness by penetration for same loading conditions. The calculation of hardness is carried out with taking help of penetration depth and the contact diameter.

3.5. Physical and mechanical characterizations

The mechanical properties of any materials are intuited by executing tests in established laboratory conscientiously through different experiments that clone the results as near as possible to actual conditions. Different factors during the test are nature (tensile, compressive shear, etc.) of the load that goes to be applying on the specimen, time duration of applied load and environment conditions, etc. applied on specimens. Different mechanical characterizations for particulate filled metal alloy composites given below:

3.5.1. Density and void content

The theoretical density of the fabricated composites can be determined by the rule of a mixture, as proposed by Aggarwal and Broutman [246] in Eq. 3.5 in terms of weight fraction. And the actual density of the said composites is dignified by the Archimedes principle by weighing the sample in air and then in water.

$$\rho_t = \frac{1}{\frac{w_p}{\rho_p} + \frac{w_m}{\rho_m}} \tag{3.5}$$

Where, ρ_t represent the theoretical density, w_p and w_m weight fraction of particulate/alloy material, ρ_p and ρ_m density of the reinforcement and alloy materials respectively.

The void contents of the indicate composites are quantified by using Eq. 3.6 given below.

$$void\ \ fraction = \frac{theoretical(\rho_t) - \exp erimental(\rho_e)}{theoretical(\rho_t)} \tag{3.6}$$

3.5.2. Hardness

The micro hardness of the particulate filled metal alloy composite is analyzed over the Walter Uhltesting machine (ASTM E92) having square based pyramidal (Angle 136° between two opposite faces) diamond indenter the quadrate value read on the 'C' scale (Figure 3.18). The value of applied load per capita is 50 gm for 15 sec period and this process is restated five times with each sample at different locations. After that the average hardness is taken to ignore malfunctioning of the results. Proceeding to perform the test, the sample should have flat and polished surface. The Vickers hardness number (VHN) is measured as [247];

$$VHN=1.854\times\frac{F}{d^{3}} \tag{3.7}$$

Where, F is load in kg, and d is the mean diagonal i.e. d= (d1+d2)/2 in mm.

Figure 3.18. Micro-hardness testing machine

3.5.3.Compressive strength

To determine the compressive strength for different composition of reinforced particulate filled metal alloy composites followed by ASTM E9-09 [233] standard on the universal testing machine (UTM) Instron 1195. The test is carried out with the specimen dimension

of 25×10×10 mm^3 at 2mm/s cross-sectional speed. The often used specimen for the compressive test is fixed from one end, and force applied from the other end of the specimen.

3.5.4. Bending strength

The flexural or bending strength of the said composites is determined by the using universal testing machine (UTM) following ASTM-E290 [233], Instron 1195 for the specimen with the standard size of 50×8×8 mm^3 having span length of 40 mm at 2mm/s cross-sectional speed (Figure 3.19). The flexural strength given as,

$$FS = \frac{3PL}{2bt^2} \tag{3.8}$$

Where, P is the maximum load, b the width of specimen and t the thickness of specimen and L is the length of the sample.

3.5.5. Impact strength

To found the impact strength of the fabricated composite material impact test is done as per ASTM-E23 [233] using impact tester with the standard specimen size of 55×10×10 mm^3 and the notch depth is 2mm (Figure 3.20). During the test machine is adjusted such that the blade on the free hanging pendulum just narrowly contracts the specimen (zero position). Since in this test practically no losses due to bearing friction, etc. (<0.3%), so the testing conditions may be appraised as ideal.

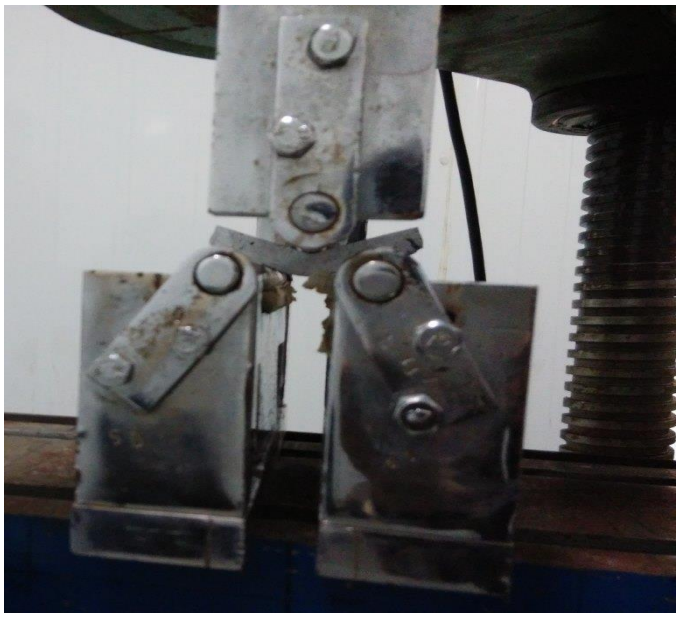

Figure 3.19. Flexural strength testing machine (UTM)

During impact test the specimens clamped in a square support and bang at their central point by a hemispherical bolt of diameter 5 mm. The appropriate values of the impact energy of different specimens are documented directly from the dial indicator.

Figure 3.20. Impact strength testing machine

3.5.6. Fracture toughness analysis

Fracture analysis (ASTM-E399) [233] of the fabricated composites is found by measuring the value of stress intensity factor (SIF) also known as fracture toughness by the use of Single Edge Notched Tension (SENT) specimens (Figure 3.21). The specific dimensions for specimen are length (L) = 50mm, thickness (B) = 5 mm, width (W) = 5 mm with the varying crack length of (1, 2, 3 and 4 mm). The specimens have a longitudinal-transverse (LT) crack plane orientation. The fracture test for specimen performed on UTM instron 1195 with the cross-head velocity of 1 mm/min. The mode-1 i.e. tensile mode used for crack opening due to the large thickness of specimen as a comparison to crack length, to elongate the crack surface in outward directions. The stress intensity factor is obtained by using Eqs. (3.9) and (3.10) [241] as;

$$K_I = \frac{P}{B\sqrt{W}}\gamma(\beta) \tag{3.9}$$

$$\gamma(\beta) = \frac{\sqrt{2tan\frac{\pi a}{2W}}}{cos\frac{\pi a}{2W}}[0.75 + 2.02\left(\frac{a}{W}\right) + 0.37(1 - sin\frac{\pi a}{3W})^3 \quad (3.10)$$

Where, P is maximum load (Stress) in N, B is a thickness of the specimen, W is the width of a specimen and 'a' is the crack length of the specimen.

Figure 3.21. Universal Testing Machines

3.6. Dynamic Mechanical Analysis

Dynamic Mechanical Analysis (DMA) of the particulate filled metal alloy composites is carried out to investigate the variation of storage modulus (E'), loss modulus (E'') and damping factor (Tan δ) as a function of temperature to characterize the thermo-mechanical response at different wt. - % of reinforcement (Figure 3.22). Dynamic Mechanical Analysis (DMA) is conducted at a fixed frequency of 1Hz heating rate of 5^0 C/min, a temperature range of 25-300^0 C on a rectangular sample with approximate dimensions of 30×10×2.5mm^3 using Perkin Elmer's instrument in a three point bending mode.

Figure 3.22. Dynamic Mechanical Analyzer

3.7. Thermo gravimetric analysis

Thermo-gravimetric analysis (TGA) measures the amount and rate of change in weight of a material as a function of temperature or time in a controlled atmosphere (Figure 3.23). Measurements are used primarily to determine the composition of materials and to predict their thermal stability at temperatures up to 1000^0C.

Figure 3.23. Thermo Gravimetric Analyzer

The technique can characterize materials that exhibit weight loss or gain due to decomposition, oxidation, or dehydration. Thermo-gravimetric analysis is most widely used the measurement of mass loss of material as a function of temperature.

3.8. Sliding wear test conditions

The sliding wear tests in dry lubricating condition is performed for reinforced filled metal alloy composite using a pin-on-disk tribometer (Model TR 20, Ducom, Bangalore, India) as per ASTM G 99 standard (Figure 3.24 and Figure 3.25). During the test the specimen (Pin) (Figure 3.26) held stationary and the disc (Figure 3.27) is rotated under dry condition and the load is applied through a lever mechanism. The tribometer has one counter body, a disc that made of EN-31 hardened steel (with hardness 60-70HRC). A fixed wear track of diameter 50 mm is used for all the tests, based on the track diameter the sliding velocity is calculated as 1.024, 2.094, 3.140, 4.188 and 5.235 m/sec respectively in the experimental work. The wear loss is measured directly as the vertical length loss of the specimen using LVDT method.

The coefficient of friction and frictional force for particulate filled metal alloy composites are also monitored continuously and the readings are recorded separately using WINDCOM 2007 software for individual test run. The major component in this research is a variation of environment temperature during sliding wear test, which is available with the sliding wear tester. The environment temperature varies from 25^0 C to 45^0 C at an interval of 5^0 C as per our Taguchi design of experiment in this analysis. The variation in temperature of the particulate filled metal alloy composites are also measured during test run through a thermocouple which get inserted in a hole placed over stationary pin holder. After sliding wear the material loss of composite is measured by a precision electronic balance with an accuracy of ±0.001 g. Finally, the specific wear rate (mm^3/N-m) is calculated as [248]:

$$Ws = \frac{\Delta m}{\rho.Vs.t.Fn} \tag{3.11}$$

Where, Ws is specific wear rate in mm^3/N-m,Δm is mass loss of composite during test(gm.),ρ is the density of the composite (g/cm^3), Vs is the sliding velocity (m/s),t is the test duration (s), and Fn is the normal load (N). The mass loss of the specimen per unit sliding distance per unit applied normal load defined as specific wear rate of composite.

Figure 3.24. Pin on Disc Tribometer Equipment

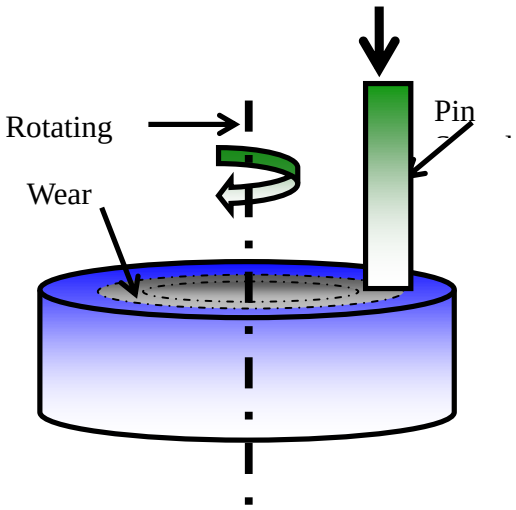

Figure 3.25. Schematic representations of the pin-on-disc wear test apparatus

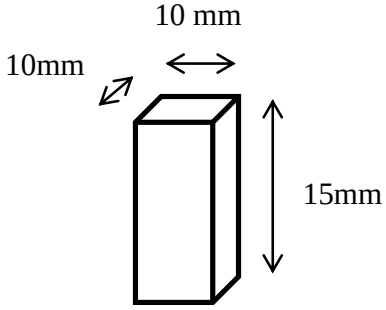

Figure 3.26. Particulate filled metal alloys composite materials pin sample

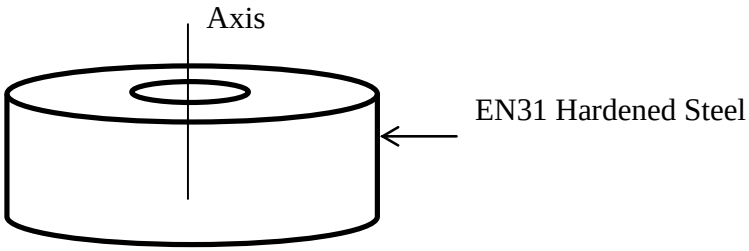

Figure 3.27. A circular disc of EN31 hardened steel

3.8.1. Experimental Design

Taguchi method is used for optimization of sliding wear rate of reinforced filled metal alloy composites for bearing application. As Taguchi method is an effective optimization tool capable of optimize simultaneously multiple variables and multiple responses. This technique is capable enough to minimize the experimental run without considerable data loss and become an effective method to solve complex problems in manufacturing sectors and gray relation analysis (GRA) therefore; different experiments are performed according to a Taguchi design of experiments. In this method, the performance characteristics represented by S/N ratio and Lower-is-Better (LB) characteristics approach that implemented as present work is purely based on the wear rate of the particulate filled metal alloy composites. In this work, five input factors i.e. sliding velocity, filler content, normal load, sliding distance and environment temperature have been selected (Table 3.11) and one output parameter such as specific wear rate by using L_{25} orthogonal array design. The S/N ratio with a LB characteristic can be expressed as [249]:

$$\frac{S}{N} = -10\log\frac{1}{n}(\Sigma y2) \tag{3.12}$$

Where, n= number of observation and y = observed data.

Finally, the analysis of variance (ANOVA) is calculated to find the significant factor setting and along with their factor ranking for better output performance.

Table 3.11. Levels of experiment variables

Control factor	Level					
	I	**II**	**IIII**	**IV**	**V**	**Units**
Sliding Velocity (A)	1.047	2.094	3.140	4.188	5.235	m/sec
Filler Content (B)	0	2.5	5	7.5	10	%
Normal Load (C)	5	15	25	35	45	N
Sliding Distance (D)	500	1000	1500	2000	2500	m
Environment Temperature (E)	25	30	35	40	45	°C

3.8.2. Taguchi design experimental analysis

Taguchi design used to get the optimum result of the different factors by using an orthogonal array. L_{25} orthogonal array to be used with the five factors and five levels, and the factors are sliding velocity, filler content, normal load, sliding distance and environment temperature respectively.

Table 3.12. Orthogonal array for L_{25} (4^5) Taguchi method

Expt. No	A (Sliding velocity)	B (Filler content)	C (Normal Load)	D (Sliding Distance)	E (Environment Temperature)
1	1	1	1	1	1
2	1	2	2	2	2
3	1	3	3	3	3
4	1	4	4	4	4
5	1	5	5	5	5
6	2	1	2	3	4
7	2	2	3	4	5
8	2	3	4	5	1
9	2	4	5	1	2
10	2	5	1	2	3
11	3	1	3	5	2
12	3	2	4	1	3
13	3	3	5	2	4
14	3	4	1	3	5
15	3	5	2	4	1
16	4	1	4	2	5
17	4	2	5	3	1
18	4	3	1	4	2
19	4	4	2	5	3
20	4	5	3	1	4
21	5	1	5	4	3
22	5	2	1	5	4
23	5	3	2	1	5
24	5	4	3	2	1
25	5	5	4	3	2

The eighth column shows the S/N ratio of the wear rate for reinforced filled metal alloy composites with different wt.-%. The overall S/N ratio is found to be in decibel (dB) unit

by the use of MINITAB 16 software Taguchi design have been done (Table 3.12). Effect of control factors shows by the figure that leads the conclusion towards a better combination of factors for reinforced filled metal alloy composites. By this method the accurate fabrication technique and the correct wt.-% of filler also found which also give its bit to wear rate of composite materials. L_{25} orthogonal array Table 3.12 shows the response for a signal to noise ratio of five factors which gives smaller the better value. From the table, it also shows that the filler particles have a most significant effect on the specific wear rate of reinforced filled metal alloy composites that followed by different parametric range for sliding velocity, sliding distance, normal load and pin temperature parameters.

3.8.3. ANOVA and the effect of factors

Analysis of variance (ANOVA) gives the better feel for the relative effect of its different factors that obtained through the decomposition of variance. Different factors to determine the specific wear rate by the ANOVA are sliding velocity, filler content, normal load, sliding distance and pin temperature.

Table 3.13. ANOVA table for specific wear rate

Source	DF	Seq. SS	Adj. SS	Adj. MS	F	P
A	4	-	-	-	-	-
B	4	-	-	-	-	-
C	4	-	-	-	-	-
D	4	-	-	-	-	-
E	4	-	-	-	-	-
Error	4	-	-	-	-	
Total	24	-		-		

DF - Degree of freedom, Seq. SS - Sequential sum of square, Adj. SS - Adjacent sum of square, Adj. MS - Adjacent sum of mean square, F – Variance, P - Test (Percentage contribution of each factor in overall performance to find out optimum specific wear rate)

Table 3.13 shows the result of ANOVA with specific wear rate for different wt.-% of reinforced filled metal alloy composites. This analysis is undertaken for a level of significance of 5% that is for a level of confidence of 95%. In Table 3.13 last columns represent the test i.e. the percentage contribution of each and individual factor on the total

variation and then the degree of influence on total results. Table 3.13 shows that significance of different parameters on outcomes of fabricated composite materials.

3.9. Surface morphology studies

The surface morphology of reinforced filled metal alloy composite is studied under field emission scanning electron microscope (FE-SEM) manufactured by FEI Nova Nano SEM 450, USA.

Figure 3.28. Field emission gun FE-SEM /EDAX

SEM machine also having energy dispersive X-ray (EDAX) with this, for measuring the different chemical composition of materials under FE-SEM. The FE-SEM is used for the high magnification images in various applications such as engineering, aerospace,

medical, electronics etc. EDAX is used to characterize the elemental or chemical analysis of the sample.

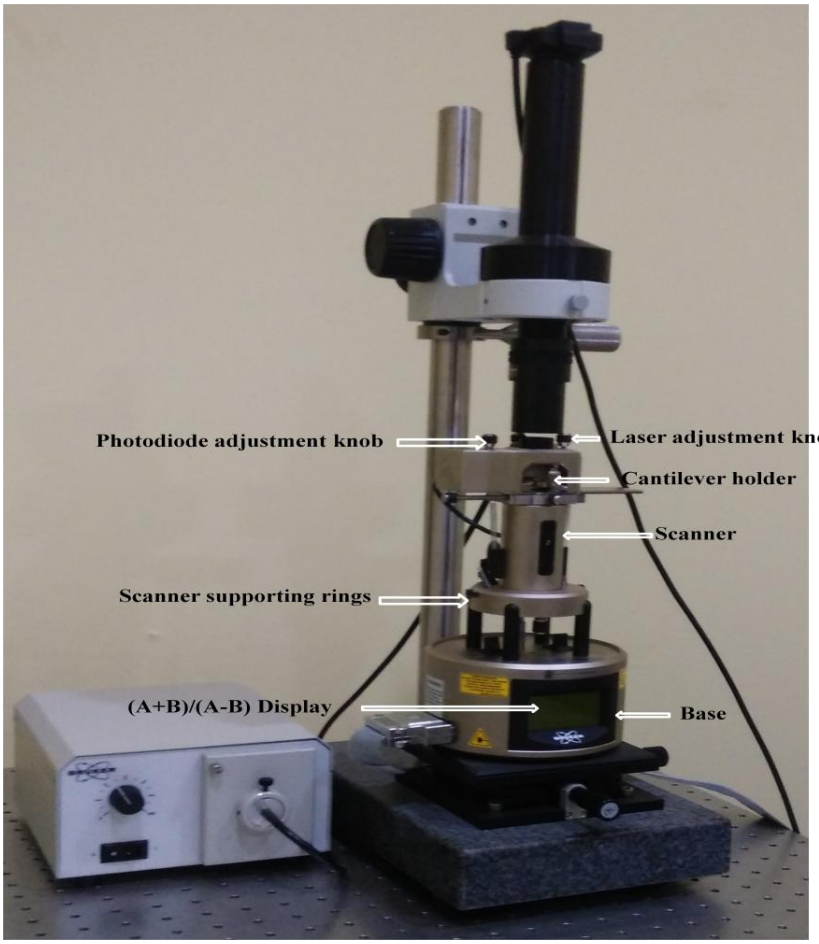

Figure 3.29. Atomic force microscopes

The atomic force microscope (AFM) that also known as scanning proves microscope is used to study about the surface profile, which thousand times better than the optical diffraction limit. It's mainly used to measure the surface roughness of the sample with high resolution.

3.10. Optimization of physical, mechanical and sliding wear behavior of the proposed composites using preference selection index (PSI) method

The optimization technique used to choose the foremost value from the set of available outcomes. This technique is one of the ancient and better ways to get the accurate solution of any problem. Different optimization methods are used for getting the optimum values such as Fuzzy Analytic Hierarchy Process (FAHP), Fuzzy Technique for Order

Preference by Similarity to an Ideal Solution (TOPSIS), Balanced Scorecard (BSC), PSI technique, etc. for different kind of applications. In the present thesis work, preference selection index (PSI) optimization technique is adopted to get the superlative result. This technique based on the idea that optimum properties of fabricated composite materials marked as nearer to exemplary explanation and shows by the highest-ranked value. The detailed PSI optimization techniques for particulate filled metal alloy composite materials are elaborated by the following points.

The various steps of PSI method can be expressed as [250]:

Step 1: Identification of the alternatives and criterions.

Step 2: After identification of alternatives and PDC a decision matrix is created.

$$D_{M\times N} = \begin{bmatrix} d_{11} & d_{12} & \dots & d_{1N} \\ d_{21} & d_{22} & \dots & d_{2N} \\ \vdots & \vdots & \dots & \vdots \\ d_{M1} & d_{M2} & \dots & d_{MN} \end{bmatrix} \tag{3.13}$$

If the numbers of alternatives are M (A_i, i=1, 2, 3… M), and numbers of PDC are N (C_j, j=1, 2, 3… N), then the decision matrix having an order of M×N is represented as:

Where, an element d_{ij} of the decision matrix $D_{M\times N}$ represents the actual value of the i^{th} alternative in term of j^{th} performance defining criteria.

Step 3: In order to measure all criterions in dimensionless units the entries of the decision matrix are normalized so that different values of the decision matrix become comparable in the range of 0-1. The normalization of the decision matrix performed according to the benefit (larger-the-better) and cost (smaller-the-better) criteria as:

$x_{ij} = \frac{d_{ij}}{d_j^{\max}}$, if j is the benefit criteria and

$x_{ij} = \frac{d_j^{\min}}{d_{ij}}$, if j is the cost criteria (3.14)

Step 4: In this step, the mean of the normalized (χ_j) value of PDC j is determined by using the equation:

$$\chi_j = \frac{1}{M}\sum_{i=1}^{M} x_{ij} \tag{3.15}$$

Step 5: In this step, preference variation value (φ_j) for each PDC is determined with the help of the following equation:

$$\varphi_j = \sum_{i=1}^{M}\left[x_{ij} - \chi_j\right]^2 \tag{3.16}$$

Step 6: In this step the deviation in the preference variation value (Δ_j) is determined for each PDC by using the following equation:

$$\Delta_j = 1 - \varphi_j \tag{3.17}$$

Step 7: In this step, the overall preference value (ζ_j) is determined with the help of the following equation:

$$\zeta_j = \frac{\Delta_j}{\sum_{j=1}^{N}\Delta_j} \tag{3.18}$$

Moreover, the total overall preference value of all the PDC should be one i.e. $\sum_{j=1}^{N}\zeta_j = 1$

Step 8: In this step, the preference selection index (ϖ_i) value for each alternative is determined by using the following equation:

$$\varpi_i = \sum_{j=1}^{N}\left(x_{ij} \times \zeta_j\right) \tag{3.19}$$

Finally, after the calculation of the ϖ_i value of each alternative, the entire alternatives are then ranked according to the ϖ_i value. The alternative with the highest ϖ_i value is ranked highest.

Chapter Summary

This chapter briefly explains properties of selected ingredients for this research work, their compositional combination variables, fabrication methodology, various testing for physical and mechanical characterization (density, void-fraction, hardness, compressive strength, flexural strength, impact strength and fracture toughness), thermo-mechanical and sliding wear behavior both experimental and FEM-modeling. Also, include the PSI

optimization technique to get the optimum result by these materials properties for fabricated composite materials.

The next chapter concluded study about the physical, mechanical and fracture toughness properties of the particulate filled metal alloy composites.

******

Chapter 4

Physical, Mechanical and Fracture Analysis of Particulate Filled Metal Alloy Composites

Chapter 4

PHYSICAL, MECHANICAL AND FRACTURE ANALYSIS OF PARTICULATE FILLED METAL ALLOY COMPOSITES

This chapter presents the measured values of the physical, mechanical and fracture toughness behaviour of particulates filled metal alloy composites. This chapter consists of two parts, the part-1 discussed the physical, mechanical and fracture toughness of the marble dust filled ZA-27 alloy composites and the part-2 discussed the same properties of CaO filled ZA-27 alloy composites. In this research work, single row deep groove ball bearing 6200 standard dimension is taken for calculation of contact stress and displacement through finite element simulation model and compared the simulated results with Hertzian theory for constant applied load.

Part I

4.1 Physical, Mechanical and Fracture analysis of Marble Dust (MD) particulate filled ZA-27 alloy composites

4.1.1 Effect of void contents on MD particulate filled ZA-27 alloy composites

The theoretical and experimental density of the marble dust particulate filled ZA-27 alloy composites are presented in Table 4.1. From Table 4.1 it is observed that the void content reduced with the increased in filler content from 0wt.% to 7.5wt.-% marble dust filled i.e. from 1.80 to 1.20% respectively. However, on further increased in filler content from 7.5wt. % to 10wt. % the void contents slowly increased to 2.62%. The lower value of density for any composite shows the insufficient bonding between matrix and reinforcing material due to the presence of voids and may be agglomeration of particulates in the matrix body during the casting process. Therefore, the resulting particulate filled alloy composite may be exhibited variations in the desired homogeneity. Furthermore, Ruch et al. [251] also clearly reported that in case of particulate filled low ductility alloy composites has not shown any significant mechanical strength in vertical casting process. The presences of these defects may be inhomogeneous mixing of matrix and reinforced particles due to which it affects the properties of composite during the performance [26]. However, void contents in most of the cases are found to be observed; it may possible to reduce by obeying proper fabrication technique. The increased in void content may be attributed to the improper filling of the gap between particulates and matrix material and there may be another

reason the increased in void content of the composites is increased of contact surface area [252].

Table 4.1. Comparison of experimental density and theoretical density

Sl.No.	Composition	Theoretical density (gm./cc^3)	Experimental density (gm./cc^3)	Void content (%)
1	ZAMD-1	5.00	4.91	1.80
2	ZAMD-2	4.89	4.81	1.64
3	ZAMD-3	4.78	4.71	1.46
4	ZAMD-4	4.68	4.62	1.28
5	ZAMD-5	4.58	4.46	2.62

4.1.2. Effect of hardness on MD particulate filled ZA-27 alloy composites

Figure 4.1 represents the hardness of marble dust particulate filled ZA-27 alloy composites with five different weight percentages of marble dust content. The hardness of the unfilled and marble dust particulate filled alloy composites are showing increased in trend (from 149Hv to 204Hv) with the increased in filler content i.e up to 7.5wt.%. However, on further increased in marble dust content i.e 10wt.% the hardness of the filled alloy composite slightly decreased (i.e 178Hv) as shown in Figure 4.

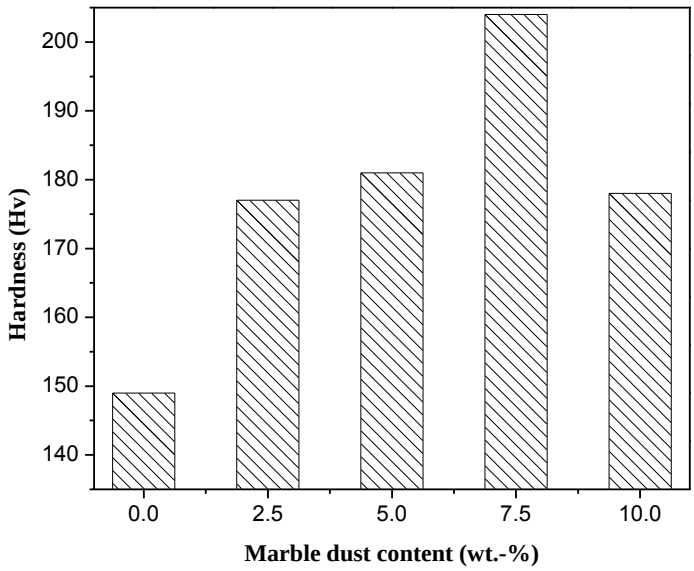

Figure 4.1. Variation of micro-hardness of MD particulate filled ZA-27 alloy composites

Kim et al. [253] explained that the hardness of particulate filled alloy composite are increased because of increased in strain energy at the periphery of the reinforced particles in the alloy matrix material. Similarly, in another study Deuis et al. [254] reported that the increased in hardness of alloy composite is only because of dispersion of higher quantity of hard ceramic particles in the matrix material as well as good interface bonding between them. Again Manojet al. [47] explained about improvement of hardness by the incorporation of SiC particulates in matrix composites is due to increase in SiC particle concentration associated with indentation up to 25wt.% of SiC. However, on further increased in SiC particulates in the matrix material the hardness trend started decreasing in nature leading to clustering of reinforcing particles. Similar, observation also reported for SiC particles filled metal alloy composites by reducing the grain size of the matrix as well as the peak hardness of the composite is higher than the alloy [255].

4.1.3. Effect of compressive strength on MD particulate filled ZA-27 alloy composites

The strength of the metal alloy composite is enhanced by the incorporation of hard ceramic particles to improve the strengthening mechanism that occurred in particulate filled metal composites. The strengthening mechanism is due to reduction in composite matrix grain size and dislocation in the matrix body resulted in thermal expansion between matrix material and the particulates. These effects include the transfer of stress from the matrix body to the particulate and the interaction between individual dislocations [256, 257]. Figure 4.2 shows the compressive strength of marble dust filled ZA-27 alloy composites and observed that with the increased in wt.-% (0wt.-% to 10wt.-%) of marble dust reinforcement the amount of compressive strength is increased up to 7.5 wt.-% MD reinforcement (i.e.665 MPa) and on further increased in filler content from 7.5wt.-% to 10 wt.-% the compressive strength (i.e. 655MPa) starts decreasing in trend. A similar observation is also reported by Jayalakshmi et al. [258], studied Mg particle filled $Ni_{60}Nb_{40}$ alloy composite and found that the composite have higher strength as compared to pure Mg alloy, they reported up to 85% increment till 5wt.-% of filler particles and later up to 10 wt.-%, there is no further enhancement in strength with respect to increase in filler particles in base alloy.

The distributions of reinforced particle in composites are strongly dependent upon the response of materials, but inhomogeneous mixing of reinforced particles for

larger amount can be the reason of decreasing in compressive strength. However, in another study Agari et al. [259] prepared Al_2O_3 particle filled ZA-27 alloy composites by centrifugal casting process and observed that for conventional filler the compressive strength is increased up to 20 wt.-% of alumina reinforcement particles and again on further addition of Al_2O_3 content beyond 20wt.-% the reduction in compressive strength is observed. This may be the formation of a cavity in between the matrix and filler particles which shows the decrement in compressive strength due to decrease in load transfer from matrix to filler particles.

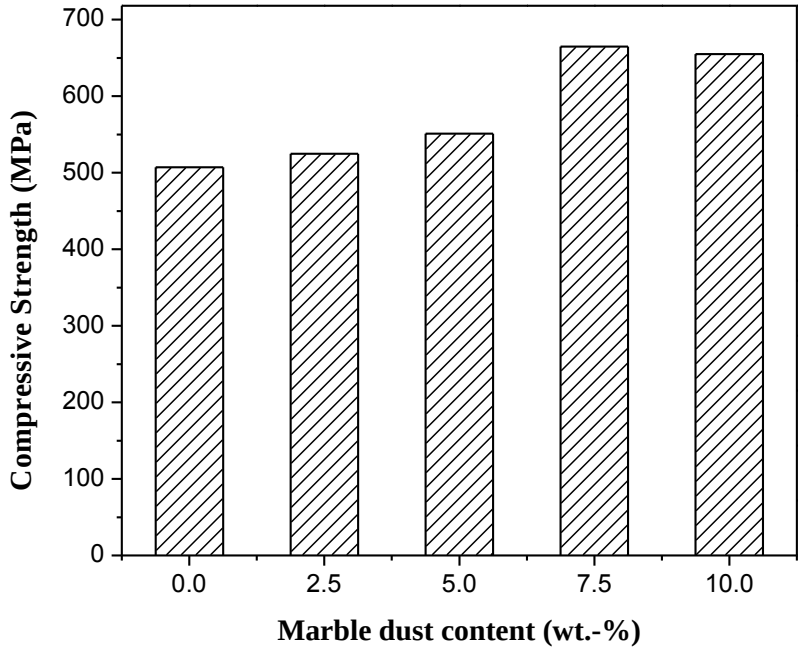

Figure 4.2. Compressive strength of MD particulate filled ZA-27 alloy composites

4.1.4. Effect of flexural strength on MD particulate filled ZA-27 alloy composites

The flexural strength of the marble dust particulate filled ZA-27 alloy composites is shown in Figure 4.3 and the magnitude of strength increases with respect to increases in wt.-% (2.5, 5, 7.5 and 10 wt.-%) of marble dust in ZA-27 alloy composites. The maximum value of flexural strength is found to be 684.34 MPa for 10wt.-% of MD filled ZA-27 alloy composites. Probably higher volume of reinforcement causes larger number of microstructure defect and increase the composite brittleness. During bending tests at the side of the specimen with prevalent tension stresses, particles are strongly loaded and cracked mainly in region under point probe of tester. In a particulate filled alloy composite generally containing strong matrix phase as well as

strong interface, therefore the crack propagation is generally taking place across the matrix and the reinforcing phase. In the present research work, the flexural strength of the unfilled and particulate filled alloy composites is showing increasing in trend with the increase in filler content in the matrix material. As far as bearing application bending strength is also one of the major parameter to improve the performance of the bearing material. A similar study is also reported by Long et al. [92] for SiC particles filled aluminium alloy composites and observed same increasing in flexural strength trend. The hardened particles of SiC mixed with matrix particles having good bonding between interfaces with matrix particle.

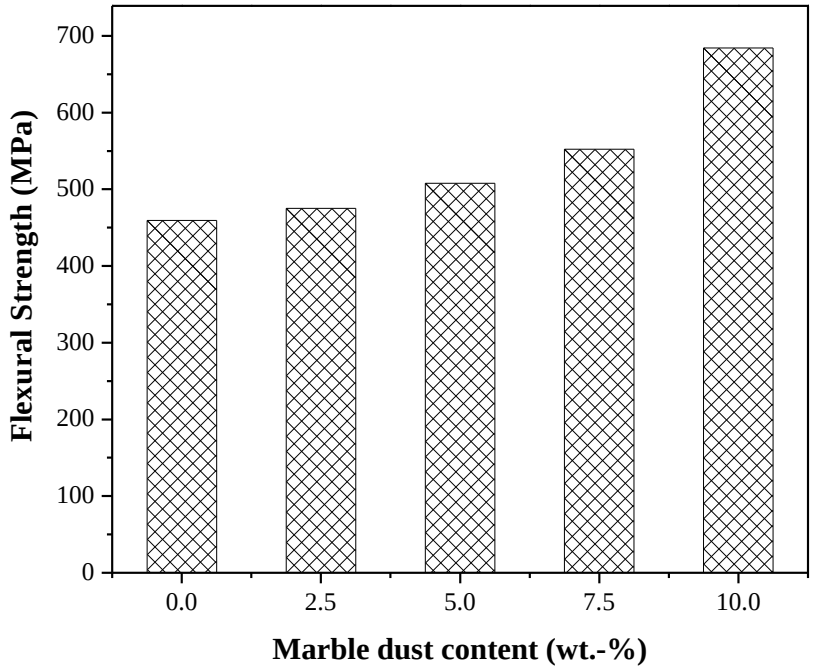

Figure 4.3. Flexural strength of MD particulate filled ZA-27 alloy composites

4.1.5 Effect of impact strength on MD particulate filled ZA-27 alloy composites

Figure 4.4 shows the impact strength of marble dust filled ZA-27 alloy composites with the variation of marble dust from 0wt.% to 10 wt.% respectively. It is observed that with the increased in increased in filler content up to certain extent the impact strength of the filled alloy composites are also increased from 3J to 6J respectively. But beyond 7.5 wt.-% marble dust filled ZA-27 alloy composites the test result shows decreased in impact load absorption. From this analysis it is also observed that with the increased in filler content in the alloy composites the density of the alloy

composites are also decreased. Therefore, marble dust filled ZA-27 alloy composites can be used in specific applications where the weight reduction of the composite is desirable. Singla et al. [47] studied the impact strength behavior of SiC filled aluminium alloy composites and concluded that with the increased in wt.-% of SiC particles, the impact strength of the filled composite also increases. The best result for impact strength is found for 25 wt.-% of SiC reinforced particles in aluminium alloy composites is 36 N-m [260]. A similar observation is also published by Mamatha et al. [26] for alumina filled ZA-27 alloy composites and the improvement of impact strength can occur due to embitterment effect, through which reinforced particles block the movement in matrix due to which the local stress concentration locations get decreased.

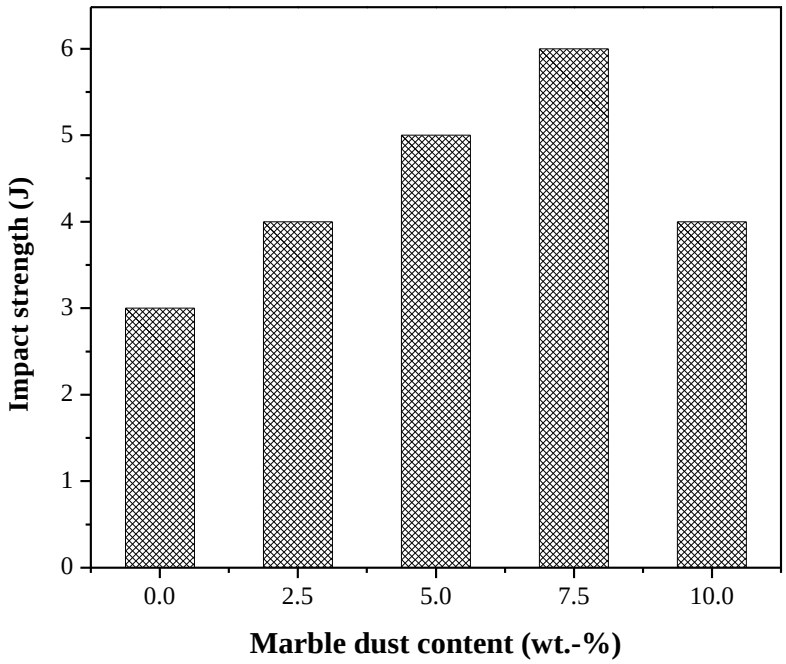

Figure 4.4. Impact strength of MD particulate filled ZA-27 alloy composites

4.1.6 Effect of stress intensity factor on MD particulate filled ZA-27 alloy composites

The magnitude of stress intensity factor for marble dust filled ZA-27 alloy composites is evaluated by using Eqs. 3.9 and 3.10 at four different crack lengths, as shown in Figure 4.5. From Figure 4.5 it is observed that the unfilled alloy composite shows lower value of SIF as compared to the particulate filled ZA-27 alloy composites. The maximum value of SIF is found at 7.5 wt.-% MD particulate filled alloy composite

(i.e. 1.899 MPa.m^1/2 for 4mm crack length). The dispersal of fine spherical particles in matrix material can be enhanced the value of fracture toughness [260]. It is noticed from Figure 4.5 that the SIF value increases with the increased in crack lengths from 1mm to 4mm respectively. The SIF value up to 7.5 wt.-% MD reinforcement swell but for 10wt.-% MD reinforcement the SIF is slightly reduced; this may be due to the presence of large amount of filler particles that incapacitated the interface bonding strength between atoms of composites. Somekawa et al. [260] studied the fracture toughness of Mg-Zn-RE alloys prepared by casting and extrusion process, the fracture toughness of the extruded magnesium is increased with grain refinement. The grain refinement for composite helps to prevent the formation of deformation twin that initiate the micro-crack. From the literature it was concluded that the SIF depends upon the different mechanical properties, such as crack size, an interface between contacting materials and on applied loading conditions on materials [47].

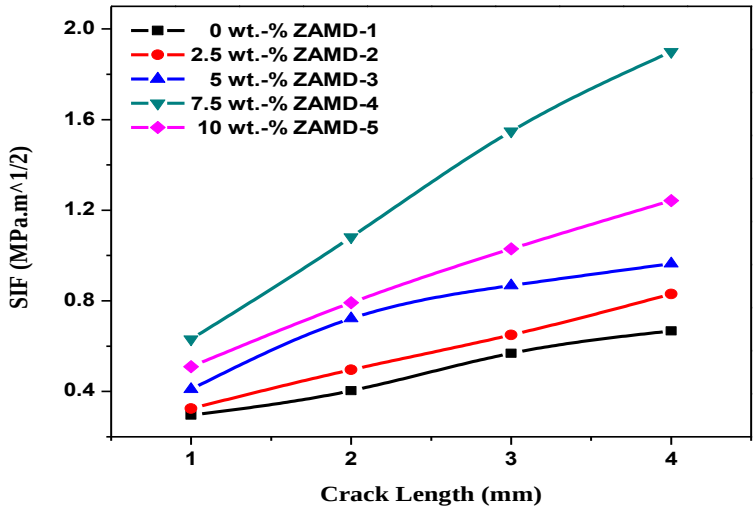

Figure 4.5. Mode I stress intensity factor for MD particulate filled ZA-27 alloy composite

Table 4.2. Stress Intensity Factor (K) of MD particulate filled ZA-27 alloy composites with different crack lengths

Sl.No.	Compositions ⇩ Crack length ⇨	1mm	2mm	3mm	4mm
1	ZAMD-1	0.2951	0.4032	0.5685	0.6672
2	ZAMD-2	0.3245	0.4962	0.6493	0.8300
3	ZAMD-3	0.4095	0.7218	0.8673	0.9638
4	ZAMD-4	0.6306	1.0813	1.5483	1.8991
5	ZAMD-5	0.5098	0.7916	1.0296	1.2425

4.1.7. Fractographs of MD particulate filled ZA-27 alloy composites

The process of examine any fractured surface after fracture test for any material is known as fractography. Where the material get separated into two or more pieces with the presence of crack after the fracture under applied stresses on it and then the fractography used to study about the surface of fractured materials [261]. Fractography generally used in engineering structures to determine the cause of failure for any particular application by the studying of fractured surfaces.

Scanning electron microscopic (SEM) fractographs are examined after fracture test of five different (0wt.-%, 2.5wt.-%, 5wt.-%, 7.5wt.-% and 10wt. - %) marble dust particulate filled ZA-27 alloy composites as shown in Figure 4.6(a-e). The SEM Fractography for unfilled ZA-27 alloy composite is shown in Figure 4.6a and the nature of micrograph is shown as ductile in behaviour. Figure 4.6b shows the SEM fractography of 2.5 wt.-% of marble dust filled ZA-27 alloy composites and observed that presence of cleavage fracture at number of places due to fracture [262].

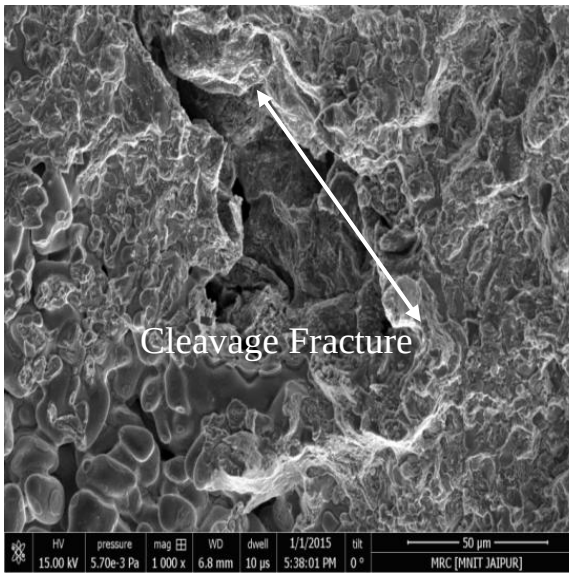

Figure 4.6a. SEM fractographs for 0 wt.-% of MD particulate filled ZA-27 alloy composites after fracture test

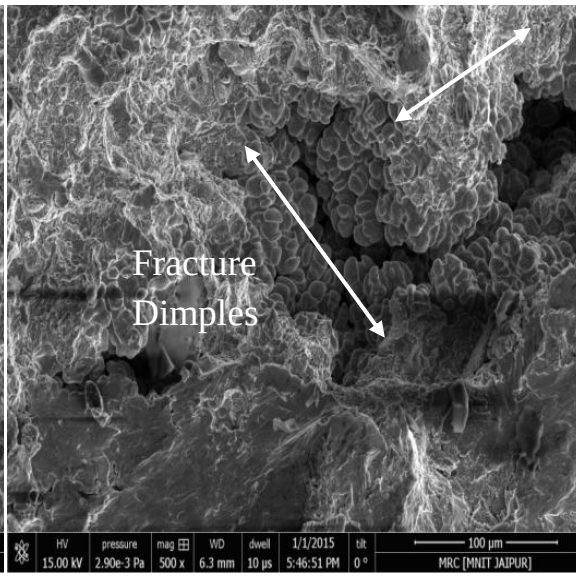

Figure 4.6b. SEM fractographs for 2.5 wt.-%of MD particulate filled ZA-27 alloy composites after fracture test

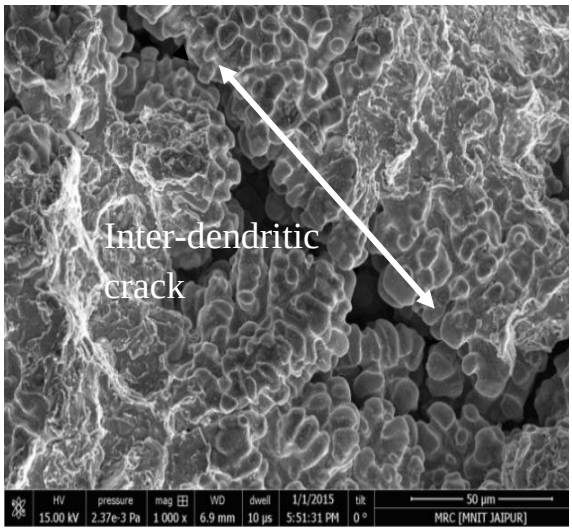

Figure 4.6c. SEM fractographs for 5 wt.-% of MD particulate filled ZA-27 alloy composites after fracture test

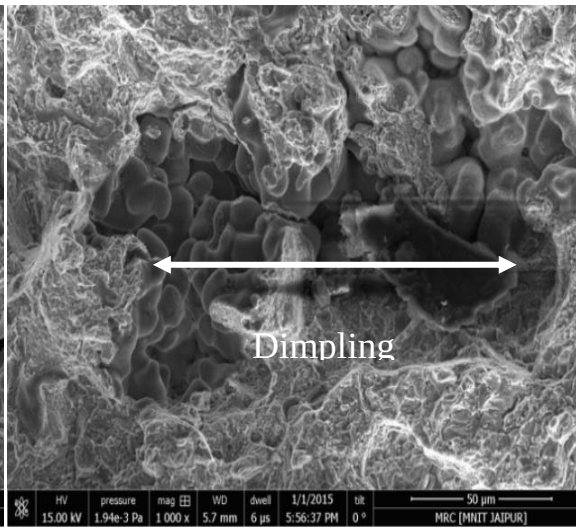

Figure 4.6d. SEM fractographs for7.5 wt.-% of MD particulate filled ZA-27 alloy composites after fracture test

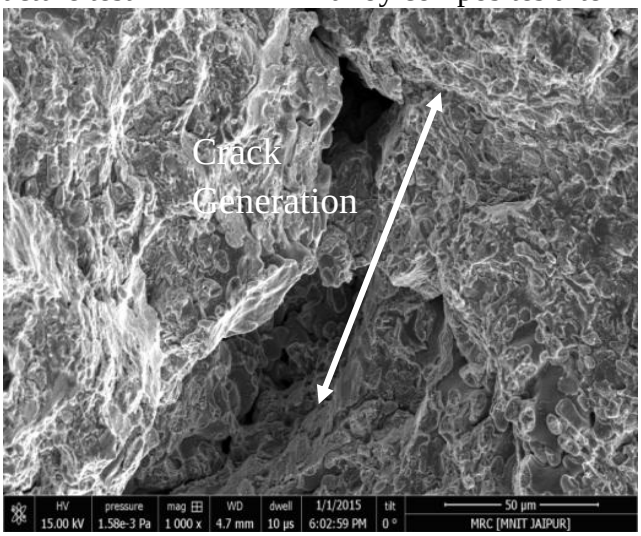

Figure 4.6e. SEM fractographs for 10 wt.-% of MD particulate filled ZA-27 alloy composites after fracture test

Figure 4.6.SEM fractographs for MD particulate filled ZA-27 alloy composites after fracture test

The fractured surface of composite consist of dimples and it is generated due to void nucleation and coalescence that produced by shear deformation or fracture at the shear plane [262,263]. As reported by Hwu et al. [263] about the presence of dimples for SiC filled alloy composites and concluded that composites interface show the atomic bonding between these two are strong enough such that at higher applied stress required breaking of bond at the interfaces. Similarly, SEM fractography for 5 wt.-% marble dust particulate filled ZA-27 alloy composite is shown in Figure 4.6c at 1000 magnification. Figure 4.6c shows the presence of crack is found due to

formation of inter-dendritic-crack [264] due to which the presence of cracks get degrades the ductility of composite materials. Figure 4.6d shows the SEM fractographs for 7.5 wt.-% of marble dust particulate filled ZA-27 alloy composites and the presence of voids or dimple is found because of applied stress at the soft ductile material, that losses the bonding between atoms of composite material during fracture process [49]. Figure 4.6e shows the fractographs of 10wt.-% of marble dust filled ZA-27 alloy composites and in fracture surface the clustered region of filler particles crack more easily and ultimately damaged the clustered region [264].

4.1.8. Effect of hardness, contact stress and deformation of MD particulate filled ZA-27 alloy composites

In this research work, single row deep groove ball bearing 6200 standard is taken for calculation of contact stress and displacement through finite simulation analysis and compared the simulated results with Hertzian theory for constant applied load. From Figure 4.7 and Table 4.3 are shown the comparison of experimental and simulated results at constant load of five different particulate filled alloy composites. The generated hardness has been determined at certain variable using the Brinell Hardness Formula. The error lies between theoretical and a simulation analysis is in between 0.005% to 1.5% respectively. The hardness of the composites is varying on varying the weight percentage of the marble dust. It is observed that on increasing the weight percentage of marble dust the hardness also increases gradually.

The contact deformation and contact stress of the entire unfilled and particulate filled ZA-27 alloy composites are calculated at constant force i.e. 500N applied on deep groove ball bearing by using ANSYS simulation software [265] as shown in Figure 4.8. Table 4.4 indicates the contact stress, displacement and stress Intensity result of particulate filled metal alloy composites at different modulus of elasticity as calculated experimentally. Table 4.5 shows the comparison of theoretical and simulated results at constant load of different particulate filled alloy composites. The generated contact stress has been determined at certain variable using the Hertzian contact theory. The error lies between theoretical and simulation analyses are lying in between 0.69% to 5.82% respectively. The percentage of error may also possible to reduce by increasing the simulation time three to four times more than the present simulation period.

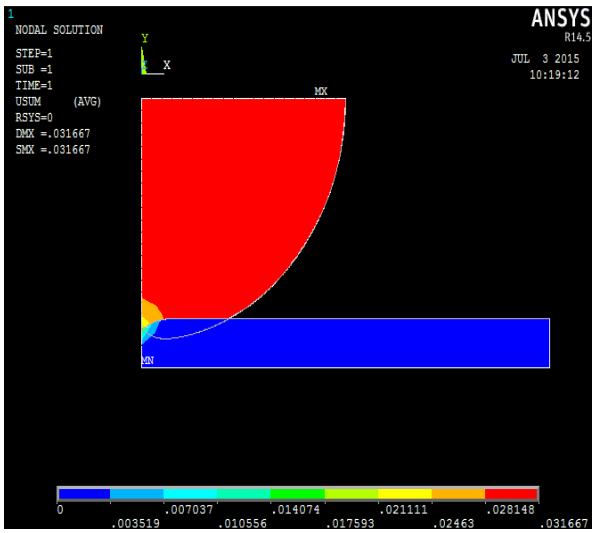

(a) 0 wt.-% MDZA-1

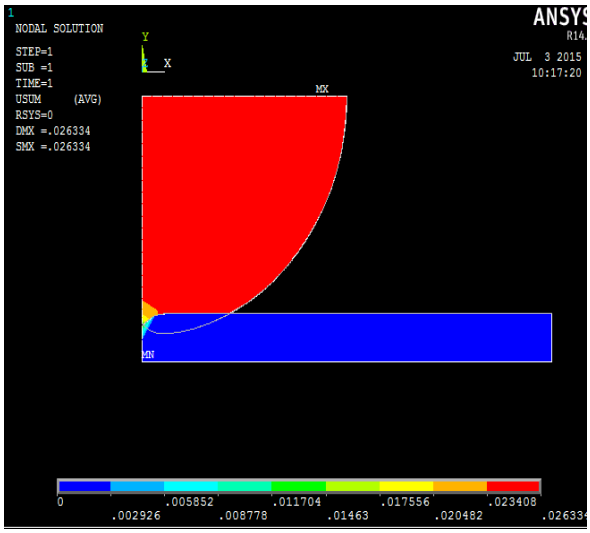

(b) 2.5wt.-% MDZA-2

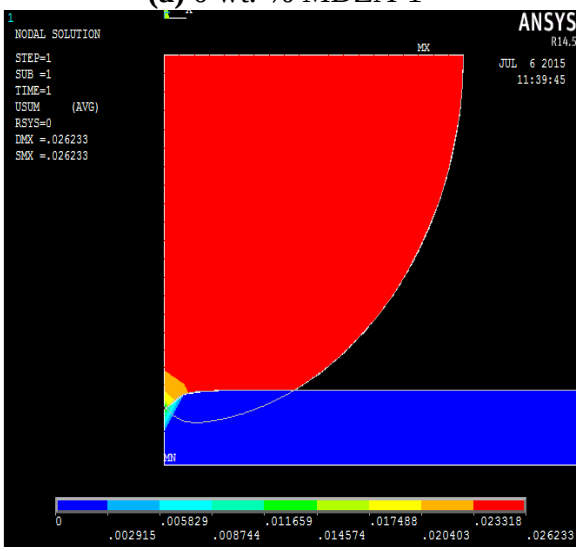

(c) 5wt.-% MDZA-3

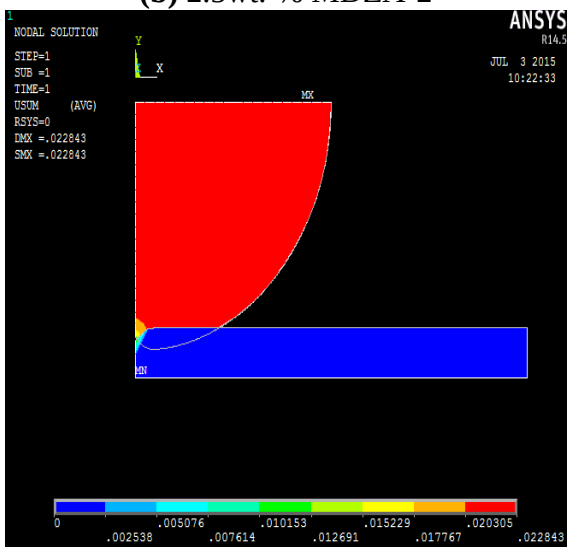

(d) 7.5wt.-% MDZA-4

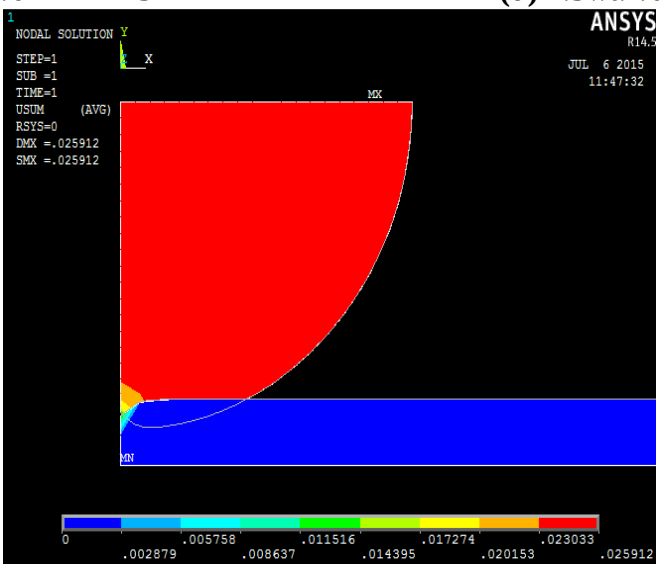

(e) 10wt.-% MDZA-5

Figure 4.7. Simulated results of penetration for MD particulate filled ZA-27 alloy composites

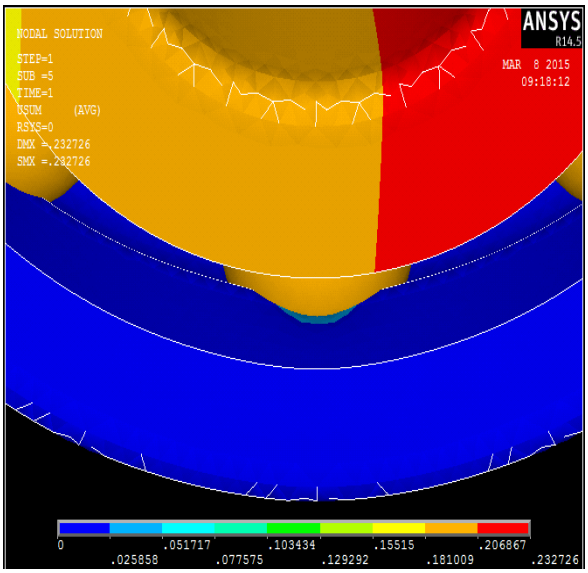

(a) 0wt.-% MDZA-1 (Displacement)

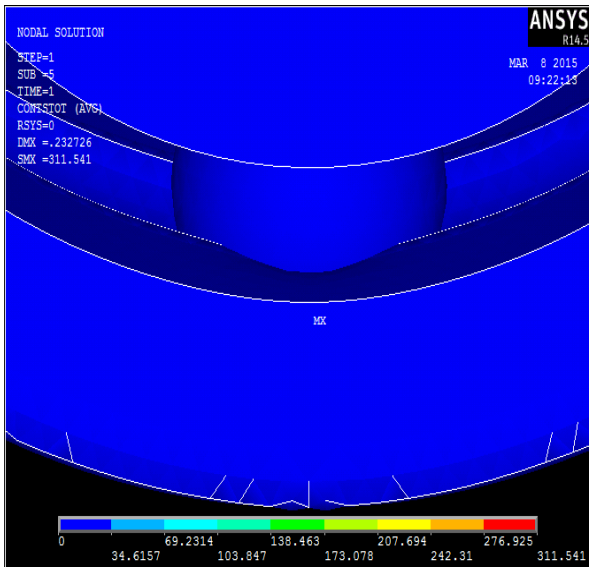

(b) 0wt.-% MDZA-1 (Contact stress)

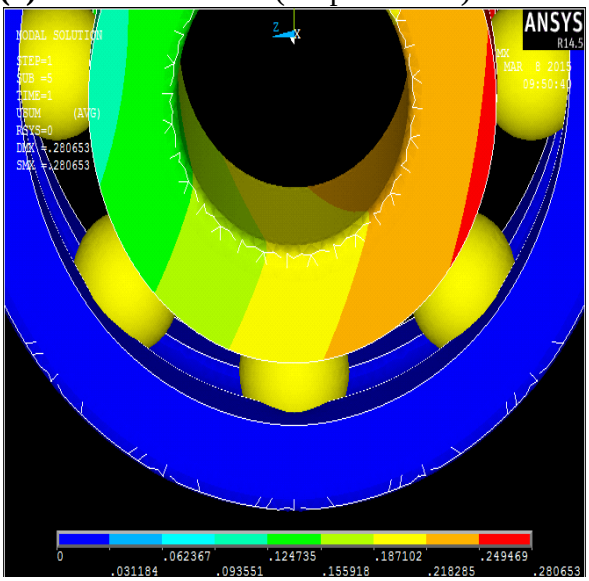

(c) 2.5wt.-% MDZA-2 (Displacement)

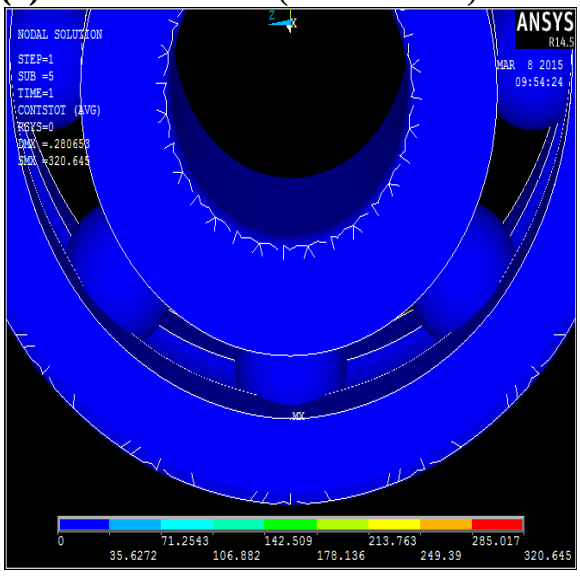

(d) 2.5wt.-% MDZA-2 (Contact stress)

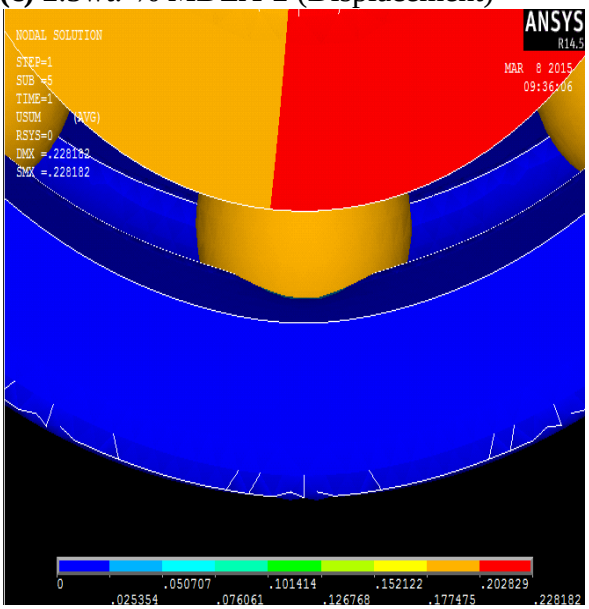

(e) 5wt.-% MDZA-3 (Displacement)

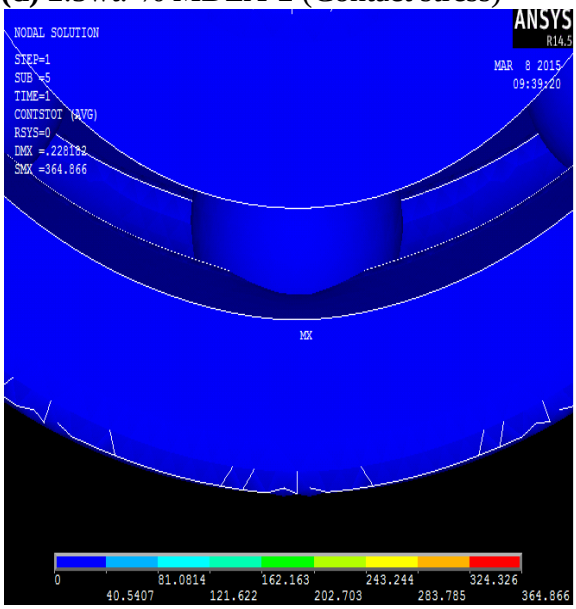

(f) 5wt.-% MDZA-3 (Contact stress)

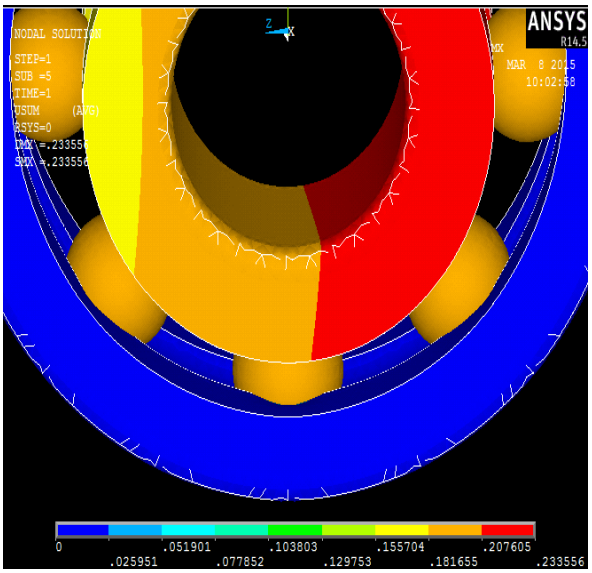

(g) 7.5wt.-% MDZA-4 (Displacement)

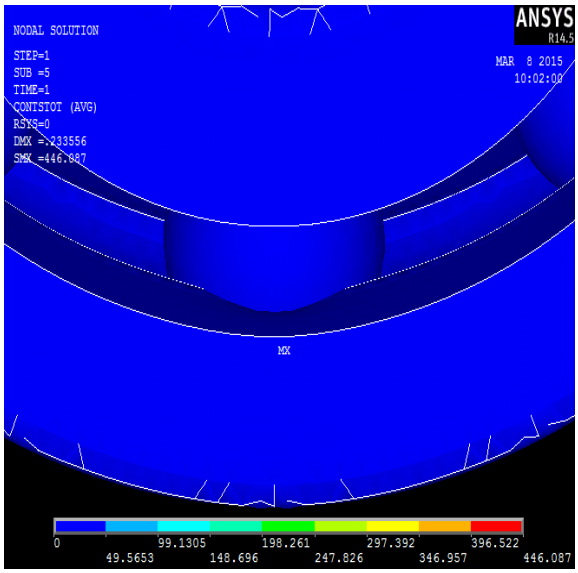

(h) 7.5wt.-% MDZA-4 (Contact stress)

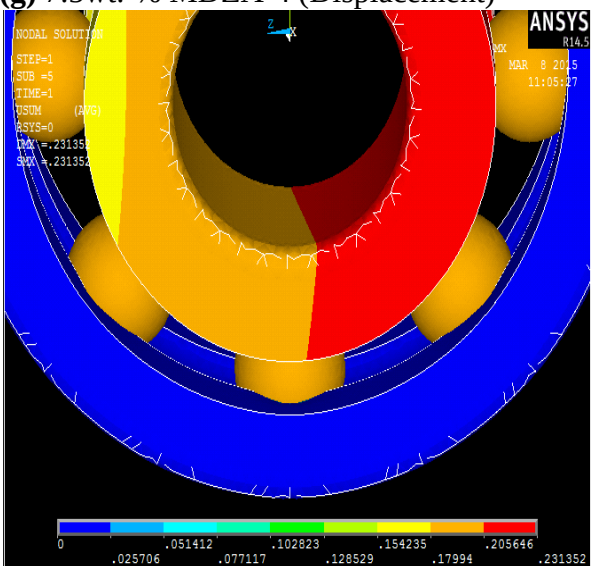

(i) 10wt.-% MDZA-5 (Displacement)

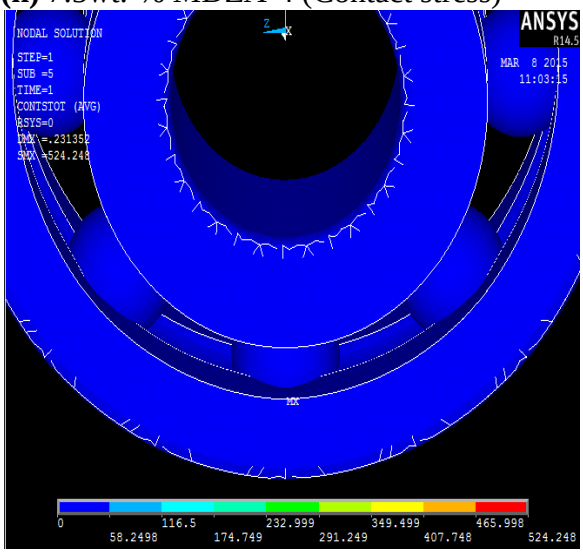

(j) 10wt.-% MDZA-5 (Contact stress)

Figure 4.8. Simulated results of displacement and contact stress analysis of MD particulate filled ZA-27 alloy composites at 500N

Table 4.3. Comparison of experimental and simulated results for the hardness of MD particulate filled alloy composites (at constant loading i.e. 30kgf)

Composite Material	Modulus of Elasticity (MPa)	Hardness (Hv)	Hardness FEA	% Error
ZAMD-1	1265.21	149	150.83	1.230
ZAMD-2	1302.18	177	181.43	0.025
ZAMD-3	1481.77	181	182.13	0.006
ZAMD-4	1811.62	204	209.14	0.025
ZAMD-5	2129.04	178	184.37	0.036

Table 4.4. Evaluations of contact stress, displacement and stress intensity factor for different wt. % of MD particulate filled ZA-27 alloy composites for 500N loading conditions

Composite Material	Modulus of Elasticity (MPa)	Contact stress (MPa)	Displacement (mm)	Stress Intensity (MPa)
ZAMD-1	1265.21	311.541	0.232726	165.698
ZAMD-2	1302.18	320.645	0.280653	170.539
ZAMD-3	1481.77	364.866	0.228182	194.059
ZAMD-4	1811.62	446.086	0.233556	237.258
ZAMD-5	2129.04	524.248	0.231352	278.829

Table 4.5. Comparison of theoretical and simulated results of the MD particulate filled alloy composites (at constant loading i.e. 500N)

Composite Material	Hertzian contact Stress (MPa)	FEA contact Stress (MPa)	Percentage Error %
ZAMD-1	315.72	313.541	0.69
ZAMD-2	322.84	318.645	1.31
ZAMD-3	350.79	364.866	3.86
ZAMD-4	401.08	426.086	5.69
ZAMD-5	446.66	474.248	5.82

Part II

4.2 Physical, Mechanical and Fracture analysis of Quicklime (CaO) particulate filled ZA-27 alloy composites

4.2.1. Effect of void contents on CaO particulate filled ZA-27 alloy composites

For successful operation of bearings, bearing materials should have some exceptional characteristics' such as to accommodate misalignment, geometrical errors, thermal stability etc. [266]. The insertion of reinforcement particles into a metal alloy fabrication or produce a composite material that played an important role to enrich and attractive amalgamation of physical and mechanical properties are as compared with the monolithic alloys so far. The theoretical density of the unfilled and particulate filled alloy composites is calculated by rule of mixture as proposed by Aggarwal and Broutman [246] and the experimental density of the same set composites is calculated

by Archimedes principle by weighing the sample in air and then in water (the detail procedure is reported in chapter 3). For CaO particulate filled ZA-27 alloy composites both the theoretical and experimental density are used to calculate the void contents of the unfilled and particulate filled alloy composites. From Table 4.6, it is observed that the value of void contents varies from 1.80 to 1.26% for unfilled alloy composite to 10wt.-% CaO particulate filled ZA-27 alloy composites. However, it is observed that the unfilled ZA-27 alloy composite shows much higher void content (i.e.1.80%) as compared to CaO filled ZA-27 alloy composites (i.e. 0.81%-1.26% for 2.5wt.-%-10wt.-% respectively). It may be due to the wetting between particulates and base alloy is better than the unfilled metal alloy composites. During solidification process the improper bonding in-between materials atom can also cause the shrinkage and gas nucleation [267].

Table 4.6. Comparison of experimental density and theoretical density of CaO particulate filled ZA-27 alloy composites

Sl. No.	Composition	Theoretical density (gm./cc^3)	Experimental density (gm./cc^3)	Void content (%)
1	ZACaO-1	5.00	4.91	1.80
2	ZACaO-2	4.93	4.89	0.81
3	ZACaO-3	4.87	4.83	0.82
4	ZACaO-4	4.82	4.77	1.03
5	ZACaO-5	4.76	4.70	1.26

The presence of some amount of porosity in composite materials is quite normal due to the feeding or insertion time and the contact surface area with air but if the porosity occurs in a large quantity than it can create problems for physical, mechanical as well as some other material properties. Therefore, after casting of composite materials applied immediate pressure to reduce the porosity of the composite and then the materials properties may be enhanced as well as strengthen the bonding force [268].

The applied pressure force the liquid's metal into present defects such as voids and construct a dense material [269]. Hashim et al. [267] found that the addition of reinforced particles into base alloy also increases the porosity it may be due to the presence of gases which formed or induced during melting of material cannot be removed by different degassing methods due to the settlement of gas bubbled by the

addition of filler particles which generally agonize by wetting conditions with the matrix .The reduction of porosity or void contents in particulate filled metal alloy composites material may be occurs due to thorough wettability in between particulate and matrix materials.

4.2.2 Effect of hardness on CaO particulate filled ZA-27 alloy composites

The hardness of any materials defined as the ability to resist the solid materials to permanent deformation or scratching, dimpling, cracks etc. under applied load [270]. The hardness for CaO particulate filled ZA-27 alloy composites is determined by using Vickers (Hv) micro-hardness tester. From Figure 4.9, it is observed that with the increased in filler content the hardness of the alloy composites is also increased up to 7.5wt.-% of CaO particulate filled. However, on further increased in filler content i.e up to 10wt.-% CaO content the hardness shows decreasing in trend in the alloy composite. The increased in hardness is utterly prominent due to the presence of hard dispersoids of solid CaO particulates that contributes positively towards increased in hardness. The increase in hardness is due to hard reinforced particle that acts as barrier to the movement of dislocations for filler particles within the matrix [49]. With the increasing in wt.-% of CaO in ZA-27 alloy, hardness increases from 148.7 Hv to 183.85Hv but then it reduces to 153.93Hv for 10wt.-% CaO particulate filled ZA-27 alloy composites. The reason for failing the hardness after 7.5wt.-% CaO filler can be the presence of porosity due the addition of large amount of filler particles in the alloy composite, which affects the bonding strength between the reinforcement and matrix materials.

As mentioned above, the hardness of the composite material is increased with the increasing in the amount of SiC particles, although the amount of porosities increased. This can be explained as follows: When the load is applied to the composite, plastic deformation occurred due to indentation. These plastic flows occurs under the restraint of the surrounding material near the indentation zone, and as the SiC particles exist at the indentation zone, these particles will hinder the plastic flow and the existence of SiC particles will restrain the plastic flow of the material more due to this indentation to fill the pore. Therefore, when the amount of SiC increases, the ceramic phase of the composite will also increase. This will lead to a remarkable reduction in the plastic flow of the material, which leads to an increase in the hardness of the composite material [271].

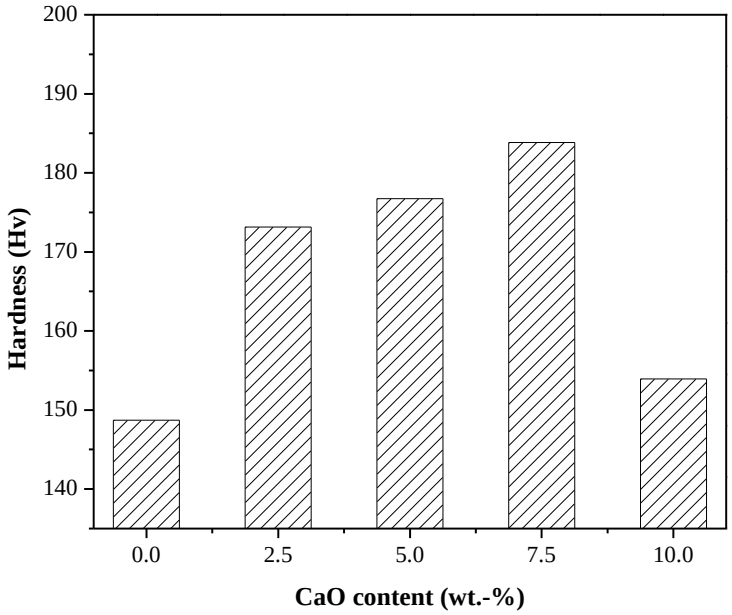

Figure 4.9. Hardness of CaO particulate filled ZA27 alloy composite

Sharma et al. [49] found in their study that with the increasing in wt.-% of zircon particles in ZA-27 alloy composites up to 5 wt.-%, hardness of the composites also increases about 10%. The zircon particles being hard dispersoids that positively contributes toward hardness of composite materials. For the bearing components low hardness is not appropriate [267] it should be as maximum as possible. Rebba and Ramanaiah [268] studied about the hardness for molybdenum disulphide (MOS_2) filled aluminium alloy composites. They found the hardness for MOS_2 filled aluminium alloy composites increases with the increasing in wt.-% of filler particles. The addition of filler particles up to 5 wt.-% and the value of hardness increases up to 4 wt.-%. Similarly, Seah et al. [272] concluded in their studies that with the increasing in wt.-% SiC particles in base alloy, the amount of hardness of the composites material also increases. The maximum hardness value is found 10 BHN for 5wt.-% of SiC content. This may be occurs due to the presence of SiC hard dispersoids particle that accord positive effect on hardness.

4.2.3 Effect of compressive strength on CaO particulate filled ZA-27 alloy composites

The compressive strength is defined as the capability of those materials to absorb or to sustain the applied compressive forced on it without any failure or deformation of material. The value of compressive strength for different wt.-% (0, 2.5, 5, 7.5 and 10)

of CaO filled ZA-27 alloy composites is shown in Figure 4.10. The increase in wt.-% of CaO particulate in alloy composite the compressive strength also increases but the increment is only up to 5wt.-% of CaO filler content (i.e.723 MPa). However, with the increased in filler content beyond 5wt.-% CaO, the compressive strength of the alloy composites is slowly decreased (i.e. 494MPa). The reason for increased in compressive strength up to 5wt.-% of CaO particulate filled ZA-27 alloy composites can be the increased in hardness of composite material up to 7.5wt.-% of CaO particulates. The presence of CaO hardened particles in ZA-27 alloy enhancing its compressive strength up to 5wt.-% but beyond it the strength is decreased because of excessive amount of filler particles in composites materials that creates the voids and diminishes the internal bonding due to which compressive strength of composite materials also decreases.

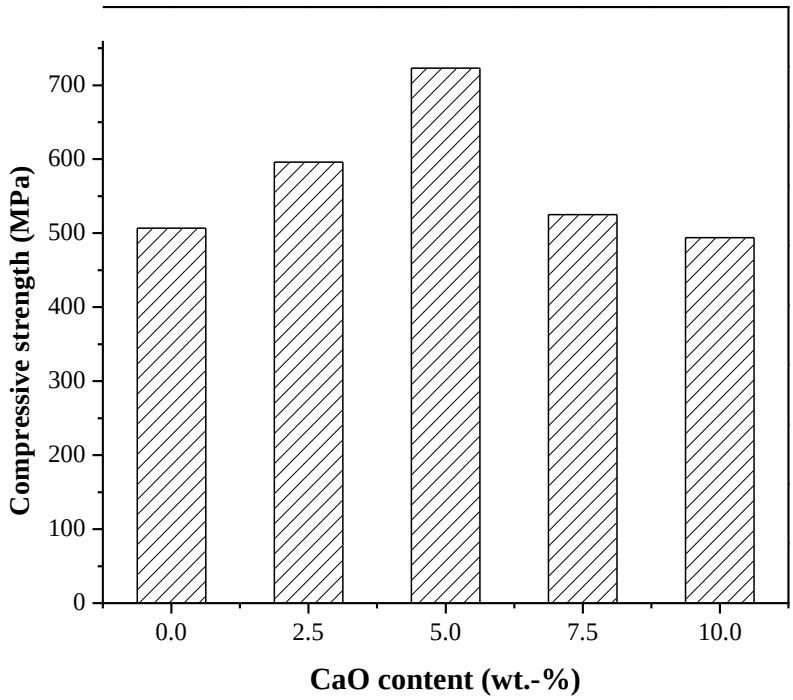

Figure 4.10. Compressive strength of CaO particulate filled ZA27 alloy composites

Shah [273] studied about the compressive strength for heat treated graphite particulates filled (up to 5 wt. - %) ZA-27 alloy composites and fabricated in vortex method. The increases in amount of graphite particulates in matrix, compressive strength also increases up to 5 wt.-% filler particles. With the heat treatment of composite materials microstructure becoming more cognate and which causes the improvement in hardness. Saravanan and Kumar [274] studied about the rice husk ash

reinforced aluminium alloy composite material, fabricated by liquid fabrication techniques with diverse wt.-% of reinforcement such as 3, 6, 9 and 12wt.-% respectively. They observed that with the increased in wt.-% of rice husk ash in base alloy, the compressive strength of composite materials also increases up to 12 wt.-% of reinforcement. This may be due to the hardening of aluminium alloy by the addition of rice husk ash as reinforcement.

The study of mechanical behaviour for graphite and albite reinforced aluminium alloy composite materials has been studied by Ramesh et al. [73]. From their study they found that both the reinforcement have different mechanical properties such as graphite particulate filled aluminium alloy composite has improvised compressive strength although albite particulate filled matrix alloy composites shows decreasing in value of compressive strength. It may be due to presence of hard graphite particles in matrix alloy act as a barrier for the movement of dislocation in composite materials.

4.2.4 Effect of flexural strength on CaO particulate filled ZA-27 alloy composites

Figure 4.11 shows the flexural strength of CaO filled ZA-27 alloy composites at five different weight percentages of CaO. The flexural strength of the particulate filled ZA-27 alloy composites is increased with the increase in CaO content up to 7.5wt.% (i.e. 459.38MPa to 937MPa).

Kumar et al. [247] fabricated silicon carbide reinforced alumina matrix composites by direct metal oxidation process. They found that with the increased in wt.-% of filler particles, flexural strength of composites also increases from 158-231 MPa for 0.35-0.43 (with 125 μm particle size of reinforcement) volume fraction of reinforced particles.

The particle size is also played an important role to strengthen the properties of materials. The smaller particles size has improvised properties as compared to larger size of reinforced particles. Similarly, Dong et al. [275] studied about the bending behaviour of SiC particulate filled aluminium alloy composites and the bending strength of the composites increased with respect to increases in wt.-% of filler particles in base alloy.

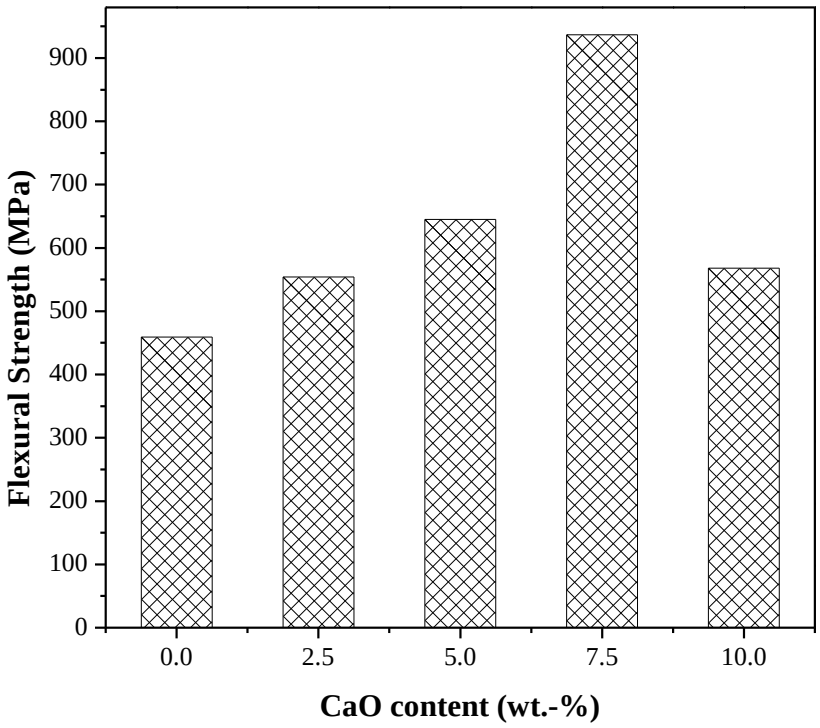

Figure 4.11. Flexural strength of CaO particulate filled ZA27 alloy composites

Again, Li et al. [276] reported that the bending strength of the alloy composite is initially increased with the increasing in sintering temperature, but then decreased after reaching their maximum values. The presence of TiC particles at the grain boundaries inhibited the grain growth of Fe_3Al. This caused a refined grain structure of composites, and consequently provided an additional contribution to the bending strength. In the first stage (before the sintering temperature corresponding to maximum values of bending strength), the densification effect is dominant and the bending strength is enhanced. In the second stage, the grain size of composites further increased with the increasing in sintering temperature. The bending strength is reduced as the grain size effect in turn becoming dominant [276].

4.2.5 Effect of impact strength on CaO particulate filled ZA-27 alloy composites

The ability of a material to sustain the impact forces up to fracture or breaking point is known as impact strength of that material or it can be also defined as the amount of energy stored in the material before fracture. The impact strength can be measured by Charpy impact test with the unit of J (Joule). Figure 4.12 shows CaO particulate filled ZA-27 alloy composites at five different weight percentages. It is observed that with the increased in filler content in the alloy material the impact strength of the

composites is also gradually increased. The increased in impact strength of a material for bearing application can be a good alternative material.

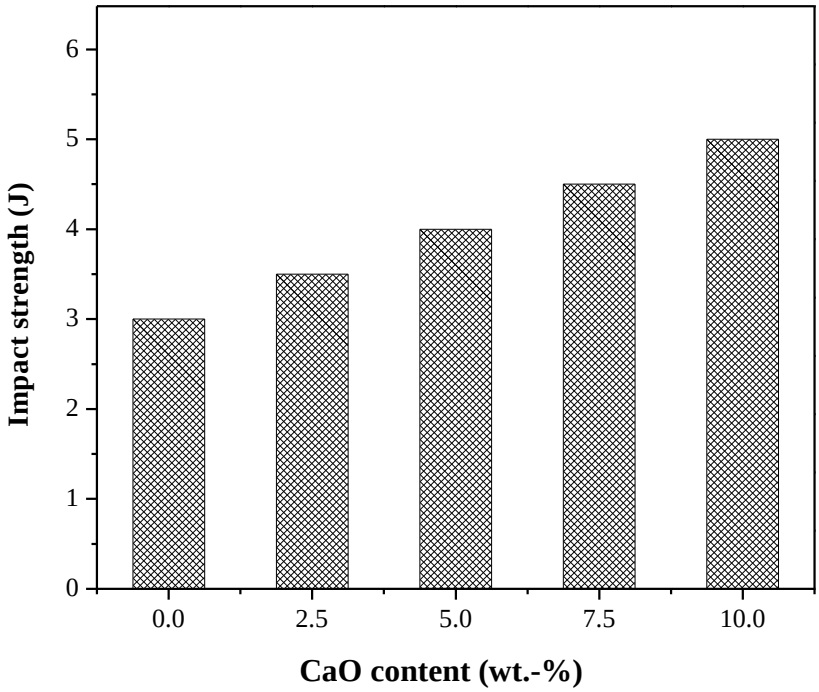

Figure 4.12. Impact strength of CaO particulate filled ZA27 alloy composites

The maximum impact strength sustain by the composites material is 5J for 10wt.-% CaO reinforcement and for unfilled ZA-27 alloy composites the impact strength is around 3J, which is minimum among the unfilled and particulate filled alloy composites. Sharma et al. [60] fabricated quartz particulate filled lead alloy composite and studied impact strength of the material which shows positive effect with the increasing in wt.-% of quartz particulates in lead alloy composite materials. The impact strength increases due to presence of hard quartz particles in composite materials which act as blockade for the movement of dislocations so that the impact strength of composite material enhances.

4.2.6. Effect of stress intensity factor on CaO particulate filled ZA-27 alloy composites

When the materials get broken into two or more pieces under the applied loading conditions known as fracture, it arises due to sudden or unexpected loading conditions. This fracture phenomenon comes in existence hundred years ago for different structural, automotive and numerous applications with the presence of cracks, voids and forbidden defects. In different metals fracture can be occurred

normally either brittle or ductile nature [277]. To overcome such types of failure the fracture behaviour of material is highly required to improve. For CaO particulate filled ZA-27 alloy composites the SIF can be calculated by using Eqs. (3.9) and (3.10) for four different crack lengths (i.e. 1, 2, 3, and 4 mm) as shown in Table 4.7 and Figure 4.13. Figure 4.13 shows the variation of SIF for different crack lengths at five different wt.-% of reinforced particulates. Figure 4.13 shows that the monolithic or unfilled ZA-27 alloy has lower value of SIF as compared to CaO particulate filled ZA-27 alloy composite materials. The fracture occurs mainly due to the presence of void, nucleation growth and coalescence in unreinforced materials as well as reinforced composite materials [49].

Table 4.7 shows the experimental values of stress intensity factor for unfilled and CaO particulate filled ZA-27 alloy composites. The different wt.-% (0, 2.5, 5, 7.5 and 10wt. - %) of CaO particulate varies in ZA-27 alloy composites with the varying in crack lengths (1, 2, 3 and 4 mm) respectively. It is observed that the value of stress intensity factor (SIF) increases with the increased in wt.-% of CaO particulate filler in ZA-27 alloy composites simultaneously with the increasing in crack lengths. The maximum value of SIF is found for 10 wt.-% (i.e. 2.0127 MPa.m^1/2 for 4mm crack length) of CaO filled ZA-27 alloy composites for 4 mm crack length.

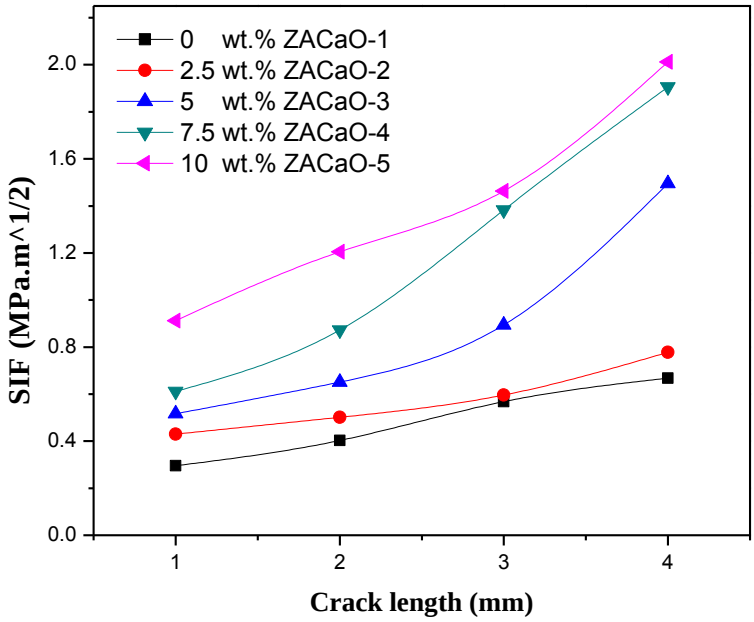

Figure 4.13. Mode I stress intensity factor for CaO particulate filled ZA27 alloy composite

Alaneme and Aluko [278] studied the fracture toughness behaviour of SiC filled aluminium alloy, fabricated by stir casting method at different wt.-% (i.e. 3, 6, 9 and 12 wt. - %) SiC content. They observed that the fracture toughness behaviour in cast as well as age hardened composite materials and noticed that in aging treatment the material shows better fracture toughness behaviour as compared to cast material, the reason for the improvement in fracture toughness may be the presence of fine coherent Mg_2Si precipitates that formed in base matrix during ageing process.

The interfacial decohesion is often observed due to the presence of undesired interfacial reaction products, such as, for example, the $MgAl_2O_4$ spinel for Mg-rich aluminum alloy matrix reinforced with Al_2O_3 particles, or the Al_4C_3 for aluminum based composites, reinforced with SiC [279,280]. Fracture of the reinforcing particles depends on the local stress acting on the particle. The large mismatch in the elastic modulus between the reinforcing particles and the metal matrix generates a constrained deformation in the matrix and a consequent concentration of stresses near the reinforcing particles. These stresses can determine cracking of the particles, fracture of the matrix and/or interfacial decohesion respectively. Fracture of the particle was greater in region with large particles and clusters, where there was a concentration of stresses and where the short interparticle distance facilitates linkage between voids and/or cracks in the particle [281,102,282, 283]. The larger particles, which also have a higher probability of containing critical flaw, generate high load transfer from the plastically deforming aluminum matrix and the elastically deforming particle, which can cause their crack. On the other hand, the smaller Al_2O_3 usually do not crack, but because of the strain differences between matrix and particle the matrix can fail by decohesion.

Table 4.7. Stress Intensity Factor (K) of CaO particulate filled ZA-27 alloy composites with different crack lengths

Sl.No.	Compositions ⇩ Crack length ⇨	1mm	2mm	3mm	4mm
1	ZACaO-1	0.2951	0.4032	0.5685	0.6672
2	ZACaO-2	0.4299	0.5012	0.5963	0.77758
3	ZACaO-3	0.5162	0.6513	0.8935	1.4953
4	ZACaO-4	0.6113	0.8725	1.3824	1.9056
5	ZACaO-5	0.9114	1.2044	1.4632	2.0127

4.2.7. Fractography of CaO particulate filled ZA-27 alloy composites after fracture test

Research in fractography area has been prospering substantially during past few years. Fractography term is used for the micro-structural study of fracture surfaces to apprehend the effect of fracture for ductile materials. The micro-structural examination of different proportion (0wt.-%, 2.5wt.-%, 5wt.-%, 7.5wt.-% and 10wt. -%) of CaO particulates filled ZA-27 alloy composite materials for fracture surface is studied by scanning electron microscopic (SEM) analysis.

Figure 4.14 (a-e) shows the different micro-structural fractographs for CaO particulates filled ZA-27 alloy composite which studied after fracture test (For different crack length 1, 2, 3 and 4mm). Figure 4.14a shows the SEM fractography of unfilled ZA-27 alloy composite and the fracture behavior has ductile in nature. Figure 4.14a shows the presence of ductile tearing with the presence of fibrous fracture in the matrix material and the presence of shrinkage cavity is also noticed due to the porosity effect in the composite materials [49]. Figure 4.14b shows the SEM fractographs of 2.5 wt.-% of CaO filled ZA-27 alloy composites. Similarly Figure 4.14c shows the fractographs for 5 wt.-% of CaO filled ZA-27 alloy composites. Figures 4.14b and 4.14c show the presence of less uniform dimple size [284].

Figure 4.14d shows the SEM fractographs for 7.5 wt.-% of CaO filled ZA-27 alloy composite and presence multiple micro cracks in the reason of agglomeration, the reason for presence of micro cracks can be the degradation in ductility of fabricated composite materials [49].

The agglomeration phenomenon in fracture material is associated with in the sequence of void nucleation, growth and coalescence [283]. The facture surface of 10 wt.-% CaO filled ZA-27 alloy composites is shown in Figure 4.14e, that clearly indicates the presence of filler particles in to matrix phase within the large deep dimple structure [285]. Reason for dimpling can be the application of stress on the soft ductile materials sample, which decreases the bonding effect in between the inter-molecules of reinforced filled metal alloy composite materials and induces porosity, and other defects.

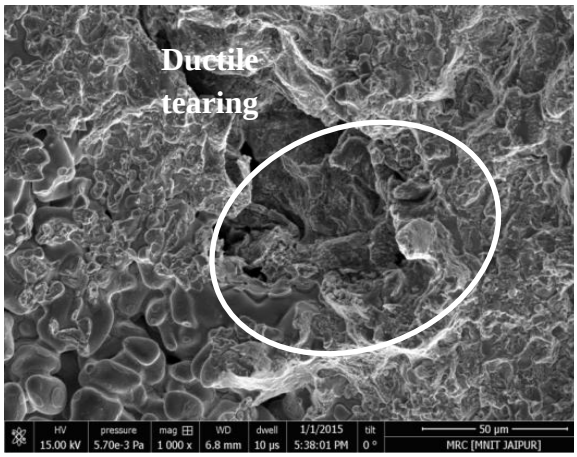

Figure 4.14a. SEM fractographs for 0 wt.-% of CaO particulate filled ZA-27 alloy composites after fracture test

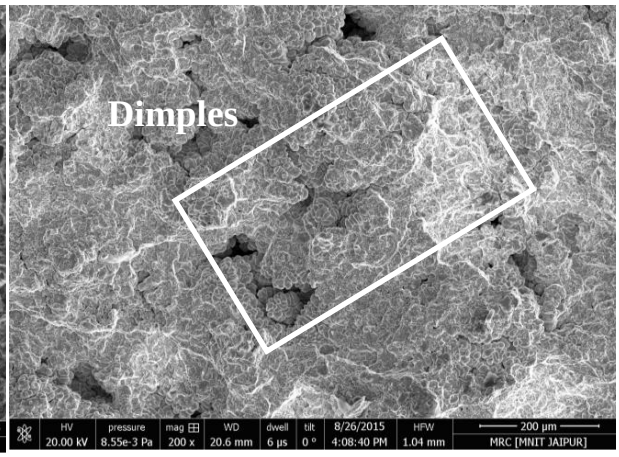

Figure 4.14b. SEM fractographs for 2.5 wt.-% of CaO particulate filled ZA-27 alloy composites after fracture test

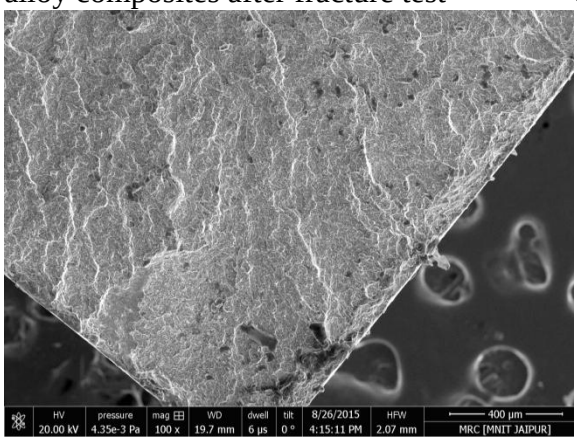

Figure 4.14c. SEM fractographs for 5 wt.-% of CaO particulate filled ZA-27 alloy composites after fracture test

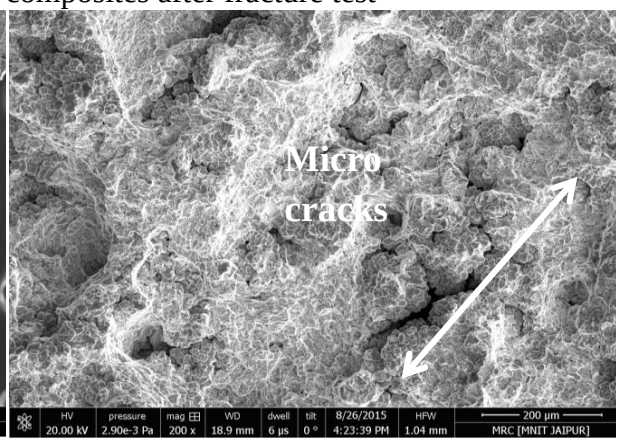

Figure 4.14d. SEM fractographs for 7.5 wt.-% of CaO particulate filled ZA-27 alloy composites after fracture test

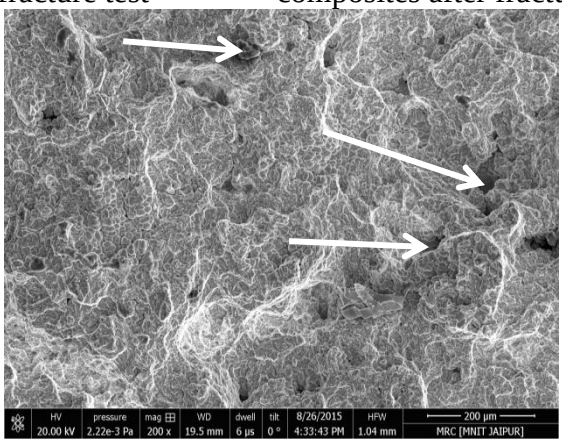

Figure 4.14e. SEM fractographs for 10 wt.-% of CaO particulate filled ZA-27 alloy composites after fracture test

Figure 4.14. SEM Fractographs of fracture surfaces for CaO particulate filled ZA-27 alloy composites after fracture test.

4.2.8. Effect of hardness, contact stress and deformation of CaO particulate filled ZA-27 alloy composites

The single row deep groove ball bearing 6200 standard design is followed for CaO particulate filled ZA-27 alloy composite materials and determine the contact stress and displacement through simulation analysis and compared it with Hertzian theory for constant applied load. It shows from Figure 4.15 and Table 4.8, the comparison of experimental as well as FEM results at constant load for different wt.-% CaO particulates filled ZA-27 alloy composites. The FEM analysis for hardness has been obtained by Brinell Hardness Formula at defined variables. After the process some error is found for theoretical and FEM analysis which lies within the range of 2.10% to 2.83% respectively. The range of hardness for the CaO filled ZA-27 alloy composite materials is varied with varying the weight percentage of filler content. The contact deformation and contact stress phenomenon in FEM for unfilled as well as for CaO filled ZA-27 alloy composites are calculated at constant load i.e. 500N applied on deep groove ball bearing with the help of ANSYS simulation software [267] as shown in Figure 4.16. Table 4.9 indicates the contact stress, displacement and stress Intensity results for unfilled and CaO filled ZA-27 alloy composite materials by varying the modulus of elasticity as calculated experimentally. Table 4.10, shows the comparison of theoretical and FEM results at constant load for unfilled and CaO particulate filled ZA-27 alloy composites. The calculated contact stress for modeled bearing composite materials is performed by using Hertzian contact theory. Therefore, between the theoretical and simulation analyses the error lies in between 1.34% to 4.86% respectively.

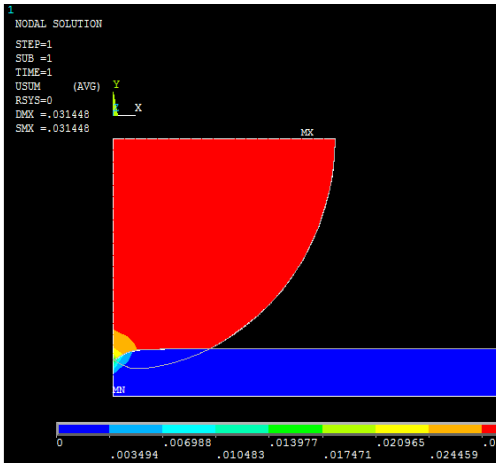

(a) 0 wt.-% CaOZA-1

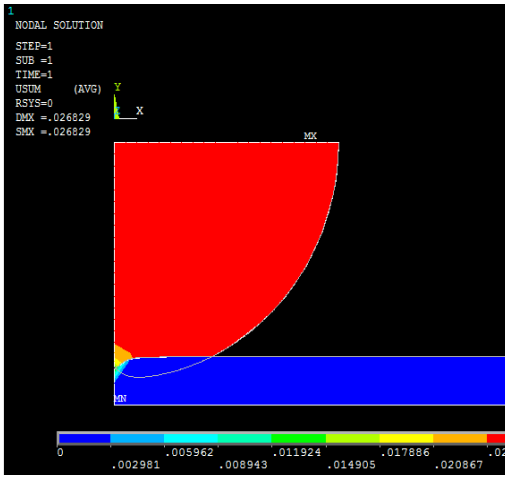

(b) 2.5wt.-% CaOZA-2

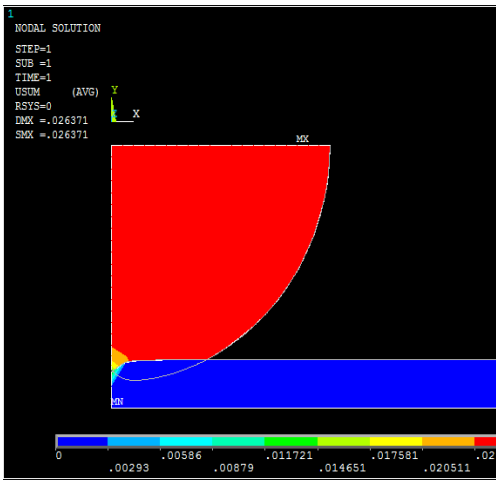

(c) 5wt.-% CaOZA-3

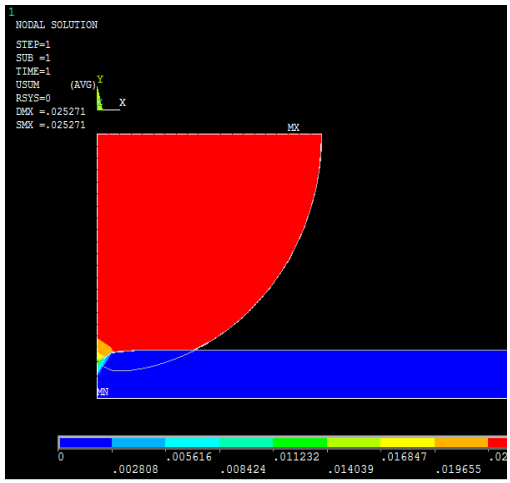

(d) 7.5wt.-% CaOZA-4

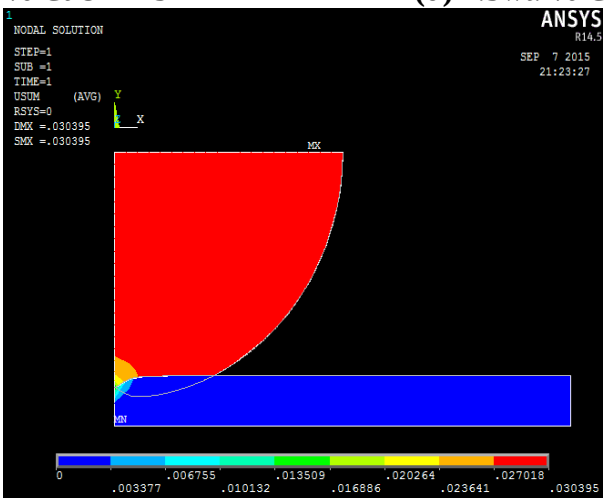

(e) 10wt.-% CaOZA-5

Figure 4.15. Simulated results of penetration for CaO particulate filled ZA-27 alloy composites

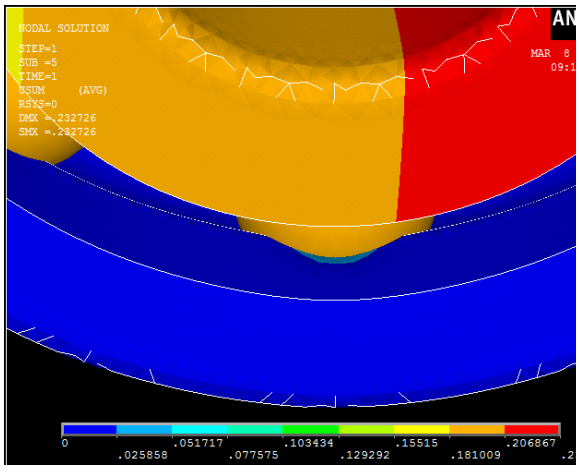

(a) 0wt.-% CaO ZA-27-1 (Displacement)

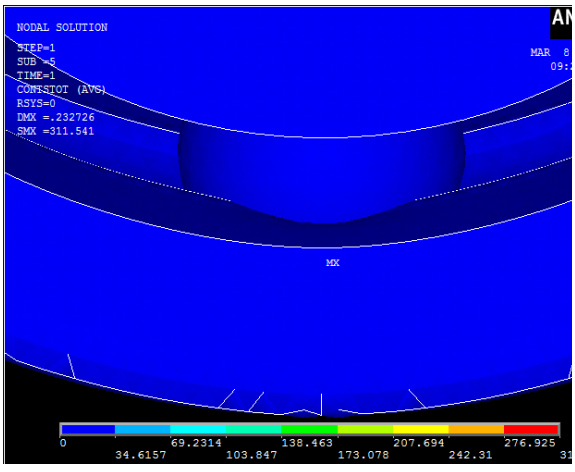

(b) 0wt.-% CaO ZA-27 -1 (Contact stress)

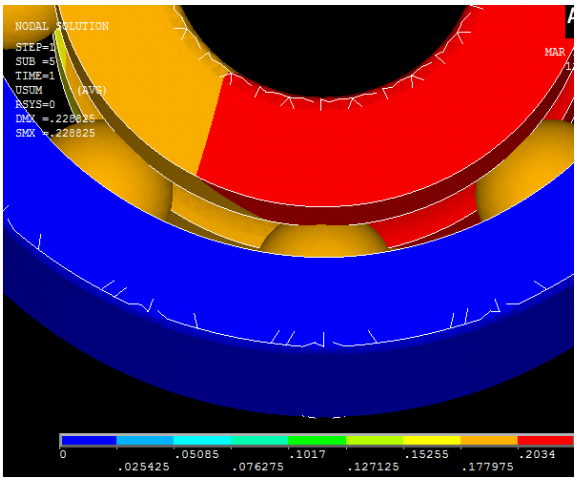

(c) 2.5wt.-% CaO ZA-27-2 (Displacement)

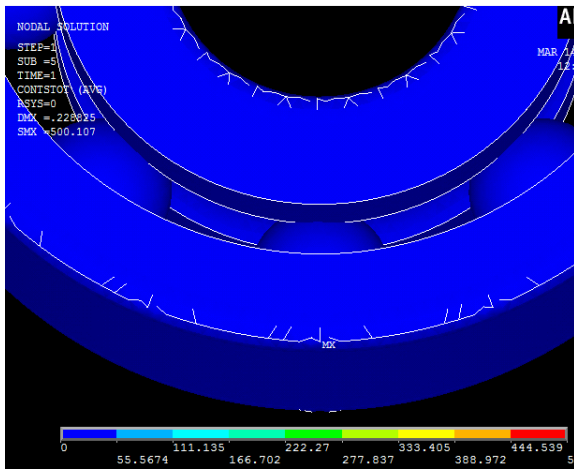

(d) 2.5wt.-% CaO ZA-27 -2 (Contact stress)

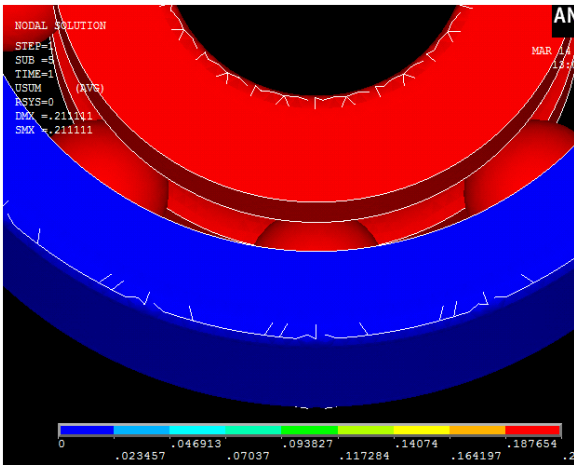

(e) 5wt.-% CaO ZA-27 -3 (Displacement)

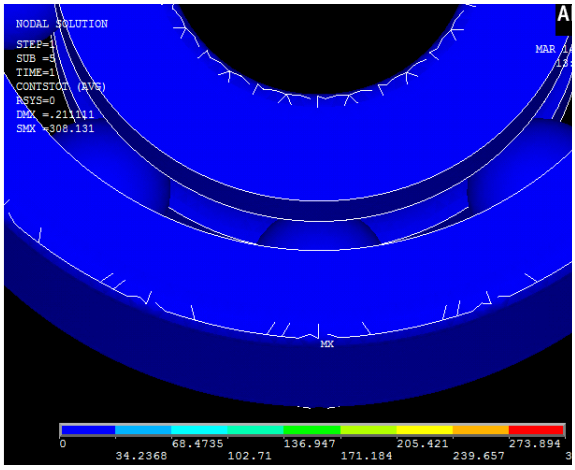

(f) 5wt.-% CaO ZA-27 -3 (Contact stress)

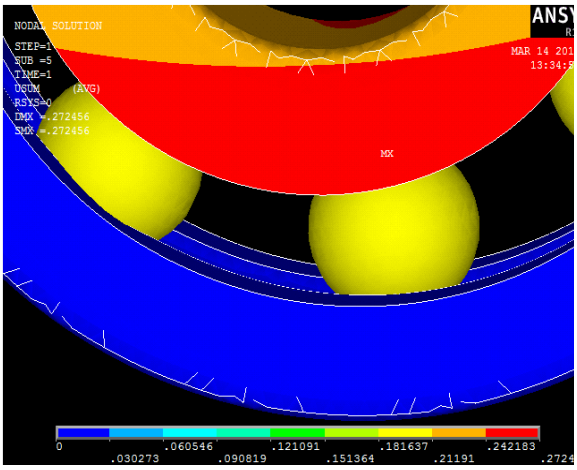

(g) 7.5wt.-% CaO ZA-27 -4 (Displacement)

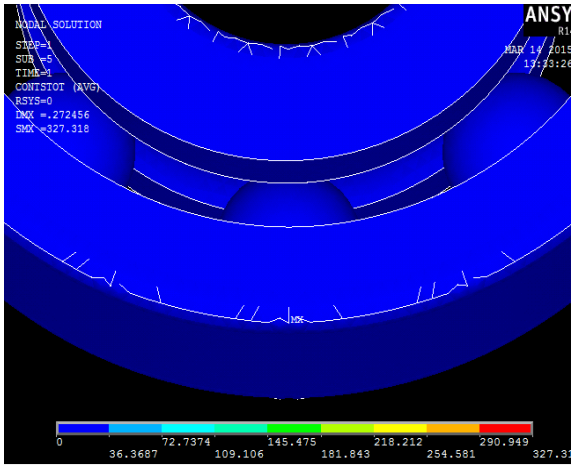

(h) 7.5wt.-% CaO ZA-27 -4 (Contact stress)

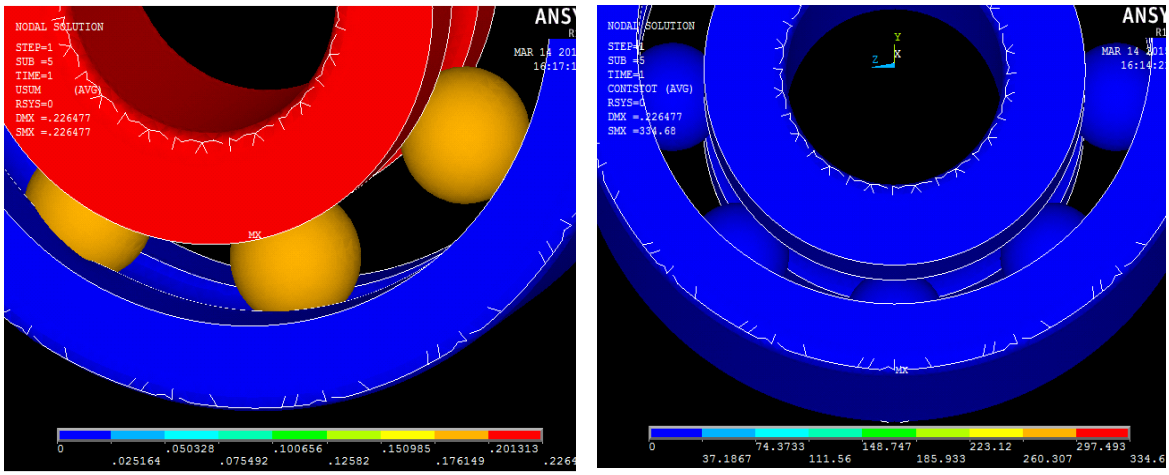

(i) 10wt.-% CaO ZA-27 -5 (Displacement)

(j) 10wt.-% CaO ZA-27 -5 (Contact stress)

Figure 4.16. Simulated results of displacement and contact stress analysis of CaO particulate filled ZA-27 alloy composites at 500N

Table 4.8. Comparison of experimental and simulated results for the hardness of CaO particulate filled ZA-27 alloy composites (at constant loading i.e. 30kgf).

Composite Material	Modulus of Elasticity (MPa)	Hardness (Hv)	Hardness FEA	% Error
ZACaO-1	1265.21	148.70	151.90	2.15
ZACaO-2	2031.00	173.16	178.06	2.83
ZACaO-3	1251.36	176.73	181.15	2.50
ZACaO-4	1330.05	183.85	189.03	2.82
ZACaO-5	1359.18	153.93	157.17	2.10

Table 4.9. Evaluations of contact stress, displacement and stress intensity factor for different wt. % of CaO particulate filled ZA-27 alloy composites for 500N loading conditions.

Composite Material	Modulus of Elasticity (MPa)	Contact stress (MPa)	Displacement (mm)	Stress Intensity (MPa)
ZACaO-1	1265.21	311.541	0.232726	165.698
ZACaO-2	2031	500.107	0.228825	265.989
ZACaO-3	1251.36	308.131	0.211111	163.884
ZACaO-4	1330.05	327.318	0.272456	173.343
ZACaO-5	1359.18	334.68	0.226477	178.004

Table 4.10. Comparison of theoretical and simulated results of the CaO particulate filled ZA-27 alloy composites (at constant loading i.e. 500N).

Composite Material	Hertzian contact Stress (MPa)	FEA contact Stress (MPa)	Percentage Error %
ZACaO-1	315.72	311.541	1.34
ZACaO-2	432.84	427.72	1.21
ZACaO-3	313.41	306.13	2.38
ZACaO-4	326.41	318.56	2.46
ZACaO-5	331.16	315.82	4.86

Part III

4.3 Physical, Mechanical and Fracture analysis of Marble Dust (MD) particulate filled Silicon Bronze alloy composites

4.3.1 Effect of void contents on MD particulate filled SiBr alloy composites

The fabricated MD filled SiBr alloy composites show the theoretical and experimental density in Table 4.11. From Table 4.11, it is observed that the void contents of the particulate filled SiBr alloy composites increases with the increasing in wt.-% of MD particulates i.e. 0.599% to 0.760% except for monolithic alloy (i.e. for 0wt.-% of filler particulates) the void content is quite higher i.e 0.824% . The presence of porosity during fabrication process is normal because of gas entrapment during stirrer process, air bubbles may be formed in liquid molten metal during feeding of reinforced particles in to matrix material at the time of casting.

Table 4.11. Comparison of experimental density and theoretical density

Sl.NO.	Composition	Theoretical density gm./cc^3)	Experimental density (gm./cc^3)	Void content (%)
1	SiBrMD-1	8.49	8.42	0.824
2	SiBrMD -2	8.34	8.29	0.599
3	SiBrMD -3	8.02	7.96	0.748
4	SiBrMD -4	7.89	7.83	0.760
5	SiBrMD -5	7.81	7.71	1.280

With the increased in MD content, the number of pores is also increased and the marble dust particles which played a significant role in weakening the composite material. The presence of voids reduce the product quality simultaneously affect the mechanical and wear characteristics of the materials and ultimately affects the end

product [286]. This was primarily attributed to increase in contact surface area due to presence of reinforcement powders in molten aluminium and pore nucleation at Al_2O_3 particulate sites (porosity associated with individual particle).

4.3.2 Effect of hardness on MD particulate filled SiBr alloy composites

Figure 4.17 shows the hardness of marble dust filled (For varying wt.-% from 0wt.-% to 10 wt.-% of MD) SiBr alloy composites. The hardness of the unfilled and particulate filled metal alloy composites is increased with the increase in weight percentages of the hard reinforcing particles i.e. up to 7.5wt.-% marble dust particulate filled alloy composites. Whereas, on further increased in filler content in the alloy composite the hardness shows slightly inferior result. The value of hardness was 113.78Hv at 0wt.-%MD and 172.93Hv at 7.5wt.-%MD. The reason for swell value of hardness can be presence of hard MD particles in SiBr alloy composites [61] that also increases the dislocation density of composite materials.

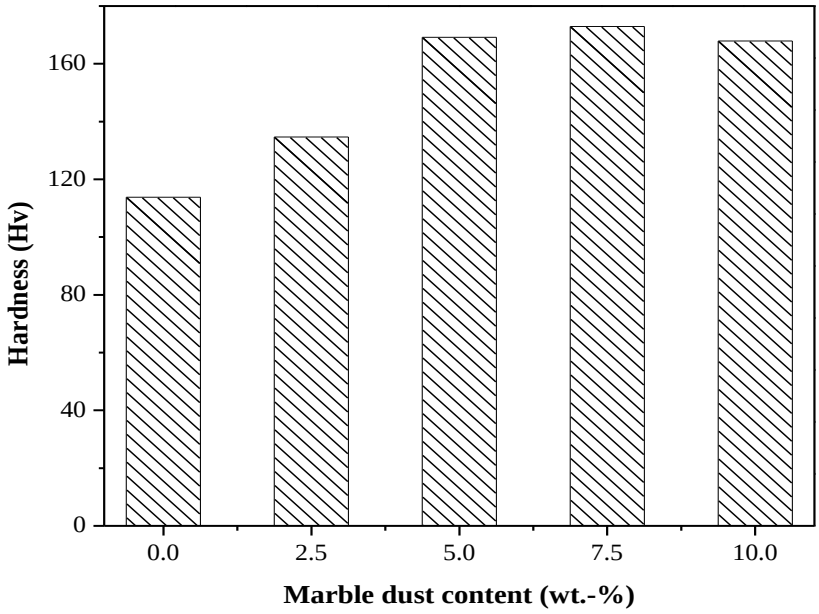

Figure 4.17. Variation of micro-hardness of MD particulate filled SiBr alloy composites

However, the unfilled SiBr alloy (i.e. 0wt.-% MD filled metal) alloy composite has lower hardness value as compared to filled SiBr metal alloy composites. The maximum value of hardness is found for 7.5wt.-% MD reinforced composites materials i.e.172.93Hv. This maximum value of hardness is found due to the presence of hard reinforced particles that plays an important role to enhance the materials

properties [78]. The same results for hardness of different composite materials are found by many other researchers by their research study [287,288]. This plastic flow occurs under the restraint of the surrounding material near the indentation zone. Therefore, the presence of pores results in lowering the hardness, and if the volume of pores increases, an accompanying decrease in hardness will result and the material appears to be softer.

4.3.3. Effect of compressive strength on MD particulate filled SiBr alloy composites

The compressive strength of a composite can primarily be attributed to significant grain refinement, the presence of reasonably distributed hard particles, and load transfer from matrix to reinforcement phase [289,290]. Figure 4.18 shows the compressive strength of five different wt.-% (0, 2.5, 5, 7.5 and 10) of MD filled SiBr alloy composites. With the increased in weight percentages of the marble dust content in the alloy composites the compressive strength increases maximum up to 70MPa i.e for 7.5wt.% marble dust filled.

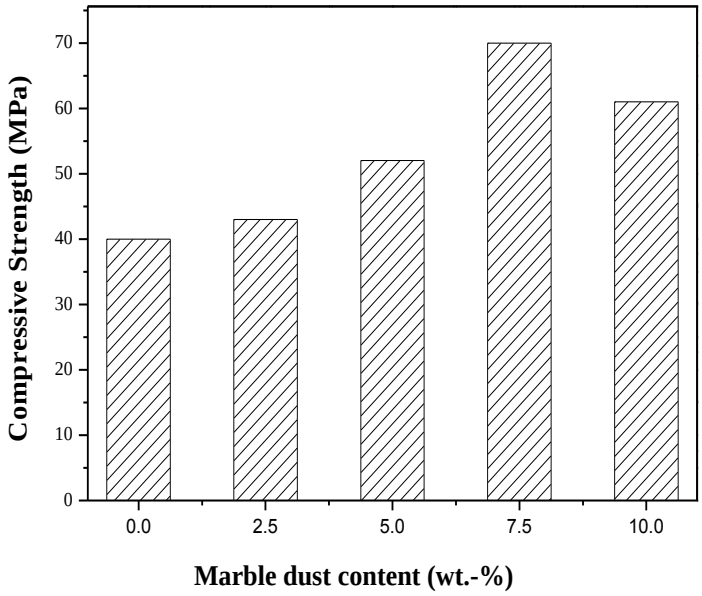

Figure 4.18. Compressive strength of MD particulate filled SiBr alloy composites

However, on further increased in filler content (from 7.5wt.% to 10wt.%) the compressive strength starts decreasing in trend (i.e. 61MPa). The reason for increasing in compressive strength up to 7.5wt.-% of MD filled SiBr alloy composites can be enhancement in hardness of materials up to 7.5wt.-% of MD particulates, that directly contingent on hardness property of composite materials. Similar, observation

is also reported by Hariharan et al. [291] for particulate filled metal composite and said that with the increasing in amount of particulates in the matrix material the compressive strength increases nearly 10% more that the unfilled base material. There may be another reason the improvement of strength in particulate filled alloy composite, that the increased in weight percentages of marble dust particles in matrix material the distance between the particle to particle decreases that causes the dislocation density increases. Therefore, more force is needed to move dislocation and hence the strength increases up to certain weight percentages of particulate filled.

4.3.4. Effect of flexural strength on MD particulate filled SiBr alloy composites

The bending or flexural strength of MD filled SiBr alloy composites is considered as a material ability to withstand the bending forces applied on composite materials without any failure of material.

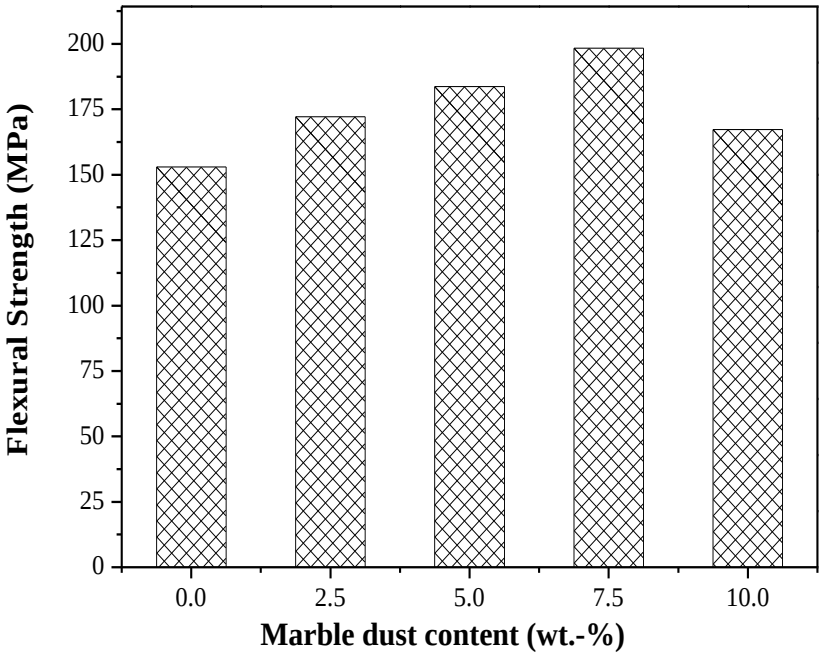

Figure 4.19. Flexural strength of MD particulate filled SiBr alloy composites

Figure 4.19, shows the three-point bending strength of MD filled SiBr alloy composites at five different weight percentages of marble dust particulates. The flexural strength of the marble dust filled SiBr alloy composites increased from 153MPa to 198.3MPa (i.e from 0wt.% to 7.5wt.% marble dust) and then decreased

from 198.4MPa to 167.3MPa (i.e from 7.5wt.% to 10wt.% marble dust) with the increased in filler percentage from 0wt.% to 10wt.% marble dust particulate.

Balak et al. [292] studied flexural strength for ZrB_2 based composite materials fabricated in SPS apparatus and noticed that lower porosity has higher flexural strength, similarly for MD particulates filled metal alloy composites have higher flexural strength in comparison of unfilled metal alloy composites due to presence of less amount of porosity (0.824% and0.599% respectively). It is also found with the inclusion of filler particulates the bonding of matrix and filler particulates get strengthen which positively affect the materials properties such as flexural strength and there by flexural strength increases up to 7.5 wt.-% MD particulate's filled SiBr alloy composites. The reason for reducing amount of flexural strength can be the presence agglomeration for higher amount of particulates in matrix material which creates low density reason and results the lowering flexural strength [293].

4.3.5 Effect of impact strength on MD particulate filled SiBr alloy composites

Materials have the ability to resist the impact forces acted on it without any fracture or breaking known as impact strength of that material, also the amount of stored energy by material before any fracture.

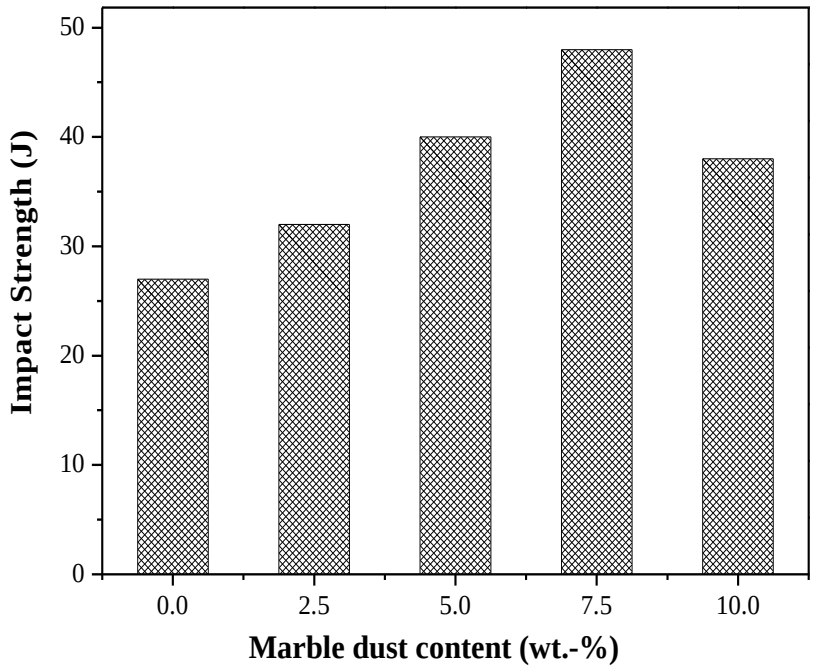

Figure 4.20. Impact strength of MD particulate filled SiBr alloy composites

Figure 4.20 shows the effect of impact strength of MD filled SiBr alloy composite materials, its shows the maximum value of impact strength at 7.5 wt.-% MD in SiBr alloy composites (i.e.48J), and for unfilled metal alloy composite the impact strength value is observed to be minimum (i.e. 27J).

Haque et al. [294] studied the mechanical behaviour of Al6061 alloy that reinforced with Cu and SiC particulates. In their study, they observed that the amount of impact strength increases up to 38MPa with the increasing in wt.-% of reinforcing particles. The reason for enhanced impact strength may be the homogeneous dispersion of SiC ceramic particulates in matrix. The increasing in impact strength shows up to 7.5 wt.-% particulates, this may be due to the applied pressure during solidification that refines the grains size [295].

4.3.6 Effect of stress intensity factor on Marble Dust particulate filled SiBr alloy composites

Figure 4.21 shows the mode 1 stress intensity factor (SIF) for marble dust filled SiBr alloy composites with different weight percentage of marble dust content. The stress intensity factor of the particulate filled alloy composites is calculated in four different crack lengths i.e from 1mm to 4mm respectively. It is observed that from the Figure 4.21, the unfilled metal alloy composites have lower SIF value as compared to marble dust filled metal alloy composite materials. The fracture phenomenon occur where the possibility of high stresses and surface imperfections take place such as voids, surface and corner cracks [296].

Table 4.12 shows the experimental value of stress intensity factor for MD filled SiBr alloy composites in different wt.-% (0, 2.5, 5, 7.5 and 10wt. - %) of MD particulate varies in SiBr alloy composites with the varying in crack lengths (1, 2, 3 and 4 mm) respectively. Table 4.12 shows the value of stress intensity factor (SIF) increases with the increasing in wt.-% of MD filler in SiBr alloy composite materials for increasing crack length values. The maximum amount of SIF is found for 10 wt.-% (i.e. 2.5391MPa.m^1/2 for 4mm crack length) MD filled SiBr alloy composites at 4 mm crack length. The defects initially have in smaller quantities but with respect to time it grows through-out thickness of materials applications, which considered as three dimensional defects in composite materials. So the increasing in crack length also increases the crack formation in materials which affect the strength of materials [296].

Table 4.12. Stress Intensity Factor (K) of MD particulate filled SiBr alloy composites with different crack lengths

Sl.No.	Compositions / Crack length	1mm	2mm	3mm	4mm
1	SiBrMD-1	0.4103	0.6723	0.7481	0.8085
2	SiBrMD -2	0.5972	0.6584	0.72076	0.7971
3	SiBrMD -3	0.6108	0.7029	0.8494	0.9847
4	SiBrMD -4	0.8492	0.9179	1.3949	1.8784
5	SiBrMD -5	0.9635	1.1478	1.6508	2.5391

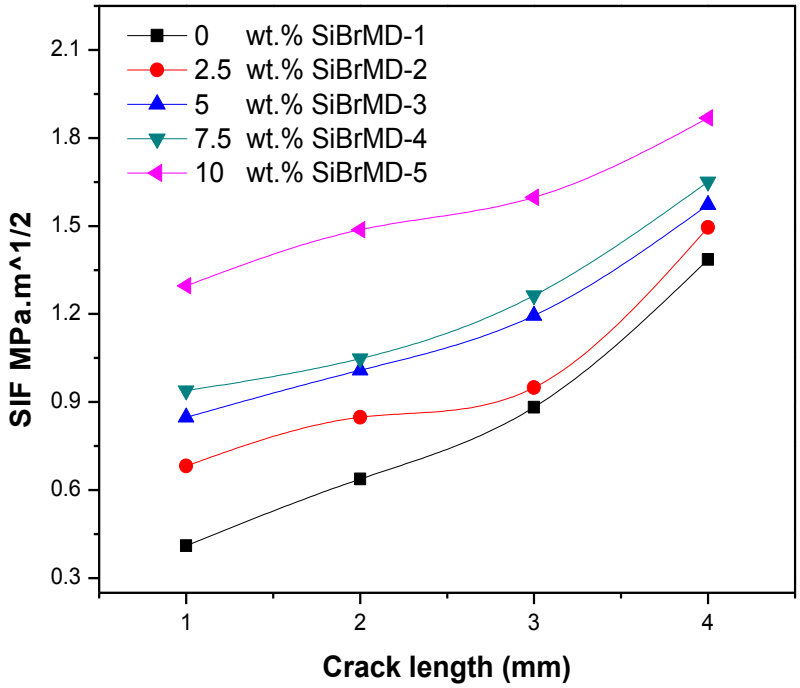

Figure 4.21. Mode I stress intensity factor for MD particulate filled SiBr alloy composite

4.3.7 Fractographs of MD particulate filled SiBr alloy composites after fracture test.

This technique is used routinely for the different failure analysis which occurred at different materials structure and examined by scanning electron microscopy [297].

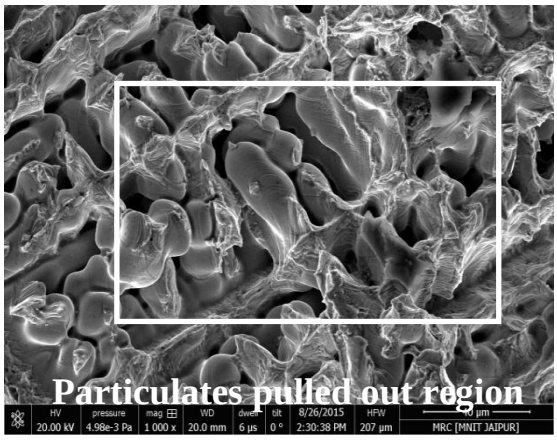

Figure 4.22a. SEM fractographs for 0 wt.-% of MD particulate filled SiBr alloy composites after fracture test

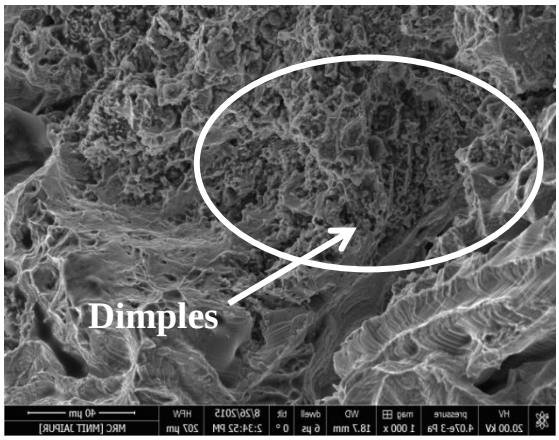

Figure 4.22b. SEM fractographs for 2.5 wt.-% of MD particulate filled SiBr alloy composites after fracture test

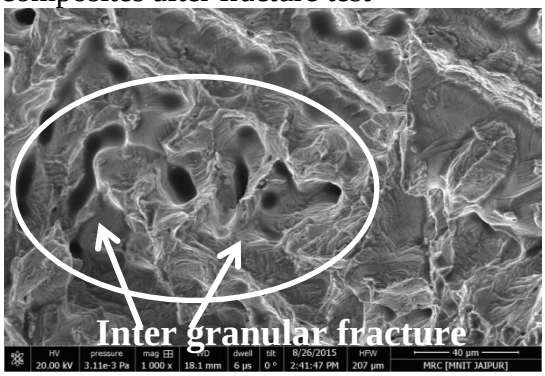

Figure 4.22c. SEM fractographs for 5 wt.-%of MD particulate filled SiBr alloy composites after fracture test

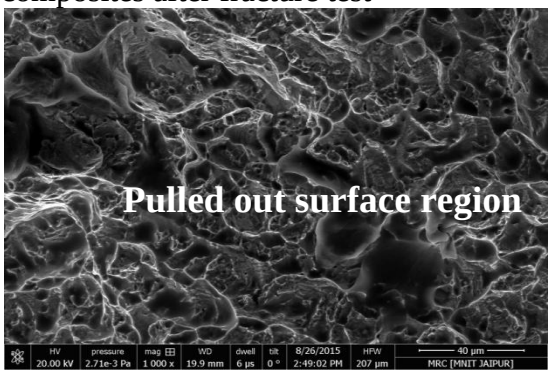

Figure 4.22d. SEM fractographs for 7.5 wt.-%of MD particulate filled SiBr alloy composites after fracture test

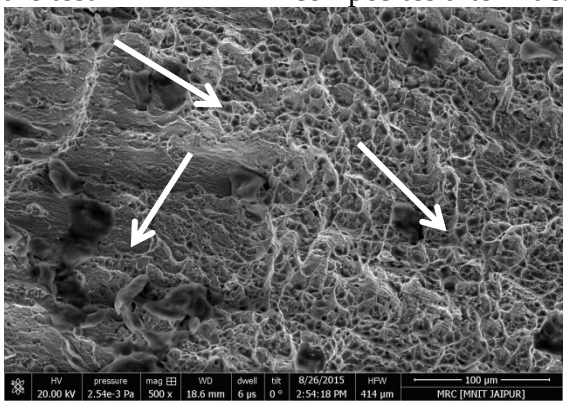

Figure 4.22e. SEM fractographs for 10 wt.-%of MD particulate filled SiBr alloy composites after fracture test

Figure 4.22. SEM Fractographs of fracture surfaces for MD particulate filled SiBr alloy composites after fracture test.

The micro-structural examination of fractured surface at different compositions (0wt.-%, 2.5wt.-%, 5wt.-%, 7.5wt.-% and 10wt. - %) of MD particulate filled SiBr alloy composite materials is studied by scanning electron microscopic (SEM) analysis.

Figure 4.22(a-e) shows the different micro-structural fractographs of MD particulates

filled SiBr alloy composite, collected after fracture test on universal testing machine (For different crack length 1, 2, 3 and 4mm). Figure 4.22a shows the fractographs for unfilled SiBr alloy composite and noticed existence of voids and dimples which impart ductile mode of fracture analysis. Figure 4.22b, shows the fractographs of 2.5wt.% MD filled SiBr alloy composite and is observed the matrix and the reinforcing particulate get de-bond which generates dimples in the composite. Figure 4.22c shows the fractographs of 5 wt.-% MD particulates filled SiBr alloy composite material.

From the Figure it observed that an intergranular fracture is formed, when the tensile force is applied on the material during fracture test the atomic bonding in between different atoms get loosen and starts to leave their actual place, which creates the gap in between those intergranulars that leads to intergranular fracture [297]. From Figure 4.22d, it is observed that in higher weight percentage of (i.e. 7.5wt.-%MD particulates) MD content is added in SiBr alloy composite, the presence of cracks in matrix get adjoining with those particulates and decline the presence of pulled out surface [298]. Figure 4.22(b, e) shows the scanning electron microscopic examination for fractured surface of 2.5 wt.-% and 10wt.-% MD filled SiBr alloy composite materials respectively and is observed that in the affected region the particulates get dispersed and creates high depth dimples due to the presence of higher amount of particulates in matrix phase.

4.3.8 Effect of hardness, contact stress and deformation of MD particulate filled SiBr alloy composites

The FEM analysis for single row deep groove ball bearing 6200 standard is modeled to calculate the contact stress and displacement and then compared with Hertzian theory at constant applied load. The comparisons of experimental as well as simulated results at constant loading condition for particulate filled metal alloy composites are shown in Figure 4.23 and Table 4.13. For the fabricated composite materials, hardness is also determined for different variables by using the Brinell Hardness Formula. The percentages of error for theoretical and simulated results of hardness are lies in between 1.69% to 2.62% respectively.

For the unfilled and particulate filled metal alloy composites, the contact deformation and contact stress are calculated at constant force i.e. 500N applied on deep groove ball bearing in ANSYS simulation software as shown in Figure 4.24.

From the Table 4.14, the experimental results for contact stress, displacement and stress Intensity results of particulate filled metal alloy composites can be observed by varying the modulus of elasticity.

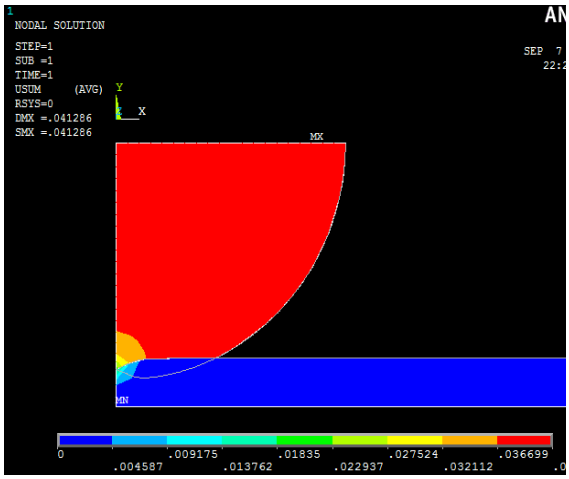

(a) 0 wt.-% MD SiBr-1

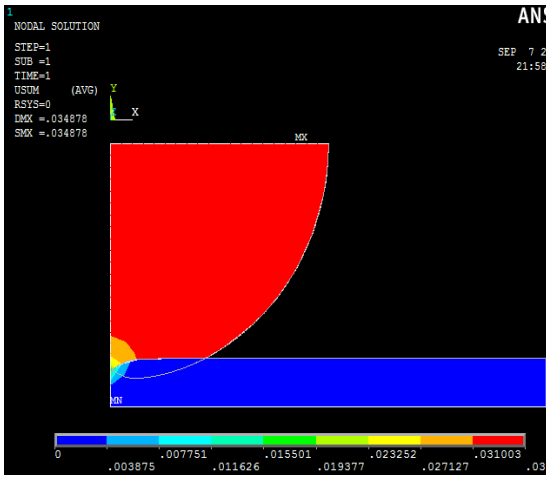

(b) 2.5wt.-% MD SiBr-2

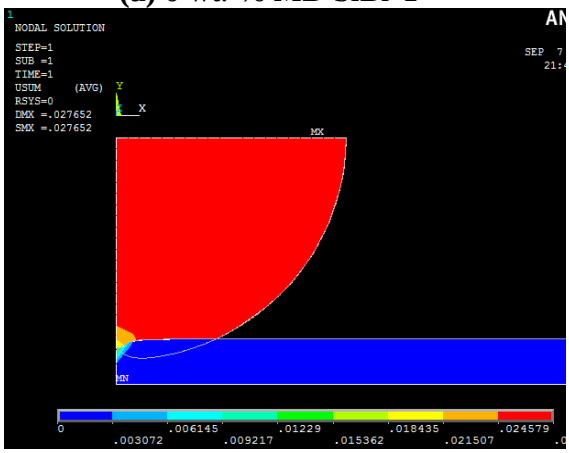

(c) 5wt.-% MD SiBr-3

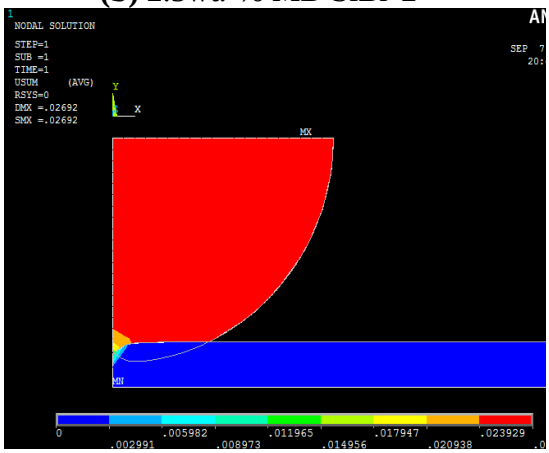

(d) 7.5wt.-% MD SiBr-4

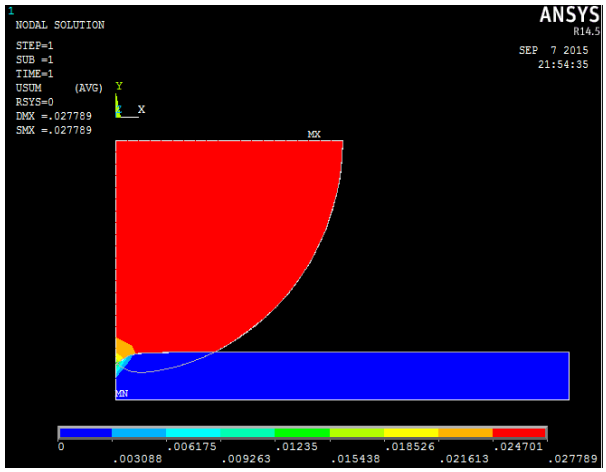

(e) 10wt.-% MD SiBr-5

Figure 4.23. Simulated results of penetration for MD particulate filled SiBr alloy composites

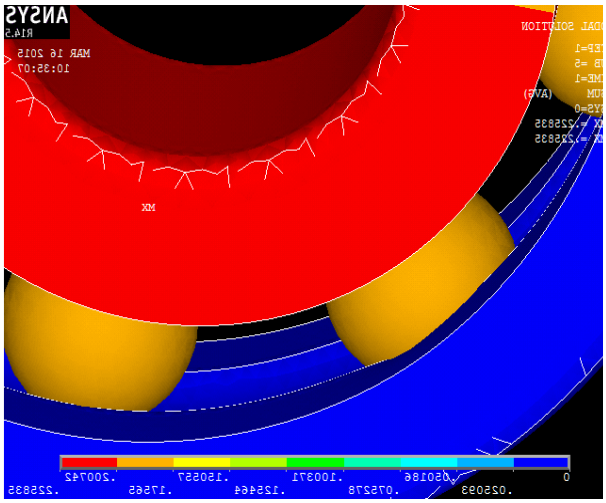

(a) 0wt.-% MD SiBr-1 (Displacement)

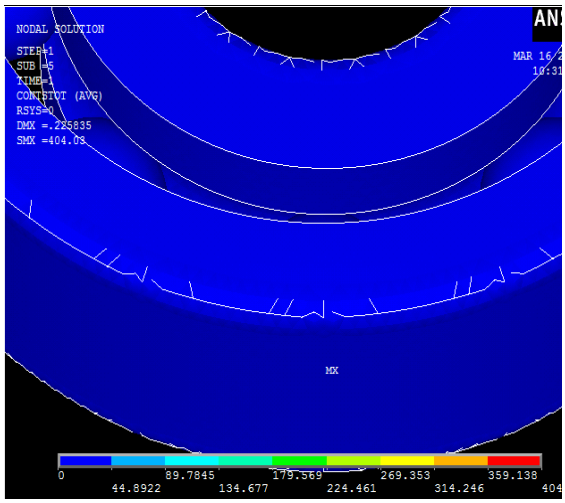

(b) 0wt.-% MD SiBr-1 (Contact stress)

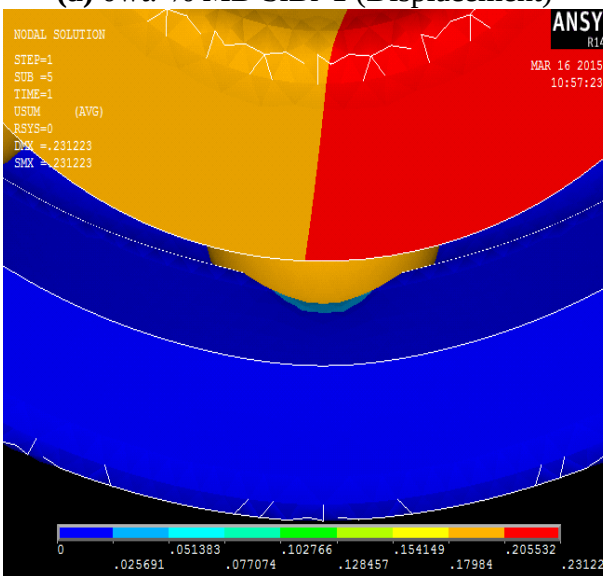

(c) 2.5wt.-% MD SiBr-2 (Displacement)

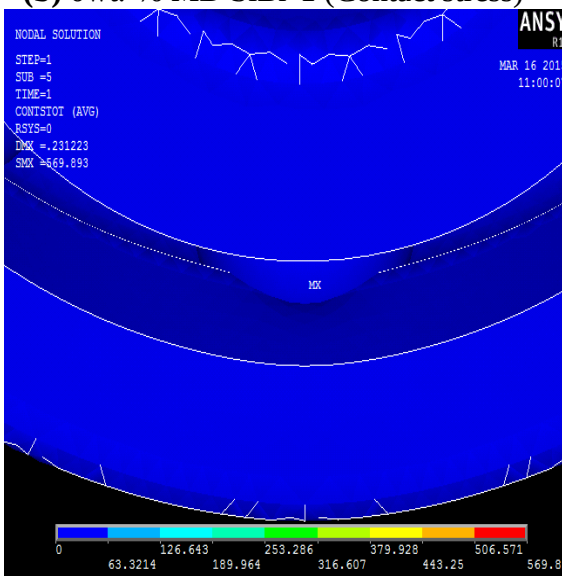

(d) 2.5wt.-% MD SiBr-2 (Contact stress)

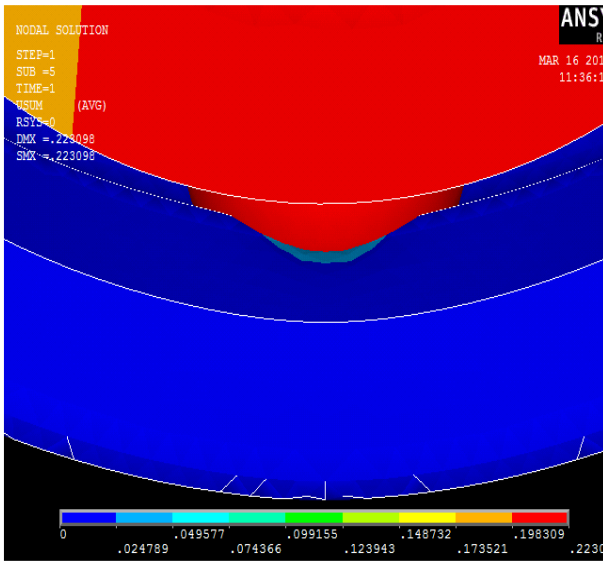

(e) 5wt.-% MD SiBr-3 (Displacement)

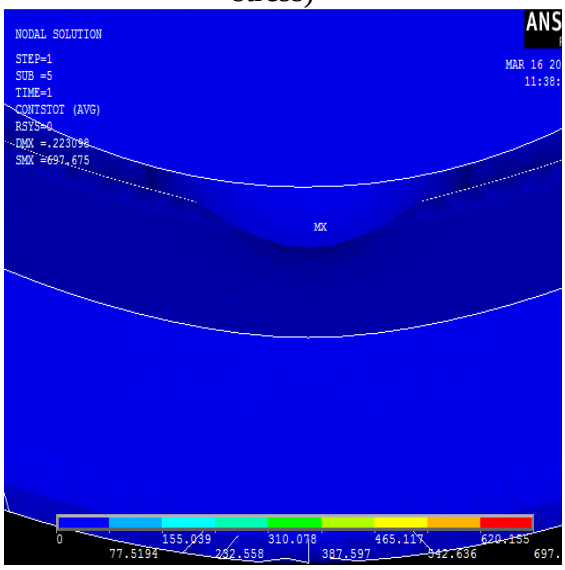

(f) 5wt.-% MD SiBr-3 (Contact stress)

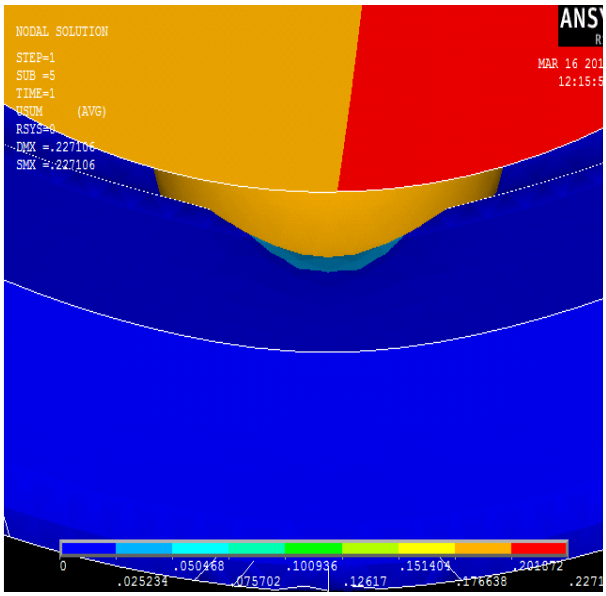

(g) 7.5wt.-% MD SiBr-4 (Displacement)

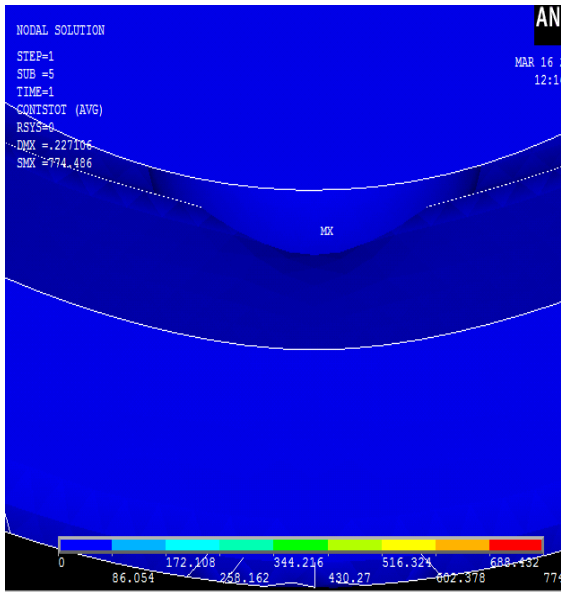

(h) 7.5wt.-% MD SiBr-4 (Contact stress)

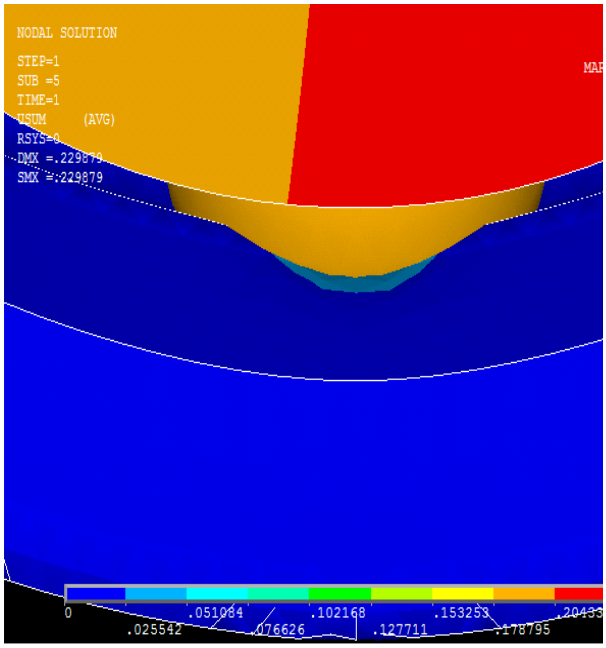

(i) 10wt.-% MD SiBr-5 (Displacement)

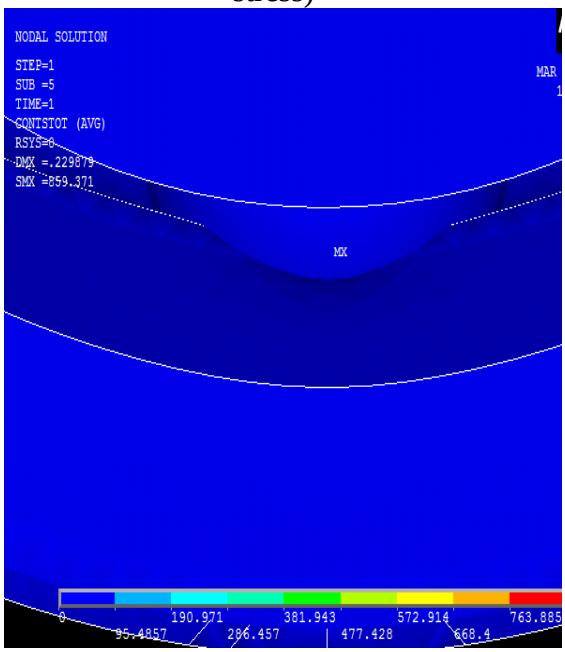

(j) 10wt.-% MD SiBr-5 (Contact stress)

Figure 4.24. Simulated results of displacement and contact stress analysis of MD particulate filled SiBr alloy composites at 500N

Table 4.15 shows the theoretical and simulated results of particulate filled metal alloy composites performed at constant load. The generated contact stress has been determined at certain variable using the Hertzian contact theory. The percentages of error for contact stress, theoretical and simulated results are lies in between 4.68% to 5.64% respectively. The percentage error for simulated results may also vary by the taking three to four times the simulation period.

Table 4.13. Comparison of experimental and simulated results for the hardness of MD particulate filled SiBr alloy composites (at constant loading i.e. 30kgf).

Composite Material	Modulus of Elasticity (MPa)	Hardness (Hv)	Hardness FEA	% Error
SiBrMD-1	1640.82	113.78	115.71	1.69
SiBrMD -2	2314.41	134.69	136.97	1.69
SiBrMD -3	2833.35	169.22	172.76	2.09
SiBrMD -4	3145.29	172.93	177.45	2.62
SiBrMD -5	3490.02	167.94	171.91	2.36

Table 4.14. Evaluations of Contact stress, displacement and stress intensity factor for different wt. % of MD particulate filled SiBr alloy composites for 500N loading conditions.

Composite Material	Modulus of Elasticity (MPa)	Contact stress (MPa)	Displacement (mm)	Stress Intensity (MPa)
SiBrMD-1	1640.82	193.177	0.225835	214.889
SiBrMD -2	2314.41	272.48	0.231223	303.105
SiBrMD -3	2833.35	333.576	0.223098	371.068
SiBrMD -4	3145.29	370.301	0.227106	411.921
SiBrMD -5	3490.02	410.887	0.229879	457.069

Table 4.15. Comparison of theoretical and simulated results of the MD particulate filled SiBr alloy composites (at constant loading i.e. 500N).

Composite Material	Hertzian contact Stress (MPa)	FEA contact Stress (MPa)	Percentage Error %
SiBrMD-1	385.46	404.03	4.82
SiBrMD -2	542.23	569.893	5.10
SiBrMD -3	660.41	697.675	5.64
SiBrMD -4	739.38	774.486	4.75
SiBrMD -5	820.97	859.371	4.68

Part IV

4.4 Physical, Mechanical and Fracture analysis of CaO particulate filled Silicon Bronze alloy composites

4.4.1 Effect of void contents on CaO particulate filled SiBr alloy composites

The theoretical and experimental densities of CaO filled SiBr alloy composites are shown in Table 4.16. It is observed that the void content in composite material increases with the increased in wt.-% of filler particulates i.e. from 0.824 % to 0.504 % up to 7.5wt.-% of CaO filled SiBr alloy composites. But beyond 7.5 wt.-% CaO filler particulate up to 10wt.-% filler the percentages of void contents get slowly increased to 1.530 %. The decrement in void content is occurred due to increase in wettability or by the diminishing threshold pressure or applied load on infiltration process [299].

Table 4.16. Comparison of experimental density and theoretical density

Sl. No.	Composition	Theoretical density ($gm./cc^3$)	Experimental density ($gm./cc^3$)	Void content (%)
1	SiBrCaO-1	8.49	8.42	0.824
2	SiBrCaO -2	8.17	8.11	0.734
3	SiBrCaO -3	8.08	8.03	0.618
4	SiBrCaO -4	7.93	7.89	0.504
5	SiBrCaO -5	7.83	7.71	1.530

The formation of porosity in composite materials is formed largely due to the cause of gas entrapment during stirrer process of fabrication or during the fabrication process the air bubbles formed in slurry either separately or as air envelope to the filler particulates, shrinkage occurs during solidification and mostly due to the volume fraction of reinforced particles in composite materials [300]. Therefore, the reduction of void content in this study reduces possibly by proper fabrication technique.

4.4.2 Effect of hardness on CaO particulate filled SiBr alloy composites

Figure 4.25 exhibited the variation of hardness for CaO filled SiBr alloy composites, which shows the remarkable improvement of micro-hardness of the composite up to 7.5wt.-% of CaO particulates. This is due to the resistance behaviour of CaO filled SiBr alloy composites against the indentation during hardness test that has been tremendously increased by the addition of CaO particles [301]. Figure 4.25, shows the micro-hardness behaviour of composite increased with the increased in weight

percentage of CaO particulates. The hardness is 119.25Hv at 0wt.-% and 140.8 Hv at 7.5wt.-% respectively.

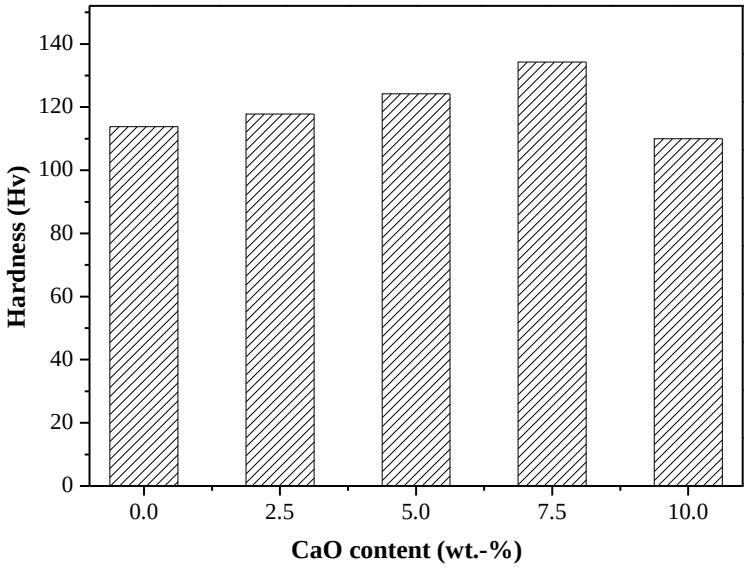

Figure 4.25. Variation of micro-hardness of CaO particulate filled SiBr alloy composites

The addition of hard reinforced particles increases the dislocation density of matrix alloy and the interaction bonding between reinforcement and matrix accumulate the micro hardness of composite materials. When the wt.-% of filler particles increases the number of dislocation in SiBr alloy also increases due to the presence of large quantity of hard CaO filler particles that steer the higher interaction in between the reinforced particulates [302]. However, the unfilled metal alloy has lower hardness value as compared to CaO filled SiBr alloy composites. The increased in value of micro-hardness in CaO filled SiBr alloy composites that directly affects the decrement of porosity in the microstructure of sample [303].

4.4.3. Effect of compressive strength on CaO particulate filled SiBr alloy composites

The value of compressive strength for different wt.-% (0, 2.5, 5, 7.5 and 10) of CaO filled SiBr alloy composites are shown in Figure 4.26. Figure shows the increment of compressive strength for (0wt.-% to 10wt. - %) CaO particulate filled alloy composites with the increasing wt.-% of filler particles (i.e. for CaO) up to 7.5 wt.-% (i.e.68 MPa) reinforcements.

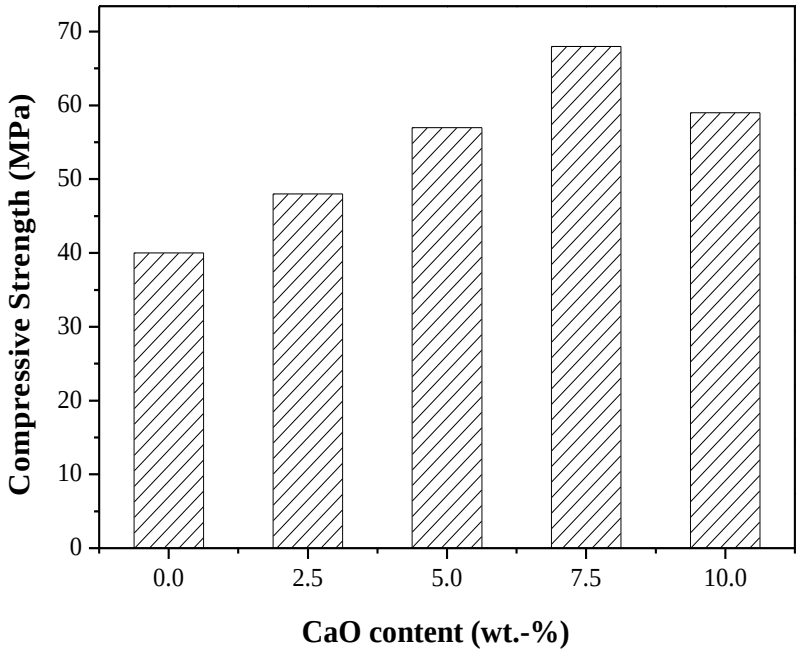

Figure 4.26. Compressive strength of CaO particulate filled SiBr alloy composites

The improvement in compressive strength of the particulate filled alloy composite is due to the strengthening effects developed in hard particulate filled alloy composites but beyond it from 7.5w.-% to 10wt.-% of filler particles value of compressive strength shows diminish behaviour. The increasing amount of hardness can be the reason of increasing compressive strength value up to 7.5wt.-% of CaO filled SiBr alloy composites. These effects include the transfer of load from matrix surface to particulate surface and interaction between the matrix dislocation and the particulates respectively. Swam et al. [304] studied about the mechanical properties ofAl6061-Tungsten carbide reinforced with Tungsten carbide (WC) and Al6061-graphite particulate with the varying wt.-% of particulates from 0wt.-% to 4wt.-%. From the study the compressive strength of the composite materials is increased due to the decreasing in interparticle space in between WC particulates, although the WC have more hardness as compared to Al6061. The WC particulates resist the deforming stresses in composite materials that enhance the compressive strength of composites [304].

4.4.4 Effect of flexural strength on CaO particulate filled SiBr alloy composites

Figure 4.27, shows the flexural strength of CaO filled SiBr alloy composites at five different particulate content. It can be seen that the flexural strength of the CaO filled SiBr alloy increased with the increase of CaO content up to 7.5 wt.-% (i.e.196.5MPa).

From the Figure it is also observed that the flexural strength of the unfilled metal alloy composite has lower flexural strength value (i.e.153MPa) as compared to CaO filled SiBr alloy composites. The flexural strength of composite material decreases from 7.5wt.-% to 10wt.-% CaO particulates, the reason for diminished flexural strength can be the presence of large amount of particulates that did not have sufficient bonding strength in between matrix material and reinforcement particulate [305].

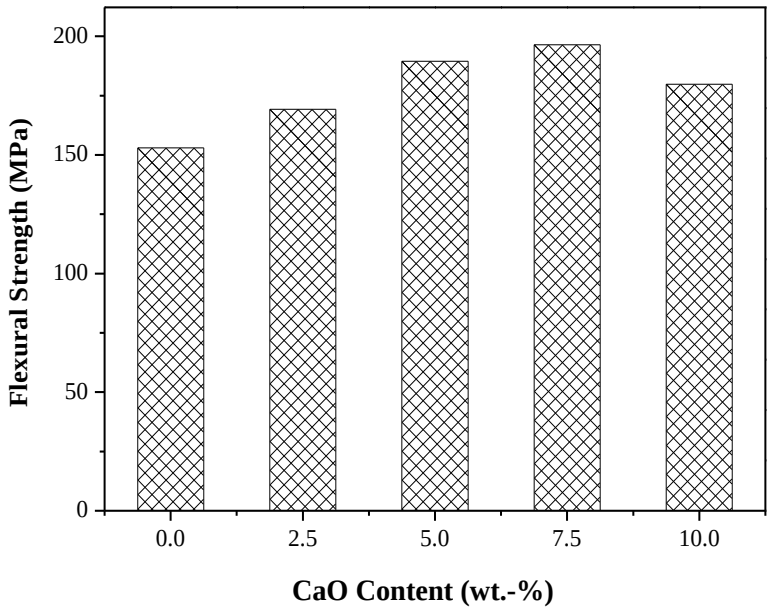

Figure 4.27. Flexural strength of CaO particulates filled SiBr alloy composites

A similar observation is also observed by Zhang et al. [305] for calculation of flexural strength of SiC particulates filled metal alloy composites. They found that the flexural strength is enhanced by 11.3% for 6 wt.-% SiC impingement in base material. When the SiC particles imbedded in the base materials can prevent the sudden expansion of crack formation and that phenomenon improvise the flexural strength of the alloy composite materials. In most of the cases, the particulate filled metal alloy composites have superior mechanical properties than the unfilled metal alloy composites that may be these metal alloy composite have higher dislocation densities as a result the thermal expansion coefficient differences the generation of dislocation.

4.4.5. Effect of impact strength on CaO particulates filled SiBr alloy composites

Figure 4.28 shows the enhancement of impact strength up to 7.5 wt.-% CaO filled SiBr alloy composites (i.e. 45J) that was much higher as compared to unfilled metal alloy composite material (i.e. 27J) [306].The improvement of impact strength up to 7.5 wt.-% of CaO particulates was found due to the presence of less amount of filler in

to base matrix materials. The hardened reinforced particles of CaO easily get trapped by base ductile materials that effectively strengthen the materials properties due to stronger adhesive force in between particulates and matrix materials atoms [307]. After 7.5 wt.-%CaO particulates, the impact strength become decreases with the increases filler particulates up to 10 wt.-% in matrix materials, the higher amount of reinforced particles shows the clustering effect which possibly develop crack phenomenon and accordingly it propagates while increases the amount of applied force, that reduces the impact strength of composite materials.

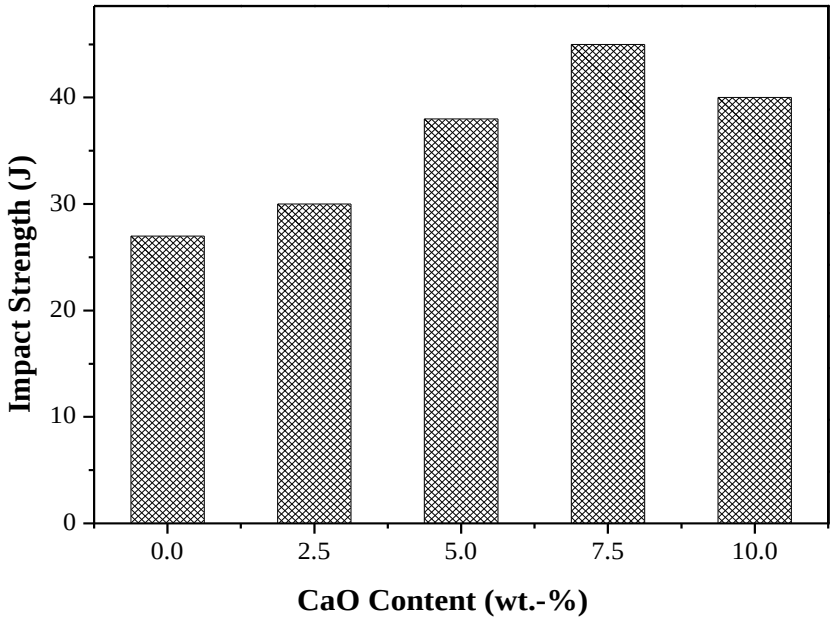

Figure 4.28. Impact strength of CaO particulate filled SiBr alloy composites

4.4.6. Effect of stress intensity factor on CaO particulate filled SiBr alloy composites

The SIF value for CaO filled SiBr alloy composites can be computed by use of equation (3.9) and (3.10) at four different crack lengths (i.e. 1, 2, 3, and 4 mm) as shown in Table 4.17 and Figure 4.29. Figure 4.29 shows the variation of SIF for different crack lengths at different wt.-% of CaO filled SiBr alloy composites materials. The unfilled alloy shows the lower value of SIF as compared to CaO filled SiBr alloy composite materials. With the increasing in demand of composite materials for various applications it's necessarily required to understand the exact mechanical behaviour of composites. From this aspect the dynamic crack propagation

phenomenon or response of cracks in composite material under applied load is a very widely studied area by theoretically as well as in experimentally [308].

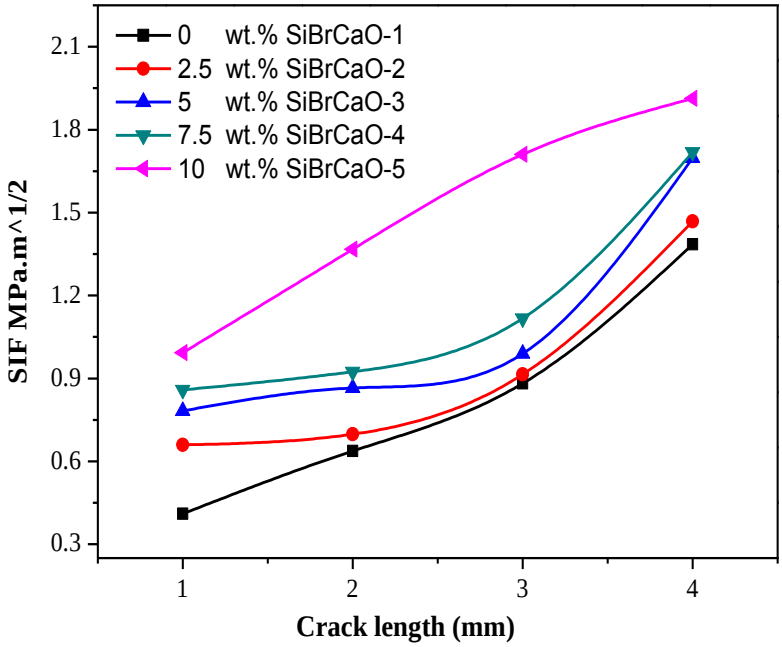

Figure 4.29. Mode I stress intensity factor for CaO particulate filled SiBr alloy composite

Table 4.17 shows the experimental value of stress intensity factor for CaO filled SiBr alloy composites. The different wt.-% (0, 2.5, 5, 7.5 and 10wt. - %) of CaO particulate varies in SiBr alloy composites with the varying crack lengths (1, 2, 3 and 4 mm). Table 4.17 shows the results of stress intensity factor (SIF) that increases with the increasing in wt.-% of CaO filled SiBr alloy composites as well as the increasing in value of crack lengths. The maximum amount of SIF is found for 10 wt.-% (i.e. 1.91338 MPa.m^1/2 for 4mm crack length) CaO filled SiBr alloy composites for 4 mm crack length.

To overcome the stress related problems there are many technique existed but only few of them have exact solution for the problem, this may be due to the complexity in mathematical analysis [308]. The maximum amount of stresses is found at the crack tips which propagate towards the failure of materials. By the stress intensity factor K, the singular stress contribution can be characterised properly [309].

Table 4.17. Stress Intensity Factor (K) of CaO particulate filled SiBr alloy composites with different crack lengths

Sl.No.	Compositions ⇩ / Crack length ⇨	1mm	2mm	3mm	4mm
1	SiBrCaO-1	0.4103	0.6723	0.7481	0.8085
2	SiBrCaO -2	0.6594	0.6979	0.8149	0.9683
3	SiBrCaO -3	0.7822	0.8652	0.9191	0.9973
4	SiBrCaO -4	0.8582	0.9238	1.1176	1.4185
5	SiBrCaO -5	0.9936	1.3671	1.71102	1.91338

4.4.7 Fractographs of CaO particulate filled SiBr alloy composites after fracture test.

Different surface failure initiation such as cracks, voids etc. can be uncovered by studying the fractured surface of the alloy composites by scanning electron microscopic analysis. The microstructural examination of different compositions (0wt.-%, 2.5wt.-%, 5wt.-%, 7.5wt.-% and 10wt. - %) of CaO particulates filled SiBr alloy composite is studied using scanning electron microscopic (SEM) analysis for fractured surface. Figure 4.31(a-e) shows the different fractographs at a magnification view for CaO particulates filled SiBr alloy composite, samples are examined after fracture test (For different crack length 1, 2, 3 and 4mm).

Figure 4.31a shows the micrographs for unfilled metal alloy composites after fracture test, in this the pulled out region shown, when the fracture test is performed on universal testing machine at applied tensile force specimen that gets brooked up and the broken matrix materials get pulled out which creates dimple type structure. Similar, observation is found for 2.5 wt.-% CaO filled SiBr alloy composite materials while analysing after fracture test (Shown in Figure 4.31b). With the presence of particulates the bonding between the matrix and particulates is strong in comparison of unfilled materials and this becomes the reason of small dimples presence.

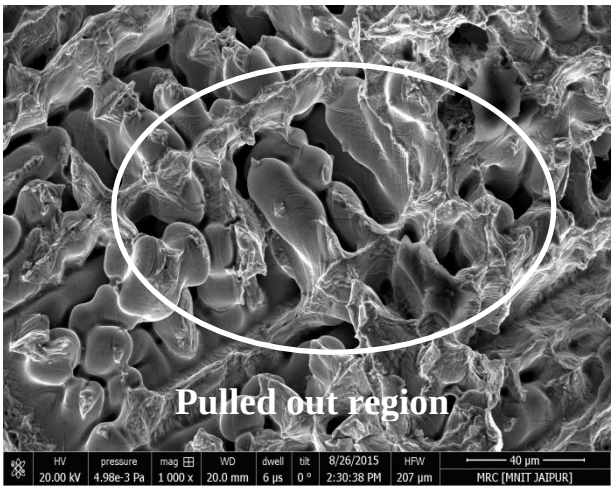

Figure 4.30a. SEM fractographs for 0 wt.-%of CaO particulate filled SiBr alloy composites after fracture test

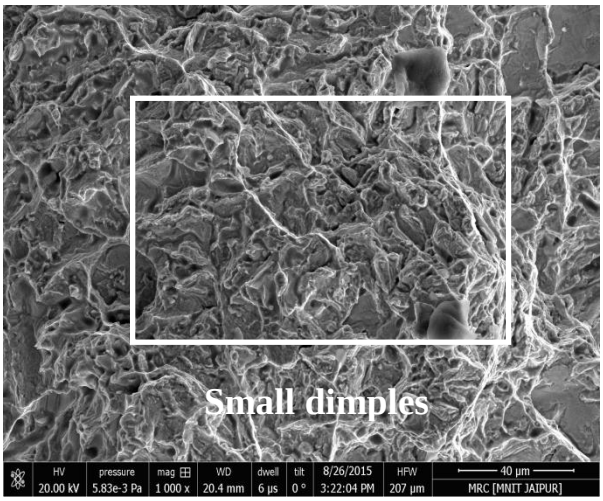

Figure 4.30b. SEM fractographs for 2.5 wt.-%of CaO particulate filled SiBr alloy composites after fracture test

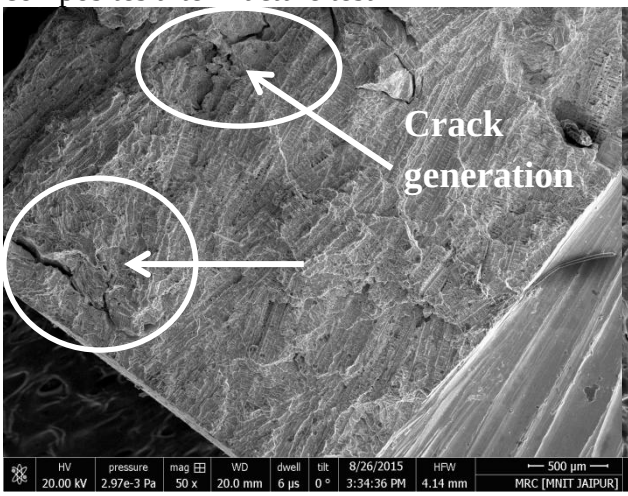

Figure 4.30c. SEM fractographs for 5 wt.-%of CaO particulate filled SiBr alloy composites after fracture test

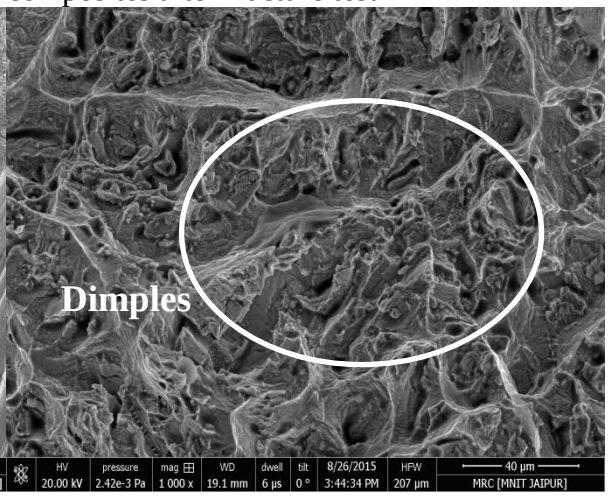

Figure 4.30d. SEM fractographs for 7.5 wt.-%of CaO particulate filled SiBr alloy composites after fracture test

Figure 4.30e. SEM fractographs for 10 wt.-% of CaO particulate filled SiBr alloy composites after fracture test

Figure 4.30. SEM Fractographs of fracture surfaces for CaO particulate filled ZA-27 alloy composites after fracture test

When the small micro voids agglomerate and growth in form of coalescence can leads toward micro cracks, same phenomenon is shown in Figure 4.31c for 5 wt.-% CaO particulates filled SiBr alloy composite materials. Or when the applied load continuously impact on specimen micro voids can creates and this leads to coalescence that generates complete fracture in specimen. Such types of micro void are generally observed at the centre on inclusion of samples [310].

Figure 4.31d shows the dimple structure at specimen surface after fracture test which examined by scanning electron microscopic analysis. The hard particulates contain by these dimples indicates the presence of ductile mode fracture in the composite materials specimen. [311,312]. Similarly, Figure 4.31e shows the scanning electron microscope for 10 wt.-% CaO filled SiBr alloy composite materials in fast fractured region, the tear ridges are found nearly plastic fracture behaviour [313]. However, at higher percentages of filler content in the matrix material the ductility nature of the composite drops but the results seems to be ductile in characteristics.

4.4.8 Effect of hardness, contact stress and deformation of CaO particulate filled SiBr alloy composites

The single row deep groove ball bearing 6200 standard was taken for the computation of contact stress and displacement by simulation analysis and then compared the outcomes with Hertzian theory at constant applied load. The comparison results of experimental as well as simulated results that performed at constant load for different wt.-% of particulate filled metal alloy composites are shown in Figure 4.31 and Table 4.18. Similarly the generated hardness experimentally and simulated results are calculated at certain variables by using the Brinell Hardness formula and the percentage of error has been found in between 0.005% to 1.5% for theoretical and simulation analyses respectively. The fabricated composite shows the increasing hardness with the increasing in wt.-% of filler particles in base metal alloy composites.

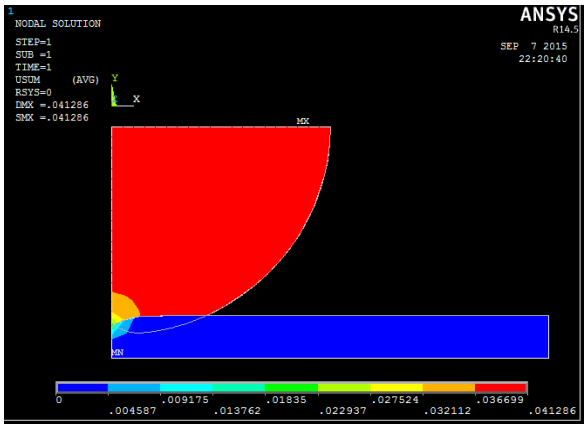

(a) 0 wt.-% CaO SiBr-1

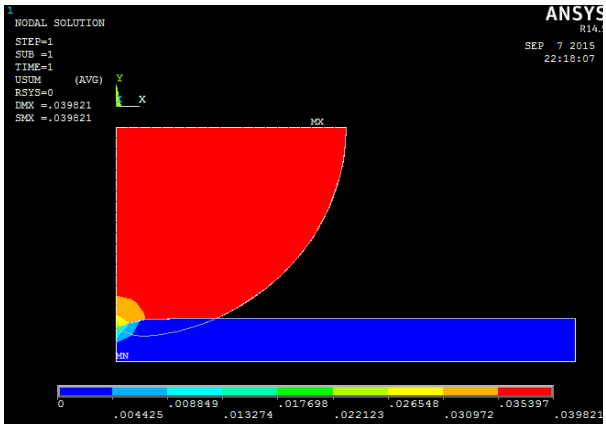

(b) 2.5wt.-% CaOSiBr -2

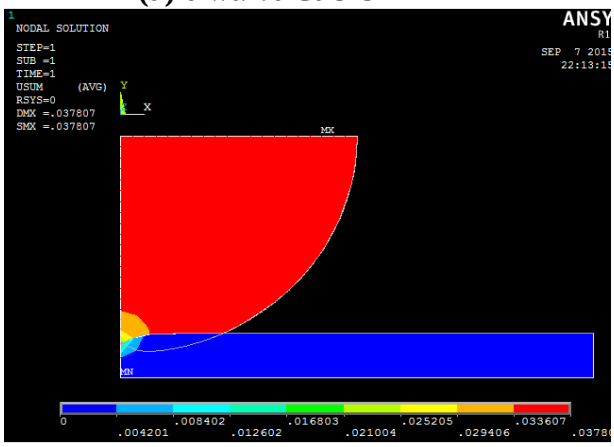

(c) 5wt.-% CaOSiBr -3

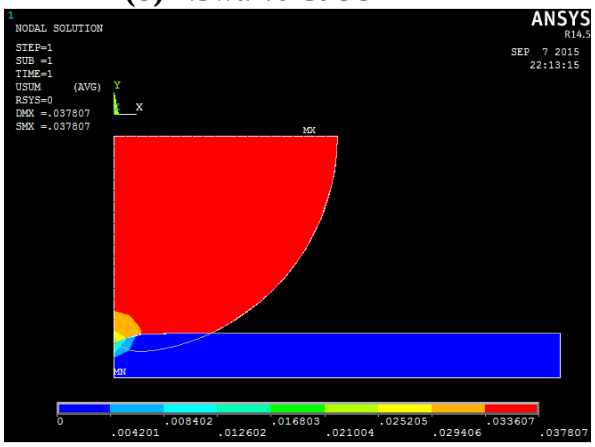

(d) 7.5wt.-% CaOSiBr -4

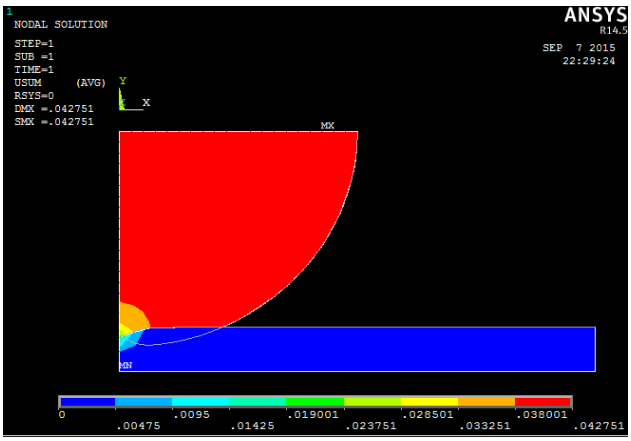

(e) 10wt.-% CaOSiBr-5

Figure 4.31. Simulated results of penetration for MD particulate filled SiBr alloy composites

Figure 4.32 shows the contact deformation and contact stress analysis for the unfilled and particulate filled metal alloy composites that are calculated at constant force i.e. 500N applied on deep groove ball bearing in ANSYS simulation software. The Table 4.19 exhibits the contact stress, displacement and stress intensity results experimentally which performed at different modulus of elasticity for particulate filled metal alloy

composites. Similarly the comparison of theoretical and simulated results is shown in Table 4.20 which performed at constant load for different particulate filled alloy composites. The Hertzian contact theory at certain variable is used to determine the contact stress analysis which performed. Table 4.20 shows the percentage of error for theoretical and simulation analyses which lies in between 0.69% to 5.82% respectively. The amount of percentage error can be varied by taken three to four times average simulation analysis.

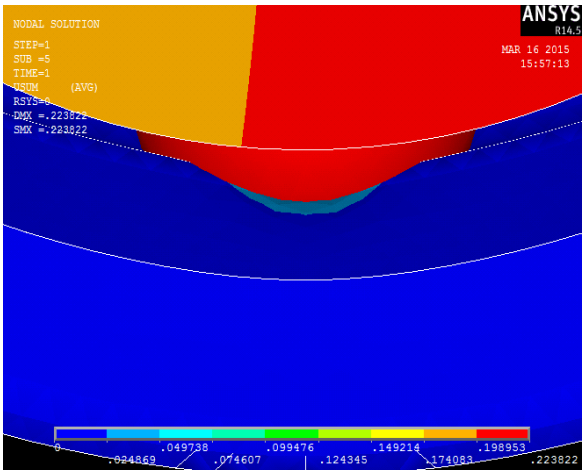

(a) 0wt.-% CaOSiBr-1 (Displacement)

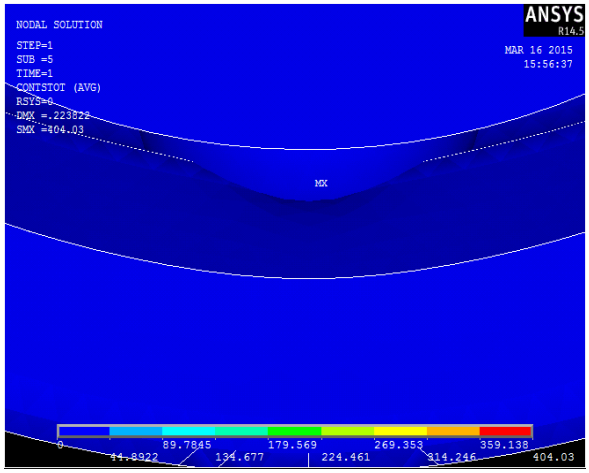

(b) 0wt.-% CaOSiBr-1 (Contact stress)

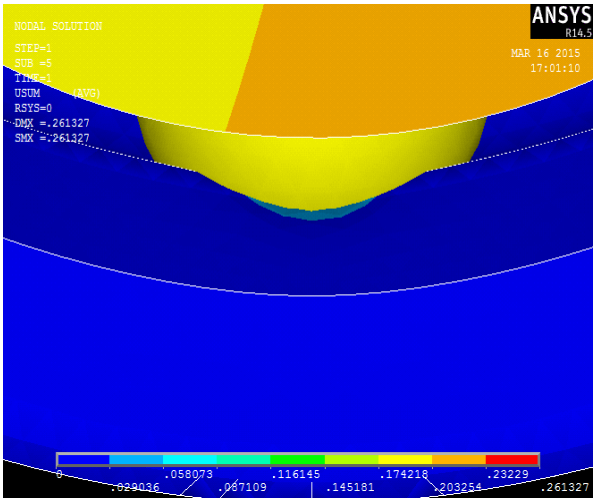

(c) 2.5wt.-% CaOSiBr-2 (Displacement)

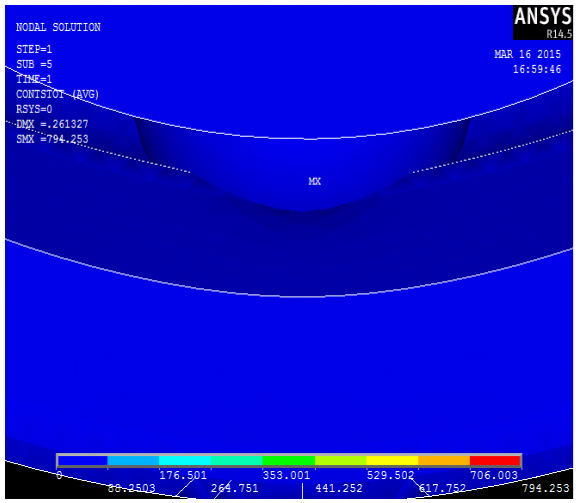

(d) 2.5wt.-% CaOSiBr-2 (Contact stress)

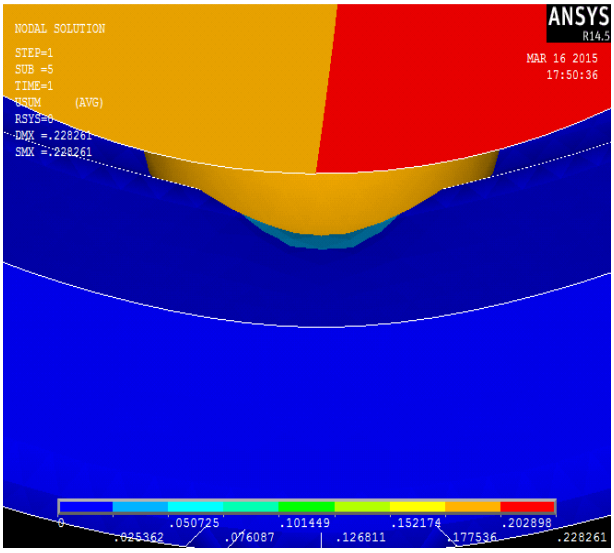

(e) 5wt.-% CaOSiBr-3 (Displacement)

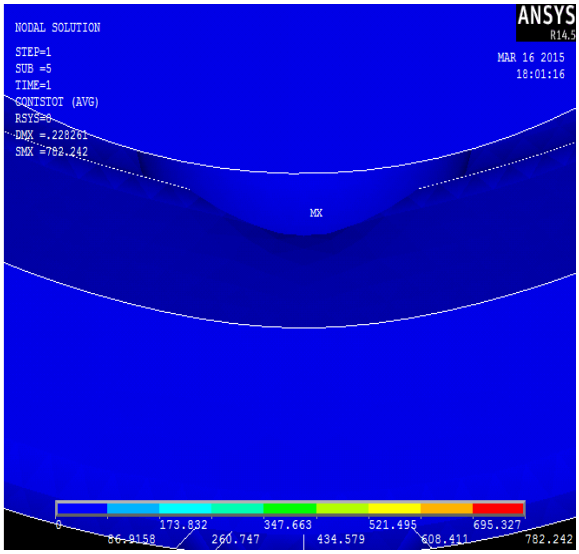

(f) 5wt.-% CaOSiBr-3 (Contact stress)

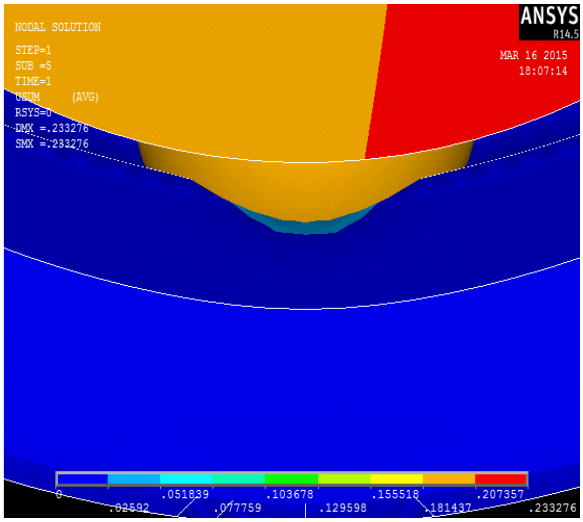

(g) 7.5wt.-% CaOSiBr-4 (Displacement)

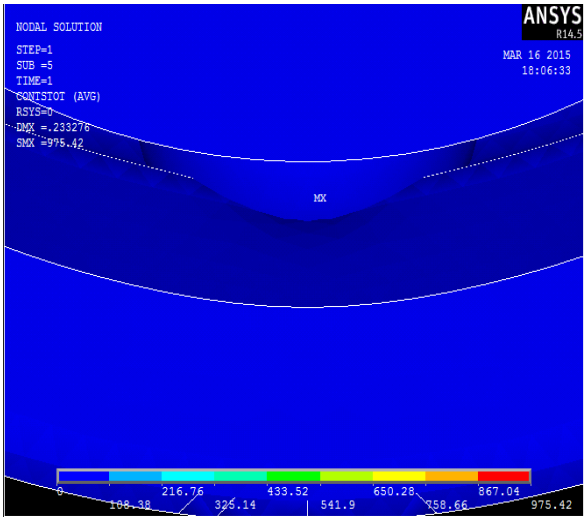

(h) 7.5wt.-% CaOSiBr-4 (Contact stress)

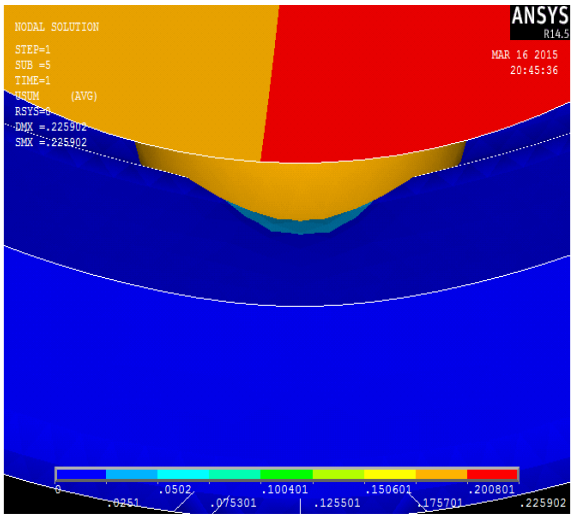

(i) 10wt.-% CaOSiBr-5 (Displacement)

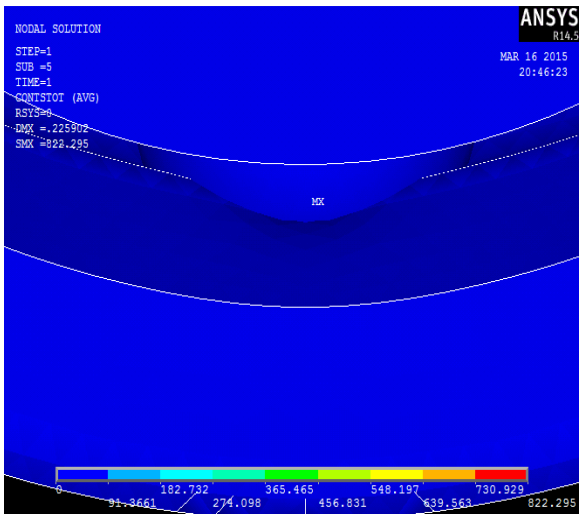

(j) 10wt.-% CaOSiBr-5 (Contact stress)

Figure 4.32. Simulated results of displacement and contact stress analysis of CaO particulate filled SiBr alloy composites at 500N.

Table 4.18. Comparison of experimental and simulated results for the hardness of CaO particulate filled SiBr alloy composites (at constant loading i.e. 30kgf).

Composite Material	Modulus of Elasticity (MPa)	Hardness (Hv)	Hardness FEA	% Error
0 wt.% CaOSiBr -1	1640.82	113.78	115.71	1.69
2.5 wt.% CaOSiBr -2	3227.43	117.83	119.96	1.81
5.0 wt.% CaO SiBr-3	3176.79	124.23	126.35	1.71
7.5 wt.% CaOSiBr -4	3961.31	134.26	136.78	1.88
10.0 wt.% CaOSiBr -5	3339.45	109.99	111.74	1.59

Table 4.19. Evaluations of Contact stress, displacement and stress intensity factor for different wt. % of CaO particulate filled SiBr alloy composites for 500N loading conditions.

Composite Material	Modulus of Elasticity (MPa)	Contact stress (MPa)	Displacement (mm)	Stress Intensity (MPa)
0 wt.% CaOSiBr-1	1640.82	193.177	0.223822	214.889
2.5 wt.% CaOSiBr-2	3227.43	377.361	0.261327	420.626
5.0 wt.% CaOSiBr-3	3176.79	374.01	0.228261	416.047
7.5 wt.% CaOSiBr-4	3961.31	466.373	0.233276	518.791
10.0 wt.% CaOSiBr-5	3339.45	393.16	0.225902	437.349

Table 4.20. Comparison of theoretical and simulated results of the CaO particulate filled SiBr alloy composites (at constant loading i.e. 500N).

Composite Material	Hertzian contact Stress (MPa)	FEA contact Stress (MPa)	Percentage Error %
0 wt.% CaOSiBr-1	385.46	404.03	4.817621
2.5 wt.% CaOSiBr-2	779.42	794.253	1.903082
5.0 wt.% CaOSiBr-3	763.24	782.242	2.489649
7.5 wt.% CaOSiBr-4	955.69	975.42	2.064477
10.0 wt.% CaOSiBr-5	802.98	822.295	2.405415

4.5. Effect of optimization on physical and mechanical behaviour of the proposed composites materials using preference selection index (PSI) method

4.5.1. Experiment results

Generally the design optimization techniques used for different engineering systems to get the modelling or simulation –based optimizations. But the different uncertainties that arises during measurement of different physical quantities, machine

manufacturing tolerance and such types other parameters, are required a reliable approach to check the optimization for that particular designs. Numerous techniques are explored to get the optimum outcomes with an affordable cost and time parameters [314]. From the past many years the selection of materials and other parameters become a contradictory topic not because of the selection of optimum parameters although required physical, mechanical, electrical, environment effect, design considerations, etc. which establish a perfect relationship in between different selection criterion as well as the elected optimized procedure for the whole processes. Mainly the different physical and mechanical properties such as, density, hardness, compressive strength, flexural strength, impact strength, fracture toughness, wear behaviour etc. affects the materials selection problems.

To resolve such type of problems there are numerous existing methods that support the materials selection problems and fulfil the materials expectations perfectly [315]. And such techniques are also known as materials optimization techniques, preference selection index (PSI) technique one of them. A detailed description of the selected criterions is given in Table 4.21. The experiment results corresponding to each criterion are listed in Table 4.22.

Table 4.21. Description of the selected criterions of particulate filled metal alloy composites

Criterions	Performance implications of criterion	Description of the individual criterion
Void content	The void content for Particulate filled metal alloy composites was calculated by using the following equation:$V_c = \frac{\rho_t - \rho_e}{\rho_t}$, where, ρ_e is the experimental and ρ_t is the theoretical density of the composite.	C-1 Lower-the-better
Hardness	The hardness used to be resistance to indentation under applied loading condition was measured on Walter Uhltesting machine having square based pyramidal (angle 136° between two opposite faces) diamond indenter the quadrate value read on the 'C' scale.	C-2 Higher-the-better
Compressive strength	The Compressive strength for particulate filled metal alloy composites was performed on universal testing machine (UTM) Instron 1195with the specimen dimension of 25×10×10 mm^3 at 2mm/s cross-sectional speed.	C-3 Higher-the-better
Flexural	The Flexural strength for particulate filled metal	C-4

strength	alloy composites was performed on universal testing machine (UTM) Instron 1195with the specimen dimension of 50 mm × 8mm × 8 mm having span length of 40 mm at 2mm/s cross-sectional speed.	Higher-the-better
Impact strength	The Impact strength for particulate filled metal alloy composites was performed on universal testing machine (UTM) Instron 1195with the specimen dimension size of 55 × 10 × 10 mm^3 and the depth under the notch is 10.2 mm.	C-5 Higher-the-better
Stress intensity factor (1mm)	The SIF for particulate filled metal alloy composites was performed on universal testing machine (UTM) Instron 1195. The specific dimensions for specimen are length (L) = 50mm, thickness (B) = 5 mm, width (W) = 5 mm with the varying crack length of 1mm.	C-6 Lower-the-better
Stress intensity factor (2mm)	The SIF for particulate filled metal alloy composites was performed on universal testing machine (UTM) Instron 1195. The specific dimensions for specimen are length (L) = 50mm, thickness (B) = 5 mm, width (W) = 5 mm with the varying crack length of 2mm.	C-7 Lower-the-better
Stress intensity factor (3mm)	The SIF for particulate filled metal alloy composites was performed on universal testing machine (UTM) Instron 1195. The specific dimensions for specimen are length (L) = 50mm, thickness (B) = 5 mm, width (W) = 5 mm with the varying crack length of 3mm.	C-8 Lower-the-better
Stress intensity factor (4mm)	The SIF for particulate filled metal alloy composites was performed on universal testing machine (UTM) Instron1195. The specific dimensions for specimen are length (L) = 50mm, thickness (B) = 5 mm, width (W) = 5 mm with the varying crack length of 4mm.	C-9 Lower-the-better

Table 4.22. Experimental results of the criterions of particulate filled metal alloy composites.

Composite	C-1 (V)	C-2 (H)	C-3 (C)	C-4 (F)	C-5 (I)	C-6 (1mm)	C-7 (2mm)	C-8 (3mm)	C-9 (4mm)
ZA-0	1.8	156	507	459.38	3	0.2951	0.4032	0.5685	0.6672
ZA-1	1.64	191.2	525	475.31	4	0.3245	0.4962	0.6493	0.83
ZA-2	1.46	215.5	551	507.72	5	0.4095	0.7218	0.8673	0.9638
ZA-3	1.28	202	665	552.19	6	0.6306	1.0813	1.5483	1.8991
ZA-4	2.62	183.5	655	684.38	4	0.5098	0.7916	1.0296	1.2425
ZA-5	0.81	181.75	596	554.05	3.5	0.4299	0.5012	0.5963	0.7775
ZA-6	0.82	185.5	723	645	4	0.5162	0.6513	0.8935	1.4953
ZA-7	1.03	193	525	937	4.5	0.6113	0.8725	1.3824	1.9056
ZA-8	1.26	161.5	494	568	5	0.9114	1.2044	1.4632	2.0127
SiBr-0	0.824	119.25	40	153	27	0.4103	0.6372	0.8817	1.3857
SiBr-1	0.599	141.25	43	172.14	32	0.6817	0.8478	0.949	1.4949
SiBr-2	0.748	177.6	52	183.7	40	0.8478	1.0088	1.1949	1.5729
SiBr-3	0.76	181.5	70	198.43	48	0.9391	1.0478	1.2635	1.6508
SiBr-4	1.28	176.25	61	167.3	38	1.2957	1.4871	1.5978	1.8684
SiBr-5	0.734	123.5	48	169.25	30	0.6594	0.6979	0.9149	1.4683
SiBr-6	0.618	130.24	57	189.54	38	0.7822	0.8652	0.9891	1.6973
SiBr-7	0.504	140.8	68	196.5	45	0.8582	0.9238	1.1176	1.7185
SiBr-8	1.53	115.25	59	179.8	40	0.9936	1.3671	1.711	1.9133

Table 4.23. Normalized matrix of particulate filled metal alloy composites.

Composite	C-1 (V)	C-2 (H)	C-3 (C)	C-4 (F)	C-5 (I)	C-6 (1mm)	C-7 (2mm)	C-8 (3mm)	C-9 (4mm)
ZA-0	0.28	0.7239	0.7012	0.4903	0.0625	1.0000	1.0000	1.0000	1.0000
ZA-1	0.3073	0.8872	0.7261	0.5073	0.0833	0.9094	0.8126	0.8756	0.8038
ZA-2	0.3452	1.0000	0.7621	0.5419	0.1042	0.7206	0.5586	0.6555	0.6923
ZA-3	0.3937	0.9374	0.9198	0.5893	0.1250	0.4680	0.3729	0.3672	0.3513
ZA-4	0.1923	0.8515	0.9059	0.7304	0.0833	0.5788	0.5093	0.5522	0.5370
ZA-5	0.6222	0.8434	0.8243	0.5913	0.0729	0.6864	0.8045	0.9534	0.8581
ZA-6	0.6146	0.8608	1.0000	0.6884	0.0833	0.5717	0.6191	0.6363	0.4462
ZA-7	0.4893	0.8956	0.7261	1.0000	0.0938	0.4827	0.4621	0.4112	0.3501
ZA-8	0.40	0.7494	0.6833	0.6062	0.1041	0.3238	0.3348	0.3885	0.3315
SiBr-0	0.6116	0.5534	0.0553	0.1633	0.5625	0.7192	0.6328	0.6448	0.4815
SiBr-1	0.8414	0.6554	0.0594	0.1837	0.6667	0.4329	0.4756	0.5991	0.4463
SiBr-2	0.6737	0.8241	0.0719	0.1961	0.8333	0.3481	0.3997	0.4758	0.4242
SiBr-3	0.6631	0.8422	0.0968	0.2118	1.0000	0.3142	0.3848	0.4499	0.4042
SiBr-4	0.3937	0.8178	0.0843	0.1785	0.7917	0.2278	0.2711	0.3558	0.3571
SiBr-5	0.6866	0.5730	0.0664	0.1806	0.6250	0.4475	0.5777	0.6214	0.4544
SiBr-6	0.8155	0.6044	0.0788	0.2023	0.7917	0.3773	0.4660	0.5748	0.3931
SiBr-7	1.0000	0.6534	0.0941	0.2097	0.9375	0.3439	0.4364	0.5087	0.3882
SiBr-8	0.3294	0.5348	0.0816	0.1919	0.8333	0.2970	0.2949	0.3323	0.3487

Table 4.24. Mean normalized, preference variation, deviation in the preference variation and overall preference values of particulate filled metal alloy composites.

Composite	Mean normalized value	preference variation value	deviation in preference variation value	overall preference values
C-1	0.5366	0.8400	0.1600	0.0344
C-2	0.7670	0.8420	0.1580	0.0341
C-3	0.4411	2.4943	1.4943	0.3219
C-4	0.4146	1.0995	0.0995	0.0214
C-5	0.4363	2.3222	1.3222	0.2849
C-6	0.5138	0.8089	0.1911	0.0411
C-7	0.5229	0.5747	0.4253	0.0916
C-8	0.5779	0.6741	0.3259	0.0702
C-9	0.5038	1.4652	0.4652	0.1002

Table 4.25. Preference selection index and ranking of the composites of particulate filled metal alloy composites

Composite	Preference selection index	Ranking
ZA-0	0.5471	**5**
ZA-1	0.5635	**4**
ZA-2	0.5292	**7**
ZA-3	0.5914	**2**
ZA-4	0.5296	**6**
ZA-5	2.0526	**1**
ZA-6	0.5807	**3**
ZA-7	0.4554	**9**
ZA-8	0.4069	**15**
SiBr-0	0.4025	**16**
SiBr-1	0.4125	**13**
SiBr-2	0.4429	**10**
SiBr-3	0.4415	**12**
SiBr-4	0.3929	**18**
SiBr-5	0.4069	**14**
SiBr-6	0.4419	**11**
SiBr-7	0.4878	**8**
SiBr-8	0.3948	**17**

Chapter Summary

This chapter has encapsulated different following points:

1) Triumphant fabrication of particulates filled metal alloy composites for different wt.-% (0, 2.5, 5, 7.5 and 10) of marble dust (MD) and quicklime (CaO) particulates has been done by the use of high temperature vacuum

casting machine (liquid fabrication technique).

2) It has been studied and observed that the void content of the composites are decreased with the increase in filler content into the matrix alloy material up to 7.5wt.% of marble dust and beyond which the void content starts increasing. The experimental and theoretical densities of the unfilled and particulate filled alloy composites are found to be in line with each other. The hardness of the composites is found to be higher than the base alloy this is mainly due to the influence of hardened particulates.
3) Mechanical properties such as compressive strength and impact strength has positive effect (665MPa and 6J respectively) up to 7.5 wt.-% MD filled ZA-27 alloy composites but the flexural strength shows the increasing effect (684.38 MPa) up to 10 wt.-% MD reinforcement.
4) Mechanical properties such as hardness, flexural strength and impact strength has favourable effect (193Hv, 937MPa and 5J respectively) up to 7.5 wt.-% CaO filled ZA-27 alloy composites but the compressive strength shows the increasing effect (723MPa) up to 5 wt.-% CaO reinforcement only.
5) From the results it is found that the mechanical properties of cast MD particulates filled SiBr alloy composite materials become consequentially permute by varying the weight percentage of MD particulates. It is found that the void content become decreases from 0.824% to 0.380 for 0wt.-% to 7.5wt.-% MD particulates filler particles. And the hardness becomes increases from 119.25Hv to 181.5Hv for 0wt.-% to 7.5wt.-% by addition of MD particulates in SiBr alloy composite materials, but the value of hardness become decreases by 176.25Hv on further increase in filler content up to 10wt.-% of MD particulates filled metal alloy composites materials, So the most exemplary results is found up to 7.5 wt.-% of MD particulates filler particles for mechanical properties.
6) Mechanical properties of cast CaO filled SiBr alloy composite materials significantly altered by varying the weight percentage of CaO particulates. It is found that void content decreases from 0.824% to 0.504% up to 7.5 wt.-% of CaO filler particles. However, the hardness of the filled alloy composites increases up to 7.5 wt.-% of CaO filler particles i.e. 140.8 Hv but on further increased in CaO particulates the hardness is shown revere in trend.
7) The magnitude of stress intensity factor (SIF) for varying crack length (1, 2, 3

and 4 mm) of MD filled ZA-27 alloy composites increases and the highest value of SIF occurs, 1.899 MPa.m^1/2 for 4mm crack length. This may be due to strong bonding between interface of reinforcement and matrix phases

8) The stress intensity factor (SIF) values for varying crack length (1, 2, 3 and 4 mm) of CaO filled ZA-27 alloy composites increases and the highest value of SIF occurs, 2.0127 MPa.m^1/2 for 4mm crack length. The reason for the increased value of SIF can be the strong bonding or relationship in between interface of particulate and matrix phases.
9) Fracture surface analysis (Fractography effect) was observed for particulates filled metal alloy composites which show the number of micro examination behavior such as dimples and cracks were observed on fractured surface of composite material which means the formation of voids and coalescence occurs during fracture process.
10) Finally the calculation of ranking order for different physical, mechanical, fracture and wear behaviour of particulate filled metal alloy composites has been done by using preference selection index (PSI) method. The sequencing of ranking was ZA-5> ZA-3-0> ZA-6 >ZA-1> ZA-0 >ZA-4 >ZA-2> SiBr-7> ZA-7 SiBr-2> SiBr-6> SiBr-3> SiBr-1> SiBr-5> ZA-8 >SiBr-0> SiBr-8> SiBr-4 for physical and mechanical properties

The next chapter presents the thermo-mechanical analysis of particulate filled metal alloy composites.

******

Chapter 5
Thermo-Mechanical Analysis of Particulate Filled Metal Alloy Composites

Chapter 5

THERMO-MECHANICAL ANALYSIS OF PARTICULATE FILLED METAL MATRIX COMPOSITES

This chapter deals with the thermo-mechanical behaviour of particulate filled metal alloy composite materials at different operating conditions such as temperature or time. The thermo-gravimetric analysis and dynamic mechanical analysis of the fabricated composite materials has been studied.

Part I

5.1 Thermo-Mechanical properties of Marble Dust (MD) particulate filled ZA-27 alloy composites

5.1.1 Effect of thermo-gravimetric analysis on MD particulate filled ZA-27 alloy composites

The thermo-gravimetric analysis technique is used to determine the weight loss of a substance in an environment with the controlled rate as a function of temperature or time. Figure 5.1 shows the thermo-gravimetric (TGA) analysis of marble dust filled ZA-27 alloy composites and observed that the enhancement of thermal stability between the temperature range of 25ºC-250ºC temperature range. Figure 5.1 shows the higher wt.-% MD reinforcement have maximum weight loss (mg) up to 900ºC temperature. The plummet order for thermo-gravimetric analysis is 10wt.-%MD>7.5wt.-%MD>5wt.-%MD>2.5wt.-%MD>0wt.-%MD respectively. This imputes that at higher temperature for thermal degradation of marble dust is 900ºC and it started to degrade from 650ºC. However, 2.5 wt.-% MD filled ZA-27 alloy composite shows more material stability as compared to unfilled ZA-27 alloy composites. From 25ºC to 650ºC almost negligible degradation is found for unfilled and filled ZA-27 alloy composites, after 650ºC materials degradation is taken place. Tangent line from A to B with the temperature range shows the highest rate of degradation of material loss for MD filled ZA-27 alloy composites. Loh et al. [316] studied about the thermo-gravimetric analysis for binder with the varying temperature range from 25 ºC to 550 ºC. They found that only 1% loss of weight is happened when temperature varies from 120 ºC to 210 ºC but from 210 to 300 ºC the weight loss of binder appreciably. The quantity of dissolved reinforcement can find out by weight loss between given tangent line A and B [317]. The stability of MD filled ZA-27 alloy

composite material till 650ºC was found due to genesis of indubitable compounds such as oxides , when the temperature increases the composite reacts with different environment gases, dust particles etc. The reason for almost negligible degradation of composite material up to 650ºC was strong bonding between binary ingredients of materials.

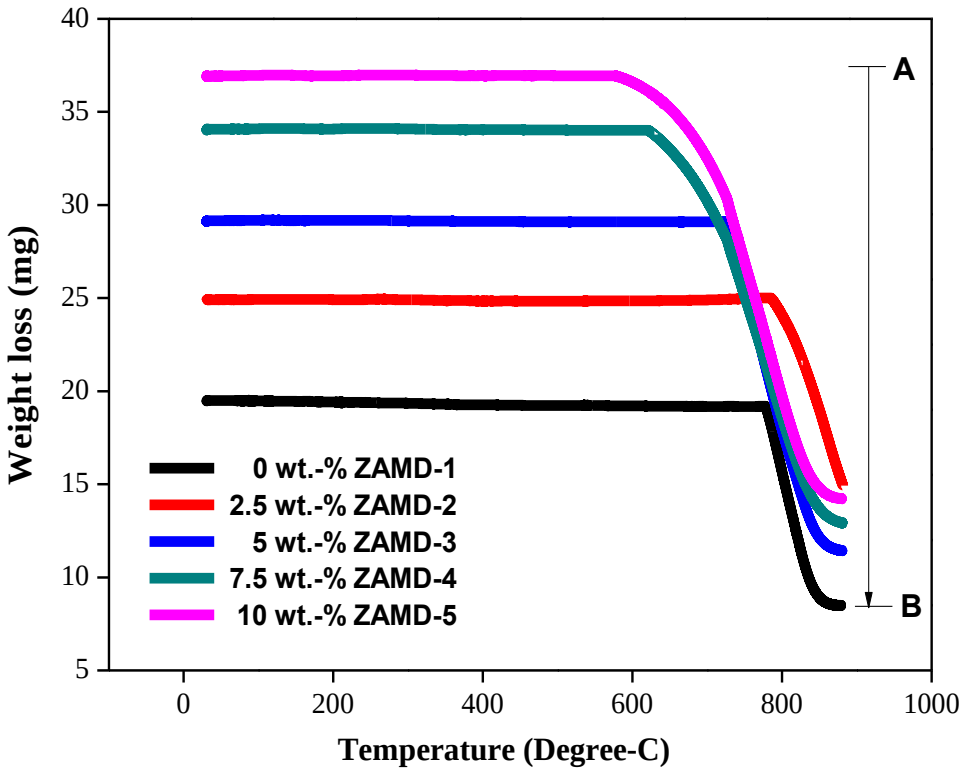

Figure 5.1 TGA result for MD particulate filled ZA-27 alloy composites

5.1.2 Effect of dynamic mechanical analysis on MD particulate filled ZA-27 alloy composites

Dynamic Mechanical Analysis (DMA) for marble dust filled ZA-27 alloy composites has been studied in this work to probe the variation of storage modulus (E'), Loss modulus (E") and Tan δ i.e. damping factor. Figures 5.2a, b, c show the storage modulus, loss modulus and Tan δ for 0, 2.5, 5, 7.5 and 10 wt.-% of marble dust filled ZA-27 alloy composites with the temperature range of 25 ºC -250 ºC respectively. Figure 5.2a shows the storage modulus (used to measure the stored energy and dissipated energy as heat for materials) of marble dust filled ZA-27 alloy composites, which shows the variation in the order of E'2.5%>E'7.5%>E'10% >E'0% > E'5%

respectively and when the temperature increases, the composite materials show the decreasing values of storage modulus for all the reinforced ZA-27 alloy composites. The decrement of storage modulus is found from 130ºC approximately and it goes diminish up to 250ºC. The loss modulus for composites material shows the increasing values with increasing temperature up to 250ºC. The maximum value of loss modulus was found in 2.5 wt.-% MD filled ZA-27 alloy composites and after that the variation order of loss modulus for other wt.-% of MD filled as E"7.5%>E"10% >E'0% > E'5% respectively (Figure 5.2b). The particle size and plastic strain of reinforcement has strong influence on damping capacity of composite materials [31]. Whereas, Figure 5.2c i.e. Tan δ graph shows the increasing values with the increase in temperature. Generally loss modulus and Tan δ provides the information about transformation change and the damping capacity in materials [318].

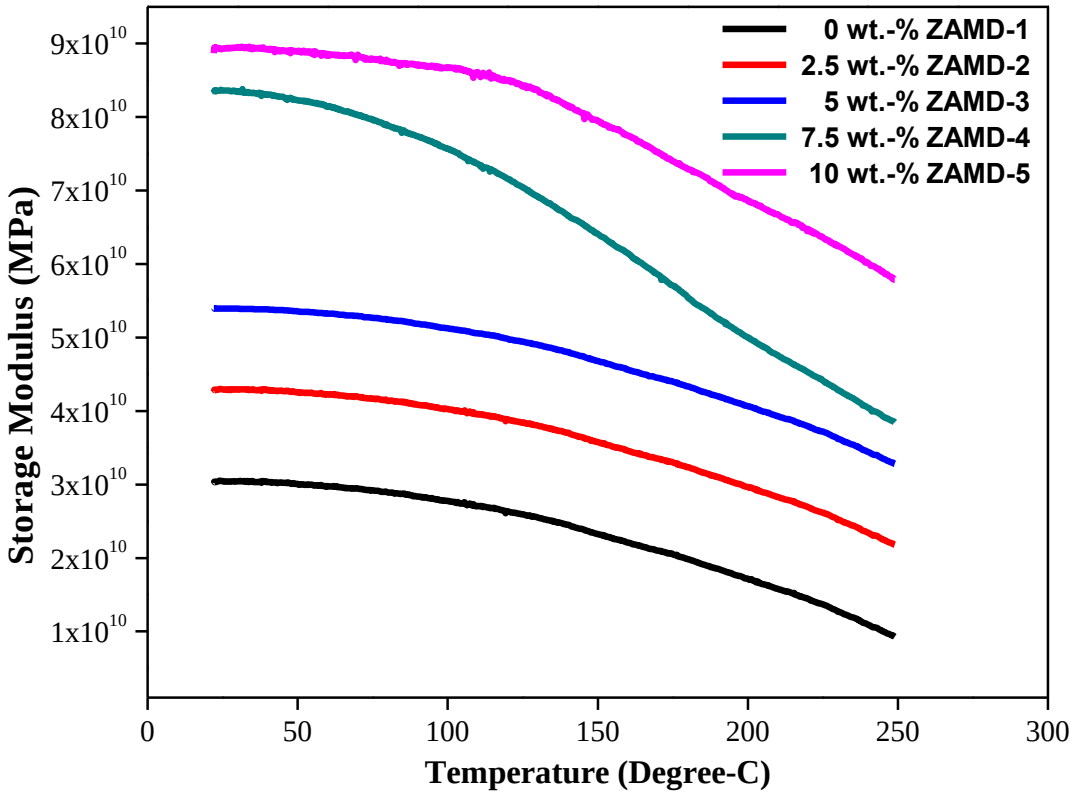

Figure 5.2a Variation of Storage modulus with temperature for MD particulate filled ZA-27 alloy composites

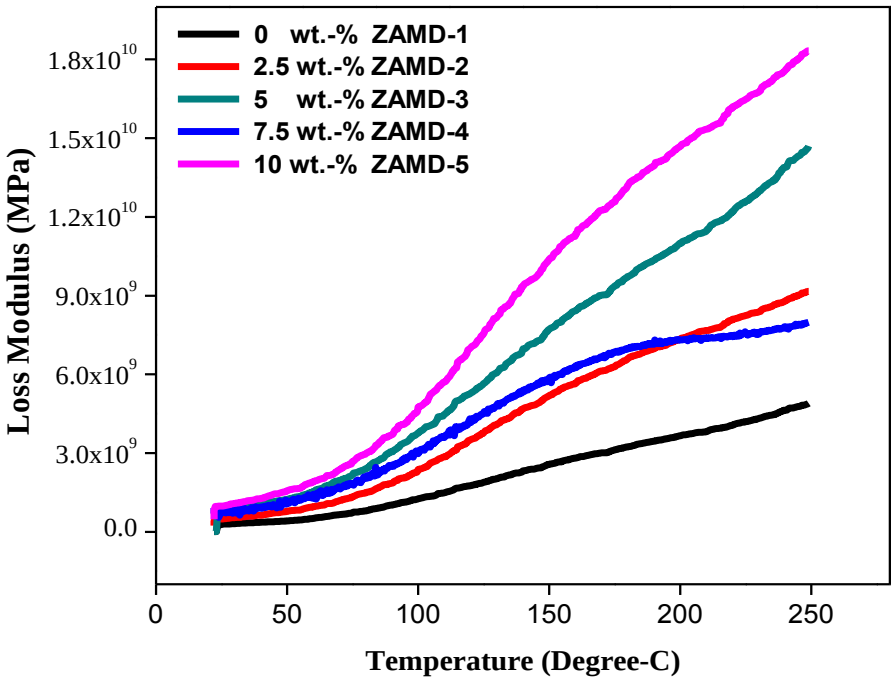

Figure 5.2b Variation of Loss modulus with temperature for MD particulate filled ZA-27 alloy composites

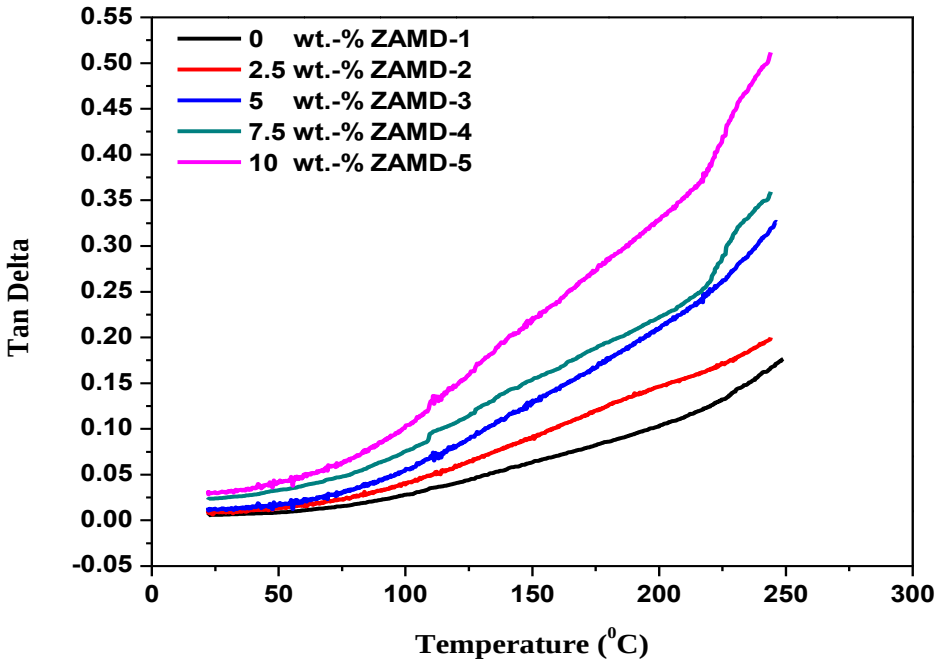

Figure 5.2c Variation of Tan delta with temperature for MD particulate filled ZA-27 alloy composites

Part II

5.2 Thermal and Thermo-Mechanical properties of Quicklime (CaO) particulate filled ZA-27 alloy composites

5.2.1 Effect of thermo-gravimetric analysis on CaO particulate filled ZA-27 alloy composites

The thermo-gravimetric (TGA) analysis for CaO filled ZA-27 alloy composites is shown in Figure 5.3. The TGA analysis is done to observe the enhancement in thermal stability of composite materials in the temperature range of 25ºC-250ºC. From the Figure it is observed that at 10wt.-% CaO filled ZA-27 alloy composites have maximum weight loss up to 650 ºC temperature and the remaining wt.-% filler have weight loss in the order of 10wt.-% CaO> 7.5wt.-% CaO>5wt.-% CaO>2.5wt.-% CaO>0wt.-% CaO respectively up to 850 ºC. By this it's concluded that the higher temperature for thermal degradation of CaO filled ZA-27 alloy composites is at 850ºC and the starting temperature for the degradation is 650 ºC. From room temperature i.e. 25 ºC to 650 ºC almost negligible degradation is taken place both unfilled as well as CaO filled ZA-27 ally composites due to the strong atomic bonding between the reinforced particles and matrix alloy, but after 650 ºC material starts to degrade for both the conditions.

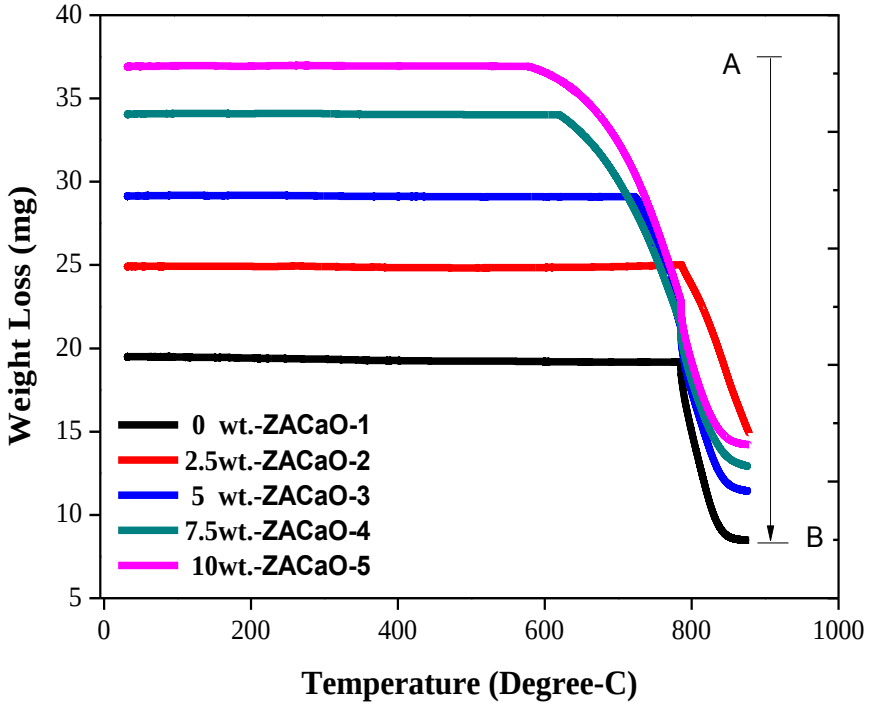

Figure 5.3 TGA result for CaO particulate filled ZA-27 alloy composites

If unfilled and CaO filled ZA-27 alloy composites get compared than we found the particulate filled composites have more thermal stability as compared to unfilled material. In the Figure 5.3 tangent line from A to B with respect to temperature range shows the highest rate of degradation of material loss for CaO filled ZA-27 alloy composites.

Ejiofor et al. [15] studied about the thermo-gravimetric analysis for zircon reinforced with Al-13.5Si-2.5Mg alloy composites fabricated by powder metallurgy fabrication techniques. They found the composite materials start to degrade at 200 ºC and extended the degradation process up to 510 ºC. Tangent line A to B in Figure 5.3 shows the total degradation which occurs during the TGA analysis with the increasing range of temperature. It may cause due to the presence of dirt particles, unwanted environment gases and the presence of other impurities when the composite material get heated up to 850 ºC.

5.2.2 Effect of dynamic mechanical analysis on CaO particulate filled ZA-27 alloy composites

The storage modulus (E'), Loss modulus (E") and damping factor (Tan δ) parameters of the investigated alloy composites are determined using DMA technique, over a temperature range of 25 to 250°C (Figure 5.4). It is observed that the diminishing trend of storage modulus (E') exhibits following order: 7.5% E' > 5% E' > 0% E' > 2.5% E' > 10% E. This infers that higher filler content (5-7.5 wt.-%) reinforcement boosts storage modulus (Figure 5.4a) of the neat alloy within workable temperature range, where as other filler content supposed to have detoriated effect on E'. Reinforcement of 2.5 wt.-% filler shows mild loss of E' till 150°C thereafter it slightly improves for further 25°C, and then decreases till 250°C. It is also observed that detoriation of E' within temperature range 150-250°C is much faster in other alloy composites except 2.5 wt.-% filler content alloy composite. However, 10 wt.-% filler content shows least E' and relatively faster deteoriation rate with temperature then others [16].

The loss modulus (E" °C) behaviour of the investigated composites are comparatively plotted in Figure 5.4b. It is observed that E" magnitude increases with temperature irrespective of filler content for all the alloy composites. Within the temperature range of 25-125°C the order of diminishing E" were: 7.5% E" > 10% E" > 5% E" > 2.5% E" ≈ 0% E", where as in temperature range 125-250°C the order of diminishing E" were: 7.5% E" > 5% E" > 10% E" > 0% E" > 2.5% E".

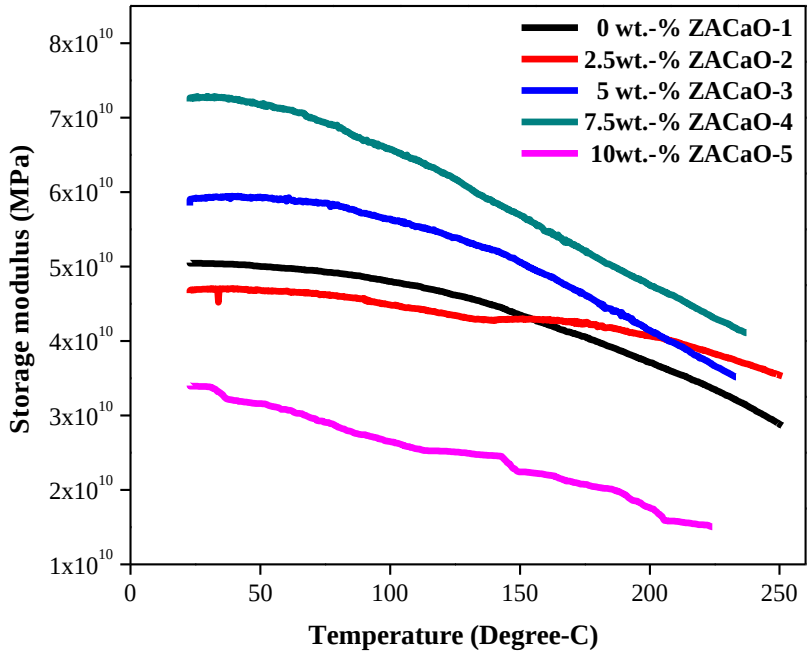

Figure 5.4a Variation of Storage modulus with temperature for CaO particulate filled ZA-27 alloy composites

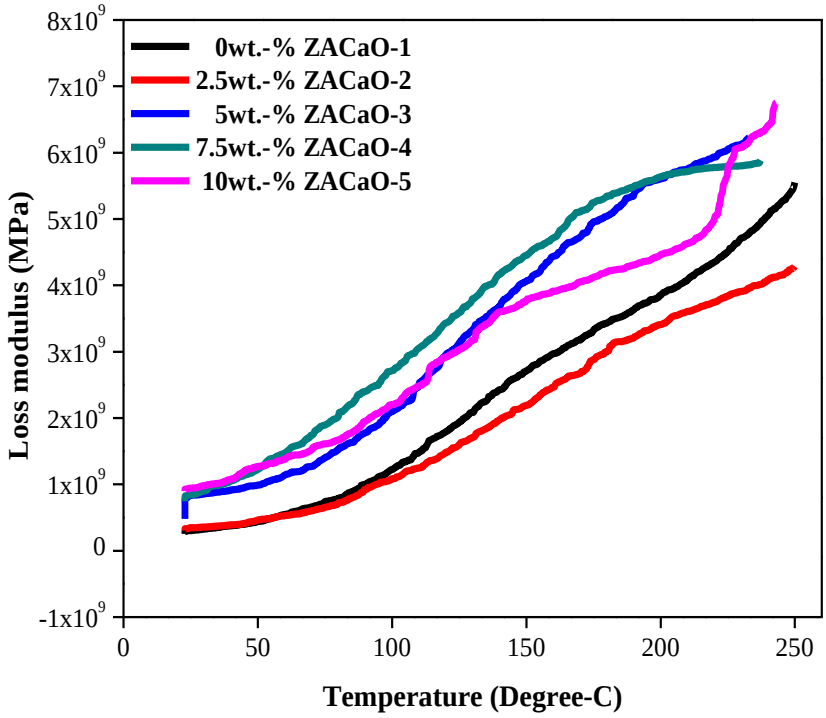

Figure 5.4b Variation of Loss modulus with temperature for CaO particulate filled ZA-27 alloy composites

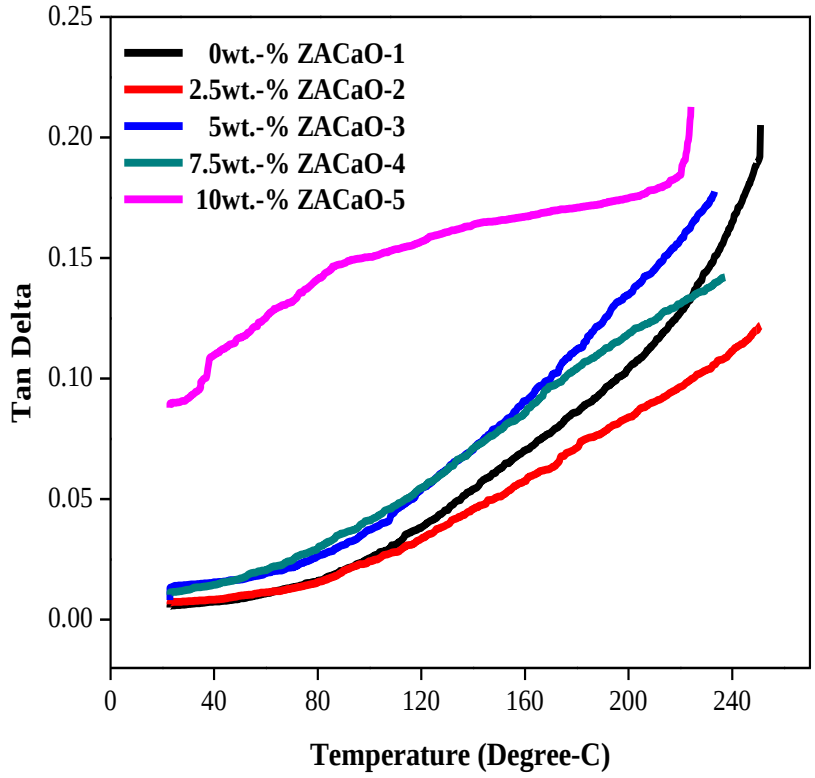

Figure 5.4c Variation of Tan delta with temperature for CaO particulate filled ZA-27 alloy composites

It might be inferred that higher filler reinforcement then 10 wt.-% leads to increase in viscous or loss modulus relative to neat except for 2.5 wt.-%. Thus, loss modulus exhibits trend reversal in-relation-to storage modulus [17].

The damping behaviour depicted by Tan δ parameter, of the investigated alloy composites are shown in plot Figure 5.4c. It infers that damping capacity property of the alloy composite shows improvement in-comparisons-to neat alloy except for 2.5 wt.-% filler content. Also, higher filler content of 10 wt.-% leads to much improved damping capacity.

It is clearly known that damping capacity depends upon interfacial adhesion between ingredients of alloyed composites. Thus, in general reinforcement of CaO particulate leads to enhancement of damping capacity. And higher content leads to better interfacial adhesion that significantly improved damping characteristics [31].

Part III

5.3 Thermal and Thermo-Mechanical properties of Marble Dust (MD) particulate filled Silicon Bronze alloy composites

5.3.1 Effect of thermo-gravimetric analysis on MD particulate filled SiBr alloy composites

The thermo-gravimetric analysis of the marble dust filled SiBr alloy composites are measured the loss in weight with respect to change in temperature. When the TGA phenomenon get started, materials shows some physical and chemical changes such as gas adsorption, desorption, decompositions, break down reactions, gas reactions etc. that leads towards the mass loss with the changes in temperature [319]. When the TGA analysis occurred the outcome weight loss graph shows the fruitful information about the material like variation in chemical composition, up to which temperature material sustains, different parameters that produced during chemical reactions. Figure 5.5 shows the weight loss effect of MD particulates filled metal alloy composites by thermo-gravimetric analysis at different varying temperatures.

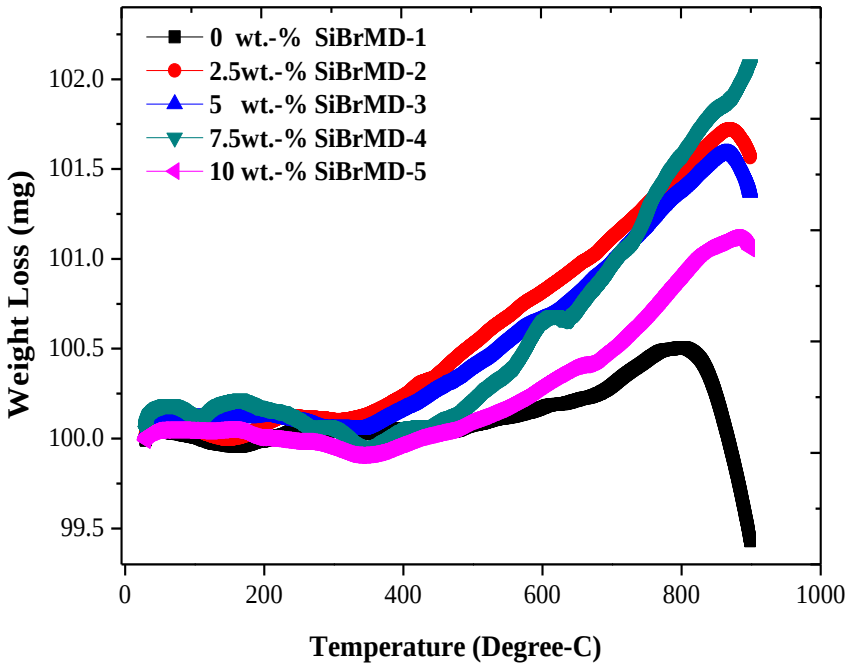

Figure 5.5 TGA result for MD particulate filled SiBr alloy composites

From Figure 5.5 it is observed, the monolithic as well as composite materials shows stability up to 400 ºC and beyond it, materials get starts to degrade or losing its ability in terms of weight loss up to 900 ºC. The sustainability of materials in terms of weight

loss maximum hold by MD particulates filled metal alloy composites as compared to monolithic alloy, especially for 7.5wt.-% compositions (Approx. 100.3 mg).

The obvious reason for materials weight loss is oxidation of materials at higher temperature [320], the reinforcement particulate imbedded in parent material or the matrix material so when the temperature get increases material loses its atomic bonding in between parent matrix material and reinforcement.

5.3.2 Effect of dynamic mechanical analysis on MD particulate filled SiBr alloy composites

The materials responses with different dynamic conditions when a periodic load applied on it that termed as dynamic storage modulus, loss modulus and Tan δ (damping factor) [321]. Generally, the dynamic mechanical analysis of any materials comprises the mechanical properties usually under sinusoidal or oscillatory behaviour with the function of temperature and time. When the load i.e. stresses applied on the materials it shows some deformation (strain) that amount in terms of phase shift and amplitude can be calculated. This section comprises the dynamic mechanical analysis of marble dust (MD) filled SiBr alloy composite materials in terms of storage modulus (E'), Loss modulus (E") and Tan δ i.e. damping factor.

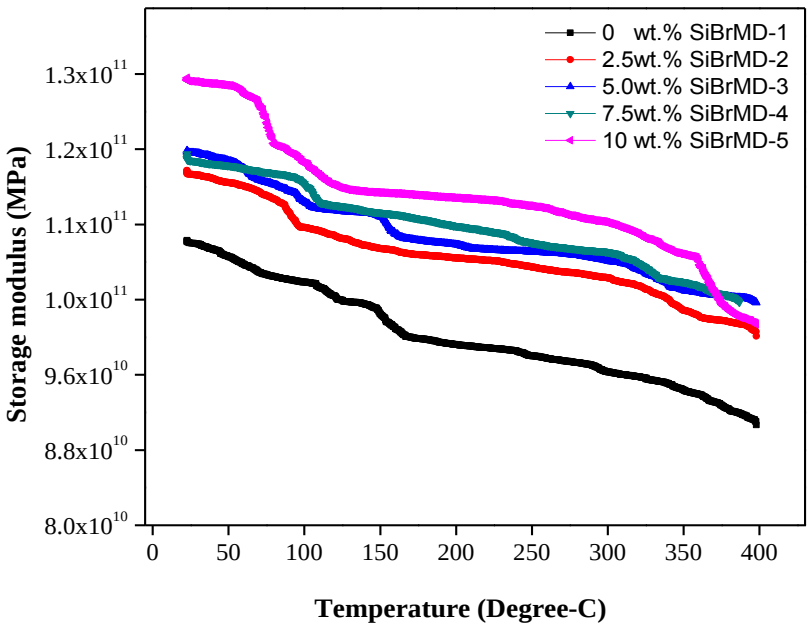

Figure 5.6a Variation of Storage modulus with temperature for MD particulate filled SiBr alloy composites

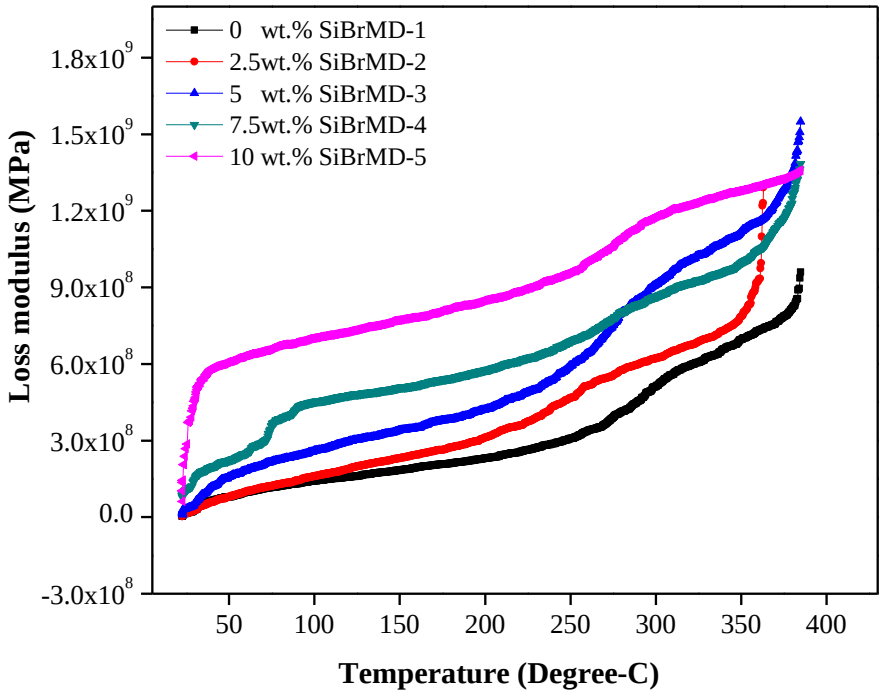

Figure 5.6b Variation of Loss modulus with temperature for MD particulate filled SiBr alloy composites

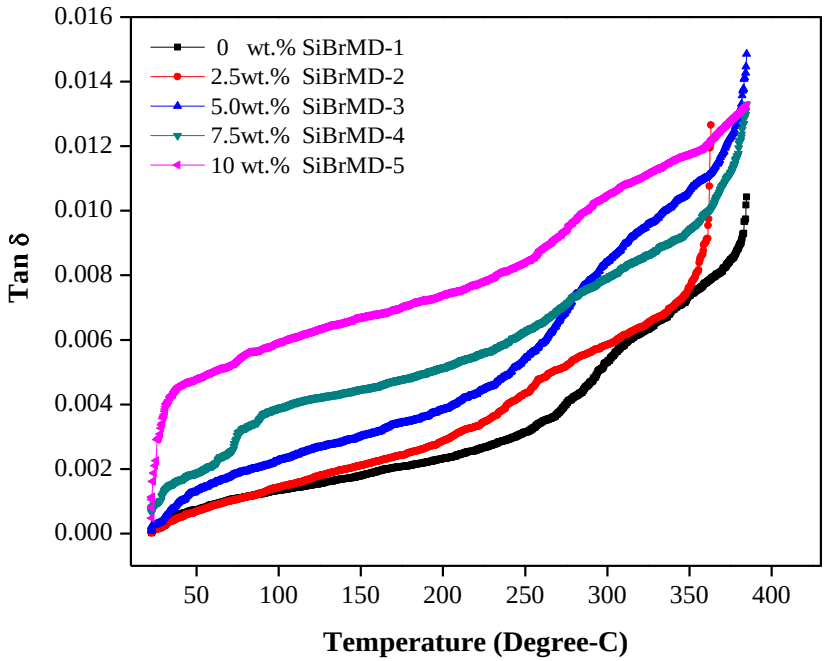

Figure 5.6c Variation of Tan delta with temperature for MD particulate filled SiBr alloy composites

In this section Figure 5.6 shows the variation of storage modulus, loss modulus and Tan δ for varying wt.-% of MD in SiBr alloy (For 0, 2.5, 5, 7.5 and 10 wt.-%) by varying temperature range from 25 ºC-400 ºC respectively. From the Figure 5.6a it is observed, the amount of storage modulus for unfilled metal alloy composite shows minimum (Approx. $1.10x10^{11}$ MPa) as compared to MD filled metal alloy composite also with the increasing amount of filler particles the range of storage modulus increases respectively, maximum storage modulus (Approx. $1.27x10^{11}$ MPa) was found for 10wt.-% MD filled metal alloy composites.

The storage modulus means the stiffness property of viscoelastic material that directly relate to energy storage capacity under the application of load that should be as maximum as possible but with the increases range of temperature materials losses its parent nature and by that the amount of storing capacity of storage modulus for composite materials also decreases.

Figure 5.6 b shows the range of loss modulus for varying wt.-% of particulates filled metal alloy composites, it is observed that the modulus value shows reveres in trend as storage modulus. As we know that the loss modulus relates to energy dissipated while applying loading condition, when the temperature increases energy get reduced and converted into vibrational energy that produces vibrations, so the amount of loss modulus should be as minimum as possible.

In the Figure 5.6b it is observed that till 125 ºC materials show approximately stable behaviour but onward it shows instability in nature. Figure 5.6c shows the graph for Tan δ (damping factor) for different wt.-% of MD filled SiBr alloy composites. It is observed, for 10 wt.-% of filler particulates have higher amount of damping factor (0.004) as compared to other wt.-% of filler particulates, and also the temperature range of materials sustainability is approximately 100 ºC beyond it materials get starts to evaporate with respect to increases temperature rate. The ration of loss modulus to storage modulus known as Tan δ means this factor is used to measure the loss of energy during operation and measure it in the form of damping factor. Similar observation is found in Xiao et al. [322] studied for Fe- 31.2Pd (at.%) alloy with the varying temperature range from 263 K to 323 K and at a fixed frequency of 0.2 Hz. They observed the increment in Tan δ is 0.002 in between the considered temperature from 263 K to 323 K. The maximum Tan δ is found for maximum temperature, it's due to relaxation processes.

Part IV

5.4 Thermal and Thermo-Mechanical properties of Quicklime (CaO) particulate filled Silicon Bronze alloy composites

5.4.1 Effect of thermo-gravimetric analysis on CaO particulate filled SiBr alloy composites

The effect on weight loss of materials in a controlled environment with respect to temperature and time factors can be examined by thermo gravimetric analysis. Figure 5.7 shows the thermal analysis of CaO filled SiBr alloy composite materials from the temperature range of 25 ºC to 900 ºC respectively. From the Figure it is observed that the material lose its weight drastically from 500 ºC onwards.

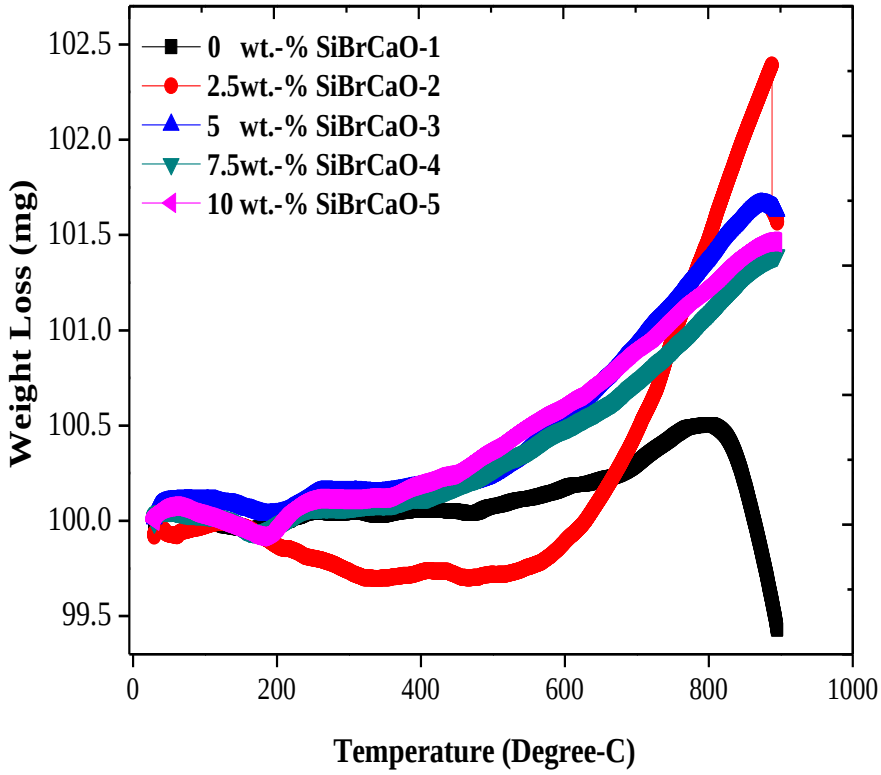

Figure 5.7 TGA result for CaO particulate filled SiBr alloy composites

The maximum sustainably is found for 10 wt.-% particulate filled material up to 500 ºC. And with the comparison of other wt.-% of filler materials i.e at 2.5 wt.-% CaO filled particulate has maximum sustainability of materials in term of weight loss up to 600 ºC. No remarkable weight loss change is found up to 500 ºC but after that drastic weight loss composite material is found with the increasing in temperature range. Thermo gravimetric analysis is used to find the energy storage capacity with respect to

temperature means up to which temperature range can sustain without losing its parent nature. From the Figure 5.7 it is observed that CaO filled SiBr alloy composite materials for bearing applications may be proposed as the material sustains its parent properties up to approx. 500 ºC.

5.4.2 Effect of dynamic mechanical analysis on CaO particulate filled SiBr alloy composites

The dynamic mechanical analysis of particulate filled metal alloy composite is characterized to find out the stiffness and damping phenomenon that expressed in terms of in phase component (i.e. storage modulus), out phase component (i.e. loss modulus) and tan delta due to applied sinusoidal force on the materials. The measurement of damping phenomenon of materials tells about the capacity of materials in form of dissipation of energy under cyclic load or the energy absorbing capacity of materials. The damping amount primarily depends upon the factors such as materials properties, temperature and frequency [323].

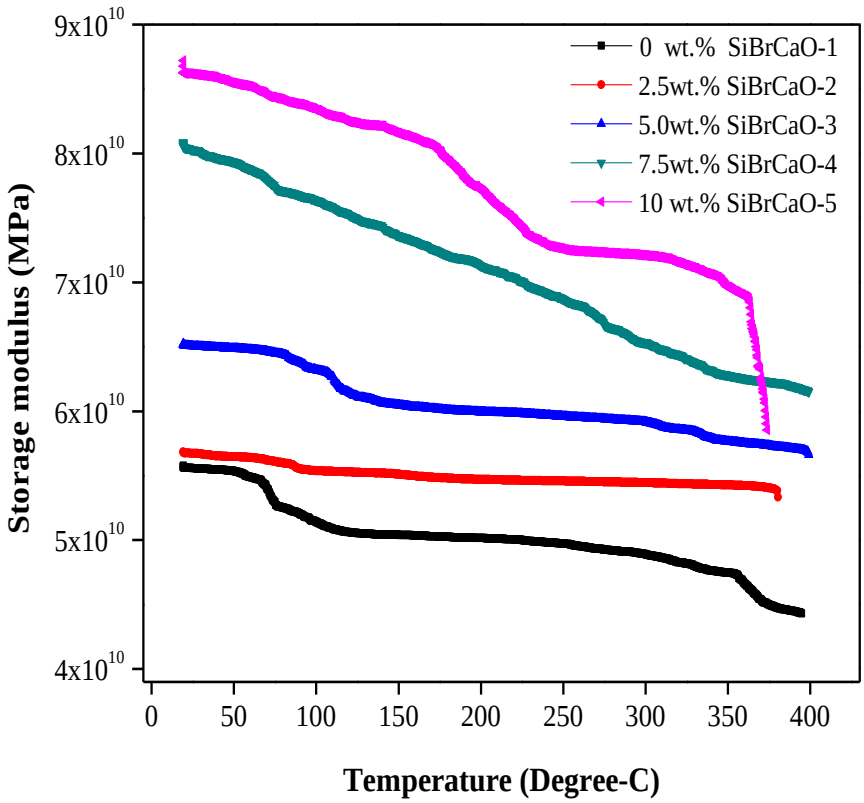

Figure 5.8a Variation of Storage modulus with temperature for CaO particulate filled SiBr alloy composites

For different wt.-% (0, 2.5, 5, 7.5 and 10) of CaO filled SiBr alloy composites, the amount of storage modulus, loss modulus and Tan δ (i.e. damping factor) are examined through Figures 5.8a, 5.8b and 5.8c with varying temperature range from 25ºC-400ºC respectively at constant frequency of 1 Hz. When the temperature starts to increases from room temperature to 400 ºC, the materials get converted its phase from solid to liquids state, so that the energy storage capacity of materials is also affected. From the Figure 5.8a, it is observed that the maximum amount of filler content in matrix material shows the maximum energy storage (Approx. 8.7x 10^{10} MPa) capacity as compared to base materials as well as other wt.-% of filler composite materials.

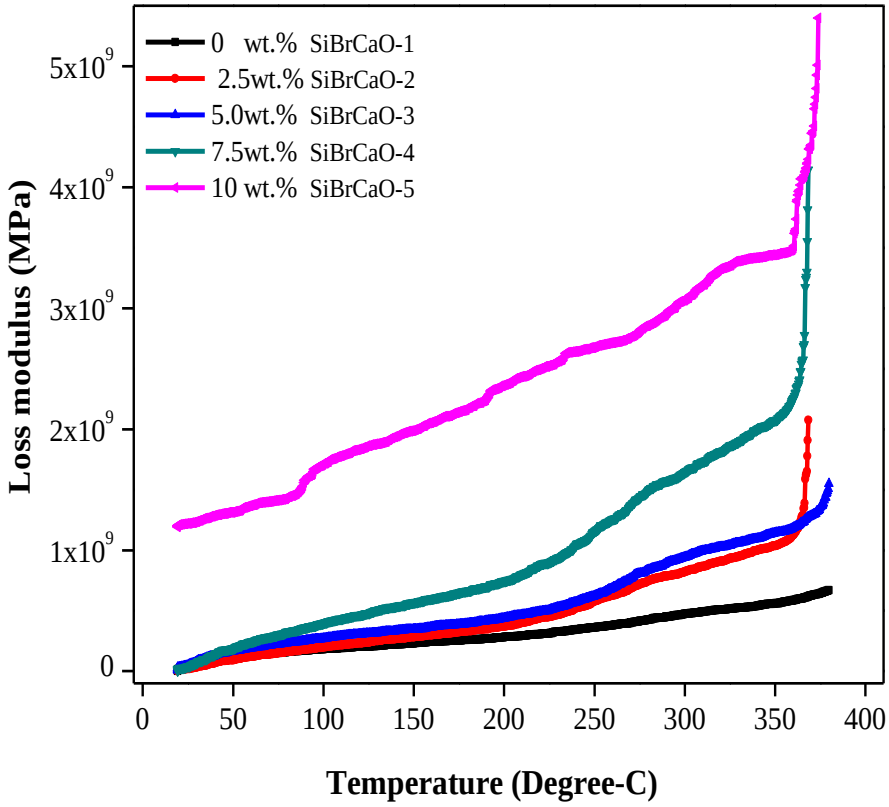

Figure 5.8b Variation of Loss modulus with temperature for CaO particulate filled SiBr alloy composites

The decrement in storage modulus with the increases in temperature is found due to softening of material that loses its atomic bonding and respectively its properties, similar observation is found in Ma et al. [324] research paper for AlxCoCrFeNi alloys with the varying temperature range from 298 to 773 K, (at frequency of 1 Hz). Figure 5.8b shows the loss modulus vs. temperature graph for CaO filled SiBr alloy composites with heating rate of 5 ºC per minute and having

constant frequency of 1 Hz. Figure 5.8b about loss modulus that shows the loss of energy in terms of heat while the working temperature get increases. Figure shows that till 150ºC materials shows the sustaining behaviour but after that drastic change was found for loss modulus.

To examine the elastic behaviour of materials two parameters has to be evaluated such as storage modulus and loss modulus. And the damping phenomenon that also called tan delta can calculate by the ratio of loss to the storage modulus [323]. Figure 5.8c shows the graph for Tan δ vs. temperature (From 25 ºC-400 ºC) and constant frequency i.e. 1 Hz. Generally the tan δ graph for materials shows the dissipation of energy, while the range of temperature gets increases. Figure shows the damping phenomenon of CaO filled SiBr alloy composite materials shows gradual increment from 25 ºC-200 ºC but after it drastic change is found up to 400 ºC; especially for 10 wt.-% filled SiBr alloy composite material. Generally what happen, when the temperature of materials get increases and the cyclic loading is applied on it that starts to deviates from its path or can say from Hooke's law, that get starts to lose stored energy and also losses material properties [324].

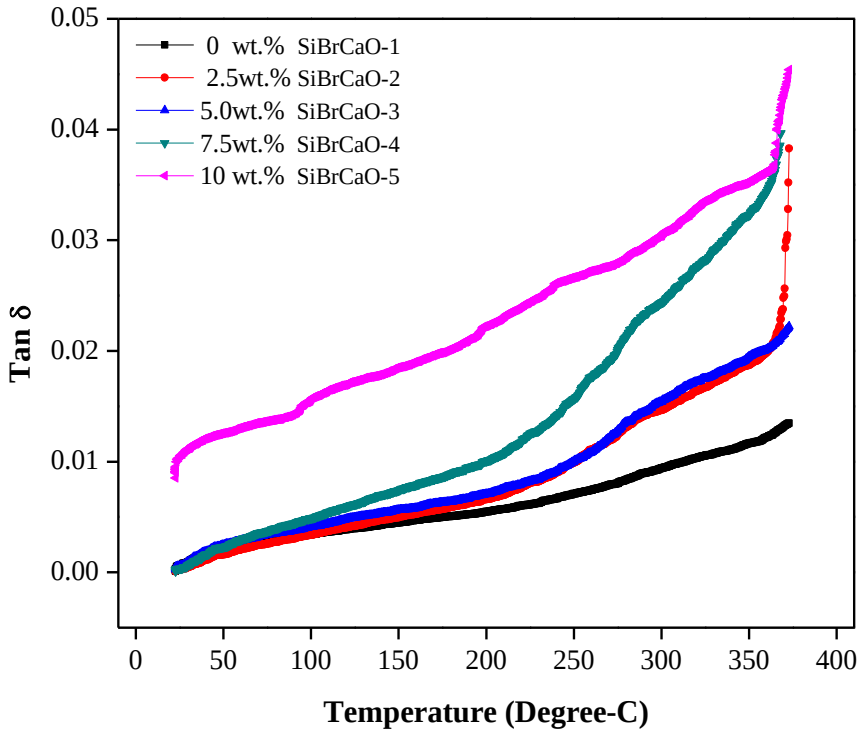

Figure 5.8c Variation of Tan delta with temperature for CaO particulate filled SiBr alloy composites

Chapter Summary

This chapter has summarized about:

- The thermo-gravimetric analysis of the entire particulate filled metal alloy composites is studied in experimentally.
- Similarly, the dynamic mechanical analysis of the particulate filled and unfilled alloy composites is performed in experimentally.

The next chapter presents the wear behaviour of particulate filled metal alloy composite materials at dry lubricating conditions, their elucidation and optimum results outcomes by method.

******

Chapter 6

Wear Behavior and Optimization of Particulate Filled Metal Alloy Composites

Chapter 6

WEAR BEHAVIOUR AND OPTIMIZATION OF PARTICULATE FILLED METAL ALLOY COMPOSITES

This chapter anthologize the results obtained from sliding wear behaviour of particulate filled metal alloy composites under steady state operating condition for bearing materials, performed on pin-on-disc tribometer. To get the optimum response of wear behaviour of composite materials, the Taguchi L_{25} orthogonal array design is applied and then analysis of variance (ANOVA) is used to find out the significant factor settings of the particulate filled alloy composites. Finally, the worn surfaces morphology of the particulate filled metal alloy composites is examined for micro-structural analysis through field emission scanning electron microscope (FESEM), for compositional analysis Energy dispersive X-ray analysis (EDAX) is performed and then Atomic force microscopic (AFM) is also studied to understand the wear mechanism and structural behaviour of the composites.

Part I

6.1 Steady state specific wear behaviour of Marble Dust (MD) particulates filled ZA-27 alloy composites

6.1.1 Effect of sliding velocity on specific wear rate of MD particulates filled ZA-27 alloy composites

Different wt.-% (0, 2.5, 5, 7.5 and 10wt.%) of marble dust particulate filled ZA-27 alloy composite specimens are tested on pin-on-disc tribometer to determine the specific wear rate by varying the sliding velocity (1.074,2.094,3.140,4.188 and 5.235 m/s) keeping all other parameters (like sliding distance (1000m), load(15N) and environment temperature (35ºC)) are remaining constant. The incorporation of marble dust into ZA-27 alloy, the specific wear resistance is increased as compared with the unfilled alloy composite irrespective of the filler percentages (Figure 6.1). However, in all the alloy composites with the increased in sliding velocity, the specific wear rate also increases. The causes for the increasing in wear rate not only because of increasing sliding velocity but also other significant control factors may also effect the wear rate of the composites i.e. the temperature or heat generated between contacted surfaces that soften the material, the environment temperature, applied normal load and sliding distance, etc. also simultaneously effect the wear rate of the unfilled and

particulate filled composites [325,326]. One of the most obvious reasons for the increasing in specific wear rate could be the presence of hard filler particles that get removed after continuous rubbing and then ultimately formation of create on the composite surface. The increasing order of wear rate is as 0wt.-% MD>2.5wt.-% MD > 5wt.-% MD > 7.5wt.-% MD >10wt.-% MD respectively.

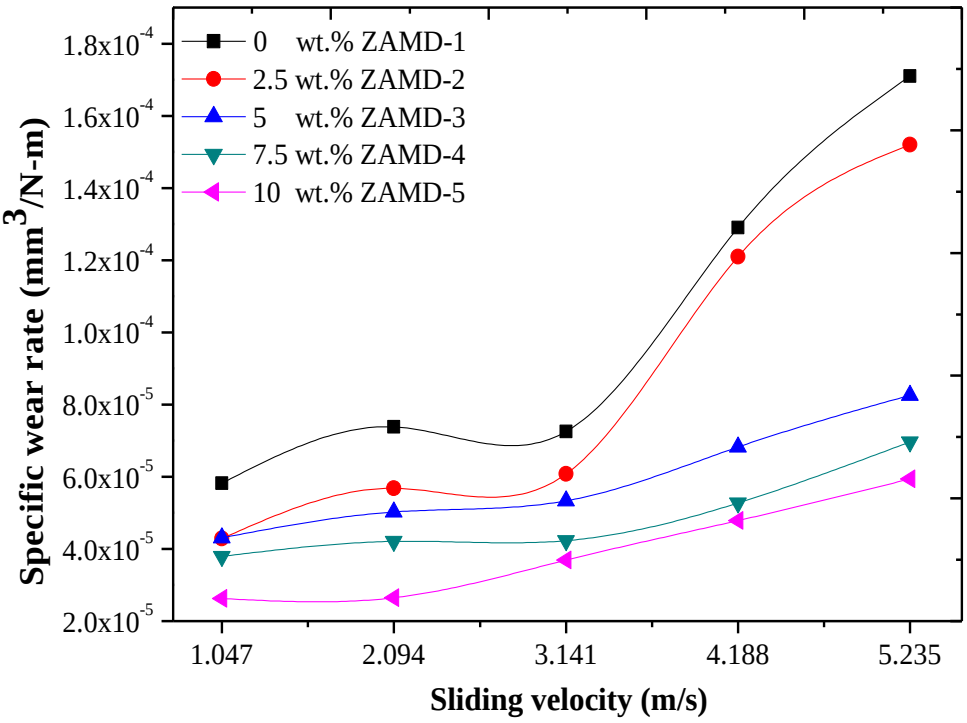

Figure 6.1 Variation of specific wear rate with sliding velocity for MD particulates filled ZA-27 alloy composites (Load: 15N, Sliding Distance: 1000m and Environment Temperature: 35°C)

6.1.2 Effect of sliding velocity on coefficient of friction of MD particulates filled ZA-27 alloy composites

Figure 6.2 shows the value of the coefficient of friction on sliding velocity of marble dust filled ZA-27 alloy composites. From Figure 6.2 it is observed that the coefficient of friction decreases initially up to 2.094 m/s sliding velocity and after that it is observed in an average values till 5.235 m/s sliding velocity. The reason for a gradually decrease in the COF can be softening of composite materials worn surface after sliding and the sub-surface with the increasing in temperature in contacted reason; these are the major factors for reduced value of COF[327]. From 2.5 to 7.5

wt.-% marble dust particulates filled ZA-27 alloy composites show almost similar pattern of coefficient of friction with the variation of sliding velocity from 2.094 m/s to 5.235 m/s including unreinforced metal alloy composites.

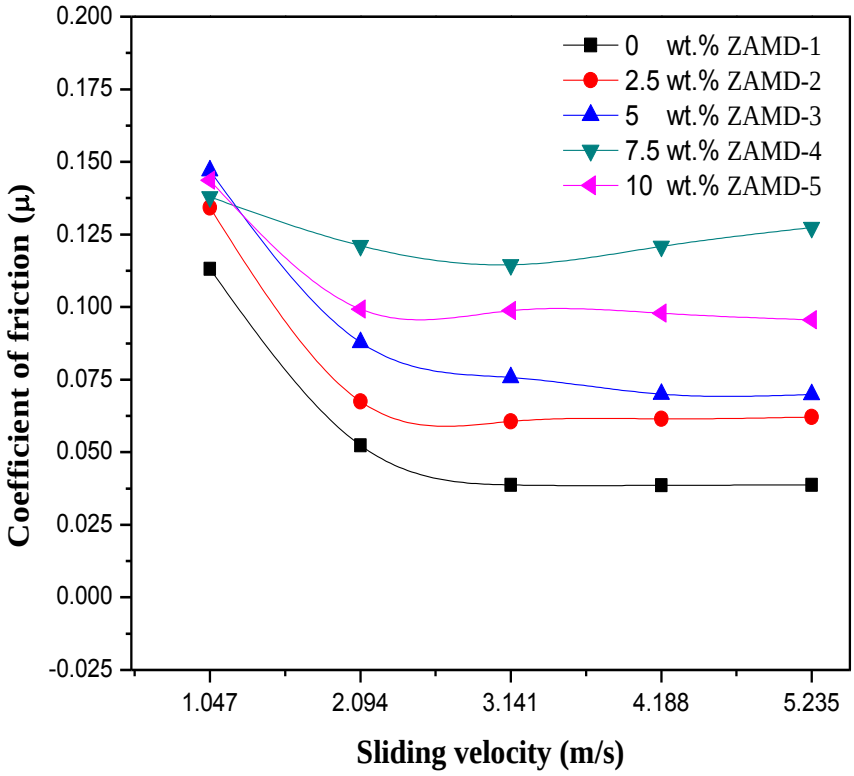

Figure 6.2 Variation of the coefficient of friction with sliding velocity for MD particulates filled ZA-27 alloy composites (Normal load: 15N, Sliding Distance: 1000m and Environment Temperature: 35°C)

When wear and friction test proceeds with the certain time period, the roughness of upper surface is reduced so that the convex peak gradually wore off due to that the COF become constant at stable stage [327]. Figure 6.1, shows the wear rate is increased with the increase in sliding velocity of the unfilled as well as particulate filled alloy composites.

Whereas, the coefficient of friction value of the particulate filled alloy composites show slightly decreasing in trend with the increased in sliding velocity. This is due to the better distribution of the marble dust particle in the ZA-27 alloy matrix that introduces the improvement in the wettability of the reinforcing phase with the matrix metal [328,329].

6.1.3 Effect of normal load on specific wear rate of MD particulates filled ZA-27 alloy composites

Figure 6.3 shows the wear rate of unfilled (unreinforced) and marble dust particulate filled ZA-27 alloy composites and it is observed that the unfilled ZA-27 alloy composite has higher specific wear rate as compared to the particulate filled ZA-27 alloy composites [330]. The maximum wear rates for all the unfilled and particulate compositions are occurred in between 35 N to 45 N loading conditions. The specific wear rate of the composite material is affected by the particle size, homogeneous mixture, hardness of the reinforcement and matrix alloy respectively [25]. There is a transition load exist at which unforeseen wear rate exist for unreinforced and marble dust filled ZA-27 alloy composites. At higher load i.e. 45N the transition occurs for unreinforced alloy from mild to severe wear [180]. Similarly, other researchers are observed a similar trend for garnet particulate filled ZA-27 alloy composites with the increased in loading capacity from 20 to 50N with an interval of 10N the wear rate increases drastically [331,332]. This is due to the presence of surface damage at contact region and ultimately material transfer at counter face [331,332].

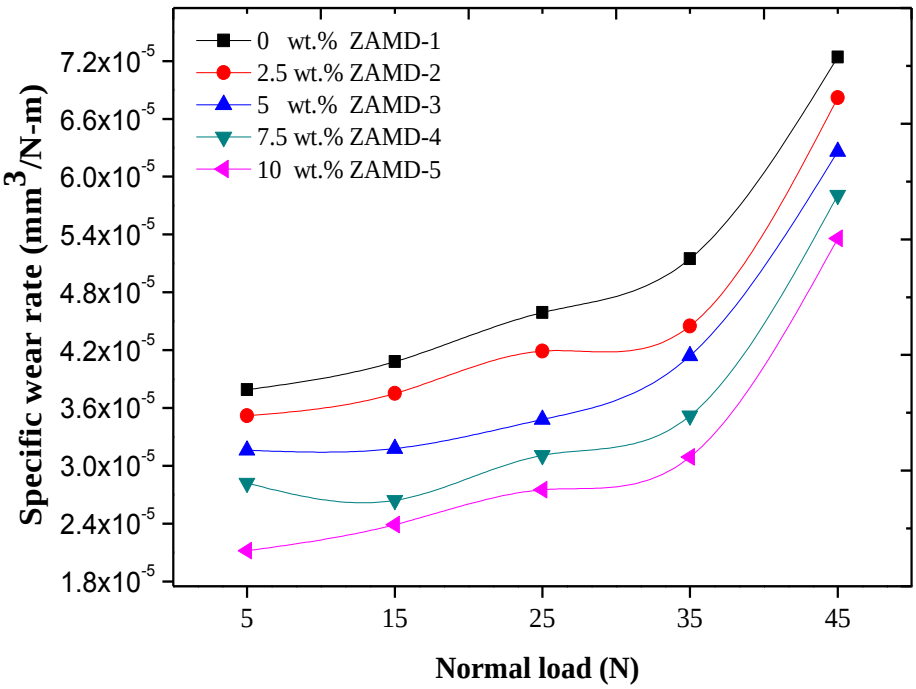

Figure 6.3 Variation of specific wear rate with normal load for MD particulates filled ZA-27 alloy composites (Sliding velocity: 2.094m/s, Sliding Distance: 1000m and Environment Temperature: 35°C)

6.1.4 Effect of normal load on coefficient of friction of MD particulates filled ZA-27 alloy composites

Figure 6.4 shows the variation of coefficient of friction under different normal loads (keeping remaining factors remains constant: Sliding velocity: 2.094m/s, Sliding Distance: 1000m and Environment Temperature: 35°C) for unfilled and particulate filled ZA-27 alloy composites. From Figure 6.4 it is observed that the coefficient of friction increases with the increasing in normal load for different wt.-% of marble dust particulate filled ZA-27 alloy composites, this can be occurred due to hard reinforced particles may be dislodged during rubbing process and get clogged between surfaces that lead higher coefficient of friction [333]. The maximum value of coefficient of friction i.e. in between 0.270 to 0.305 is found for 2.5 wt.-% of marble dust particulate filled ZA-27 alloy composite [332]. The coefficient of friction is generally observed stable for all the composites at different loading conditions but for Cu/MMC and Al/MMC composites the coefficient of friction is varied in between 0.2 and 0.45 due to dependency on filler content, loading conditions and sliding distance [85;331].

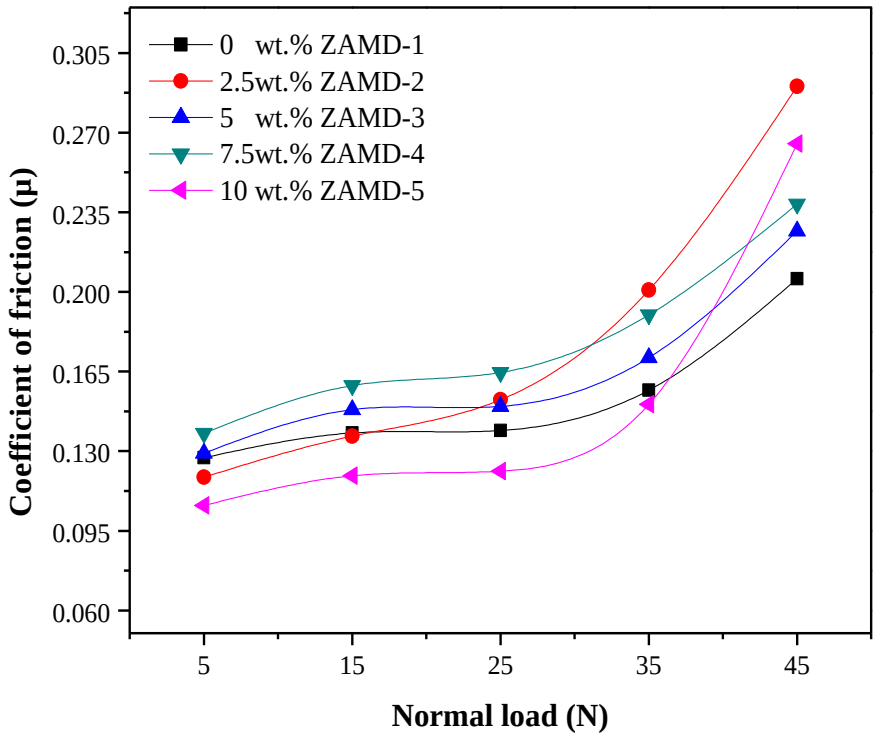

Figure 6.4 Variation of the coefficient of friction with normal load for MD particulates filled ZA-27 alloy composites (Sliding velocity: 2.094m/s, Sliding Distance: 1000m and Environment Temperature: 35°C)

6.1.5 Taguchi design experimental analysis for MD particulates filled ZA-27 alloy composites

The overall S/N ratio is found to be 83.16 dB by using MINITAB 16 software for the proposed particulate filled ZA-27 alloy composites (Table 6.1).

Table 6.1 shows the response for the signal to noise ratio of five factors that give smaller the better characteristics.

Expt. No.	Sliding Velocity (m/sec)	Filler Content (wt. -%)	Normal Load (N)	Sliding Distance (m)	Environment Temperature (°C)	Spe. Wear Rate $\frac{mm3}{N-m}$	S/N Ratio (db)
1	1.047	0	5	500	25	0.0002432	72.281
2	1.047	2.5	15	1000	30	0.0000408	87.793
3	1.047	5	25	1500	35	0.0001731	75.234
4	1.047	7.5	35	2000	40	0.0001623	75.794
5	1.047	10	45	2500	45	0.0001208	78.359
6	2.094	0	15	1500	40	0.0002161	73.307
7	2.094	2.5	25	2000	45	0.0000734	82.687
8	2.094	5	35	2500	25	0.0000598	84.460
9	2.094	7.5	45	500	30	0.0000381	88.377
10	2.094	10	5	1000	35	0.0000438	87.165
11	3.14	0	25	2500	30	0.0000587	84.630
12	3.14	2.5	35	500	35	0.0003108	70.150
13	3.14	5	45	1000	40	0.0000372	88.577
14	3.14	7.5	5	1500	45	0.0005720	64.852
15	3.14	10	15	2000	25	0.0000921	80.714
16	4.188	0	35	1000	45	0.0000811	81.825
17	4.188	2.5	45	1500	25	0.0000362	88.816
18	4.188	5	5	2000	30	0.0000838	81.537
19	4.188	7.5	15	2500	35	0.0000286	90.876
20	4.188	10	25	500	40	0.0000526	85.582
21	5.235	0	45	2000	35	0.0000060	104.375
22	5.235	2.5	5	2500	40	0.0000638	83.898
23	5.235	5	15	500	45	0.0000437	87.186
24	5.235	7.5	25	1000	25	0.0000201	93.919
25	5.235	10	35	1500	30	0.0000470	86.549

From Table 6.1 it is also concluded that filler particles have most significant effect on the specific wear rate of marble dust filled ZA-27 alloy composites that followed by sliding velocity, sliding distance, normal load and environment temperature. Figure 6.5 leads the conclusion towards a better combination of factor settings for marble dust filled ZA-27 alloy composites.

Table 6.1 Experimental design of L_{25} orthogonal array

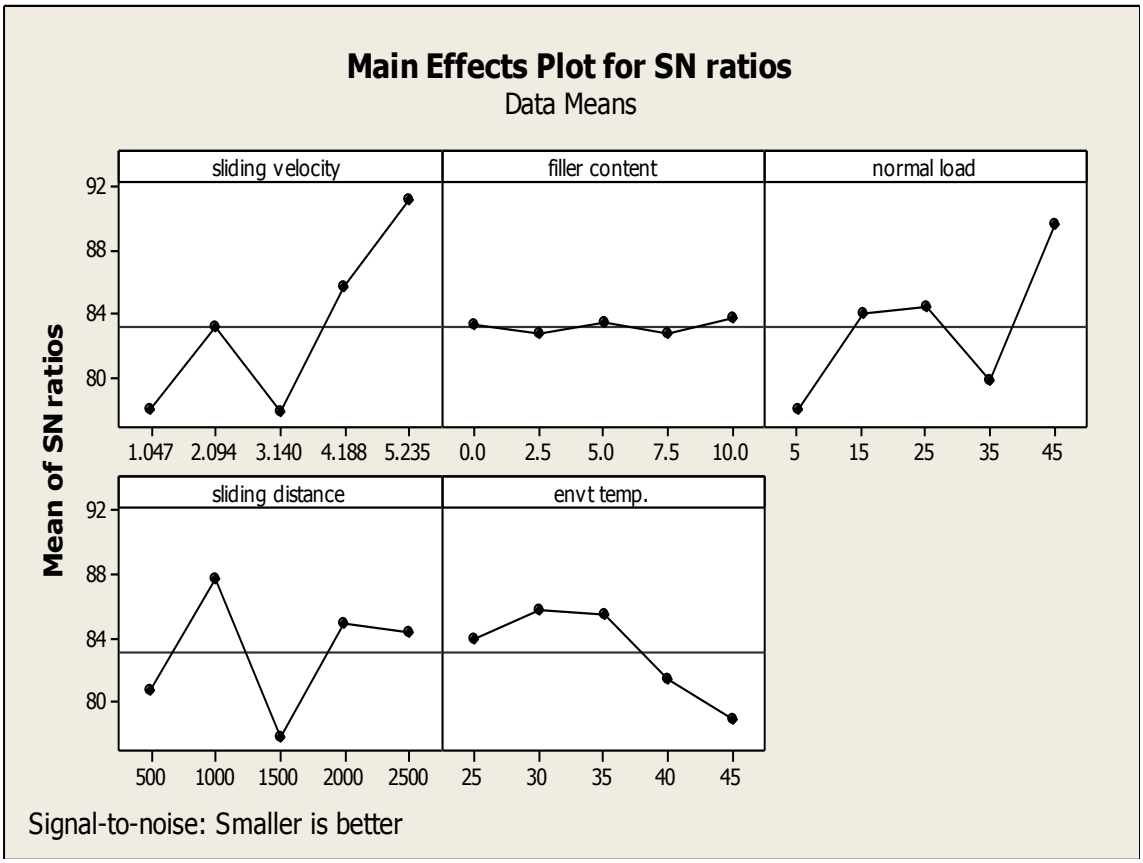

Figure 6.5 Effect of control factors on wear rate (For MD filled ZA-27 alloy composites)

6.1.6 ANOVA and the effect of factors for MD particulates filled ZA-27 alloy composites

Table 6.2 shows the result of ANOVA with specific wear rate for different wt.-% of marble dust filled ZA-27 alloy composites. This analysis is undertaken for a level of significance of 5% that shows a level of confidence up to 95%. In Table 6.2 the last column represents the p-test i.e. the percentage contribution of each and individual factor on the total variation and then the degree of influence on total results. Table 6.2 shows the load (C) [p=0.124%], sliding distance (D) [p=0.185%] and environment temperature (E) [p=0.368%], have most significant influence on the specific wear rate of the marble dust filled ZA-27 alloy composites but the filler content (B) [p=0.997]

and sliding velocity (A) [p=0.066] show the greatest significance on specific wear rate of the alloy composites. It is cleared that the filler content has most significance contribution as compared to other factors.

Table 6.2 ANOVA table for specific wear rate MD particulates filled ZA-27 alloy composite)

Source	DF	Seq SS	Adj SS	Adj MS	F	P
A	4	638.22	638.22	159.55	5.40	0.066
B	4	3.67	3.67	0.92	0.03	0.997
C	4	418.91	418.91	104.73	3.55	0.124
D	4	311.96	311.96	77.99	2.64	0.185
E	4	169.12	169.12	42.28	1.43	0.368
Error	4	118.13	118.13	29.53		
Total	24	1660.01				

DF - Degree of freedom, Seq SS - Sequential sum of square, Adj SS - Adjacent sum of square, Adj MS - Adjacent sum of mean square, F – Variance, P - Test (Percentage contribution of each factor in overall performance to find out optimum specific wear rate)

6.1.7 Surface morphology of unfilled and MD particulates filled ZA-27 alloy composites

The surface morphology is commonly used to analyse geometric features of material that also known as grain structure. The field emission scanning electron microscopy (FE-SEM) of typically worn surfaces of the marble dust (100 µm) filled ZA-27 alloy composite is presented in Figure 6.6. Figure 6.6a shows the wear surface for unfilled metal alloy composites that have 0.018 % void contents that are more as compared to 7.5wt.-% marble dust filled ZA-27 alloy composites. The surface shows the homogeneous in nature due to the absence of filler particles as well as unworn surfaces. Therefore, the presence of different micro cracks, voids and such types of problem may be less. However, the effect of sliding velocity (at higher velocity: 5.235m/s) for unfilled ZA-27 alloy composite shows very rough surface and the worn surface shows the area where matrix material is worn out (Figure 6.1 and Figure 6.6b). Figure 6.6c, 6.6e, 6.6g and 6.6i show marble dust particulate filled ZA-27 alloy composites for the unworn condition.

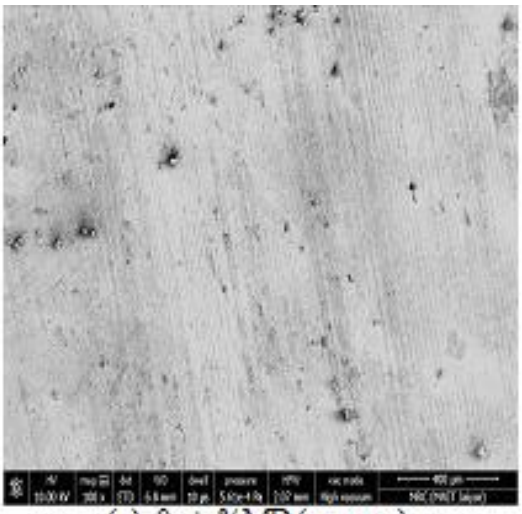

(a): 0wt.-%MD (unworn)

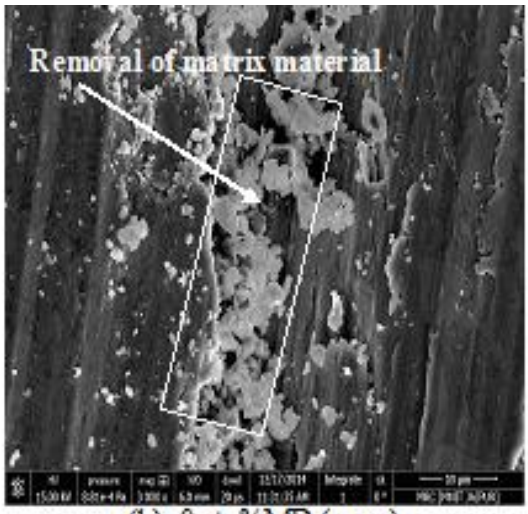

(b): 0wt.-%MD (worn)

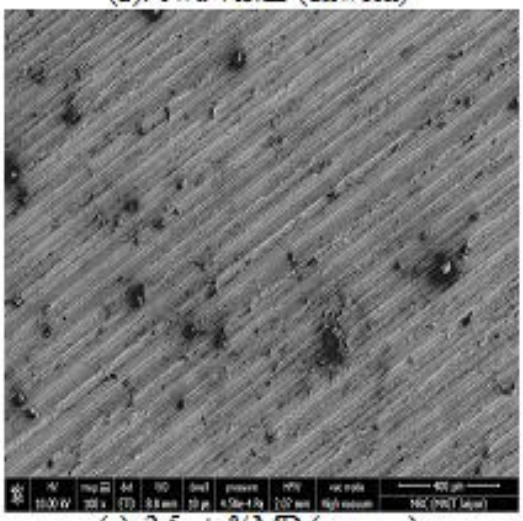

(c): 2.5wt.-%MD (unworn)

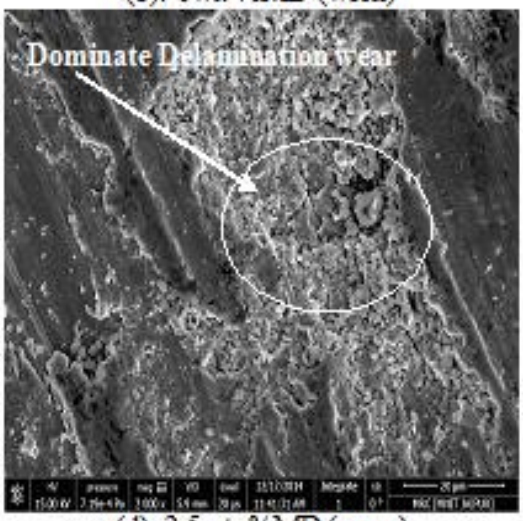

(d): 2.5wt.-%MD (worn)

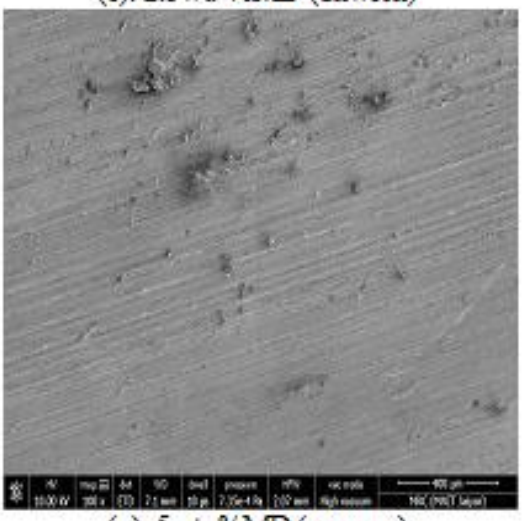

(e): 5wt.-%MD (unworn)

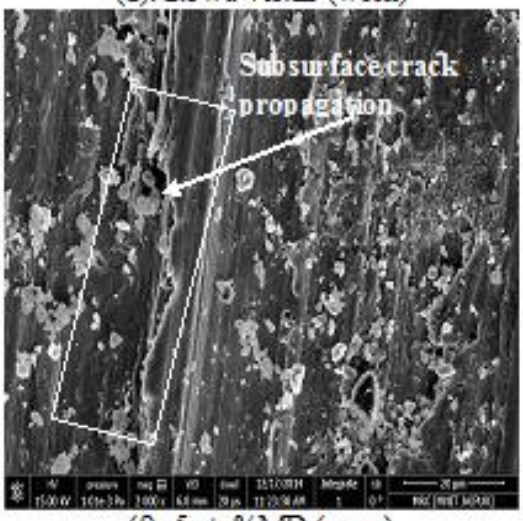

(f): 5wt.-%MD (worn)

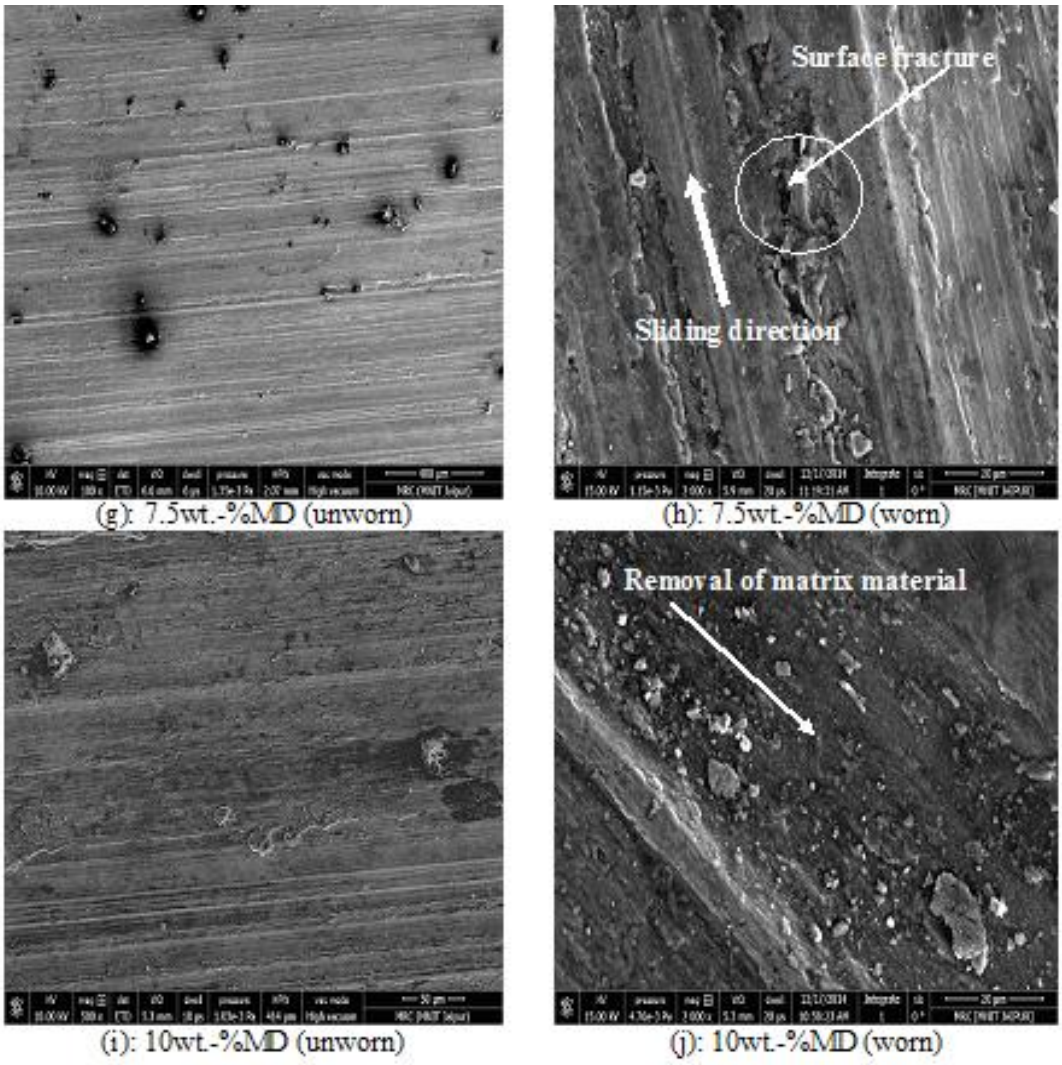

Figure 6.6 Scanning electron micrograph of unfilled and particulates filled ZA-27 alloy composites under steady state condition with varying sliding velocity (At constant: Normal load: 15N, Sliding Distance: 1000m and Environment Temperature: 35°C)

These surfaces are shown a clear structure with lesser numbers of grooves on the upper surface of the filled composite and these grooves are mainly due to the presence of voids in the composite. Figure 6.6d shows 2.5wt.-% of marble dust filled ZA-27 alloy composite at 5.235m/s sliding velocity at constant normal load: 15N, sliding distance: 1000m and environment temperature: 35^0C respectively. At higher sliding velocity the upper surface protective layer of the marble dust filled particles can no longer remain stable and huge numbers of wear strips are formed which distinctly visible as shown in Figure 6.6d (Figure 6.1).

The materials are removed on the surface of the composite in the form of flank type debris. Figure 6.6f shows the effect of sliding velocity in steady state conditions at constant normal load: 15N, sliding distance: 1000m and environment temperature: 35^0C respectively for 5wt.-% of marble dust filled ZA-27 alloy composites. In Figure 6.6f at higher sliding velocity (5.235m/s), the sliding wear tracks are clearly visible. As compared to unfilled and 2.5wt.-% marble dust filed ZA-27 alloy composites the wear rate of 5wt.-% marble dust filled alloy composite shows lesser wear rate (Figure 6.1). Similarly, atomic force microscope analysis is conducted for worn surfaces of MD filled ZA-27 alloy composite materials to check the roughness peeks for different wt.-% of filler particulates that shown in Figures 6.9 (a) to (e). From Figure 6.6f shows, the subsurface crack propagation as shear strain induced during rubbing between disc and pin materials as caused finally delamination wear [334]. However, with the increased in filler content in the matrix material the wear rate drastically reduced as the hard filler particles behave as a protecting surface as shown in Figure 6.1 (Figures 6.6h, i). As the wear rate reduced for 10wt.-% marble dust filled composites as compared to other unfilled and 7.5wt.-% marble dust filled composites but the surface fracture is clearly evident in Figure 6.6h. Therefore, under similar boundary conditions the upper surface materials are completely removed and the shear strain is increased due to rubbing between the dust particles and matrix materials, thus ultimately causing the removal of the surface layers by delamination (Figure 6.6j).

Figure 6.7 shows the effect of normal load on the specific wear rate of the marble dust filled ZA-27 alloy composites at constant velocity: 2.094m/s, sliding distance: 1000m and environment temperature: 35ºC respectively. Figure 6.7a shows the micrograph of unfilled ZA-27 alloy composite at low load i.e. 5N. At lower loading conditions the unfilled alloy composite shows generally delamination wear, that confirms the presence of worn surfaces and crack initiation / propagation. However, with the increased in normal load from 5N to 45N for the same unfilled ZA-27 alloy composite the wear rate drastically increases at constant velocity: 2.094m/s, sliding distance: 1000m and environment temperature: 35ºC respectively as shown in Figure 6.7b. As compared to Figure 6.7a the fracture location is quite increased and the locally damaged matrix material reaches to fracture surface. Figures 6.7c and 6.7d show the wear rate of the particulate filled (2.5wt.-% of marble dust) ZA-27 alloy composites at low and high loading condition by keeping the other parameters remaining constant.

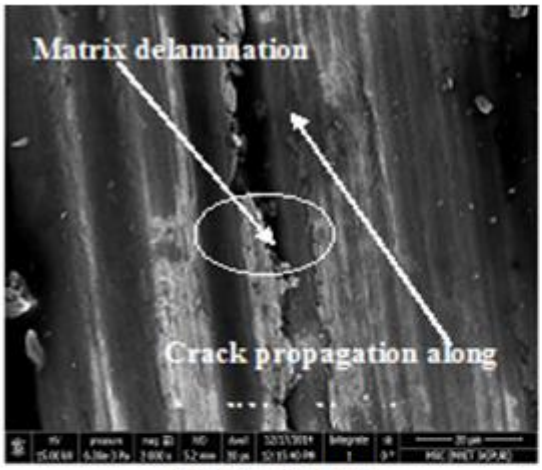

(a): 0wt.-%MD

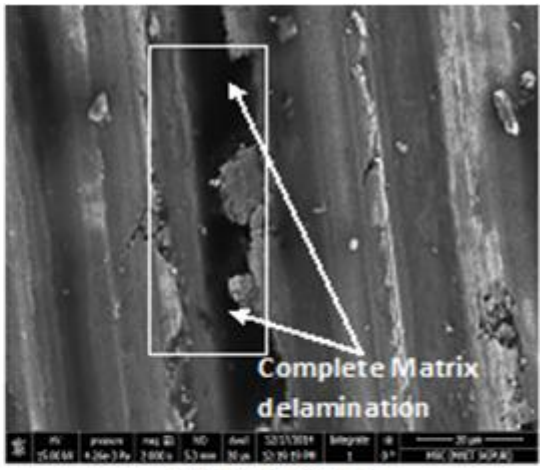

(b): 0wt.-%MD

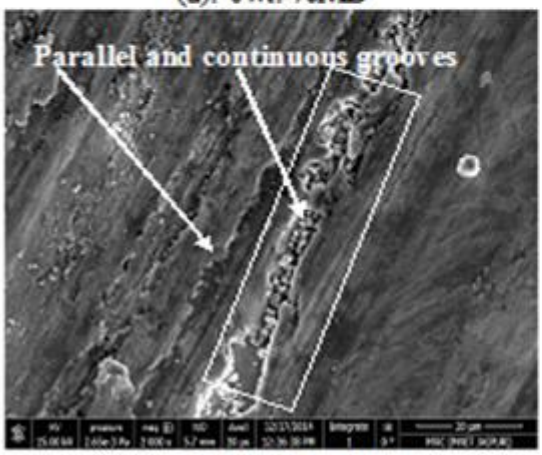

(c): 2.5wt.-%MD

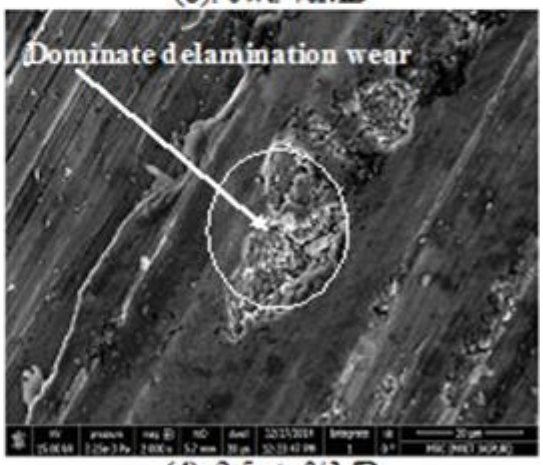

(d): 2.5wt.-%MD

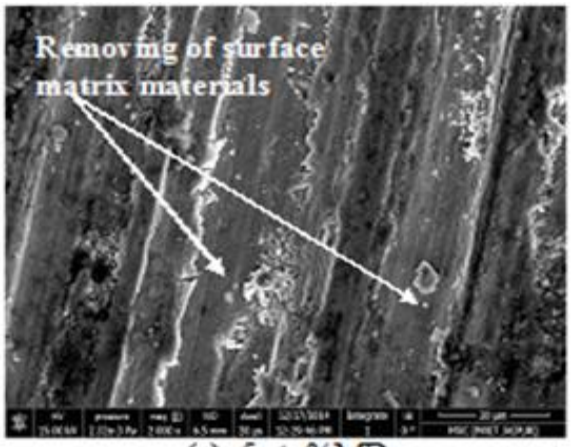

(e): 5wt.-%MD

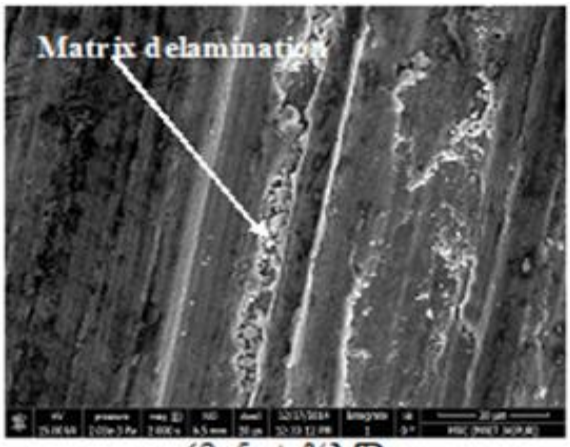

(f): 5wt.-%MD

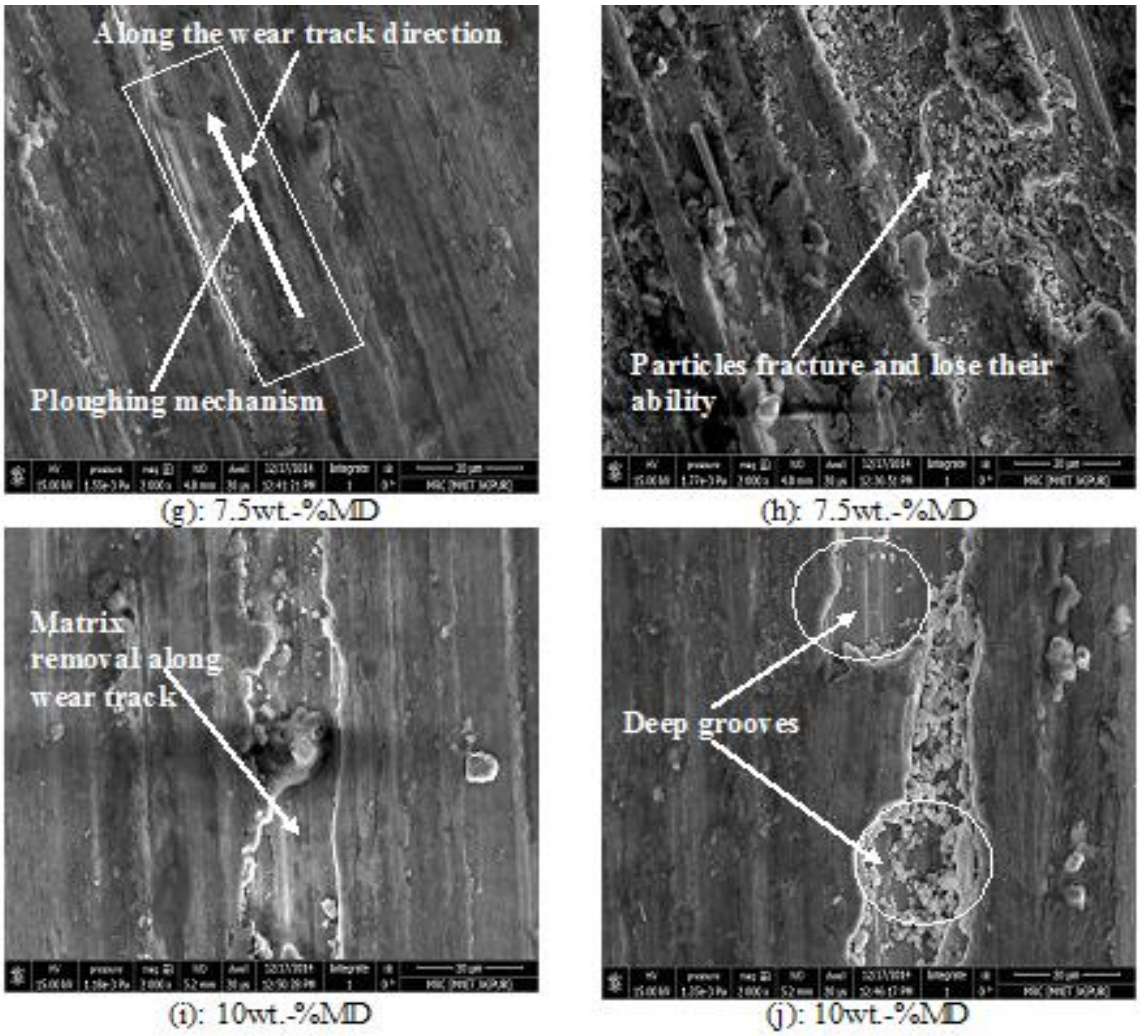

Figure 6.7 Scanning electron micrograph of unfilled and particulates filled ZA-27 alloy composites under steady state condition with varying normal load (At constant: Sliding velocity: 2.094m/s, Sliding Distance: 1000m and Environment Temperature: 35°C)

At low load the above said composite micrograph shows both parallel and continuous grooves as shown in Figure 6.7c and the abrasive wear mechanism is observed at low loads, but with the increased in normal load from 5N to 45N the wear plays the dominating role [335].

Similarly, with the increased in filler content from 2.5wt.-% to 5wt.-% under similar operating condition (Figures 6.7e, f) the microstructure wear mechanism show different pattern as compared with Figure 6.7c, d. From Figure 6.7e it is observed that at low normal load condition the surface micrograph shows removing of surface matrix materials and cracks get nearer to the surface with the increased in shear strain

thus that causes at higher load excessive wear (Figure 6.7f). However, on further increased in filler content from 5wt.-% to 7.5wt.-% of marble dust in the matrix material the wear rate further reduced as shown in Figure 6.3 and micrograph (Figure 6.7g). The presence of micro-ploughing can occur due the hardened asperities on the contacted surfaces [336]. The improvement in wear resistance of the particulate filled ZA-27 alloy composites at low load is attributed to the presence of the hard marble dust particles that form a thin glassy layer at the contact surface between the composite and the disc counter face (Figure 6.7h). A similar observation is observed for SiC particle filled metal composites [337]. Again on further increased in marble dust particles from 7.5wt.-% to 10wt.-% in the matrix material and the wear rate still played a dominating role as shown in Figure 6.3 and micrograph in Figures 6.7i, j respectively. It is observed that, as the load increases, the wear track on the worn surfaces changes gradually from scratches to deep grooves (Figure 6.7j).

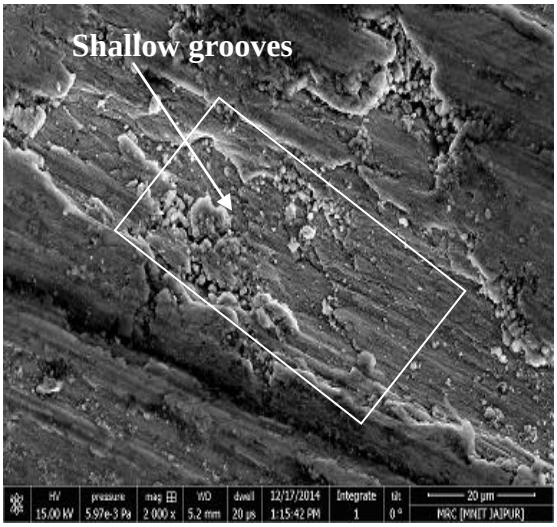

(a): 0wt.-%MD

(b): 0wt.-%MD

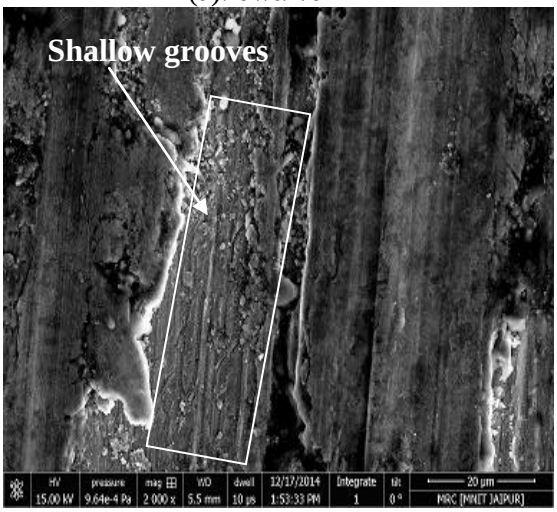

(c): 2.5wt.-%MD

(d): 2.5wt.-%MD

(e): 5wt.-%MD

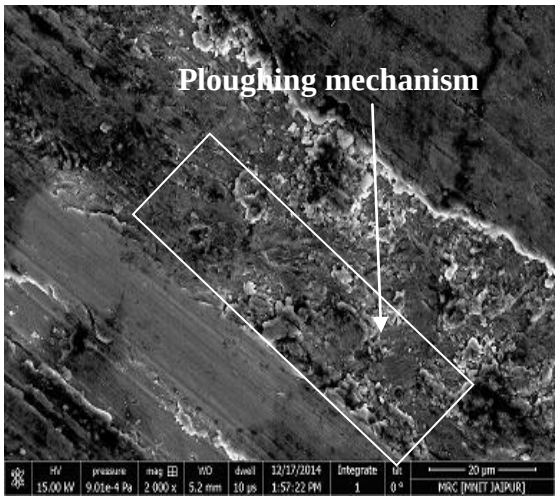

(f): 5wt.-%MD

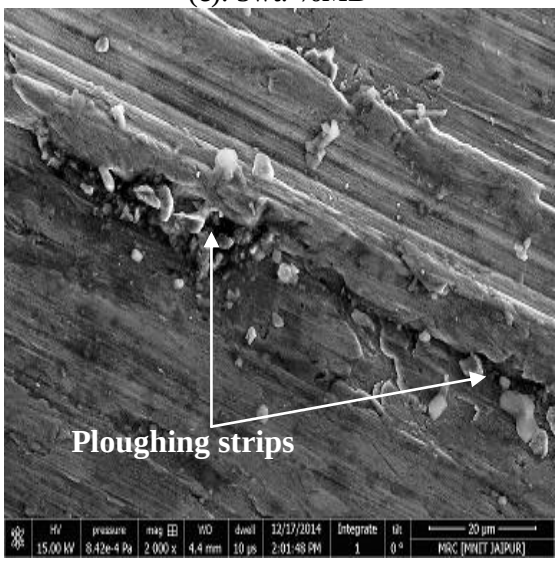

(g): 7.5wt.-%MD

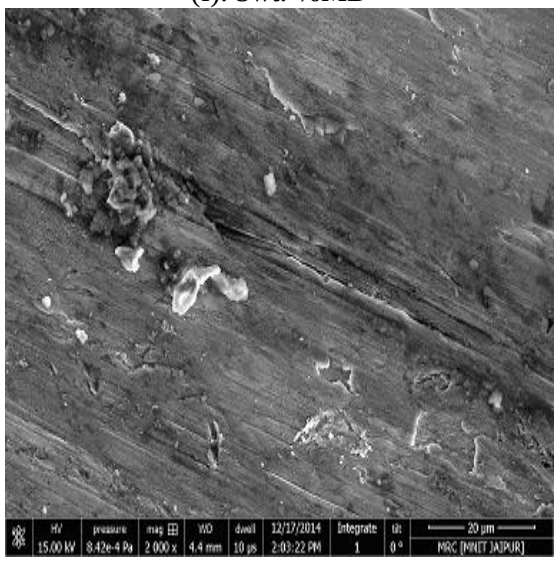

(h): 7.5wt.-%MD

(i): 10wt.-%MD

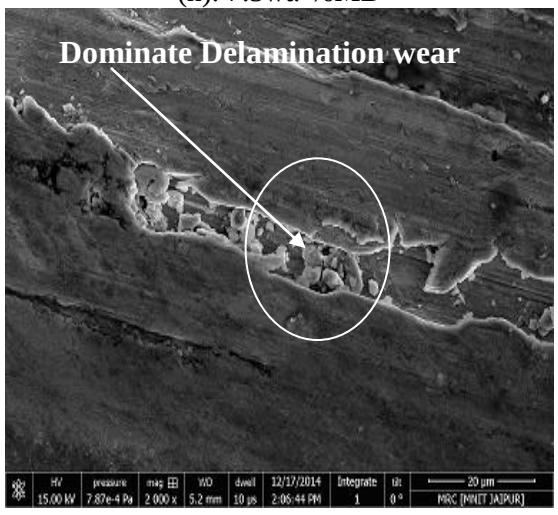

(j): 10wt.-%MD

Figure 6.8 Scanning electron micrographs of unfilled and particulate filled ZA-27 alloy composites (Taguchi Design of Experiment)

Figure 6.8 (a-j) shows the surface morphology of composite materials at different test conditions for L_{25} Taguchi design (Table 6.1). The composite materials

strongly follow the interaction in between the reinforced particles and matrix, and this follows the performance of different properties of composite materials for numerous applications. The sliding wear test is performed on pin-on-disc tribometer to get the wear behaviour of composite material with varying conditions with time. During wear when two surfaces are in contact that generated a deformation regarding wear debris, ploughing, surface roughness and many more which directly and indirectly affect the performance of composites materials. Figure 6.8a shows the surface microstructure for unreinforced particulate filled ZA-27 alloy composites in which presence of wear debris and shallow grooves shown due to continuous contact of two surfaces during running (See Table 6.1, Expt. Run 1). However, with the increasing in sliding velocity and normal load the contact pressure between surfaces also increases (Figure 6.8b) and due to that ploughing, voids and debris like problems occurs (See Table 6.1, Expt. Run 6). Figure 6.8c shows the presence of 2.5 wt.-% of marble dust as filler in ZA-27 alloy composites (See Table 6.1, Expt. Run 2). It shows the shallow grooves and ploughing due to the plastic deformation of present asperities by generated frictional heat and stresses [338].

However, with the increase in sliding velocity, normal load and sliding distance of the same composite, the wear rate also increases as compared to that of Figure 6.8d. Such observations have been reported by various researchers, such as Yu et al. [339] have reported that the wear resistances of MMCs increase with the content of SiC reinforcement. They infer that the shape and size of the reinforcement have a greater influence on the wear resistance of the filled composites (See Table 6.1, Expt. Run 7). Figure 6.8e shows the microstructure for 5wt.-% marble dust filled ZA-27 alloy composites at 3.14 m/s sliding velocity. The microstructure shows the presence of crack, when two surfaces are in contact and having higher shear force, cracks form in both transverse and longitudinal directions [338]. So the increasing in sliding velocity can be the reason for surface vandalization through a crack, debris and such like trouble (See Table 6.1, Expt. Run 13). Similarly, with the increase in sliding velocity of the similar weight percentage of the composites (Figure 6.8f), in this case, the wear debris and agglomeration forms during sliding wear between two contacted surfaced at different varying conditions of sliding velocity, load and environment temperature. When sliding velocity increases, deep scratches in between contacted region occurs and due to that wear debris produced, therefore the hardened wear debris impact other regions and again produced debris or voids (See Table 6.1, Expt.

Run 18). During casting, the fabrication technique is also played an important process to characterize the wear performance of composite material because the interaction or homogeneity between filler and matrix is an important factor which can affect the friction and wear properties of composites. For 7.5wt.-% of marble dust filled ZA-27 alloy composites the wear characterises of the composite shows smooth surface and ploughing strips are very sharp as shown in Figure 6.9d. In this case, surface ploughing seems to be an important mechanism of material removal under dry sliding conditions both in the case of composites as well as the base alloy. Given the above observation it can be concluded that at higher loads, the main wear mechanism is delamination wear, causing excessive fracture of the reinforcement and the matrix resulting in deterioration of the wear resistance of the composite (See Table 6.1, Expt. Run 4).

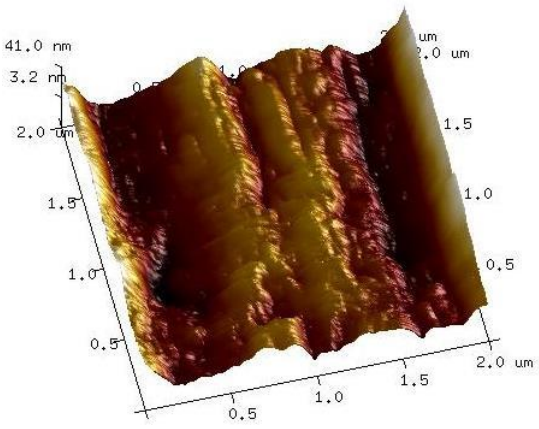

(a): 0 wt.-% MD (worm)

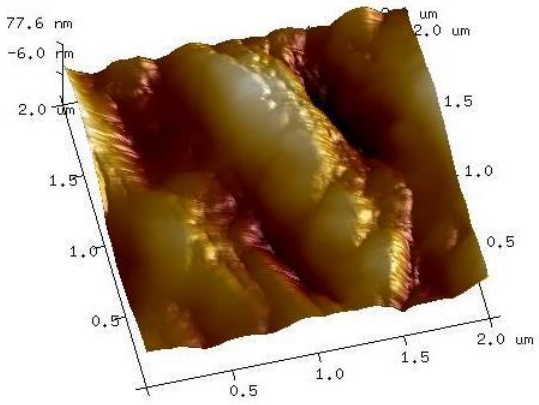

(b): 2.5 wt.-% MD (worm)

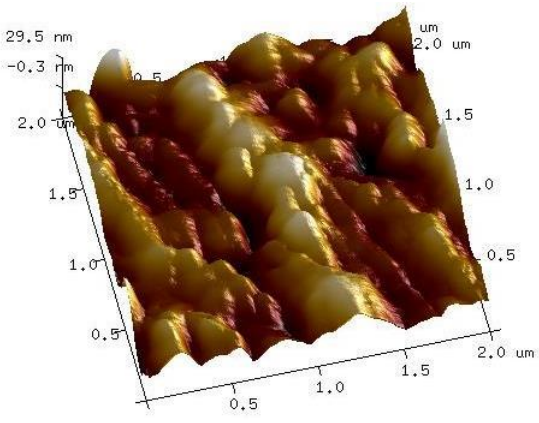

(c): 5 wt.-% MD (worm)

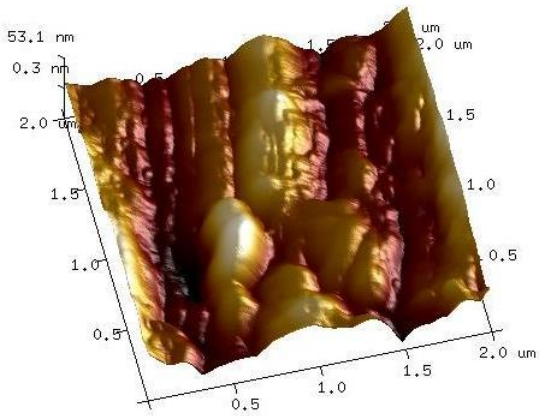

(d): 7.5 wt.-% MD (worm)

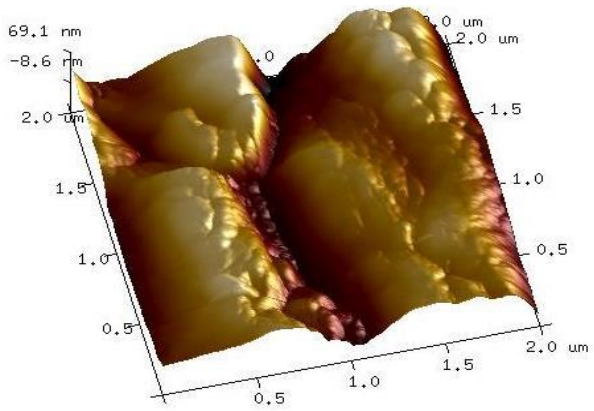

(e): 10 wt.-% MD (worn)

Figure 6.9 AFM micrographs of MD particulates filled ZA-27 alloy composites (a) 0 wt.-% MD (b) 2.5 wt.-% MD (c) 5 wt.-% MD (d) 7.5 wt.-% MD and (e) 10 wt.-% MD

Again at higher sliding velocity, lower normal load and lower sliding distance the wear rate is reduced as compared with Figure 6.8g and also, the macroscopic observation reveal the presence of the microgrooves on the surface of the composite that provides sufficient evidence for the abrasive effect of the reinforcing particles as evident from Figure 6.8h (See Table 6.1, Expt. Run 14).

Figure 6.8i shows 10wt.-% marble dust filled ZA-27 alloy composite under low load condition (See Table 6.1, Expt. Run 10) and wear loss is nominal as in this case marble dust plays a major role due to higher percentages of marble dust is included. Similarly, with the increased in sliding velocity for the same composite i.e. 10wt.-% marble dust filled ZA-27 alloy composite the wear loss is slightly increased that may be due to the filled composite that can be able to withstands high stresses without plastic deformation and it is very effective in reducing the wear rate (Figure 6.8j). Hence, it can be concluded that the ability of the sheared reinforcement layers to adhere the disc sliding surface decides the effectiveness of the particles in reducing the wear rate of the composite materials (See Table 6.1, Expt. Run 20).

6.1.8 Energy dispersive X-ray analysis (EDAX) of unfilled and MD particulates filled ZA-27 alloy composites

Energy dispersive X-ray analysis (EDAX) is used as an X-Ray technique to identify the composition of any materials, by it compositions analysed in the form of peaks. By EDAX elements mapping, and image analysis for material is also possible. From Figure 6.10(a-e) shows the different peaks form for the different compositions of marble dust filled ZA-27 alloy composites (0wt.-% to 10wt.-% of MD particulates). The EDAX is done only for steady state wear analysis of the particulate filled alloy

composites under varying sliding velocity. Figure 6.10a shows the EDAX graph of the wear samples at 1.047m/s sliding velocity for unfilled ZA-27 alloy composite and also observed that the presence of Zn and Al as major constituents. Figure 6.10a shows the sliding wear analysis of the unfilled alloy composite at sliding velocity 1.047m/s. At lower velocity the surface rubbing only taking place. Similarly, for 2.5wt.-% of marble dust filled alloy composites the EDAX graph shows the following constituents Zn, Fe, Ca, O, Al, etc., whereas the major constituents were Zn, Al, Fe and Ca. As Zn and Al and remaining Fe and Ca the minor constituents of marble dust (Figure 6.10b). Therefore, it is cleared that after wear analysis the constituents remaining intact with the composite material.

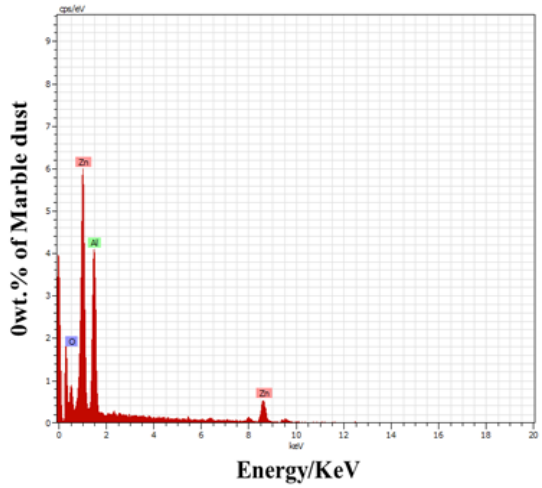

(a)

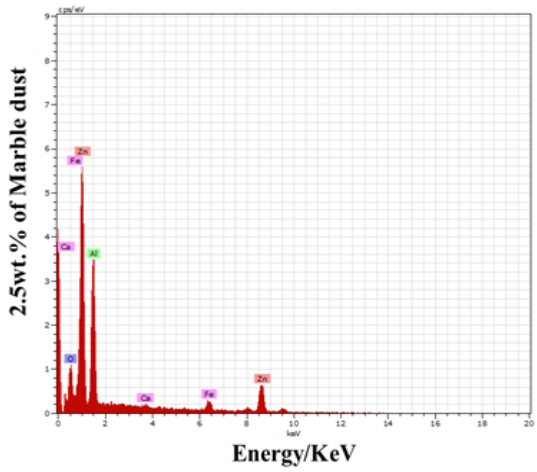

(b)

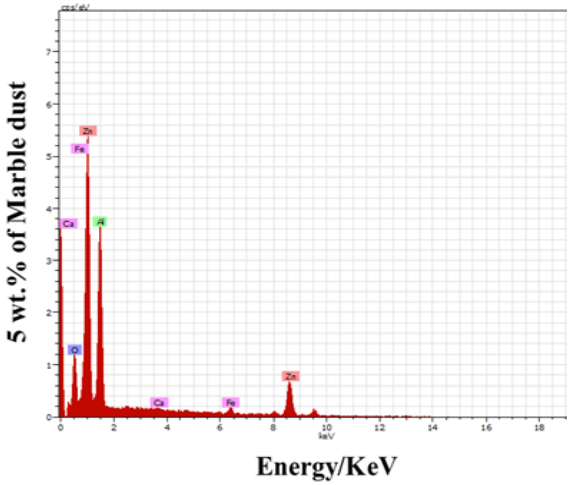

(c)

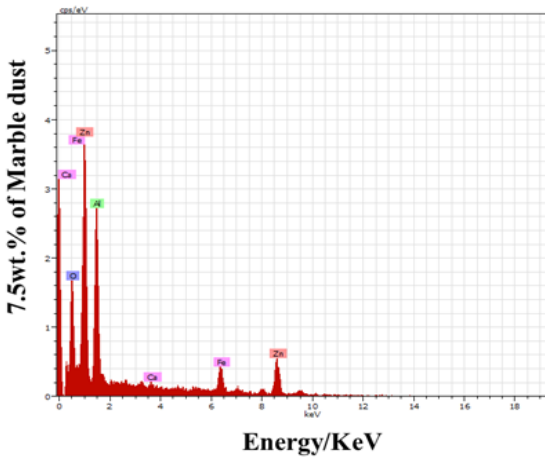

(d)

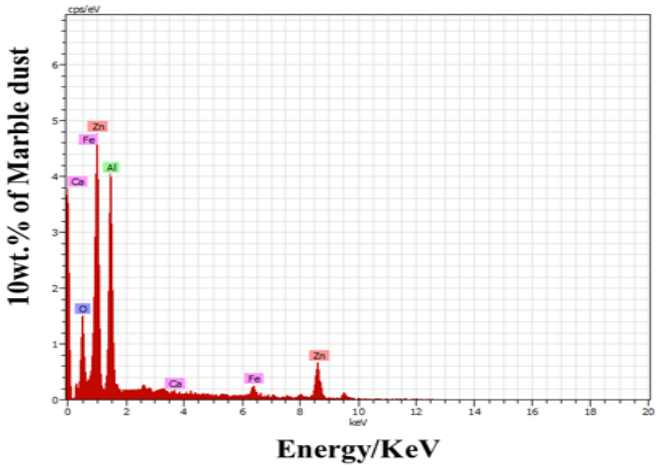

(e)

Figure 6.10 EDAX spectrums of MD particulates filled ZA-27 alloy composite. (a) 0wt.% MD (b) 2.5wt.% MD (c) 5wt.% MD (d) 7.5wt.% MD and (e) 10wt.% MD

This indicates that the wear debris and agglomeration forms during sliding wear between two contacted surfaced at different varying conditions of sliding velocity, load and environment temperature. Again Figure 6.10c shows the 5wt.-% of marble dust filled ZA-27 alloy composites for EDAX peak. From EDAX graph shows the major peaks are Zn, Fe, Ca and Al but as compared with Figure 6.10b the peak ratio is slightly lesser.

This may be due to the increase of filler materials in the base material or may be at higher weight percentages of filler content the base material starts wear out during sliding wear. However, with the increased in sliding velocity from 1.047m/s to 4.188m/s for 7.5wt.-% marble dust filled ZA-27 alloy composites the wear rate drastically increases with respective to lower sliding velocity as shown in Figure 6.10d. From EDAX graph (Figure 6.10d) it is still further clear that the major constituents further reduced the peak range as compared with the Figures 6.10a, b and c. This is mainly due to the increase of filler content in the base matrix alloy material. Finally, Figure 6.10e shows the EDAX peak of the 10wt.-% of marble dust filled ZA-27 alloy composite at higher sliding velocity i.e. 5.235m/s and shows similar characteristic as discussed for other weight percentages of marble dust filled alloy composites. Thus, it follows from the above observation that the most significant feature of severe wear that the marble dust particles should remain intact during wear to support the applied load and act as effective abrasive elements.

Part II

6.2 Steady state specific wear behaviour of Quicklime (CaO) particulates filled ZA-27 alloy composites

6.2.1 Effect of sliding velocity on specific wear rate of CaO particulates filled ZA-27 alloy composites

The computed SWR (from the data obtained via test runs on pin-on-disk tribometer), for all the investigated alloy composites at various laid down velocities (i.e. 1.047 to 5.235 m/s) are shown in Figure 6.11. In this plot the parameters like sliding distance (1000m), load (15N) and environment temperature (35ºC) are kept constant.

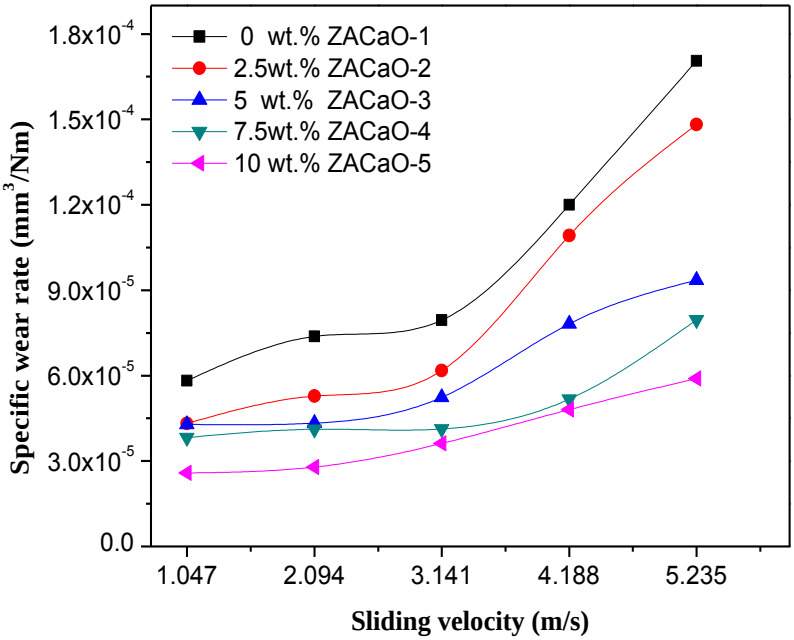

Figure 6.11 Variation of specific wear rate with sliding velocity for CaO filled ZA-27 alloy composites (Load: 15 N, Sliding distance: 1000 m and Environment temperature: 35°C)

The plotted Figure 6.11, makes following observations: (i) SWR of the investigated composites shows increasing trend with sliding velocity irrespective of filler content (ii) SWR is diminishing in magnitude with filler content, consequently the order of SWR as 0wt.-% CaO> 2.5wt.-% CaO> 5wt.-% CaO> 7.5wt.-% CaO> 10wt.-% CaO, across all sliding velocity. This may make an inference that higher (10 wt. - %) filler reinforcement leads to lowest SWR between the interfacing and rubbing surfaces. The improved behaviour of 10 wt.-% CaO particulate filled alloy composite may be attributed to strong interface bonding between matrix-filler that intact material against

wear out phenomenon [191]. Similar, results are reported by Ranganath et al. [30] while investigating sliding wear behaviour of garnet filled ZA-27 alloy composites. They reported that with the increased in wt.-% of garnet particles the wear rate decreases about the neat alloy.

6.2.2 Effect of sliding velocity on the coefficient of friction of CaO particulates filled ZA-27 alloy composites

The coefficient of friction on different sliding velocity (1.047 to 5.235 m/s) during the test runs for the specimens is plotted in Figure 6.12, while other parameters (like Normal load: 15N, Sliding Distance: 1000m and environment temperature: 35°C respectively) are kept constant. From this Figure, it is observed that: (i) COF seems to be in an increasing trend with sliding velocity irrespective of test specimens (ii) COF shows declining in magnitude with filler content, therefore, the order of COF is 0wt.-% CaO> 2.5wt.-% CaO> 5wt.-% CaO> 7.5wt.-% CaO> 10wt.-% CaO. This may make an inference that higher (10 wt. - %) filler reinforcement leads to lower COF (<0.2) between interfacing of rubbing surfaces. Similarly, the same composition leads to minimal SWR as indicated form Figure 6.11.

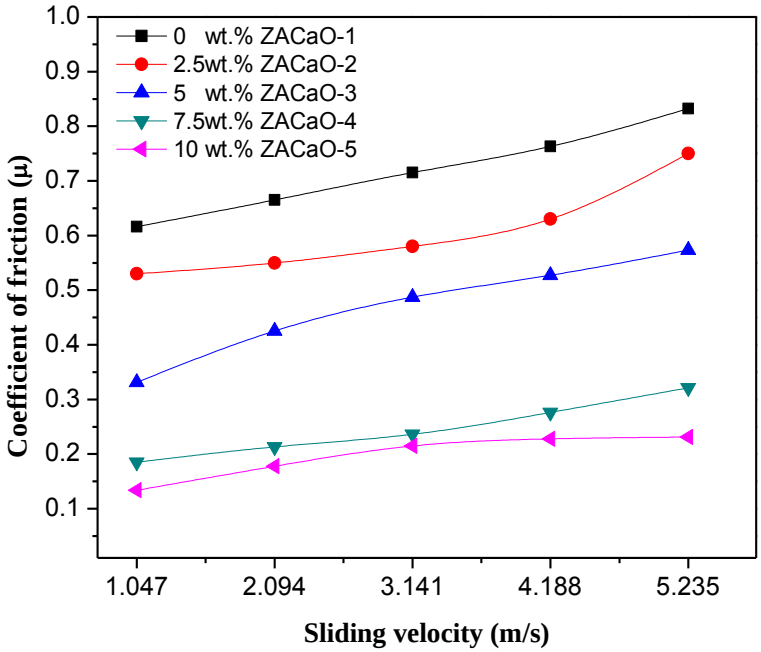

Figure 6.12 Variation of the coefficient of friction with sliding velocity for CaO particulates filled ZA-27 alloy composites (Normal load: 15 N, Sliding distance: 1000 m and Environment temperature: 35°C)

This might be attributed the proper interaction between reinforced particles and matrix alloy. During sliding process, the produced asperities, fluctuates by their positions that cause stick-slip oscillation condition for frictional profiles [340].

6.2.3 Effect of normal load on specific wear rate of CaO particulates filled ZA-27 alloy composites

The effect of normal load (5 to 45 N) on the SWR of the investigated alloy composites are plotted in Figure 6.13. The following observations could be made: (i) The SWR tends to have increasing in trend with normal load irrespective of filler content of the investigated composites (ii) the order of diminishing SWR magnitude with filler content as 0 wt.-% CaO > 2.5 wt.-% CaO > 5 wt.-% CaO > 7.5 wt.-% CaO > 10 wt.-% CaO irrespective of normal load condition. Thus, higher (10 wt. - %) filler content lead to lowest SWR across all loads under steady state condition. They might attributed to the presence of reinforced particles in a matrix that reduces the effective area of fraction with the counter area and by this matrix shepherd to a small surface abrasion in the composites counter face [341] (iii) it is also observed that unfilled alloy tends to higher SWR about filled alloy composites.

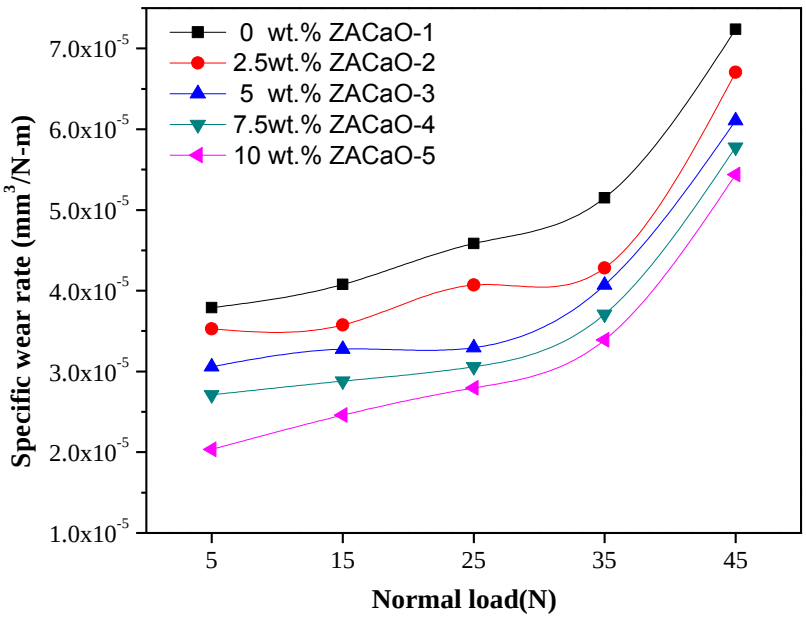

Figure 6.13 Variation of specific wear rate with normal load for CaO particulates filled ZA-27 alloy composites (Sliding velocity: 2.094 m/s, Sliding distance: 1000 m and Environment temperature: 35°C)

6.2.4 Effect of normal load on the coefficient of friction of CaO particulates filled ZA-27 alloy composites

The coefficient of friction on normal load (5 to 45 N) under steady state condition of CaO particulates filled ZA-27 alloy composites is plotted in Figure 6.14. The following inference could be drawn: (i) The COF tend to have increased in trend with normal load irrespective of filler content of the investigated composites. The contact surface during sliding is in elastoplastic state and by that the actual contacted become nonlinear with applied load, this results in the variation of COF with the increasing value of applied normal load [342]. (ii) The COF shows diminishing magnitude with filler content (i.e. 0wt.-% CaO> 2.5wt.-% CaO> 5wt.-% CaO> 7.5wt.-% CaO> 10wt.-% CaO) irrespective of normal load conditions. Thus, higher (10 wt. - %) filler content lead to lowest COF across all loads under steady state condition. (iii) It is also observed that neat specimen tends to show higher COF relative to filled composites. Similar, observations are made by Ozsarac et al. [343] while studying the wear behaviour of sliding bearings and they reported that COF for bearings show increase in values with the increased in the normal load.

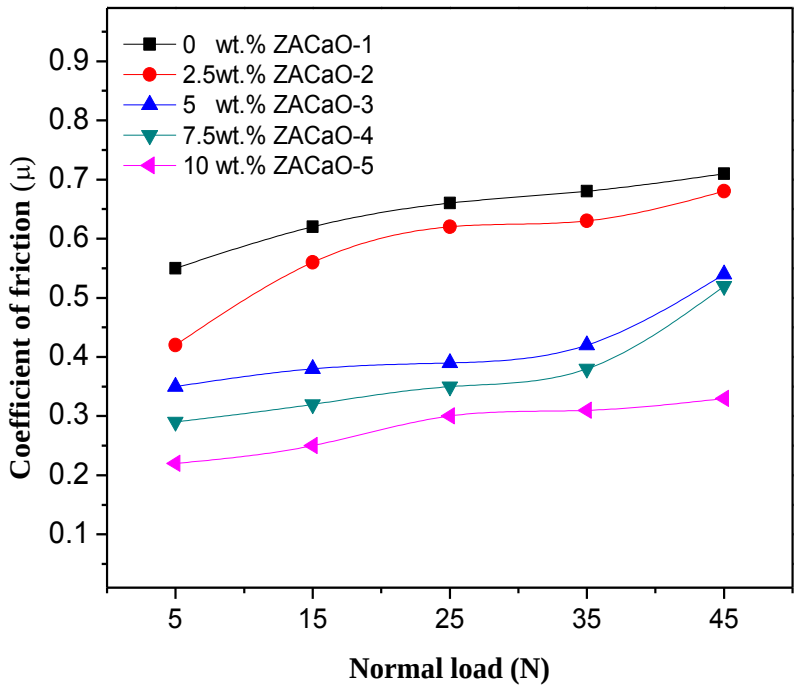

Figure 6.14 Variation of the coefficient of friction with normal load for CaO particulates filled ZA-27 alloy composites (Sliding velocity: 2.094 m/s, Sliding distance: 1000 m and Environment temperature: 35°C)

6.2.5 Taguchi design experimental analysis for CaO particulates filled ZA-27 alloy composites

To understand the correlation between SWR and its controlling variables Taguchi design of Experiment approach is applied in this work.

Table 6.3 Experimental design of L_{25} orthogonal array

Expt. No.	Sliding Velocity (m/sec.)	Filler Content (wt. -%)	Normal Load (N)	Sliding Distance (m)	Environment Temperature (°C)	Specific Wear Rate $\frac{mm3}{N-m}$	S/N Ratio (db)
1	1.047	0	5	500	25	2.432E-04	72.281
2	1.047	2.5	15	1000	30	6.782E-05	83.373
3	1.047	5	25	1500	35	1.648E-05	95.661
4	1.047	7.5	35	2000	40	2.980E-06	110.516
5	1.047	10	45	2500	45	1.505E-05	96.449
6	2.094	0	15	1500	40	3.602E-05	88.869
7	2.094	2.5	25	2000	45	8.138E-06	101.790
8	2.094	5	35	2500	25	7.062E-06	103.021
9	2.094	7.5	45	500	30	2.781E-05	91.116
10	2.094	10	5	1000	35	1.693E-04	75.427
11	3.14	0	25	2500	30	1.544E-05	96.227
12	3.14	2.5	35	500	35	1.034E-05	99.710
13	3.14	5	45	1000	40	1.832E-05	94.741
14	3.14	7.5	5	1500	45	5.564E-05	85.092
15	3.14	10	15	2000	25	2.738E-05	91.251
16	4.188	0	35	1000	45	5.210E-05	85.663
17	4.188	2.5	45	1500	25	3.014E-05	90.417
18	4.188	5	5	2000	30	4.120E-05	87.702
19	4.188	7.5	15	2500	35	6.118E-05	84.268
20	4.188	10	25	500	40	1.693E-05	95.427
21	5.235	0	45	2000	35	8.057E-06	101.877
22	5.235	2.5	5	2500	40	7.963E-05	81.978
23	5.235	5	15	500	45	6.450E-05	83.809
24	5.235	7.5	25	1000	25	2.612E-05	91.661
25	5.235	10	35	1500	30	1.136E-05	98.892

Taguchi DOE approach enables the establishment of ranking order of controlling variables that significantly affects SWR within least experimental test runs, thereby leads to satisfactory conclusions [248]. In this research work, the controlling factors that practically governs SWR and there intact levels are depicted in Table 3.11. Thus, there are five controlling variables and there five levels as per Table 3.11. For

experimental test runs L_{25} orthogonal array is used (as depicted in Table 6.3) and S/N ratio is computed using MINITAB 16. The S/N ratio is computed for smaller-the-better value (SWR should be least) and found to be 91.49 dB (Figure 6.15). The order of significant effect on SWR such as normal load<sliding distance<environment temperature<sliding velocity<filler content as depicted form Figure 6.15. Thus, filler content is the major variable that governing the SWR of the investigated alloys composites. The Table 6.3, also states wear performance of the investigated alloy composites under different sets of controlling variables, for judging there suitability across numerous applications.

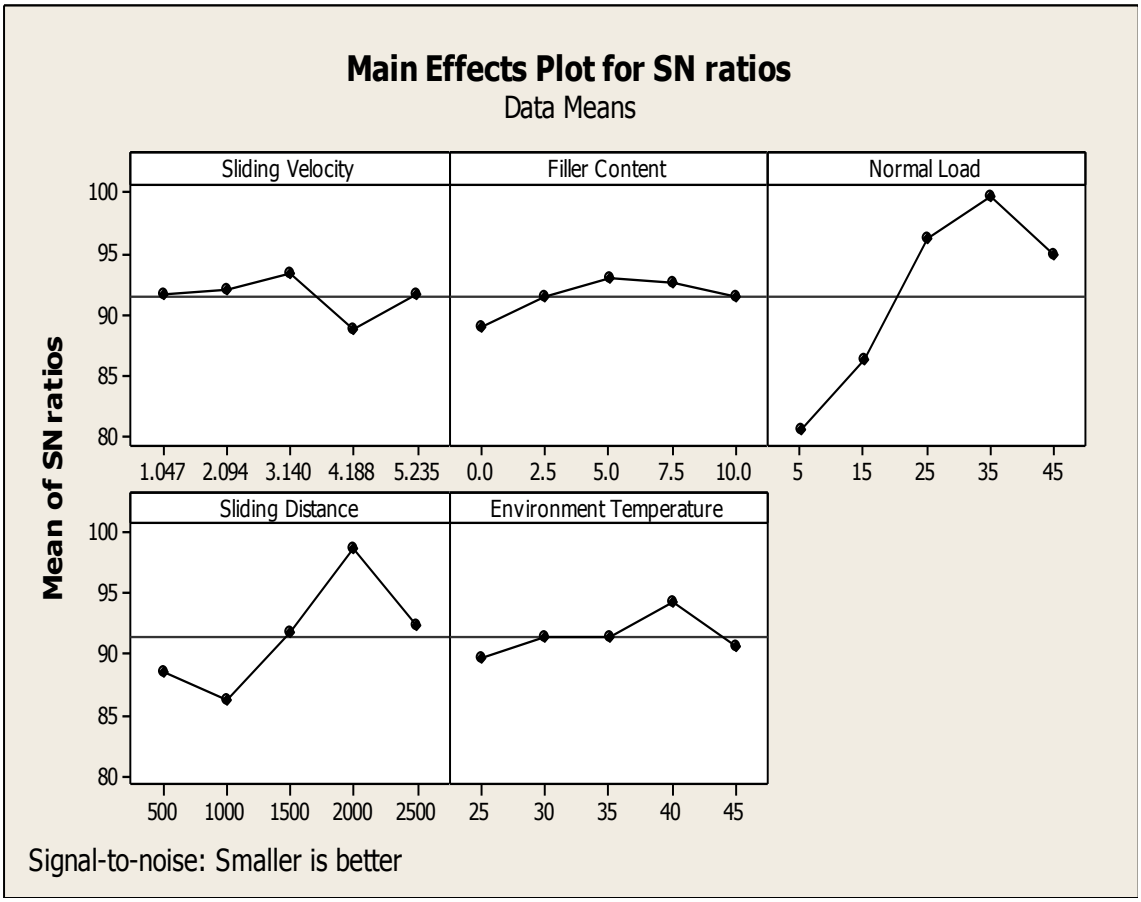

Figure 6.15 Effect of control factors on wear rate of CaO particulates filled ZA-27 alloy composites

6.2.6 ANOVA and the effect of factors for CaO particulates filled ZA-27 alloy composites

The SWR for the investigated alloy composites is analyse by ANOVA (analysis of variance) that presented in Table 6.4. The ANOVA analysis is performed with 5% level of significance and 95% level of confidence. The p-test column in Table 6.4 signifies percentage contribution of individual factor variables on the total variations

and the degree of influence on output results (i.e. SWR). It is observed that order of influence on SWR: Normal load (C) [p = 0.008 %] < Sliding distance (D) [p = 0.049 %] < Environment temperature (E) [p = 0.557 %] < Sliding velocity (A) [p = 0.559 %] < Filler content (B) [p = 0.635 %]. Thus, it concluded that filler content in the investigated alloy composites contributes majorly in controlling the SWR or have the greatest impact about other variables.

Table 6.4 ANOVA table for specific wear rate (CaO particulates filled ZA-27 alloy composite)

Source	DF	Seq SS	Adj SS	Adj MS	F	P
A	4	59.17	59.17	14.79	0.85	0.559
B	4	48.04	48.04	12.01	0.69	0.635
C	4	1231.50	1231.50	307.87	17.76	0.008
D	4	446.17	446.17	111.54	6.44	0.049
E	4	59.59	59.59	14.90	0.86	0.557
Error	4	69.33	69.33	17.33		
Total	24	1913.79				

DF - Degree of freedom, Seq SS - Sequential sum of square, Adj SS - Adjacent sum of square, Adj MS - Adjacent sum of mean square, F – Variance, P - Test (Percentage contribution of each factor in overall performance to find out optimum specific wear rate)

6.2.7 Surface morphology of unfilled and CaO particulates filled ZA-27 alloy composites

The surface morphology of worn surfaces studied via field emission scanning electron microscopic (FESEM), for steady state conditions were reported in Figure 6.16 and Figure 6.17, while Figure 6.18 presents worn surfaces from Taguchi DOE test runs. The micrograph of each investigated alloy composite enables us to understand wear phenomenon prevailed across the interface of the composite-counter surface of tribometer.

The Figure 6.16, shows micrograph of each investigated alloy composites having highest SWR under steady state condition with varying sliding velocity, keeping constant Normal load: 15 N, Sliding Distance: 1000 m and Environment temperature: 35°C respectively. From Figure 6.12, it is clear that higher SWR corresponds to highest sliding velocity i.e. 5.235 m/s, irrespective of filler content. The neat alloy composite micrograph Figure 6.16a depicts removal and fragmented matrix material over the rubbing surface with a lot of debris particles. The reason for

this could be the presence of highest void content ~ 0.018% and absence of any hardened filler content, that otherwise could lead to matrix strengthen and enhancement in its mechanical properties. With the addition of filler content, void content and cracking tendency of the composites are observed to decrease and could be validated by Figures 6.12-6.15. The higher wear rates are observed at higher sliding velocities but with diminished magnitudes in order of filler content. The interfacial bonding might go to be better with filler content in the neat alloy. The weak matrix-filler interfacial bonding may lead to bulk removal of material hence grooves formation as shown in Figure 6.16b for 2.5 wt.-% filler content. As the filler content increases in 5 wt.-% (Figure 6.16c) the material mechanical properties enhances, leading to diminishing wear rates. Also the back flow of debris over the sliding surface and their compactness over the rubbing surface, protect the base material and reduces effective wear rate. The subsurface crack propagation is there that accelerated wear rate. The ploughing action might lead to higher wear rates in composites having 7.5 wt.-% CaO filler (Figure 6.16d) and 10 wt.-% CaO filler (Figure 6.16e). It is found that the detached debris, creators or cavities may collapse [342; 344; 339] during the sliding wear process and then they form a ploughing strip, that also help to reduce the wear of contacted surfaces.

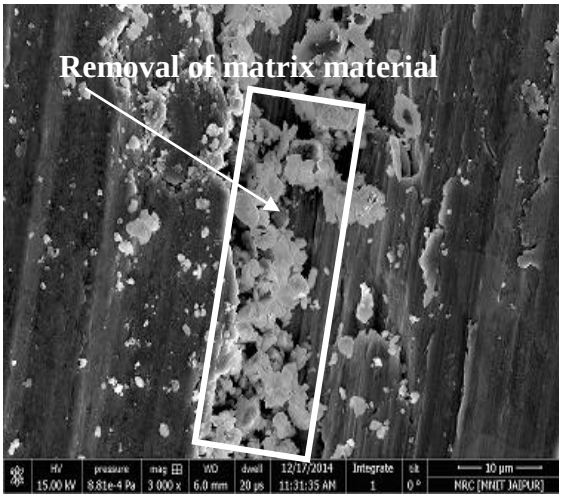

(a) 0 wt.-% CaO (worn)

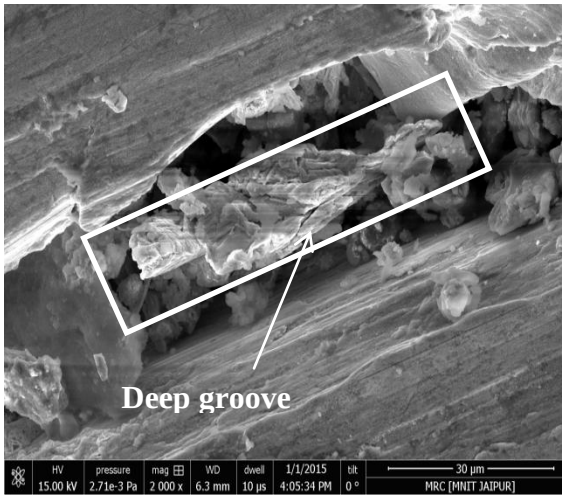

(b) 2.5 wt.-% CaO (worn)

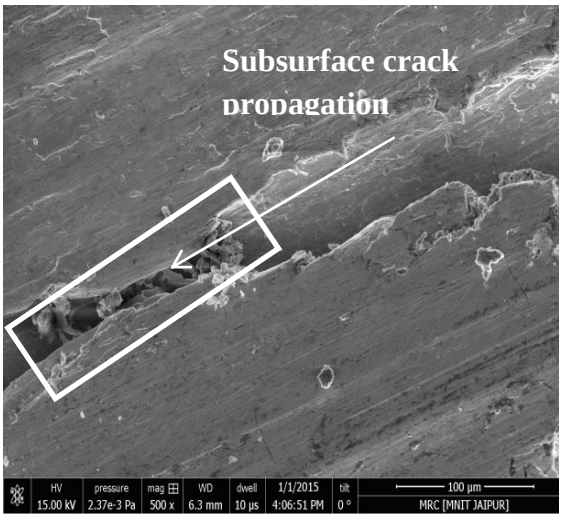

(c) 5 wt.-% CaO (worn)

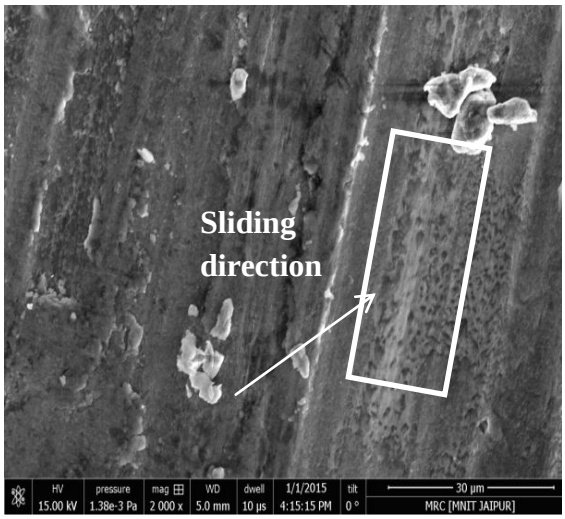

(d) 7.5 wt.-% CaO (worn)

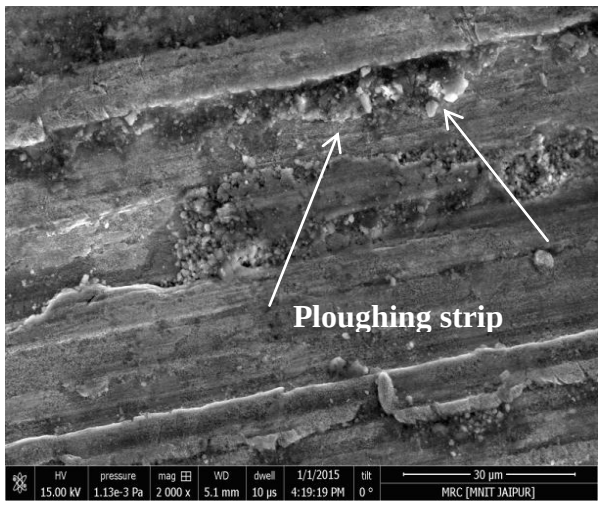

(e) 10 wt.-% CaO (worn)

Figure 6.16 Scanning electron micrograph of CaO particulates filled ZA-27 alloy composites under steady state condition with varying sliding velocity (Normal load: 15 N, Sliding Distance: 1000 m and Environment temperature: 35°C)

The Figure 6.17, shows micrograph of investigated alloy composites having highest SWR under steady state condition with varying normal load, keeping constant sliding velocity: 2.094 m/s, sliding distance: 1000 m and environment temperature: 35°C. From the Figure 6.14, the highest load i.e. 45 N leads to highest SWR, irrespective of filler content and the AFM micrographs are also presented in Figure 6.19. The micrograph of neat alloy composite at 5 N loading is shown in Figure 6.17a. It is observed that the lower normal load may also increase the delamination of the matrix. At rubbing interface due to relative motion between moving surfaces, shear stress are generated at meeting area of surfaces. This shear force produces frictional forces that in-turns generates frictional heat consequently, asperities are produced at

the contacting surfaces [342]. The AFM micrograph verifies the same as the surface undulations are very high and these leads to acceleration delaminating of the matrix by ploughing action leads to more wear (Figure 6.19a).

The micrograph of 2.5 wt.-% filler content alloy composites at 15 N loading is shown in Figure 9b. It is observed that the specimen surface exhibited different damages like surface crack and shallow craters [344]. Similar observations are found for the micrograph of 7.5 wt.-% filler content alloy composites at 25 N loading and shown in Figure 6.17d. The corresponding AFM micrographs shown in Figure 6.19b and Figure 6.19d shows the decrease in ploughing action, leads to relatively smoother surface hence decrease in wear rate.

The worn micrograph are shown in Figures 6.17c and 6.17e for 5 wt.-% and 10 wt.-% filler content alloy composites at higher loading i.e. 45 N respectively. The wear occurrence along sliding direction is clearly observed. The AFM micrograph shown in Figure 6.19c for 5 wt.-% filler content shows relatively lesser plateaus. However, AFM micrograph shown in Figure 6.19e for 10 wt.-% filler content shows least plateaus, responsible for lowest wear rate. One of the reasons for increasing wear rate is the higher value of COF at higher loading condition [339]. When the normal load get increases at the counter surfaces of pin sample and rotating disc than the expedition of cracks may convert into grooves or craters.

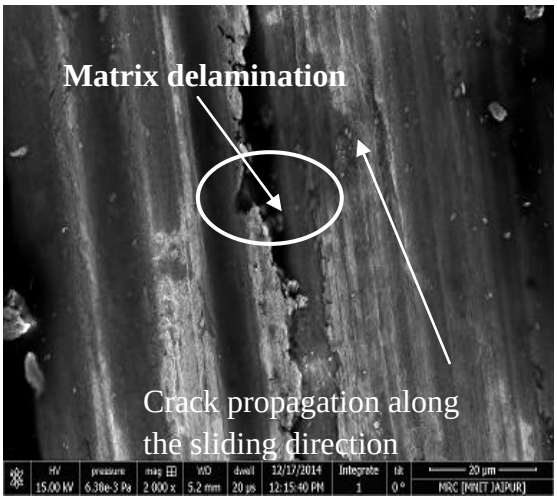

(a) 0 wt.-% CaO (worn)

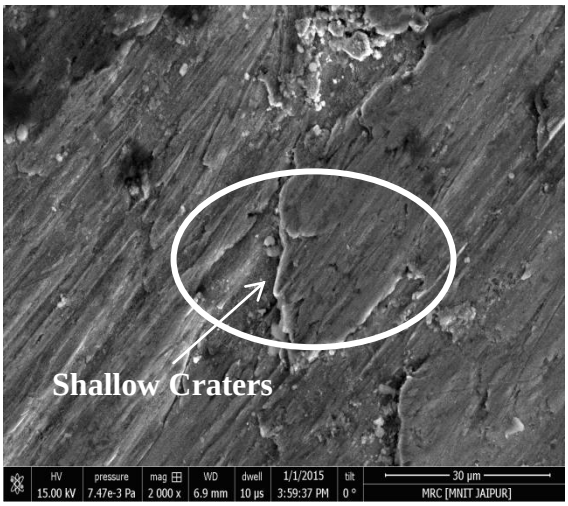

(b) 2.5 wt.-% CaO (worn)

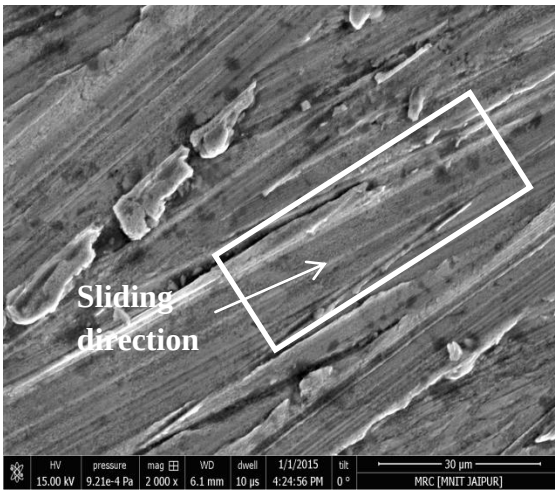

(c) 5 wt.-% CaO (worn)

(d) 7.5 wt.-% CaO (worn)

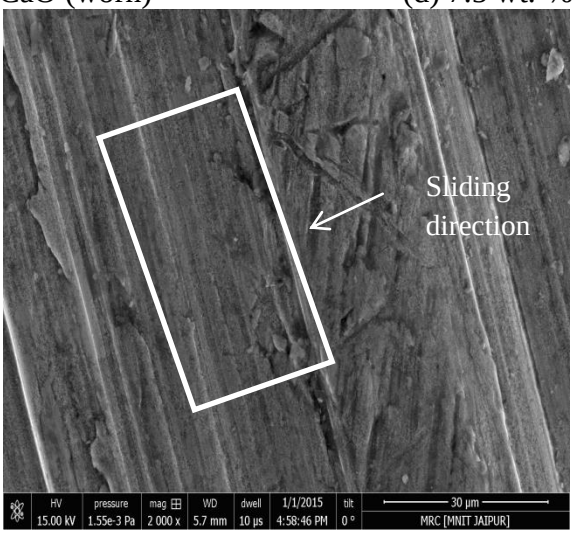

(e) 10 wt.-% CaO (worn)

Figure 6.17 Scanning electron micrograph of CaO filled ZA-27 alloy composites under steady state condition with varying normal load (Sliding velocity: 2.094 m/s, Sliding distance: 1000 m and Environment temperature: 35°C)

The micrographs shown in Figure 6.18, presents highest SWR of the investigated alloy composites under Taguchi designed experimental test runs (Table 6.3). During sliding wear of two surfaces the underlying wear mechanisms, debris particulates and surface roughness reported to affecting the wear performance. The micrograph (Figure 6.18a) of neat alloy composite shows shallow grooves, lesser ploughing surfaces with adhesive wear type. This may attribute to the low sliding velocity of 1.047 m/s, a lower load of 5 N over the smaller distance of 500 m at a mild temperature of 25°C (Exp. Run 1, Table 6.3). The lower mechanical properties of neat alloy might lead to maximum wear rate.

The micrograph (Figure 6.18b) of 2.5 wt.-% CaO particulate filled alloy composite shows highest wear rate (Exp. Run 22, Table 6.3) with sliding velocity

5.235 m/s, 5 N normal load over the distance of 2500 m, at a temperature of 40°C. It might be attributed to intense interfacial heat generated due to highest rubbing velocity together with higher environment temperature, might lead to softening of rubbing surface, that might cause dislodging of material form surface and formation of pits. The small wear particles could be observed and more ploughing action responsible for higher wear rates.

The micrograph as shown in Figure 6.18c, for 5 wt.-% CaO particulate filled alloy composite shows highest wear rate (Exp. Run 23, Table 6.3) with sliding velocity 5.235 m/s, 15 N normal load over the distance of 500 m, at a temperature of 45°C. The Figure shows debris particles, shallow grooves, micro cracks and ploughing action due to plastic deformation of the surface while rubbing.

(a) 0 wt.-% CaO (worn)

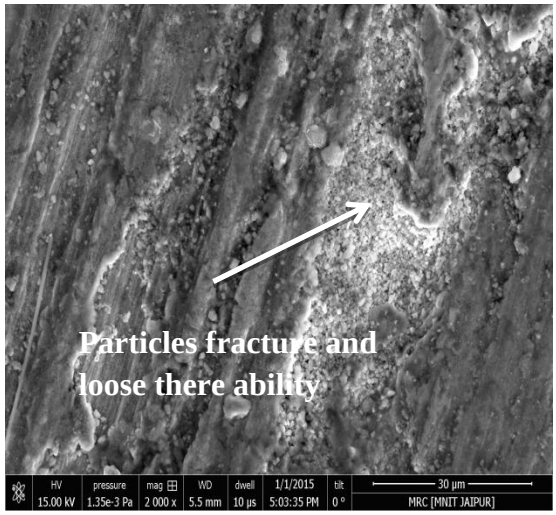

(b) 2.5 wt.-% CaO (worn)

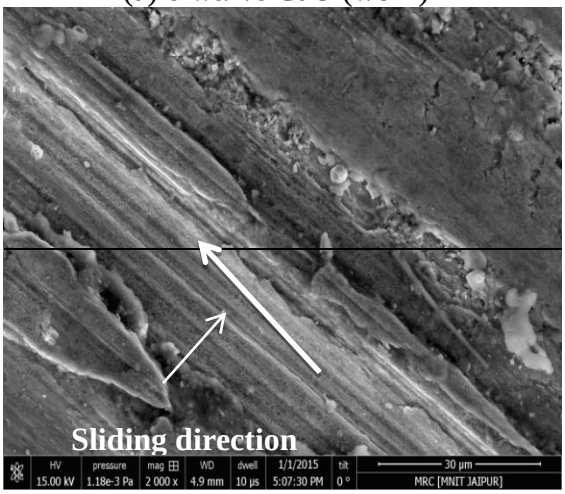

(c) 5 wt.-% CaO (worn)

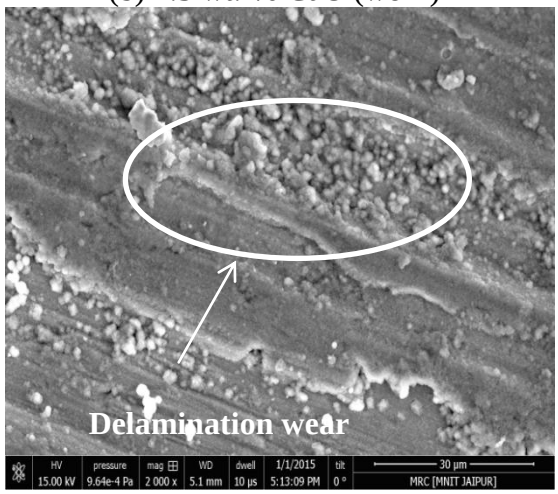

(d) 7.5 wt.-% CaO (worn)

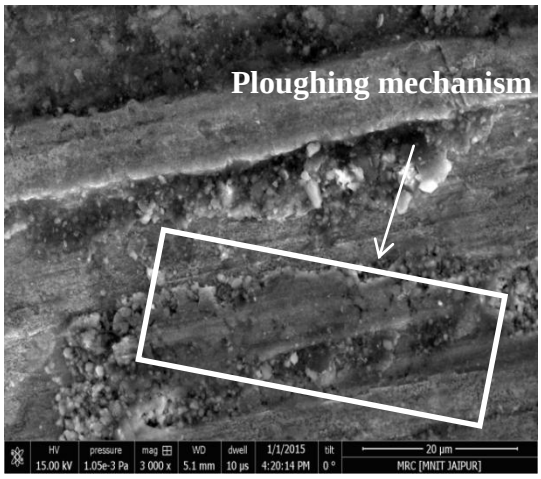

(e) 10 wt.-% CaO (worn)

Figure 6.18 Scanning electron micrographs of CaO particulates filled ZA-27 alloy composites (Taguchi Design of Experiment)

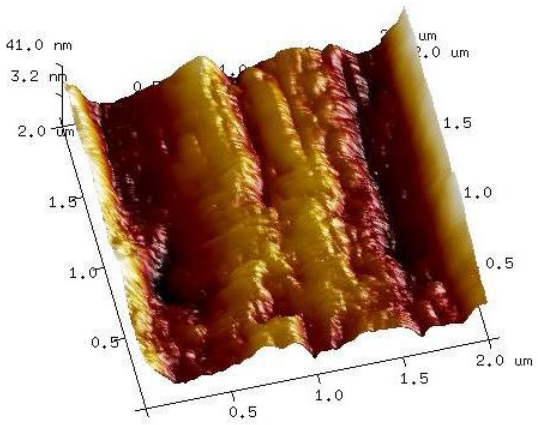

(a) 0 wt.-% CaO (worn)

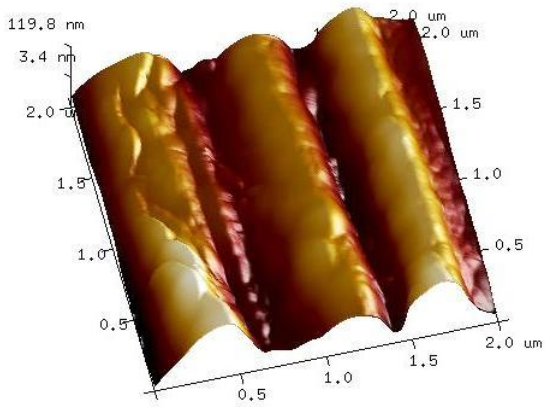

(b) 2.5 wt.-% CaO (worn)

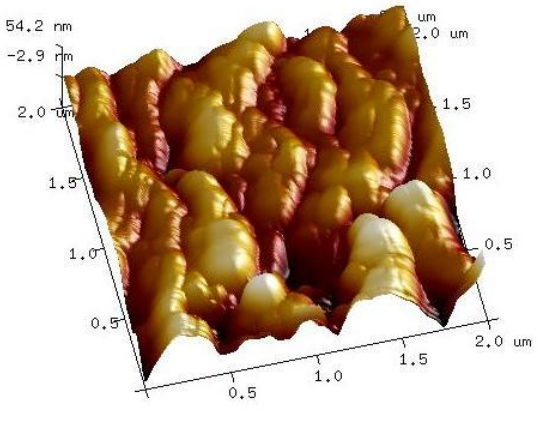

(c) 5 wt.-% CaO (worn)

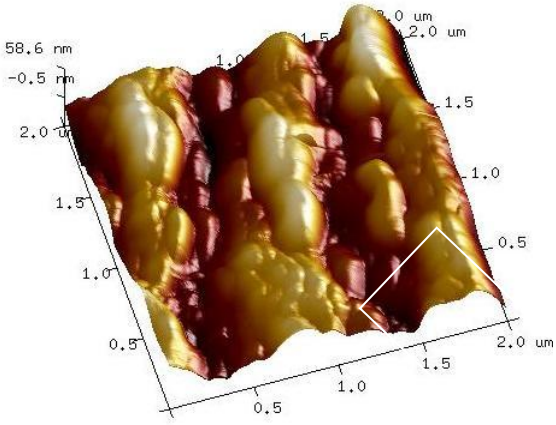

(d) 7.5 wt.-% CaO (worn)

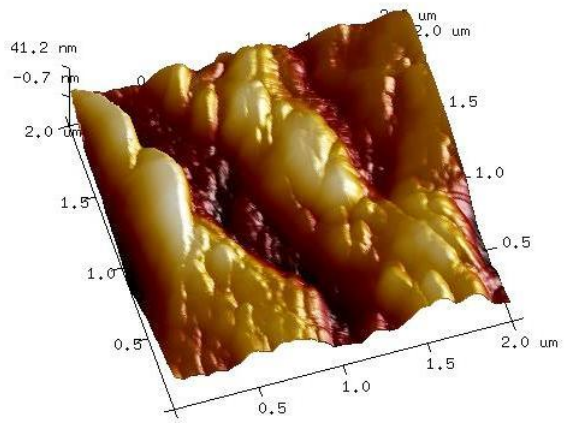

(e) 10 wt.-% CaO (worn)

Figure 6.19 AFM micrographs of CaO particulates filled ZA-27 alloy composite (a) 0 wt.-% CaO (b) 2.5 wt.-% CaO (c) 5 wt.-% CaO (d) 7.5 wt.-% CaO and (e) 10 wt.-% CaO

The high velocity rubbing generates high frictional heat aided by highest environment temperature together with high-stress magnitude, leads to higher shear forces, material softening and crack formation both in transverse and longitudinal directions. These factors might lead to higher wear rate.

The micrograph showing highest wear rate for 7.5 wt.-% CaO particulate filled alloy composite is shown in Figure 6.18d, (Exp. Run 19, Table 6.3) with sliding velocity 1.188 m/s, 15 N normal load over the distance of 2500 m, at a temperature of 35°C. It is observed that delimitation wear occurs at the interface under higher a applied load, that results in exposure of under laid material at most of the places and too many wear debris. Too many wear debris particles might lead to three-body abrasive type wear that accelerate wearing of rubbing surfaces, hence higher wear rates.

The micrograph as shown in Figure 6.18e for 10 wt.-% CaO particulate filled alloy composite against (Exp. Run 10, Table 6.3) sliding velocity 2.094 m/s, 5 N normal load over the distance of 1000 m, at a temperature of 35°C shows maximum wear rate. The presence of heavy filler content might lead to ploughing action over the surface resulting in the formation of series of small pits and too many wear debris particles that acts as abrasives which future accelerates wear rates. Similar, observations have been reported by Yu et al. [339] while studying SiC filler reinforcement in MMC's. Also, fabricating casting technique might influences wear and friction performance of the alloy composites.

6.2.8 Energy dispersive X-ray analysis (EDAX) of unfilled and CaO particulates filled ZA-27 alloy composites

EDAX spectrums of the investigated alloy composite material were shown in Figure 6.20.

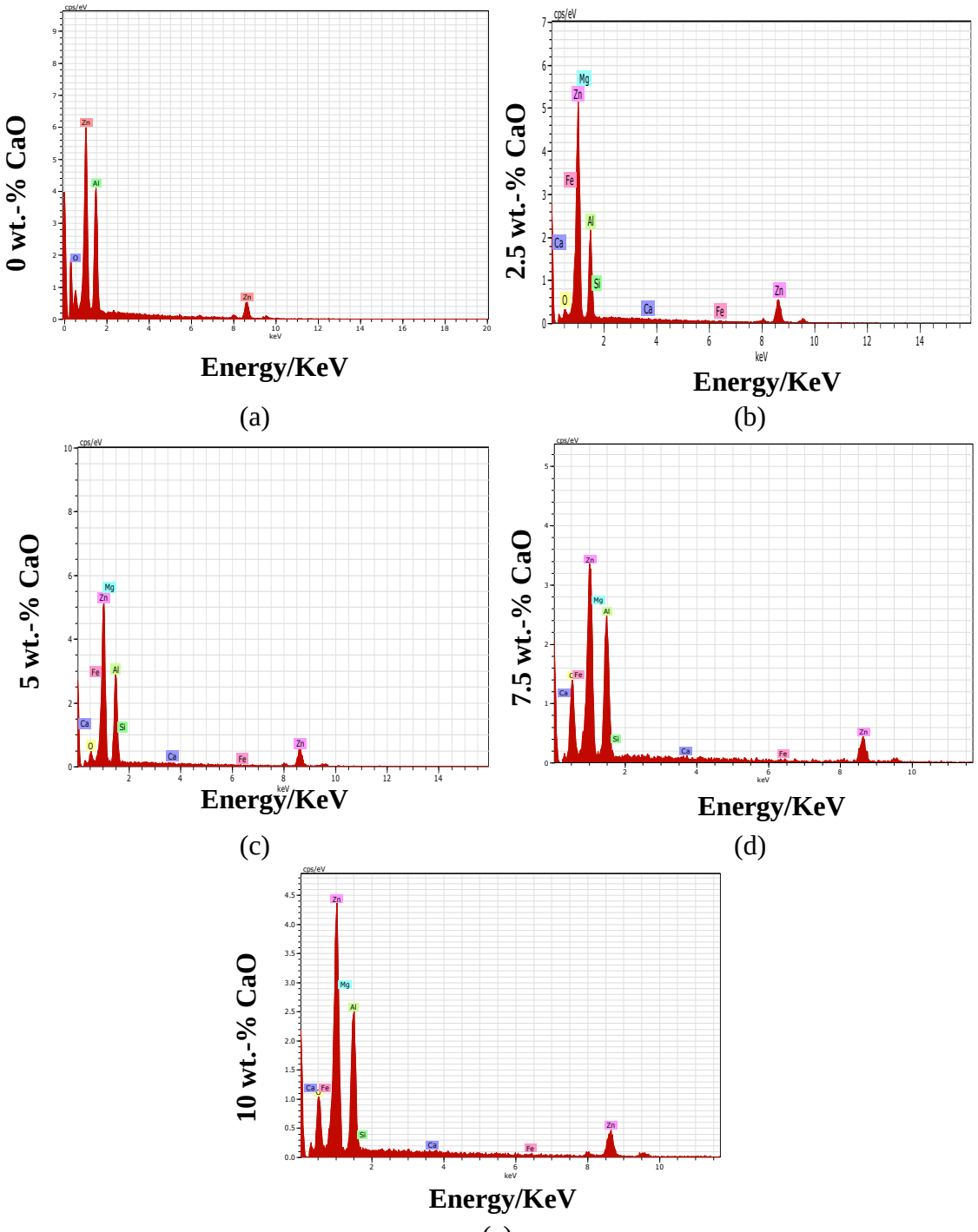

Figure 6.20 EDAX spectrum of CaO particulates filled ZA-27 alloy composite (a) 0 wt.-% CaO (b) 2.5 wt.-% CaO (c) 5 wt.-% CaO (d) 7.5 wt.-% CaO and (e) 10 wt.-% CaO

The plot clearly verifies the presence of different elements present in input material (i.e. composition of ZA-27 as shown in Table 3.1 and filler material i.e. CaO particulate) used for the preparation of various alloy composites.

Part III

6.3 Steady state specific wear behaviour of Marble Dust (MD) particulates filled Silicon Bronze (SiBr) alloy composites

6.3.1 Effect of sliding velocity on specific wear rate of MD particulates filled SiBr alloy composites

Figure 6.21 shown the effect of sliding velocity on the specific wear rate of MD filled SiBr alloy composites. The specific wear rate of the MD particulate filled SiBr alloy composites is shown decreasing in wear rate with the increased in sliding velocity with constant sliding distance (1000m), normal load (15N) and environment temperature (35ºC) respectively [345].

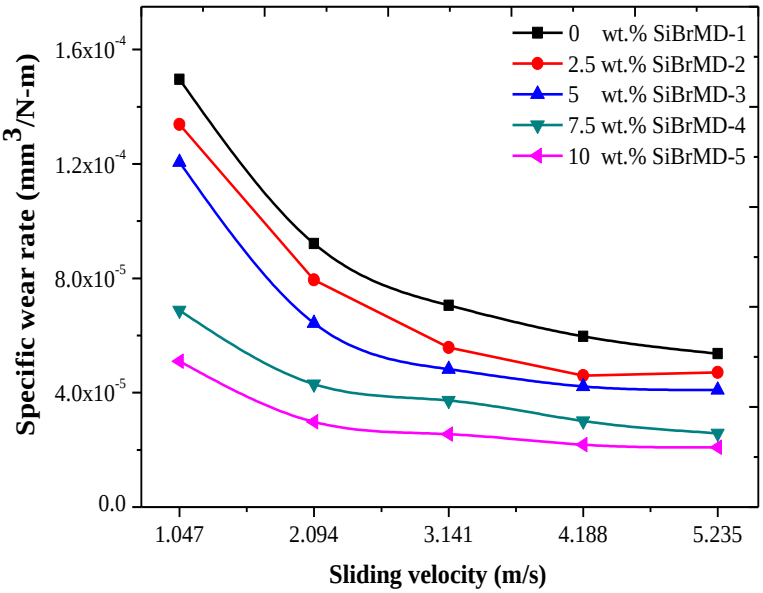

Figure 6.21 Variation of specific wear rate with sliding velocity for MD particulates filled SiBr alloy composites (Load: 15N, Sliding Distance: 1000m and Environment Temperature: 35°C)

However, the unfilled alloy composite is shown maximum wear rate as compared to other particulate filled alloy composites. The maximum value of SWR is found only for 1.047 m/s sliding velocity but beyond it the SWR decreases for all wt.% of MD particulates filled SiBr alloy composite materials up to 5.235m/s sliding velocity. The loading condition at the time of sliding wear process is exceptionally large which initiated wear at the beginning in Hertzian line contact condition. During the

continuous sliding process the counter face area of pin sample and disk surface, the interface temperature is slightly increased but the contact pressure decreases simultaneously which become the reason for decreasing wear intensity of composite materials by decreasing slope of steady state wear rate [346]. The increasing order of wear rate of the unfilled and particulate filled alloy composites is as 0wt.% MD>2.5wt.% MD>5wt.% MD>7.5wt.% MD>10wt.% MD respectively (Figure 6.21).

6.3.2 Effect of sliding velocity on coefficient of friction of MD particulates filled SiBr alloy composites

Figure 6.22 shows the resulting value of the coefficient of friction for MD particulates filled SiBr alloy composites by varying sliding velocity from 1.047m/s to 5.235 m/s whereas the remaining factors remaining constant (Normal Load: 15N, Sliding Distance: 1000m and Environment Temperature: 35°C) respectively.

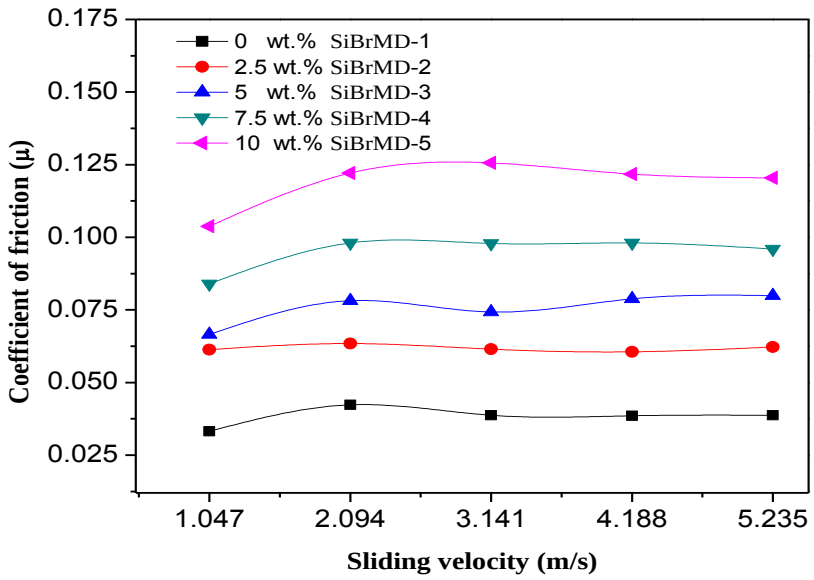

Figure 6.22 Variation of the coefficient of friction with sliding velocity for MD particulates filled SiBr alloy composites (Load: 15N, Sliding Distance: 1000m and Environment Temperature: 35°C)

From Figure 6.22 it is observed that the value of the coefficient of friction (COF) initially increases up to 2.094m/s sliding velocity but further increased in sliding velocity COF show almost homogenous in nature up to 5.23 m/s sliding velocity. The homogeneous nature of coefficient of friction for composite materials occurs due to the presence of asperities while sliding wear process got swing their positions with the

new positions got to convicted stick-slip oscillation condition for COF of fabricated composite materials [347].

The reason for initial maximization of COF from 1.047m/s to 2.094m/s can be the existence of hardened particulates MD filler in SiBr alloy composites. The maximum value of COF is found approximately 0.125 for 10wt.-% MD particulate filled SiBr alloy composite from 2.094m/s to 5.235 m/s sliding velocity (Figure 6.22). The minimum value of COF is found for monolithic alloy (unfilled), this may be due to the presence of different factors such as asperity, adhesion, debris plowing, etc. [249,348], and the large quantity of these factors reduces the COF for composite materials.

6.3.3 Effect of normal load on specific wear rate of MD particulates filled SiBr alloy composites

Figure 6.23 shows the outcome graph for specific wear rate (SWR) for both unfilled and MD particulates filled SiBr alloy composites with varying a normal load from 5N to 45N. It is observed that the resulting value of specific wear rate decreases with the increased in normal load.

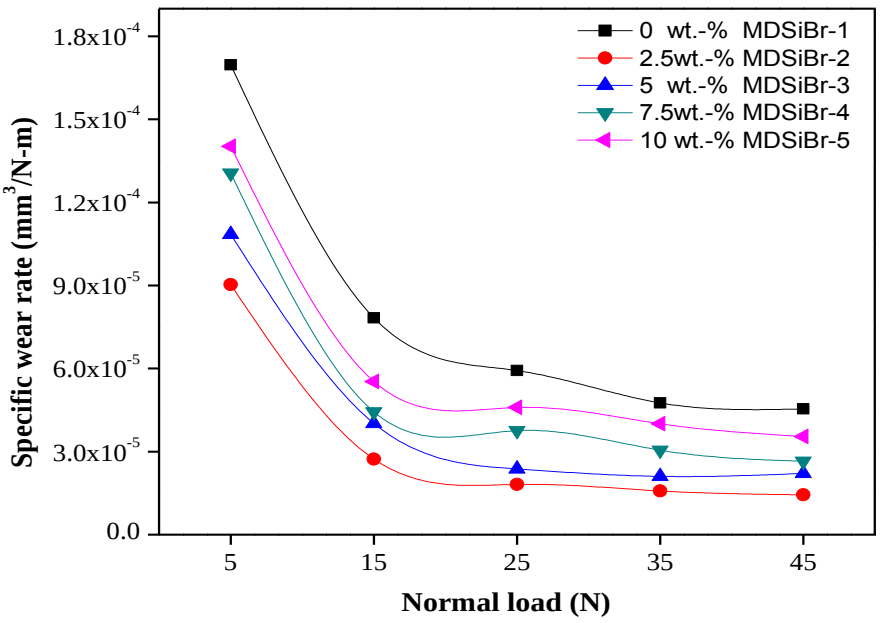

Figure 6.23 Variation of specific wear rate with normal load for MD particulates filled SiBr alloy composites (Sliding velocity: 2.094m/s, Sliding Distance: 1000m and Environment Temperature: 35°C)

From this analysis the unfilled alloy composite is shown maximum wear rate as compared with the particulate filled alloy composites (Figure 6.23). The MD filled alloy composites the hard MD particulates played major role to reduce the wear rate of the composites and simultaneously it is also clear that the particulate filled alloy composites were shown higher hardness (Figure 4.17) and minimum void content as compared with the unfilled alloy composites except in case of 10wt.% MD particulate filled SiBr alloy composites have higher void content (Table 4.11).

The lower value of SWR concluded the good agreement with wear resistance, and this occurs due to the size and thickness of reinforced particles or tribo film thickness of particulates, that rescue the materials surface by having rarely pull out of reinforced particulates from the counter surface of fabricated composite materials [349].

When the sliding wear occurs in between a counter face surfaces of pin sample and disk, plough and grooves become generated and these leads toward acute plastic deformation at higher loading condition, which form the oxide surface known as a mechanically mixed layer (MML). This MML allow the surfaces for smooth sliding and by which reducing specific wear rate as observed by Zhang and Wang [349].

6.3.4 Effect of normal load on the coefficient of friction of MD particulates filled SiBr alloy composites

Figure 6.24 shows the trend of the coefficient of friction with respect to varying normal load for five different weight percentages of MD particulates filled SiBr alloy composites.

The coefficient of friction of particulate filled alloy composites is higher than the unfilled alloy composites except in case of 10wt.% MD filled composite.

The higher coefficients of friction of the particulate filled alloy composites were due to the presence of hard marble dust particles at the interface between the two contacting surfaces i.e. disc as well as the sample.

The counter surface of pin sample and the disk has contact usually in elasto-plastic state and this increase while applied load also increases during sliding. Therefore, the increased value of surface roughness by increasing normal load during sliding wear process also lead the amount of coefficient of friction [350, 351].

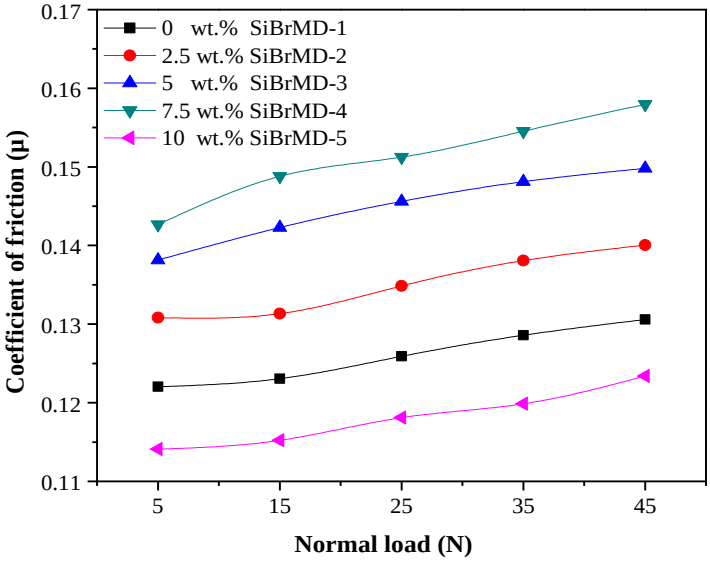

Figure 6.24 Variation of the coefficient of friction with normal load for MD particulates filled SiBr alloy composites (Sliding velocity: 2.094m/s, Sliding Distance: 1000m and Environment Temperature: 35°C)

6.3.5 Taguchi design experimental analysis for MD particulates filled SiBr alloy composites

The results for various combinations of factor settings were obtained by conducting the dry sliding wear experimental analysis as per orthogonal array design. The experimental results were analyzed by the commercially available software MINITAB 16 used for the design of experimental techniques. Table 6.5 indicated the experimental results an average of two replicas each experimental run for specific wear rate of the alloy composites and then the output results were transferred into signal-to-noise rate (S/N ratio). The overall S/N ratio for unfiled and MD particulates filled SiBr alloy composites is found to be 101.70 dB as shown in Table 6.5.

The corresponding main effect between the input factors i.e. sliding velocity, filler content, normal load, sliding distance and environment temperature on the performance output i.e. specific wear rate of the alloy composites were reported in Figure 6.25. From this graph it is observed that normal load seems to be more significant as compared with other factors. The significance of each factor is determined from the inclination on the main effect plot i.e. a factor which is more inclined about the mean line will have the most significant effect.

Table 6.5 Experimental layout of L_{25} orthogonal array

Expt. No.	Sliding Velocity (m/sec)	Filler Content (wt. -%)	Normal Load (N)	Sliding Distance (m)	Environment Temperature (°C)	Spe. Wear Rate $\frac{mm3}{N-m}$	S/N Ratio (db)
1	1.047	0	5	500	25	2.836E-04	70.946
2	1.047	2.5	15	1000	30	1.206E-04	78.373
3	1.047	5	25	1500	35	1.338E-05	97.469
4	1.047	7.5	35	2000	40	9.111E-06	100.80
5	1.047	10	45	2500	45	1.606E-05	95.886
6	2.094	0	15	1500	40	2.101E-05	93.553
7	2.094	2.5	25	2000	45	7.236E-05	82.810
8	2.094	5	35	2500	25	2.724E-05	91.295
9	2.094	7.5	45	500	30	2.268E-05	92.889
10	2.094	10	5	1000	35	1.807E-04	74.863
11	3.14	0	25	2500	30	7.385E-05	82.634
12	3.14	2.5	35	500	35	3.309E-04	69.607
13	3.14	5	45	1000	40	2.975E-05	90.531
14	3.14	7.5	5	1500	45	2.382E-04	72.462
15	3.14	10	15	2000	25	5.424E-05	85.314
16	4.188	0	35	1000	45	6.414E-05	83.857
17	4.188	2.5	45	1500	25	3.037E-05	90.351
18	4.188	5	5	2000	30	2.635E-04	71.585
19	4.188	7.5	15	2500	35	4.762E-05	86.444
20	4.188	10	25	500	40	4.129E-05	87.682
21	5.235	0	45	2000	35	8.222E-06	101.70
22	5.235	2.5	5	2500	40	6.608E-05	83.598
23	5.235	5	15	500	45	1.833E-04	74.735
24	5.235	7.5	25	1000	25	5.991E-05	84.450
25	5.235	10	35	1500	30	1.616E-05	95.830

Figure 6.25 also concluded the significance of individual factor on output performance of the unfilled and particulate filled alloy composites i.e. sliding velocity at level one, filler content at level five, normal load at level five, sliding distance at

level three and environment temperature at level four were shown significant level on output of the composites.

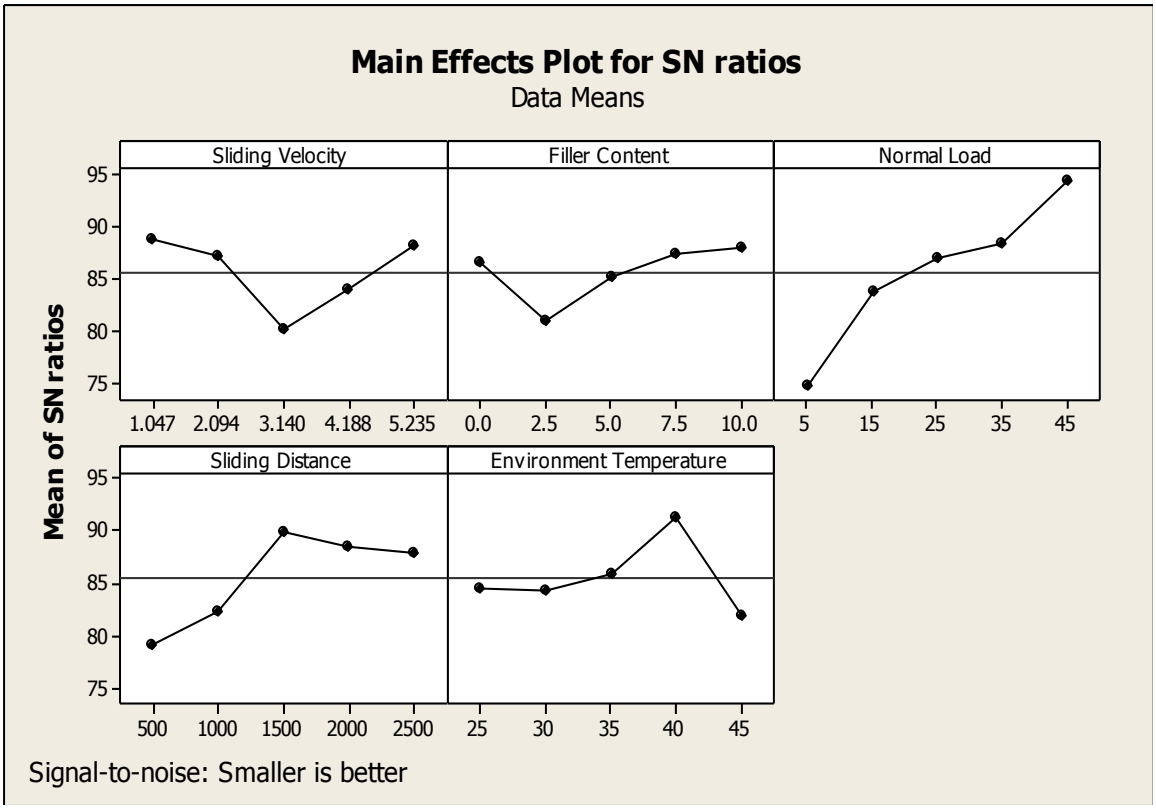

Figure 6.25 Effect of control factors on wear rate for MD particulates filled SiBr alloy composites

6.3.6 ANOVA and the effect of factors for MD particulates filled SiBr alloy composites

Analysis of variance (ANOVA) is performed to determine the most significant factor that affects the performance characteristic of the unfilled and particulate filled alloy composites, and it also determined the percentage contribution of each factor on output.

It is observed from Table 6.6 that normal load [p=0.017%], sliding velocity [p=0.161%] and sliding distance [p=0.077%] respectively to ascertain the specific wear rate of unfilled and MD particulates filled SiBr alloy composite have significant effect, but the remaining factors such as filler content [p=0.288%] and environment temperature [p=0.171%] show the least significant effect on specific wear rate of fabricated composite materials.

Table 6.6 ANOVA table for specific wear rate (MD particulates filled SiBr alloy composite)

Source	DF	Seq SS	Adj SS	Adj MS	F	P
A	4	253.05	253.05	63.26	2.93	0.161
B	4	156.93	156.93	39.23	1.82	0.288
C	4	1035.16	1035.16	258.79	12.00	0.017
D	4	419.75	419.75	104.94	4.87	0.077
E	4	241.54	241.54	60.38	2.80	0.171
Error	4	86.27	86.27	21.57		
Total	24	2192.71				

DF - Degree of freedom, Seq SS - Sequential sum of square, Adj SS - Adjacent sum of square, Adj MS - Adjacent sum of mean square, F – Variance, P - Test (Percentage contribution of each factor in overall performance to find out optimum specific wear rate)

6.3.7 Surface morphology of unfilled and MD particulates filled SiBr alloy composites

The microstructural analysis of worn surfaces has been examined by the Scanning electron microscopy (SEM) that used to scrutinize the geometric features of worn surfaces of samples on same magnification level for the contrast purpose. Figure 6.27 shows the micro-graph of unfilled and MD particulate filled SiBr alloy composites under steady state condition by varying at constant normal Load: 15N, Sliding Distance: 1000m and Environment Temperature: 35°C respectively. Figure 6.27a shows 0wt.% of MD particulate filled SiBr alloy composite at lower sliding velocity 2.904m/s, normal load 15N, sliding distance 1000m and environment temperature 25^0C respectively. From micro-graph at lower sliding velocity an array of shallow grooves is observed on the composite surface along the sliding direction. Similar observation is found in Prasad [352] study, he studied about the microstructural behavior for zinc based alloy matrix reinforced with SiC particulates. In his study he found with the increasing value of sliding velocity the presence of groove in counter surfaces also increases. With the increasing sliding velocity, the limit and extremity of composite materials deformation increased. However, with the increased in sliding velocity to 3.141m/s for 2.5wt.% MD (Figure 6.27b) particulate filled alloy composite the worn surface is completely deteriorated, and the protective layer is broken up while sliding with the formation of enormous wear strips along the sliding direction.

Similarly, in case of 5wt.% MD particulate filled alloy composite with further increased in sliding velocity i.e. 4.188m/s the worn surface losses the hard marble dust particles from the surface due to high shear strain is produced between the disc surface and the composite alloy surface along with interface temperature is increased during sliding that therefore delaminated the surface due to removal of hard particles from the alloy composite (Figure 6.27c) [198]. Again with further increased in sliding velocity to 5.235m/s for 7.5wt.% MD particulate filled alloy composite, at higher sliding speed the reinforced particulates can be played as a third body once removed from the composite surface [30]. Therefore, the composite surface shows cavities and large grooved on the worn surface and reinforced particles automatically pulled out from the surface (Figure 6.27d). The grooves is formed parallel to the sliding directions [353], it's a continuous process which get produced different deformation such as grooves, cracks, ploughing etc. while the sliding wear formed for some period of time, during the process both the counter body rubbed to each other which produces heating zone and get removed or pulled out contacted materials. Similarly, the microstructure of 10wt.-% MD particulates filled SiBr alloy composite materials (Figure 6.27e) did not assemble any large grooves or wear formation because the density of reinforced particulates on microstructure shows higher value with the increasing volume fraction and by that did not produces acute adhesion [354, 182]. The MD particulates filled SiBr alloy composite shows minimum wear rate as compared to monolithic alloy, which could be possible by the prevention of plastic deformation at the counter face of sample and disk [198].

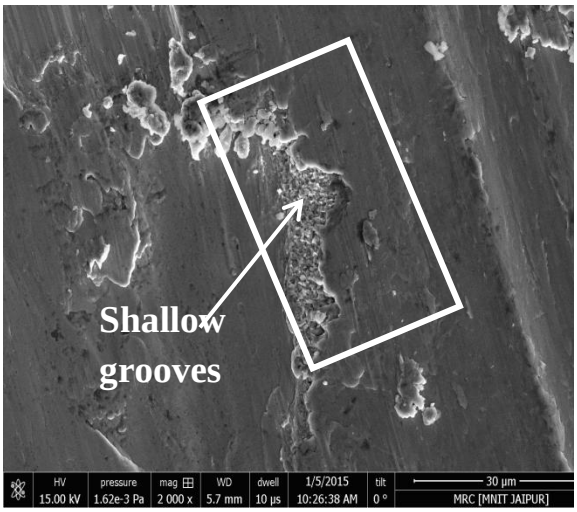

(a) 0wt.-% MD (worn)

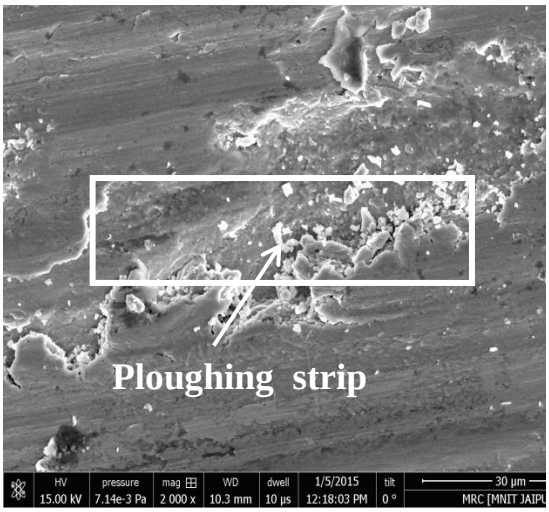

(b) 2.5wt.-% MD (worn)

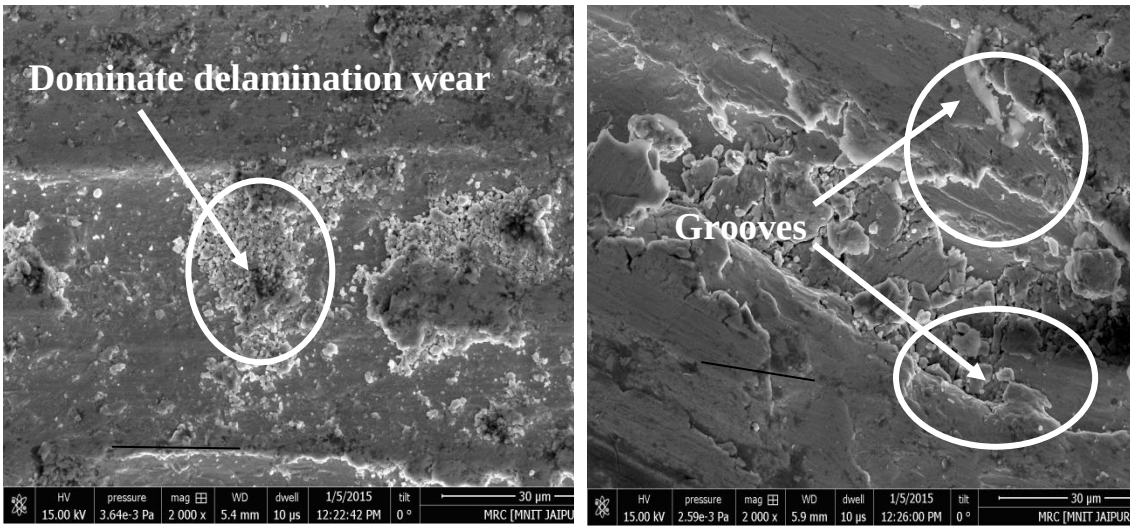

(c) 5wt.-% MD (worn) (d) 7.5wt.-% MD (worn)

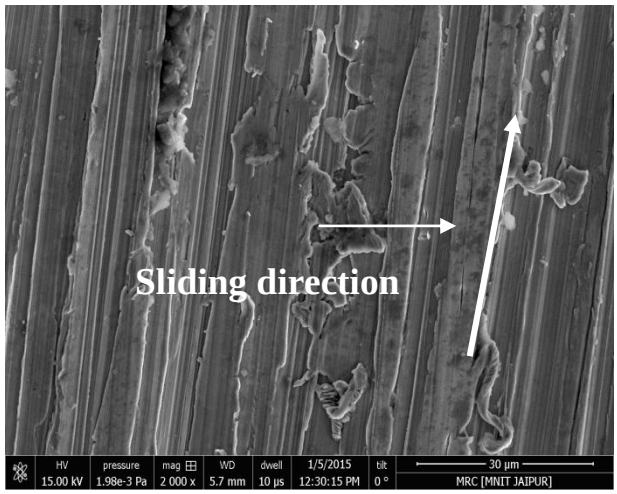

(e)10 wt.-% MD (worn)

Figure 6.26 Scanning electron micrograph of particulates filled SiBr alloy composites under steady state condition with varying sliding velocity (At constant: Normal load: 15N, Sliding Distance: 1000m and Environment Temperature: 35°C)

Figure 6.27(a-e) shows the result of specific wear rate of MD particulates filled SiBr alloy composite materials with varying normal load from 5N to 45N while other parameters remain constant such as sliding velocity: 2.094m/s, sliding distance: 1000m and environment temperature: 35ºC respectively. Figure 6.27a studied the worn surface micrographs for unfilled alloy composite at low load condition i.e. 5N which shows the presence of crack on the surface**.** The presence of cracks on the surface after sliding wear process commences the fracture phenomenon, and this paramount the delamination wear [355]. However, as compared with AFM micrographs which used to check the profile of worn surfaces of composite materials after sliding wear at different varying parameters to check the perimeter width and

depth of the wear [356]. For 0wt.-% MD particulate filled alloy composite the exact surface resolution after wear process is performed which shows homogeneous tips around the contacted surface area due to which higher amount of SWR get noticed for composite materials (Figure 6.29a).

When the load of wear process become increases from 5N to 45 N remaining parameters constants such as sliding velocity: 2.094m/s, sliding distance: 1000m and environment temperature: 35ºC the specific wear rate is decreased for MD particulates filled SiBr alloy composite materials (compared with Figure 6.23). Therefore, the microstructure image of 2.5 wt.-%MD particulates filled alloy composite worn surfaces (Figure 6.27b) did not shows the large grooves or ploughs which work as wear initiators, so the absence of these groves and ploughs leads towards the better wear resistance for composite materials. The ploughing mechanism is shown in Figure 6.27c for 5wt.-% MD particulates filled metal alloy composites. The MD particulates filled composite materials show least amount of SWR for the addition of MD particulates in alloy composites as compared to monolithic alloys. Similarly, the relative AFM micrographs for 2.5wt.-% and 10wt.-% (Figure 6.29b and Figure 6.29e) have the least value of SWR as compared to other filled alloy composites that may be due to the presence of reduced ploughing action or decreed grooves. However, with the increased in volume fraction of filler particulates the composite materials have also enhanced the wear resistance because the matrix alloy furthermore got strengthen and the inclusion of filler particles resist or reduced the penetration, cutting formation of debris and plastic deformation [357].

Similarly, the AFM micrographs for 5 wt.-% and 7.5wt.-% MD particulates filled alloys were shown (Figure 6.29c and Figure 6.29d) that is correlated with the SWR of 5 wt.-% and 7.5wt.-% MD particulates filled metal alloy composites shows the serrated and worn tips for AFM micrographs for the worn surface profile that shows the height of tip, which means the wear of surface towards the vacillation of materials properties leads [358]. The parallel and continuous grooves were shown in Figure 6.27d for 7.5 wt.% MD filled SiBr alloy composite. The groves have been seen by the abrasion wear mechanism at lower applied normal loads [180], while the deep grooves on the composite surfaces were found by an obvious reason of adhesion (Figure 6.27e).

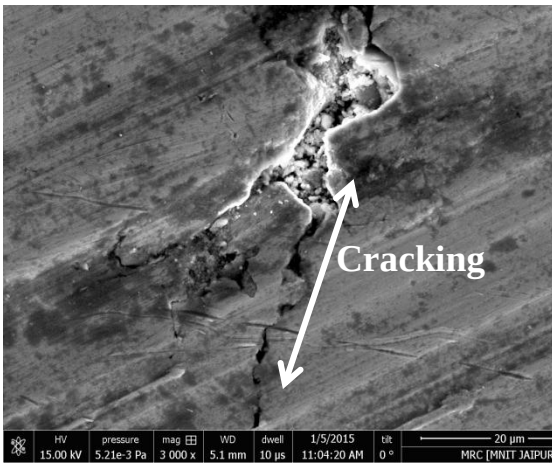

(a) 0wt.-% MD (worn)

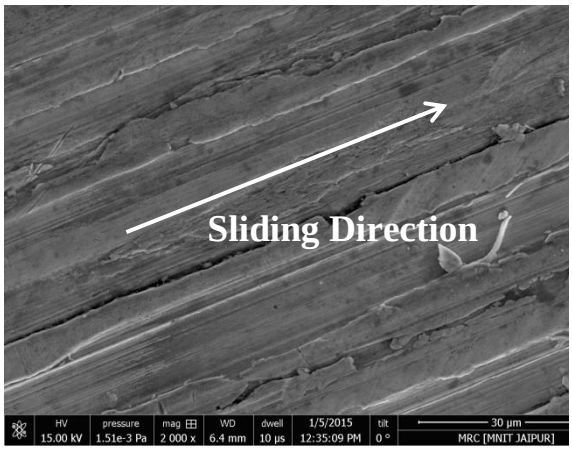

(b) 2.5wt.-% MD (worn)

(c) 5wt.-%MD (worn)

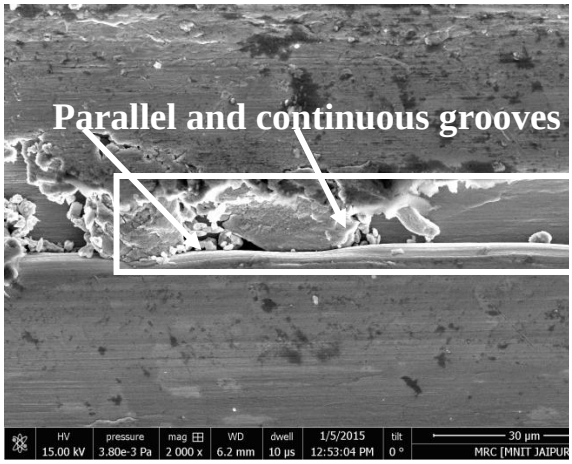

(d) 7.5wt.-%MD (worn)

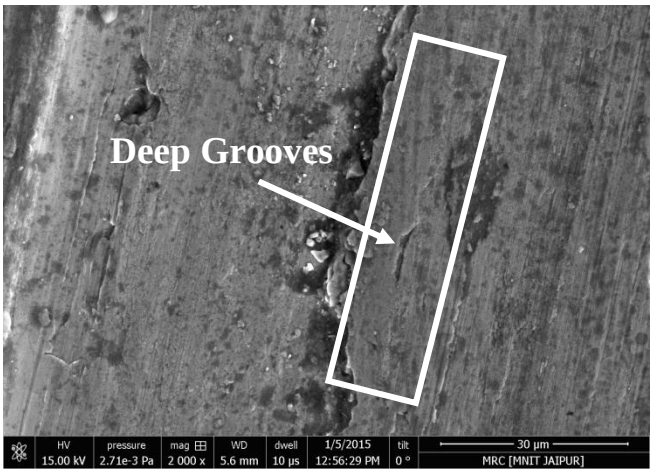

(e)10wt.-% MD (worn)

Figure 6.27 Scanning electron micrograph of particulates filled SiBr alloy composites under steady state condition with varying normal load (At constant: Sliding velocity: 2.094m/s, Sliding Distance: 1000m and Environment Temperature: 35°C)

The microstructure studies of L_{25} Taguchi design experimental test runs for MD particulates filled SiBr alloy composite materials were shown in Figure 6.28. The

micrographs were shown in Figure 6.28 has highest SWR for fabricated composite materials under L_{25} Taguchi design of experimental test run (Table 6.5). Figure 6.28a shows the micrographs for test run 6 which shows the lowest value of SWR i.e. 2.101E-05 $\frac{mm3}{Nm}$ for 0wt.-% of MD particulates filled alloy composites. From Figure 6.28a it shows the composite materials has a lower value of SWR at 15N loading condition and 2.094m/s sliding velocity as compared to other test run process so at lower SWR the probability of groove and debris presence become less which also shown in Figure 6.28a.

The micrographs (Figure 6.28b and 6.28c) for 2.5wt.-% and 5wt.-% of MD particulates filled SiBr alloy composites lowest SWR (Exp. Run 2, and Exp. Run 3, Table 6.5) at 1.047m/s sliding velocity and 15N, 25N loading conditions over the sliding distance of 1000m and 1500m at a temperature of 30-35°C respectively. Figure 6.28b and 6.28c reported both the ploughing and delamination wear mechanism respectively during sliding wear process under controlled operating condition. Similarly, Figure 6.28d and 6.28e show the micrographs of 7.5 wt.-% and 10wt.-% MD particulate filled SiBr alloy composites (Exp. Run 9, and Exp. Run 5 Table 6.5) show the grooves and materials removal phenomenon [359]. The material removal phenomenon takes place at composite counter face surface due to the delamination of sub surface layers. At the time of wear the thick oxide layer that spread over the materials surface brakes while applying a large amount of load and this leads toward materials removal from the surfaces in the form of debris particles or delamination wear [360].

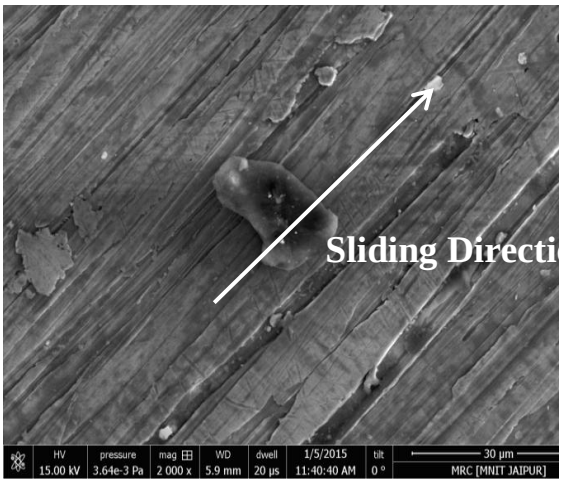

(a) 0wt.-% MD (worn)

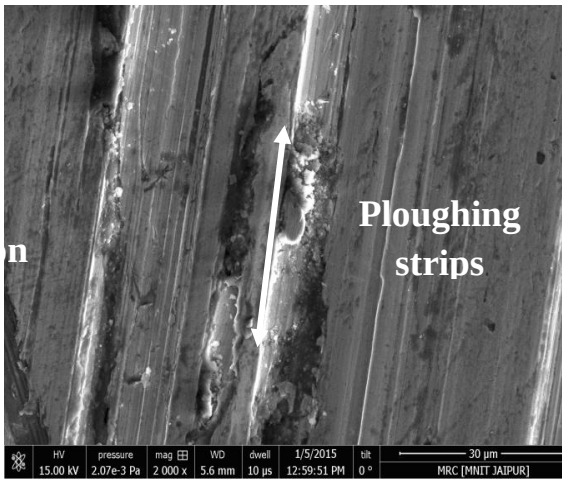

(b) 2.5wt.-% MD (worn)

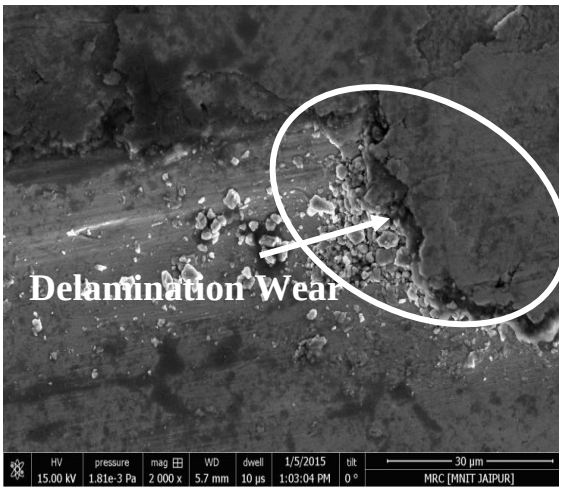

(c) 5wt.-% MD (worn)

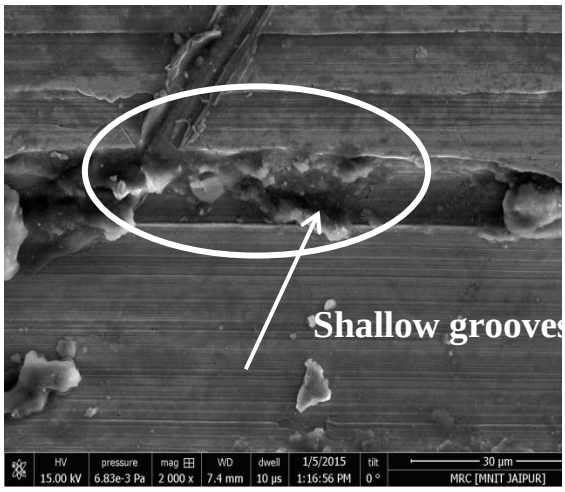

(d) 7.5wt.-% MD (worn)

(e)10wt.-% MD (worn)

Figure 6.28 Scanning electron micrograph of MD particulate filled SiBr alloy composites (Taguchi Design of Experiment)

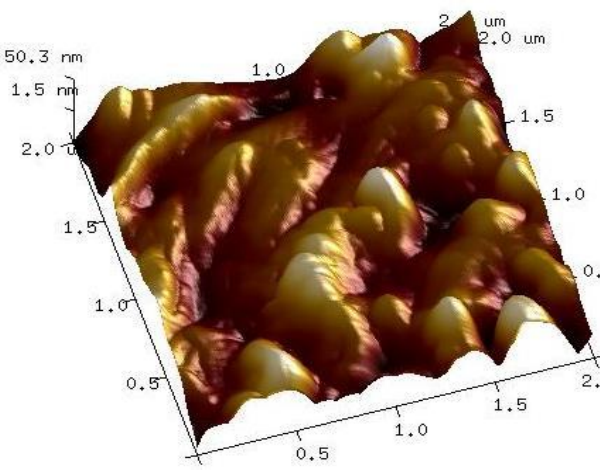

(a) 0 wt.-% MD (worn)

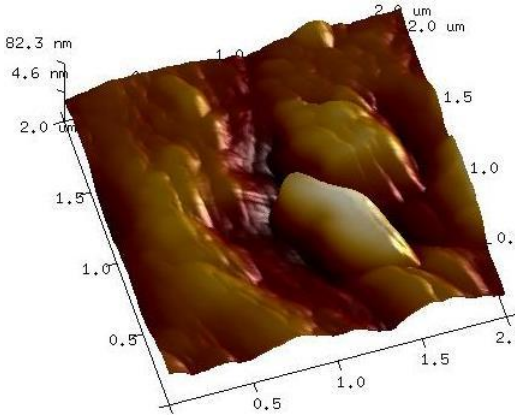

(b) 2.5 wt.-% MD (worn)

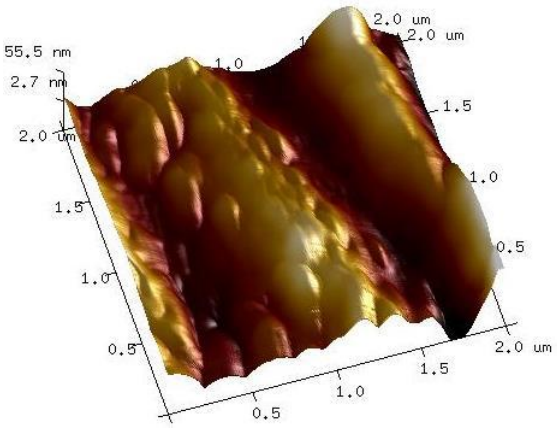

(c) 5 wt.-% MD (worn)

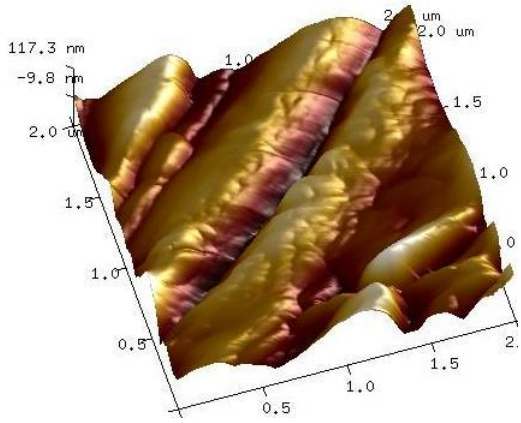

(d) 7.5 wt.-% MD (worn)

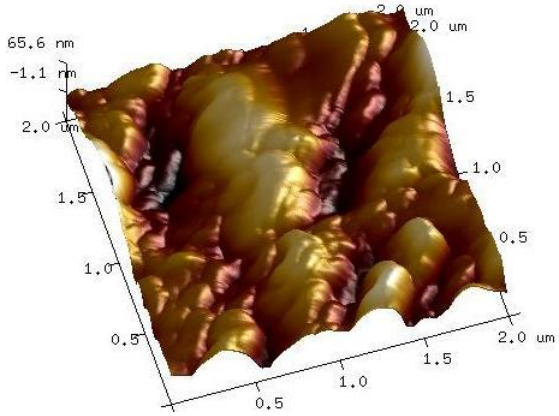

(e) 10 wt.-% MD (worn)

Figure 6.29 AFM micrographs of MD particulates filled SiBr alloy composite (a) 0 wt.-% MD, (b) 2.5 wt.-% MD (c) 5 wt.-% MD (d) 7.5 wt.-% MD and (e) 10 wt.-% MD

6.3.8 Energy dispersive X-ray analysis (EDAX) of unfilled and MD particulates filled SiBr alloy composites

The EDAX spectrum to scrutinize the presence of different materials compositions of MD filled SiBr alloy composite materials were shown in Figure 6.30. From the Figure, it's clearly seen the presence of different input materials such as matrix and reinforced materials (For SiBr alloy material composition as shown in Table 3.3 and reinforced particulates of MD particle) for the fabrication of composite materials were shown by different peaks.

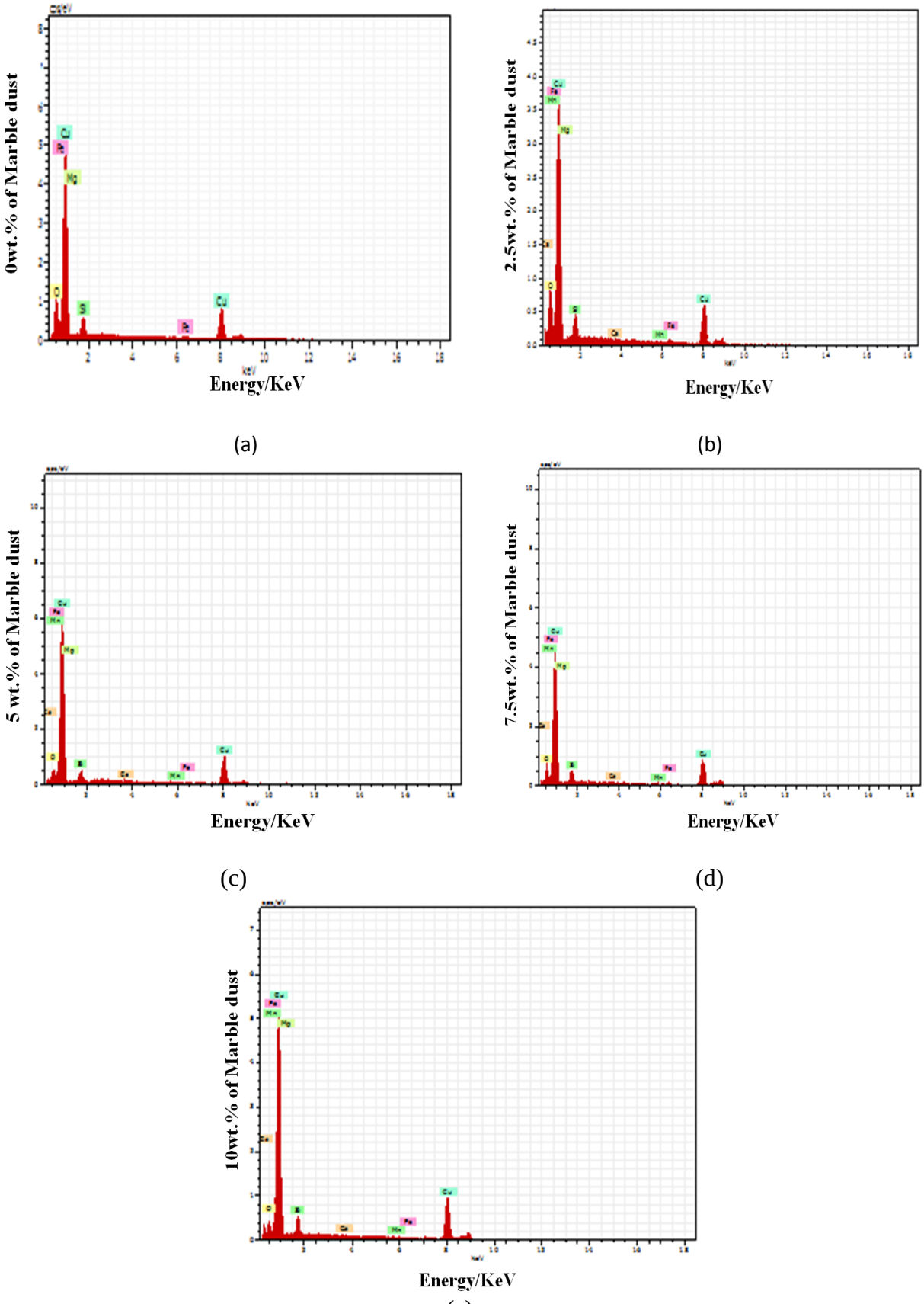

Figure 6.30 EDAX spectrum of MD particulates filled SiBr metal alloy composite. (a) 0wt.-% MD (b) 2.5wt.-% MD (c) 5wt.-% MD (d) 7.5wt.-% MD and (e) 10wt.-% MD.

Part IV

6.4 Steady state specific wear behaviour of Quicklime (CaO) particulates filled SiBr alloy composites

6.4.1 Effect of sliding velocity on specific wear rate of CaO particulates filled SiBr alloy composites

The specific wear rate results were plotted against sliding velocity as observed in Figure 6.31 for unfilled and particulate filled metal alloy composites. For which different wt.-% (0, 2.5, 5, 7.5 and 10wt.%) Of CaO filled SiBr alloy composites were tested on pin-on-disc tribometer at varying sliding velocity (1.074, 2.094, 3.140, 4.188 and 5.235 m/s) while the other operating parameters remain constant such as: sliding distance (1000m), normal load(15N) and environment temperature (35ºC). Figure 6.31 shows a maximum value of specific wear rate for unfilled alloy as compared to CaO filled SiBr alloy composites.

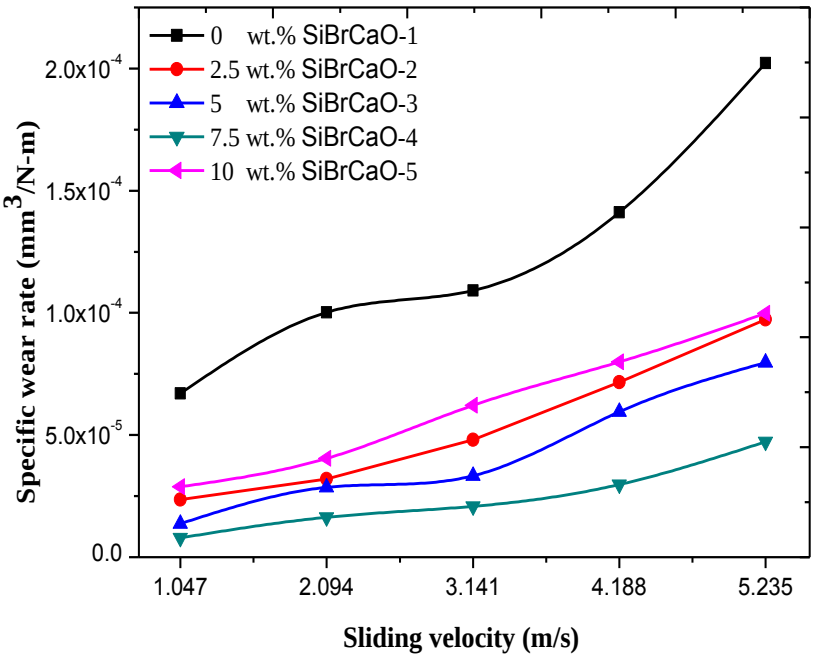

Figure 6.31 Variation of specific wear rate with sliding velocity for CaO particulates filled SiBr alloy composites (Load: 15N, Sliding Distance: 1000m and Environment Temperature: 35°C)

The outcomes of specific wear rate have a correlation with hardness when the hardness of particulate filled alloy material is increased, the composites show decreased in wear rate. The different parameters such as weight fraction of reinforced particulates, geometry/size, particle distribution and morphology of composite surface

were taken care during sliding wear process to calculate the specific wear rate of the unfilled/ particulate filled composite materials, and this also becomes the fundamental difference between monolithic and the alloy composite materials [361]. Jin et al. [327] studied the dry sliding wear behaviour for $Mg_2B_2O_5$ whisker reinforced 6061Al matrix composite. In this study, they found the increased in wear rate as a function of sliding velocity at a constant load of 15 N.

This result is due to the proper wettability between particulate and matrix material in the composite. The increased in wear rate is in order of 0wt.-% CaO>10wt.-% CaO> 2.5wt.-% CaO> 5wt.-% CaO>7.5wt.-% CaO respectively. The apparent reason for the higher value of specific wear rate with the increased in sliding velocity is the presence of CaO particles in SiBr alloy composites, which get dispersed from their place after continuous rubbing of counter face materials during sliding wear process.

6.4.2 Effect of sliding velocity on the coefficient of friction of CaO particulates filled SiBr alloy composites

The correlation between the coefficient of friction and sliding velocity of CaO filled SiBr alloy composites were shown in Figure 6.32.

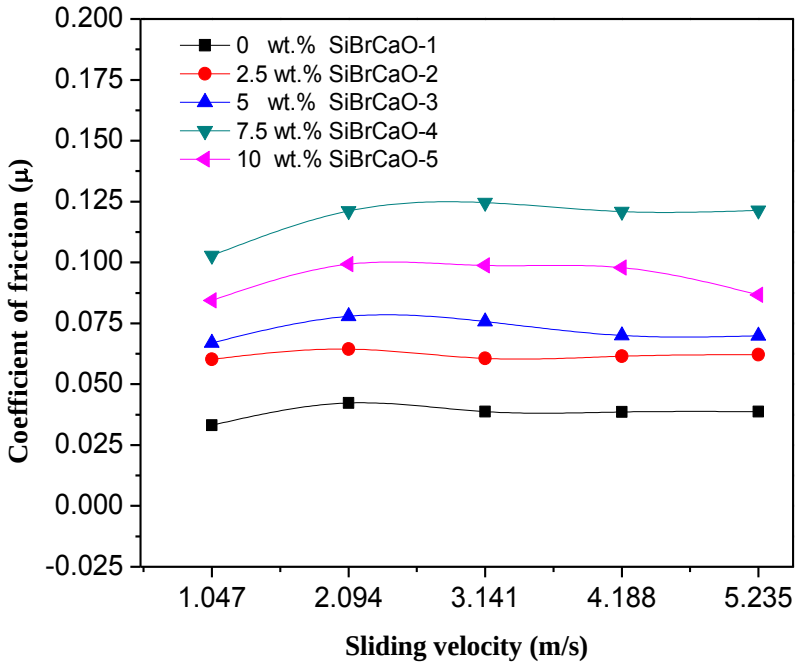

Figure 6.32 Variation of the coefficient of friction with sliding velocity for CaO particulates filled SiBr alloy composites (Load: 15N, Sliding Distance: 1000m and Environment Temperature: 35°C)

It is observed that the value of coefficient of friction (COF) increases with the increased in weight percentage of the composite. At 7.5wt.-% of CaO filled SiBr alloy composite shows the highest value of COF that is 0.125 approximately at 4.188m/s sliding velocity, similarly other weight fractions also show the approximately constant value of COF from the 2.084m/s to 4.188m/s sliding velocity range respectively. Initially, the value of COF increases from 1.047m/s to 2.097 m/s but beyond it, the value of COF remain constant. The presence of hard reinforced particulates from the worn surface of composite material sample can be the reason of initial rise in COF because the hard asperities act like a cutting tool that tries out to damage the surface of the material in term of scratches or grooves. On the other hand, plastic deformation in between counter faces of pin and disk sample can be partially responsible for the higher value of COF. The excess amount of plastic deformation would occur at higher sliding speed due to the heat affected zone at counterpart of composite material with disk materials [362].

6.4.3 Effect of normal load on specific wear rate of CaO particulates filled SiBr alloy composites

The specific wear rate result is plotted against applied load in Figure 6.33 for CaO filled SiBr alloy composites.

The specific wear rate of both unfilled and CaO filled SiBr alloy composites is decreased with the increased in normal load from 5N to 45N (Fig. 6.33). The maximum wear rate for CaO filled SiBr alloy composite is found at low loads i.e. about 5N load. The reasons for higher wear rate at initial normal loading (i.e. 5N load) can be the transition phenomenon and the transition loading increases by the increment in wt.-% of CaO reinforcement particle in the alloy composites. When the value of applied load is increased, the wear rate decreased for all wt.-% of particulate filled SiBr alloy composites and finally, the particulate filled alloy composites trend is same as the unfilled metal alloy [363] as specific wear rate depends on the hardness of the composites [364].

Baskaran et al. [365] studied the wear behaviour for AA7075–TiC particulate filled metal alloy composite materials at varying loading conditions and found that the wear rate for composite materials abruptly decreases which means the wear resistance capacity of composite materials is maximum for different loading conditions.

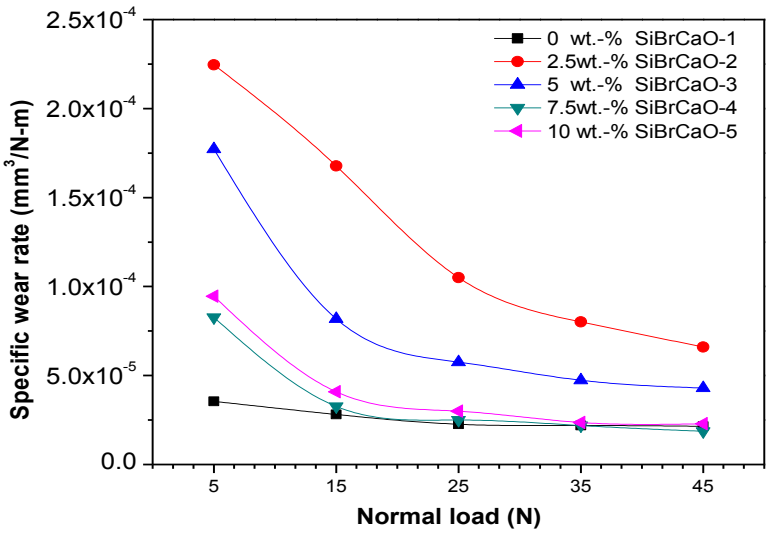

Figure 6.33 Variation of specific wear rate with normal load for CaO particulates filled SiBr alloy composites (Sliding velocity: 2.094m/s, Sliding Distance: 1000m and Environment Temperature: 35°C)

6.4.4 Effect of normal load on the coefficient of friction of CaO particulates filled SiBr alloy composites

The coefficient of friction for CaO filled SiBr alloy composites on varying load is shown in Figure 6.34.

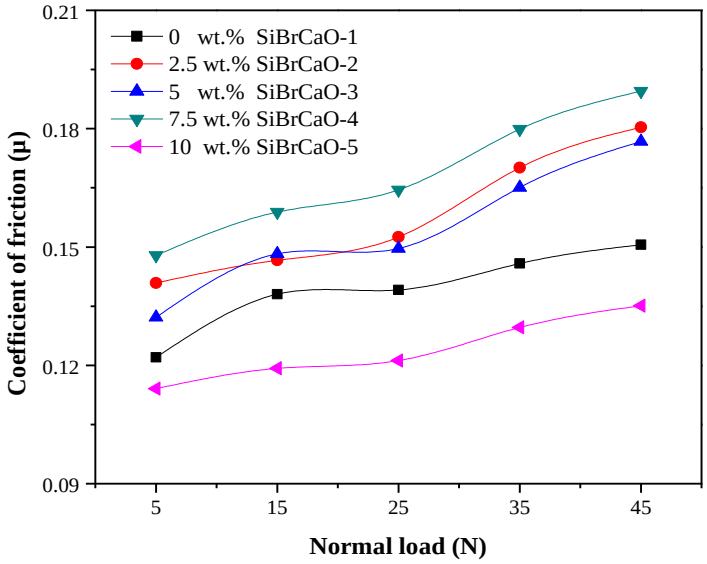

Figure 6.34 Variation of the coefficient of friction with normal load for CaO particulates filled SiBr alloy composites (Sliding velocity: 2.094m/s, Sliding Distance: 1000m and Environment Temperature: 35°C)

From Figure 6.34, it is observed that the trend of coefficient of friction remain constant from 5N to 25N applied loading condition for different wt.-% of CaO filled SiBr alloy composites, but beyond 25N to 45N the value of coefficient of friction is increased from 0.164 to 0.189 for 7.5wt.-% of CaO filled SiBr alloy composites, that shows the CaO particulate has remarkable effect on the coefficient of friction for the alloy composite [366]. It is also observed that the value of the coefficient of friction increases at low loads.

6.4.5 Taguchi design experimental analysis for CaO particulates filled SiBr alloy composites

Table 6.7 shows the experimental results for specific wear rate of CaO filled SiBr alloy composites and their corresponding signal-to-noise ratio for each experiment. Also the total mean signal-to-noise ratio for the 25 experiments is calculated as 106.33 dB by using MINITAB 16 software.

The corresponding response plot for the particulate filled SiBr alloy composites factor settings were presented in Figure 6.35. From Figure 6.35 one can be observed that the effect of individual factor level of significance on the specific wear rate of the particulate filled alloy composites i.e. the factor with highest inclination line is more significant than the factor with a lower angle of inclination. Therefore, the factor sliding velocity, normal load and environment temperature respective show more significant as compared with other factors (Figure 6.35).

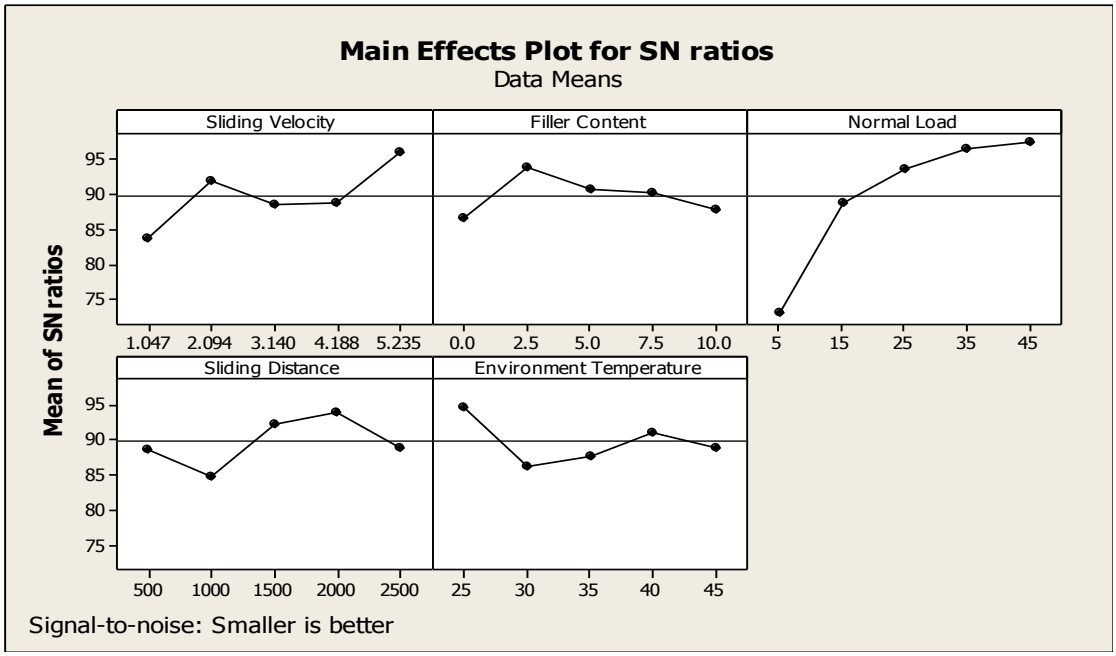

Figure 6.35 Effect of control factors on wear rate for CaO particulates filled SiBr alloy composites

Table 6.7 Experimental layout of L_{25} orthogonal array

Expt. No.	Sliding Velocity (m/sec)	Filler Content (wt. -%)	Normal Load (N)	Sliding Distance (m)	Environment Temperature (°C)	Spe. Wear Rate $\frac{mm3}{N-m}$	S/N Ratio (db)
1	1.047	0	5	500	25	2.836E-04	70.946
2	1.047	2.5	15	1000	30	1.367E-04	77.285
3	1.047	5	25	1500	35	4.684E-05	86.588
4	1.047	7.5	35	2000	40	2.004E-05	93.962
5	1.047	10	45	2500	45	3.326E-05	89.562
6	2.094	0	15	1500	40	2.101E-05	93.551
7	2.094	2.5	25	2000	45	4.824E-06	106.33
8	2.094	5	35	2500	25	7.169E-06	102.89
9	2.094	7.5	45	500	30	2.268E-05	92.887
10	2.094	10	5	1000	35	6.452E-04	63.806
11	3.14	0	25	2500	30	7.385E-05	82.633
12	3.14	2.5	35	500	35	1.225E-05	98.237
13	3.14	5	45	1000	40	1.487E-05	96.554
14	3.14	7.5	5	1500	45	2.212E-04	73.104
15	3.14	10	15	2000	25	2.503E-05	92.031
16	4.188	0	35	1000	45	6.414E-05	83.857
17	4.188	2.5	45	1500	25	5.360E-06	105.41
18	4.188	5	5	2000	30	1.631E-04	75.751
19	4.188	7.5	15	2500	35	3.742E-05	88.538
20	4.188	10	25	500	40	3.097E-05	90.181
21	5.235	0	45	2000	35	8.222E-06	101.70
22	5.235	2.5	5	2500	40	8.496E-05	81.416
23	5.235	5	15	500	45	2.619E-05	91.637
24	5.235	7.5	25	1000	25	7.988E-06	101.95
25	5.235	10	35	1500	30	6.927E-06	103.18

6.4.6 ANOVA and the effect of factors for CaO particulates filled SiBr alloy composites

For different wt.-% of CaO filled SiBr alloy composites materials the outcomes of analysis of variance (ANOVA) with specific wear rate were listed in Table 6.8. This analysis of variance is undertaken for a level of significance of 5% that is for a level of confidence of 95%. The p-test i.e. the percentage contribution for an individual factor is shown in Table 6.8. Table 6.8 shows that the factors, normal load (C) [p=0.012%], sliding distance (D) [p=0.272%] and sliding velocity (A) [p=0.151%] have most influences on the specific wear rate of the CaO filled SiBr alloy composite but the other factors such as filler content (B) [p=0.445%] and environment temperature (E) [p=0.337%] have the least effect on specific wear rate of the filled alloy composites. From this analysis, it is observed that filler content has the most significant contribution as compared to other factors.

Table 6.8 ANOVA table for specific wear rate (CaO particulates filled SiBr alloy composite)

Source	DF	Seq SS	Adj SS	Adj MS	F	P
A	4	414.57	414.57	103.64	3.08	0.151
B	4	155.94	155.94	38.99	1.16	0.445
C	4	1982.50	1982.50	495.62	14.74	0.012
D	4	258.20	258.20	64.55	1.92	0.272
E	4	210.45	210.45	52.61	1.56	0.337
Error	4	134.48	134.48	33.62		
Total	24	3156.14				

DF - Degree of freedom, Seq SS - Sequential sum of square, Adj SS - Adjacent sum of square, Adj MS - Adjacent sum of mean square, F – Variance, P - Test (Percentage contribution of each factor in overall performance to find out optimum specific wear rate)

6.4.7 Surface morphology of unfilled and CaO particulates filled SiBr alloy composites

The scanning electron microscopy is used to analyse the surface morphology or geometric features of all the particulate filled alloy composite materials on the same magnification for the comparison purpose. The microstructure for worn surfaces of CaO (100 μm) filled SiBr alloy composites by field emission scanning electron microscopy (FESEM), steady state condition were shown in Figure 6.36, Figure 6.37 and Figure 6.38 shows the microstructure of worn surfaces after Taguchi DOE test

run. Each microstructure for different test conditions explains the micro-examination behaviour across the counter face of composite. The worn surfaces of the fabricated composite materials as shown in Figure 6.36, Figure 6.37 and Figure 6.38 indicated that the proportion of material is removed after counter face process by micro machining effect that affected the reinforcement or filler phase of the composite material by oxidation [367].

Figure 6.36 shows the microstructure behaviour of each examined CaO filled SiBr alloy sample having highest specific wear rate at steady state condition with the varying value of sliding velocity from 1.047 m/s to 5.235 m/s while other parameters such as normal load: 15N, sliding distance: 1000m and environment temperature: 35°C remains constant throughout the experiment respectively. From Figure 6.31, it is accessible that the specific wear rate for CaO filled SiBr alloy composite material as well as for monolithic alloy were found maximum for the highest sliding velocity i.e. 5.235m/s. Figure 6.36a shows the worn surface morphology of the unfilled alloy where the presence of reinforced particles becomes negligible. In Figure 6.36a, shallow grooves were found due to the presence of large amount of void content ~ 0.824% and due to which the interfacial bonding in between the particle is not so strong and due to that the material is removed from surfaces during sliding wear process and formed number of shallow grooves on the composite surface. There should be high infiltration pressure applied on the sample after fabrication to enrich the wettability of composite material but if the sufficient pressure is not applied than it showed improper bonding between matrix and reinforced which leads to removal of material during sliding wear process, shown in Figure 6.36b for 2.5wt.-% CaO filled SiBr alloy composite material [368]. Figure 6.36c shows the regular and continuous wear mark [369] along with the sliding wear direction. As the filler content increases to 7.5wt.-% (Figure 6.36d) the specific wear rate decreases as compared to other wt.-% of reinforced particulates as well as a monolithic alloy. During sliding wear process when the contact between the pin and counter face occur frictional heat is developed, that is influenced by sliding velocity. The sliding velocity and frictional heat behave reciprocal to each other. When the heat is generated at a counter part of surfaces, materials get softer which lowers the bonding strength of reinforcement and matrix.

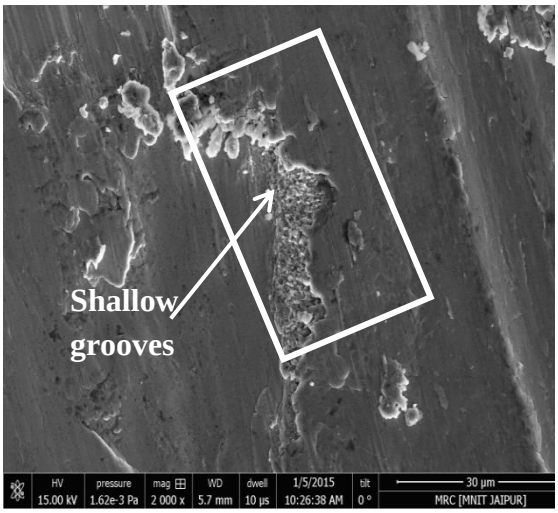

(a) 0wt.-% CaO (worn)

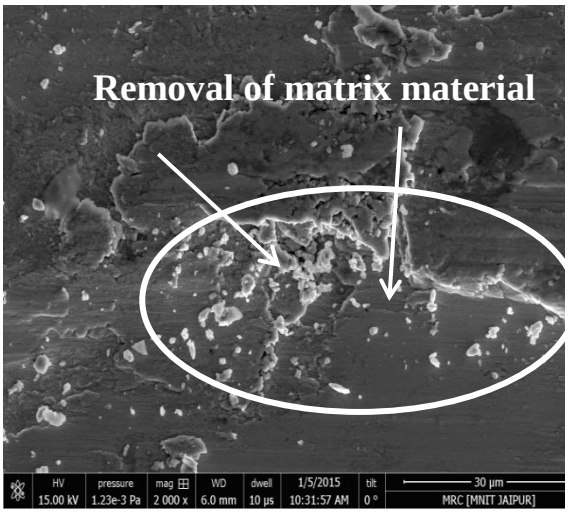

(b) 2.5wt.-% CaO (worn)

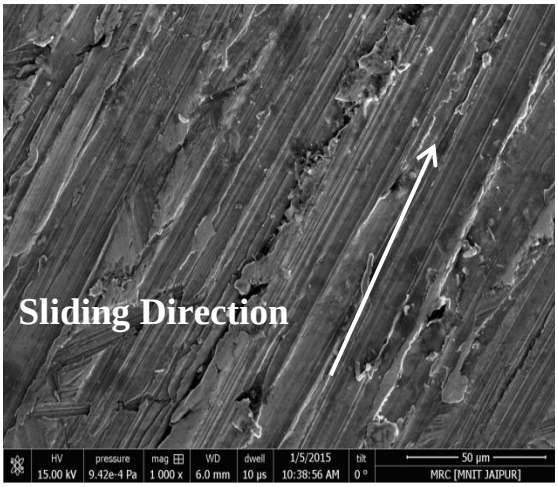

(c) 5wt.-% CaO (worn)

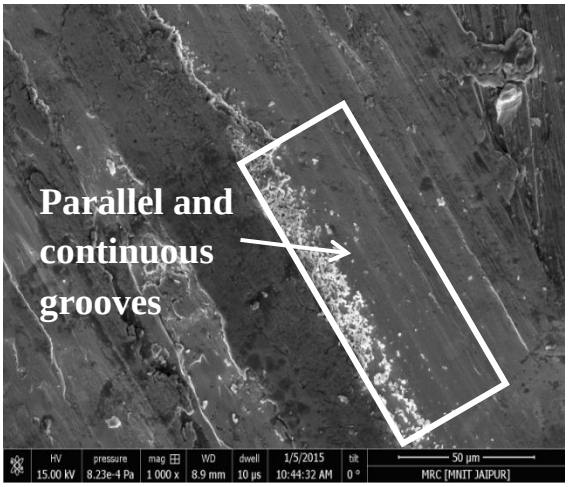

(d) 7.5wt.-% CaO (worn)

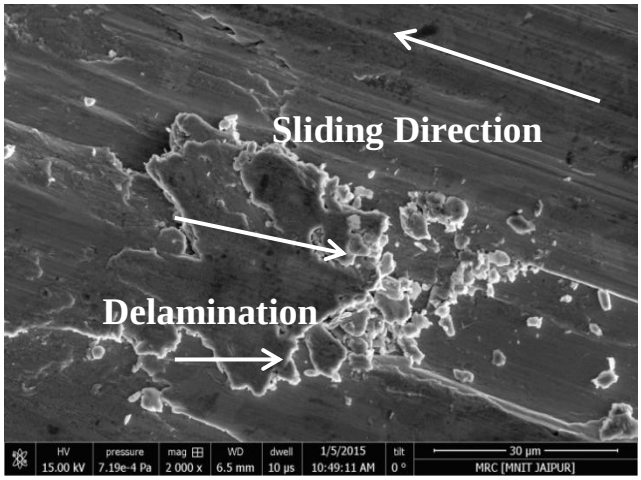

(e)10 wt.-% CaO (worn)

Figure 6.36 Scanning electron micrograph of particulates filled SiBr alloy composites under steady state condition with varying sliding velocity (At constant: Normal load: 15N, Sliding Distance: 1000m and Environment Temperature: 35°C)

This phenomenon easily occurs at a higher sliding velocity that pulls out the reinforced particles from softer materials i.e. pin material creates continuous grooves [370] (shown in Figure 6.36d). Similarly, the delamination wear occurs at higher sliding velocity, and higher applied a load (shown in Figure 6.36e).The higher sliding velocity presented, the higher wear rate as shown in Figure 6.31 for 10 wt.-% of CaO filled SiBr alloy composite materials [370].

Figure 6.37 shows the surface micrographs for different wt.-% of CaO filled SiBr alloy composite materials under steady state condition with varying applied load while keeping other factors constant such as sliding velocity: 2.094 m/s, sliding distance: 1000 m and environment temperature: 35°C. From Figure 6.33 it is found that the value of specific wear rate decreases on increasing in applied load from 5N to 45N. The maximum value of specific wear rate (SWR) shows at a very lower value of load which is 5N, irrespective of filler content and the wear sample surfaces with high resolutions AFM process is used as plotted in Figure 6.39. The micrographs for CaO filled SiBr alloy composite materials at 5N loading are shown in Figure 6.37a. It shows the presence of crack that occurred during sliding wear process and sliding process the load applied on the pin sample, and counter face is majorly applicable on sharp edges of reinforced particles that tend towards crack initiation in the composite materials [371]. The AFM micrographs were also used for surface resolutions, for 0wt.-% filler particulates it shows the homogeneous tips around the surface area and which also shows the less SWR value for the above material (Figure 6.39a). Figure 6.37b and Figure 6.37c showed the surface micrographs for 2.5 wt.-% and 5wt.-% of CaO filled SiBr alloy composites respectively. When the counter face of both pin and disk surfaces rub each the target material gets soften due to heat generated at the contact zone but at lower load i.e. 5N the 2.5 wt.-% and 5wt.-% particulate filled alloy show maximum wear rate may be due to improper interfacial bonding in between reinforced and matrix material where the hard particles get pulled out form the surfaces and leads towards ploughing mechanism [371]. Similarly, AFM micrographs for 2.5 wt.-% and 5wt.-% filler particles shows (Figure 6.39b and Figure 6.39c) sharp and worn tips by which tip wear occurs which leads towards uncertainty of obtained material properties [358].

Figure 6.37d and Figure 6.37e show the micrographs for 7.5wt.-% and 10wt.-% CaO filled SiBr alloy composites respectively. These two volume contents show the least SWR as compared to other wt.-% of filler particulates. Similarly, the corresponding

AFM micrographs for 7.5wt.-% and 10wt.-% (Figure 6.39d and Figure 6.39e) filler particulates show reduced ploughing action, due to decreasing specific wear rate of composites materials (From Fig. 6.37).

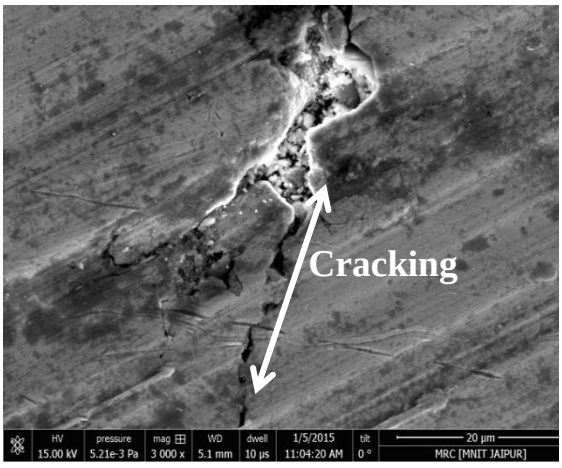

(a) 0wt.-% CaO (worn)

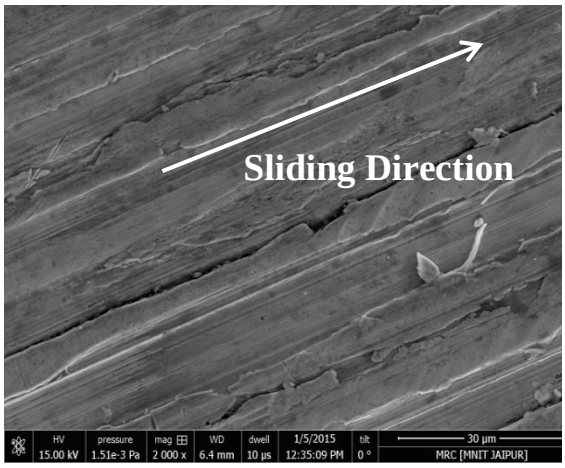

(b) 2.5wt.-% CaO (worn)

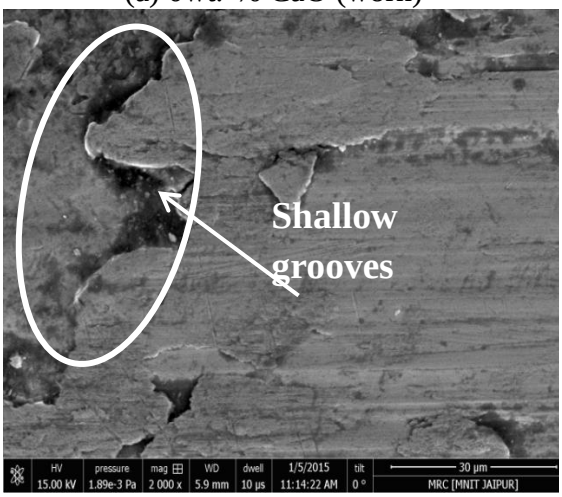

(c) 5wt.-% CaO (worn)

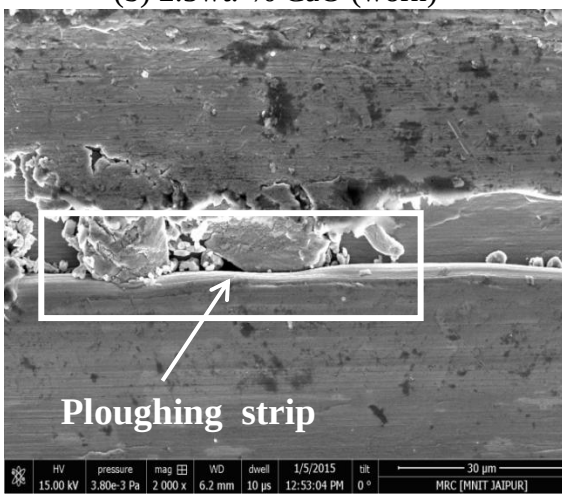

(d) 7.5wt.-% CaO (worn)

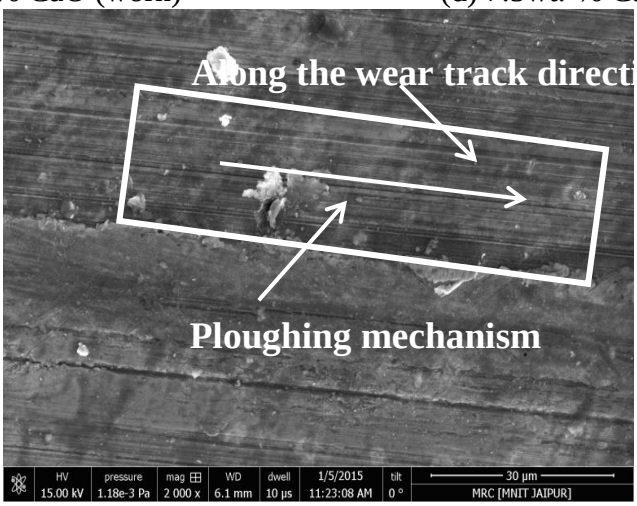

(e)10wt.-% CaO (worn)

Figure 6.37 Scanning electron micrograph of particulate filled SiBr alloy composites under steady state condition with varying normal load (At constant: Sliding velocity: 2.094m/s, Sliding Distance: 1000m and Environment Temperature: 35°C)

To understand the mechanical behaviour due to metal oxidation of composite materials, the micro-structural studies has been carried out [247]. The microstructure studies of CaO filled SiBr alloy composite materials for L_{25} Taguchi design experimental test runs shown in Figure 6.38. The micrographs shown in Figure 6.38 has highest SWR for fabricated composite materials under L_{25} Taguchi design of experimental test run (Table 6.7). Figure 6.38a shows the micrograph for first test run (i.e. Exp. Run 1, Table 6.7). This shows the lowest wear rate (2.836E-$^{04}\frac{mm3}{Nm}$**)** for 0wt.-% of particulate filled metal alloy composites. The wear rate of composite material shows lower value at lower load. The lower value of SWR indicated that the homogeneity during sliding wear process at a low velocity of 1.047 m/s and a lower load of 5N, that has less debris and by that the SWR also shows less amount for fabricated composite material. From Figure 6.38a, the homogeneous and continuous sliding direction is clearly visible in the unfilled SiBr alloy composite. The micrograph (Figure 6.38b) for 2.5wt.-% of CaO filled SiBr alloy composite material shows highest SWR (Exp. Run 7, Table 6.7) at 2.094m/s sliding velocity and 25N load over the sliding distance of 2000 m at a temperature of 40°C. When the two surfaces of pin and disk were rubbed to each other during sliding wear process at 2.094 m/s sliding velocity, the heat is generated at the counter face and therefore, the reinforcing hard particles get loosen from the matrix material. The micro-ploughing phenomenon at that position of composite material could be the reason for maximum wear rate.

Figure 6.38c shows the micrograph for 5wt.-% CaO filled SiBr alloy composite material that shows highest specific wear rate (Exp. Run 8, Table 6.7) with the sliding velocity 2.094m/s, normal load 35N over the sliding distance of 2500m at a temperature of 25°C. The micrograph shows the presence of dense filler particles and the stirring process during fabrication is resulted in the formation of agglomeration in few portions of the alloy composite. Numerous grooves or ploughs were formed during the sliding wear process. By these grooves, micro ploughing and similar type of worn surfaces were observed under the application of higher loads [372]. Similar, phenomenon of micro-ploughing is also found at 7.5 wt.-% of CaO filled SiBr alloy composite where maximum specific wear rate (Exp. Run 24, Table 6.7) is observed with sliding velocity 5.235 m/s, load 25 N over sliding distance of 1000 m at a temperature 25°C as shown in Figure 6.38d. The micrograph as shown in Figure 6.38e

for 10 wt.-% CaO filled SiBr alloy composite against (Exp. Run 25, Table 6.7) the sliding velocity of 5.235 m/s, 35 N normal load over a distance of 1500 m, at a temperature of 30°C shows maximum wear rate. During sliding wear test at higher sliding velocity, the reinforcement particles pull out from the pin surface in the form of debris [369] that pushed at the edge as wear scar (Fig. 6.38e).

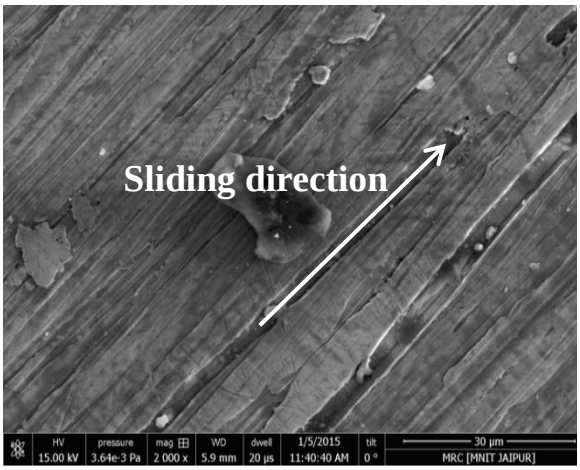

(a) 0wt.-% CaO (worn)

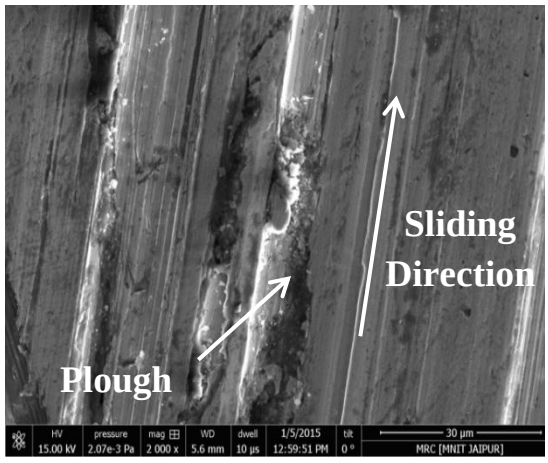

(b) 2.5wt.-% CaO (worn)

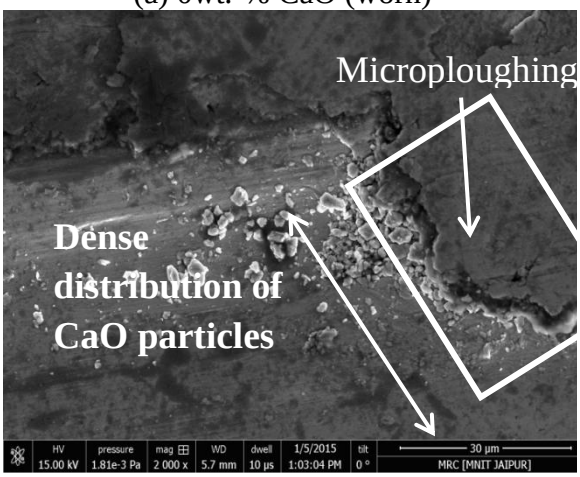

(c) 5wt.-% CaO (worn)

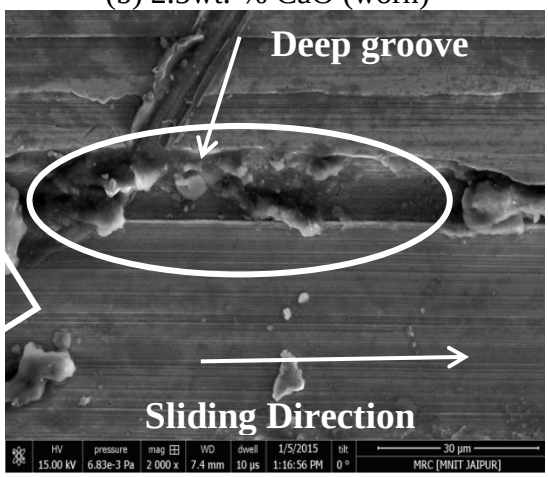

(d) 7.5wt.-% CaO (worn)

(e)10wt.-%CaO (worn)

Figure 6.38 Scanning electron micrographs of particulate filled SiBr alloy composites (Taguchi Design of Experiment)

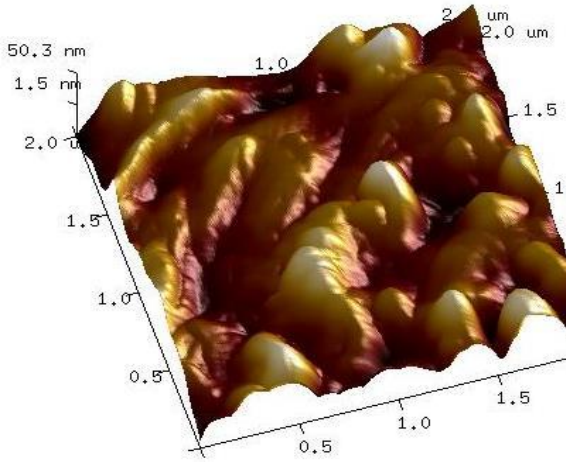

(a) 0 wt.-% CaO (worn)

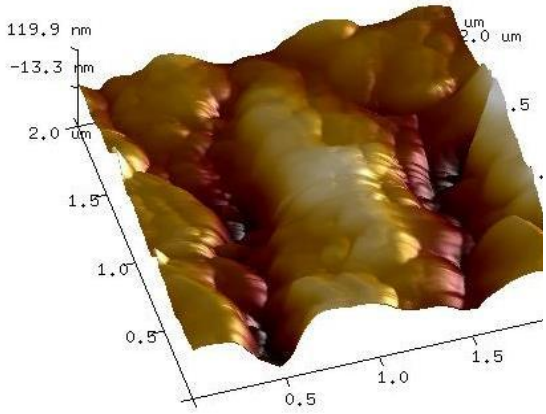

(b) 2.5 wt.-% CaO (worn)

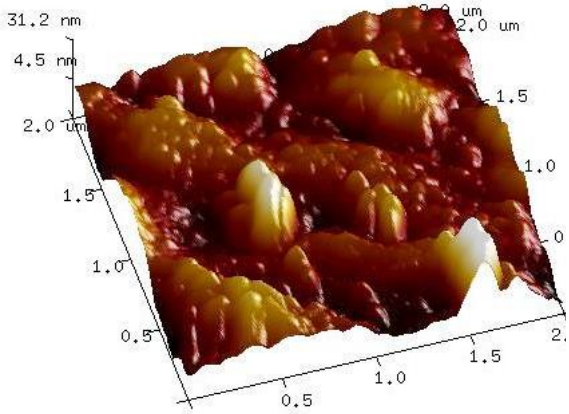

(c) 5 wt.-% CaO (worn)

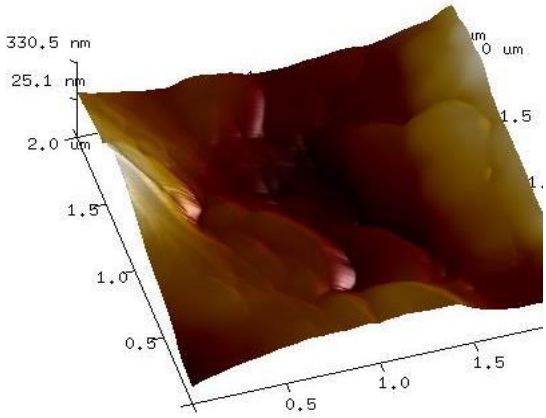

(d) 7.5 wt.-% CaO (worn)

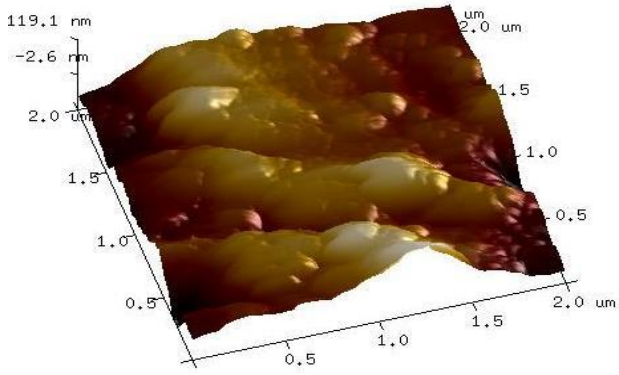

(e) 10 wt.-% CaO (worn)

Figure 6.39 AFM micrographs of CaO particulates filled SiBr alloy composite (a) 0 wt.-% CaO (b) 2.5 wt.-% CaO (c) 5 wt.-% CaO (d) 7.5 wt.-% CaO and (e) 10 wt.-% CaO

6.4.8 Energy dispersive X-ray analysis (EDAX) of unfilled and CaO particulates filled SiBr alloy composites

The EDAX analysis is carried out to confirm the presence of reinforcing particulates and elements of the matrix material. Figure 6.40 shows the EDAX spectrums of the scrutinize CaO filled SiBr alloy composites. From the plot, it distinctly substantiates the presence of input matrix materials (Such as SiBr alloy as shown in Table 3.3 and reinforced particulates i.e. CaO particles) and reinforced materials.

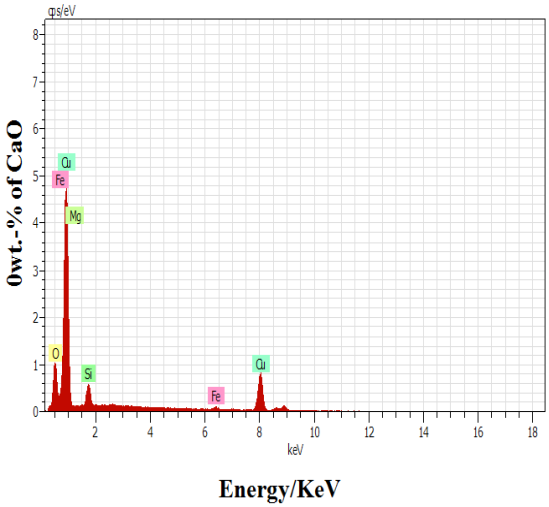

(a)

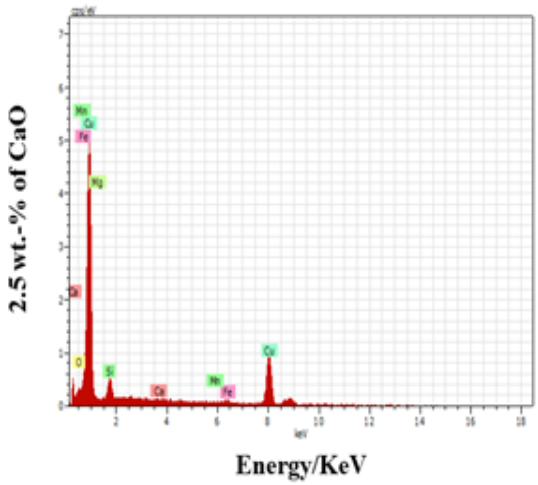

(b)

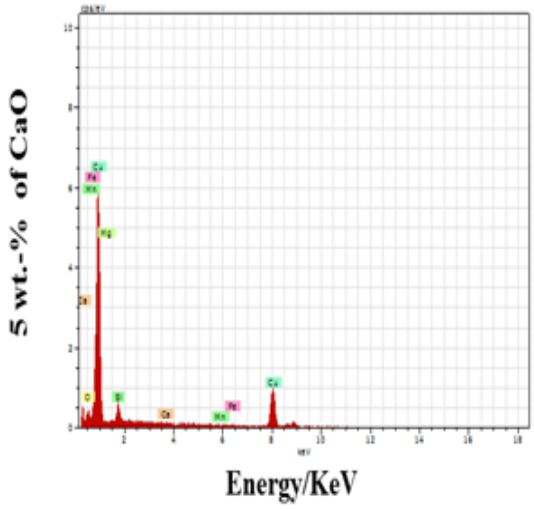

(c)

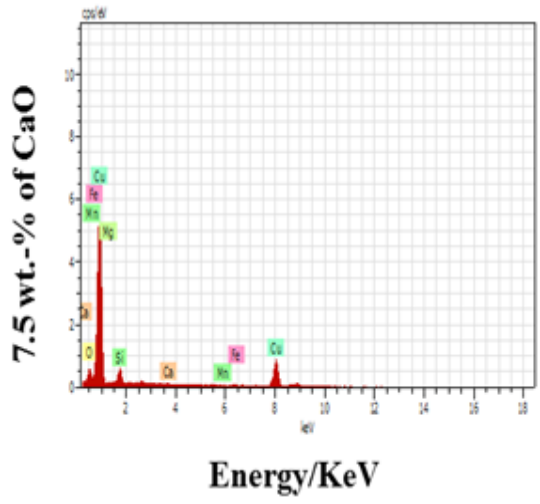

(d)

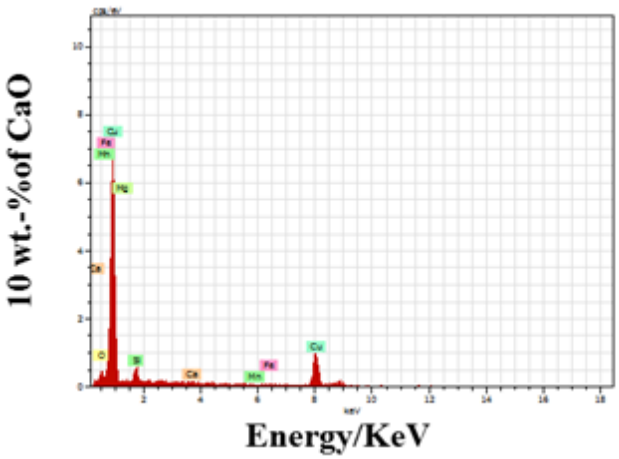

(e)

Figure 6.40 EDAX spectrum of CaO particulates filled SiBr metal alloy composite. (a) 0wt.% CaO (b) 2.5wt.% CaO (c) 5wt.% CaO (d) 7.5wt.% CaO and (e) 10wt.% CaO

6.5 Effect of optimization on wear behaviour of the proposed composites materials using Preference Selection Index (PSI) method

6.5.1 Experiment results

The selection of a most prominent materials from the numerous feasible alternatives, that having its unique characteristics, applications, advantages and limitations, the researcher or the designer should have the proper perception regarding the functional selection for different applications and also should have exhaustive knowledge or information to consider the accurate criterion for specific engineering design and applications. It's a very challenging task for any design engineer to select accurate materials for the design and development of different components used for numerous applications. The selection parameter plays an important role for any design engineers because if improper parameters were chosen, may often escort immense loos in terms of cost, component/product life, etc. So it's very obligatory for any designer to identify the need and choose accurate materials accordingly and fulfil the functionality in respect of minimum cost inclusion and maximum accomplishment [373].

From the past, plenty amount of research had been reported for the selection of accurate materials by using different multi-attribute decision-making methods. It's a very commercial tool that widely used for the selection of best possible alternative solution of any given application, different methods that become used to get the alternative solutions as weighted product method (WPM), technique for order preference by similarity to ideal solution (TOPSIS), analytical hierarchy process

(AHP), graph theory and matrix representation approach (GTMA), etc. And now-a-days preference selection index (PSI) method most widely used method due to its pleasing quality such as in this method there's no need to shows the relative importance in between the different attributes that cannot be ignored in other methods. So this method can be used, where the different conflicts can occur in deciding the importance of different attributes. By using the overall preference value and preference selection index for each and individual alternatives, can get the best possible alternative that having higher rank order [374].

The PSI procedure used to found the best solution for the chosen alternative values of particulate filled metal alloy composite materials during wear analysis through POD tribometer test analysis. Firstly the materials properties been normalized to extinguish the differences and set the values in a preferred range order. This procedure is performed according to the benefit of outcomes such as smaller the better or larger the better, for the wear analysis it should be smaller the better. In this research work, ten selected performance defining criteria`s (PDCs) is selected to analyse the wear analysis for eighteen experimental values of particulate filled metal alloy composite materials as given in Table 6.10 and 6.11. The decision matrix for PSI method is calculated from Eq. 3.13 and revolutionize the performance values (Shown in Table 6.10) in the range of [0, 1]. After calculation from Eq. 3.14 and 3.15 getting the normalised matrix for all the preferred alternatives, mean normalized, preference variation, deviation in the preference variation and overall preference values (Table 6.12) is calculated, and these values finally lead the ranking order of chosen attributes for composite materials (Table 6.13). A comprehensive elucidation of the selected criterions for optimization outcomes is given in Table 6.9. And the experiment results correspondingly for each criterion and condition were listed in Table 6.10 to Table 6.13.

Table 6.9 Description of the selected criterions.

Criterions	Description of the individual criterion	Performance implications of criterion
Wear	It is the specific wear rate for sliding wear behaviour of composite materials performed on POD tribometer at 1.047 m/s sliding velocity while keeping other parameters constant such as, Normal load: 15N, Sliding Distance: 1000m and Environment Temperature: 35°C	C-1 Lower-the-better

Wear	It is the specific wear rate for sliding wear behaviour of composite materials performed on POD tribometer at 2.094 m/s sliding velocity while keeping other parameters constant such as, Normal load: 15N, Sliding Distance: 1000m and Environment Temperature: 35°C	C-2 Lower-the-better
Wear	It is the specific wear rate for sliding wear behaviour of composite materials performed on POD tribometer at 3.141 m/s sliding velocity while keeping other parameters constant such as, Normal load: 15N, Sliding Distance: 1000m and Environment Temperature: 35°C	C-3 Lower-the-better
Wear	It is the specific wear rate for sliding wear behaviour of composite materials performed on POD tribometer at 4.188 m/s sliding velocity while keeping other parameters constant such as, Normal load: 15N, Sliding Distance: 1000m and Environment Temperature: 35°C	C-4 Lower-the-better
Wear	It is the specific wear rate for sliding wear behaviour of composite materials performed on POD tribometer at 5.235 m/s sliding velocity while keeping other parameters constant such as, Normal load: 15N, Sliding Distance: 1000m and Environment Temperature: 35°C	C-5 Lower-the-better
Wear	It is the specific wear rate for sliding wear behaviour of composite materials performed on POD tribometer at 5N normal load while keeping other parameters constant such as, Sliding velocity: 2.094m/s, Sliding Distance: 1000m and Environment Temperature: 35°C	C-6 Lower-the-better
Wear	It is the specific wear rate for sliding wear behaviour of composite materials performed on POD tribometer at 15N normal load while keeping other parameters constant such as, Sliding velocity: 2.094m/s, Sliding Distance: 1000m and Environment Temperature: 35°C	C-7 Lower-the-better
Wear	It is the specific wear rate for sliding wear behaviour of composite materials performed on POD tribometer at 25N normal load while keeping other parameters constant such as, Sliding velocity: 2.094m/s, Sliding Distance: 1000m and Environment Temperature: 35°C	C-8 Lower-the-better
Wear	It is the specific wear rate for sliding wear behaviour of composite materials performed on POD tribometer at 35N normal load while keeping other parameters constant such as, Sliding velocity: 2.094m/s, Sliding Distance: 1000m and Environment Temperature: 35°C	C-9 Lower-the-better

Wear	It is the specific wear rate for sliding wear behaviour of composite materials performed on POD tribometer at 45N normal load while keeping other parameters constant such as, Sliding velocity: 2.094m/s, Sliding Distance: 1000m and Environment Temperature: 35°C	C-10 Lower-the-better

Table 6.10 Experimental results of the criterions.

Composite	C-1	C-2	C-3	C-4	C-5	C-6	C-7	C-8	C-9	C-10
ZA-0	5.82E-05	7.38E-05	7.95E-05	1.20E-04	1.71E-04	3.79E-05	4.08E-05	4.59E-05	5.15E-05	7.24E-05
ZA-1	4.29E-05	5.68E-05	6.08E-05	1.21E-04	1.52E-04	3.52E-05	3.75E-05	4.19E-05	4.45E-05	6.82E-05
ZA-2	4.31E-05	5.02E-05	5.33E-05	6.82E-05	8.26E-05	3.16E-05	3.18E-05	3.48E-05	4.14E-05	6.26E-05
ZA-3	3.79E-05	4.21E-05	4.23E-05	5.27E-05	6.96E-05	2.82E-05	2.64E-05	3.11E-05	3.52E-05	5.81E-05
ZA-4	2.63E-05	2.65E-05	3.69E-05	4.79E-05	5.94E-05	2.12E-05	2.39E-05	2.75E-05	3.09E-05	5.36E-05
ZA-5	4.32E-05	5.28E-05	6.18E-05	1.09E-04	1.48E-04	3.53E-05	3.58E-05	4.07E-05	4.28E-05	6.71E-05
ZA-6	4.29E-05	4.33E-05	5.24E-05	7.82E-05	9.36E-05	3.06E-05	3.28E-05	3.30E-05	4.07E-05	6.11E-05
ZA-7	3.82E-05	4.12E-05	4.12E-05	5.17E-05	7.96E-05	2.71E-05	2.88E-05	3.06E-05	3.71E-05	5.78E-05
ZA-8	2.58E-05	2.78E-05	3.62E-05	4.81E-05	5.90E-05	2.03E-05	2.46E-05	2.80E-05	3.39E-05	5.44E-05
SiBr-0	2.36E-05	5.97E-05	8.06E-05	9.21E-05	9.96E-05	2.55E-05	3.76E-05	5.93E-05	7.83E-05	8.97E-05
SiBr-1	1.21E-04	6.43E-05	4.83E-05	4.22E-05	4.09E-05	1.09E-04	4.02E-05	3.38E-05	3.10E-05	3.22E-05
SiBr-2	1.34E-04	7.95E-05	5.58E-05	4.60E-05	4.72E-05	1.51E-04	5.44E-05	3.76E-05	3.05E-05	2.65E-05
SiBr-3	5.10E-05	2.98E-05	2.55E-05	2.18E-05	2.09E-05	1.40E-04	5.53E-05	4.59E-05	4.01E-05	3.54E-05
SiBr-4	6.88E-05	4.30E-05	3.73E-05	3.01E-05	2.58E-05	9.03E-05	4.73E-05	3.10E-05	2.58E-05	2.44E-05
SiBr-5	2.36E-05	3.20E-05	4.81E-05	7.17E-05	9.72E-05	2.25E-04	1.68E-04	1.05E-04	8.01E-05	6.60E-05
SiBr-6	1.36E-05	2.86E-05	3.33E-05	5.95E-05	7.96E-05	1.77E-04	8.18E-05	5.75E-05	4.73E-05	4.30E-05
SiBr-7	7.88E-06	1.64E-05	2.08E-05	2.97E-05	4.73E-05	8.27E-05	3.27E-05	2.50E-05	2.18E-05	1.86E-05
SiBr-8	2.88E-05	4.05E-05	6.22E-05	8.00E-05	9.98E-05	9.45E-05	4.09E-05	3.00E-05	2.37E-05	2.29E-05

Table 6.11 Normalized matrix.

Composite	C-1	C-2	C-3	C-4	C-5	C-6	C-7	C-8	C-9	C-10
ZA-0	0.14	0.22	0.26	0.18	0.12	0.54	0.59	0.54	0.42	0.26
ZA-1	0.18	0.29	0.34	0.18	0.14	0.58	0.64	0.60	0.49	0.27
ZA-2	0.18	0.33	0.39	0.32	0.25	0.64	0.75	0.72	0.53	0.30
ZA-3	0.21	0.39	0.49	0.41	0.30	0.72	0.91	0.80	0.62	0.32
ZA-4	0.30	0.62	0.56	0.46	0.35	0.96	1.00	0.91	0.71	0.35
ZA-5	0.18	0.31	0.34	0.20	0.14	0.58	0.67	0.61	0.51	0.28
ZA-6	0.18	0.38	0.40	0.28	0.22	0.66	0.73	0.76	0.54	0.30
ZA-7	0.21	0.40	0.50	0.42	0.26	0.75	0.83	0.82	0.59	0.32
ZA-8	0.31	0.59	0.57	0.45	0.35	1.00	0.97	0.89	0.64	0.34
SiBr-0	0.33	0.27	0.26	0.24	0.21	0.80	0.64	0.42	0.28	0.21
SiBr-1	0.07	0.26	0.43	0.52	0.51	0.19	0.59	0.74	0.70	0.58
SiBr-2	0.06	0.21	0.37	0.47	0.44	0.13	0.44	0.66	0.71	0.70
SiBr-3	0.15	0.55	0.82	1.00	1.00	0.15	0.43	0.54	0.54	0.53
SiBr-4	0.11	0.38	0.56	0.72	0.81	0.22	0.51	0.81	0.84	0.76
SiBr-5	0.33	0.51	0.43	0.30	0.22	0.09	0.14	0.24	0.27	0.28
SiBr-6	0.58	0.57	0.62	0.37	0.26	0.11	0.29	0.43	0.46	0.43
SiBr-7	1.00	1.00	1.00	0.73	0.44	0.25	0.73	1.00	1.00	1.00
SiBr-8	0.27	0.40	0.33	0.27	0.21	0.21	0.58	0.83	0.92	0.81

Table 6.12 Mean normalized, preference variation, deviation in the preference variation and overall preference values.

Composite	Mean normalized value	preference variation value	deviation in preference variation value	overall preference values
C-1	0.2661	0.8348	0.1651	0.0709
C-2	0.4267	1.0049	0.0049	0.0021
C-3	0.4817	0.6155	0.3845	0.1652
C-4	0.4178	0.8065	0.1934	0.0821
C-5	0.3461	0.9185	0.0814	0.0351
C-6	0.4767	1.5635	0.5635	0.2421
C-7	0.6356	0.8533	0.1467	0.0630
C-8	0.6844	0.6546	0.3453	0.1483
C-9	0.5983	0.6541	0.3459	0.1486
C-10	0.4467	0.9026	0.0973	0.0418

Table 6.13 Preference selection index and ranking of the composites.

Composite	Preference selection index	Ranking
ZA-0	0.3940	**16**
ZA-1	0.4435	**13**
ZA-2	0.5134	**8**
ZA-3	0.5967	**5**
ZA-4	0.7157	**2**
ZA-5	0.4515	**12**
ZA-6	0.5217	**7**
ZA-7	0.5985	**4**
ZA-8	0.7111	**3**
SiBr-0	0.4407	**14**
SiBr-1	0.4583	**11**
SiBr-2	0.4117	**15**
SiBr-3	0.5104	**9**
SiBr-4	0.5508	**6**
SiBr-5	0.2341	**18**
SiBr-6	0.3792	**17**
SiBr-7	0.7588	**1**
SiBr-8	0.4851	**10**

From the normalized matrix (shown in Table 3) it is shown that the entire element were normalized in between the close interval [0, 1]. After that the mean of the normalized (χ_j) value of PDC j is determined by using the Eqt. 3. The preference variation value (φ_j) for each PDC and deviation in the preference variation value (Δ_j) is calculated for each and individual alternatives (By Eqt. 4 & 5). Lastly the overall preference value (ζ_j) is calculated (Eqt. 6) to get the optimum alternative value by PSI method. Finally, the overall preference selection index ϖ_i for the overall alternatives is calculated by using Eq 7. After the overall calculations, alternatives were arranged in a sequence of preference selection index and the maximum amount of PSI ranked as one that means it has the maximized optimal contribution in comparison of other fabricated particulate filled metal alloy composite materials during wear behaviour analysis (Shown in Table 5). Finally, the ranking order of wear analysis from PSI method for particulate filled metal alloy composite materials is done and sequenced as SiBr-7>ZA-4>ZA-8>ZA-7>ZA-3>SiBr-4>ZA-6>ZA-2>SiBr-3>SiBr-8>SiBr-1>ZA-5>ZA-1>SiBr-0>SiBr-2>ZA-0>SiBr-6>SiBr-5.SiBr-7 (SiBr alloy reinforced with 7.5 wt.-% CaO) shows the optimal performance among all particulate filled metal alloy composites considered in this study.

Chapter Summary

The experimental inquisition of particulate filled metal alloy composites has accompanied the following specific points:

1. The steady state condition to calculate SWR for varying sliding velocities and normal load for particulate filled metal alloy composite materials keeping other parameters constant.
2. The steady state condition to calculate the coefficient of friction with varying sliding and normal load for particulate filled metal alloy composite materials.
3. The prime value of particulate filled metal alloy composites calculated by Taguchi method by using L25 orthogonal array.
4. By the study of analysis of variance (ANOVA) for particulate filled metal alloy composites it's found that which factor plays most consequential effect in specific wear rate for a composite material in comparison of other factors.
5. The micro structural analysis for particulate filled metal alloy composites done by FESEM/EDAX and AFM at varying sliding speeds and load wear

mechanism which accountable for the wear behaviour of fabricated composite materials.

6. Finally, the PSI method is used to sequencing the wear behaviour of particulates filled metal alloy composites at varying conditions.

The next chapter postulates the summary and conclusion of the research findings drawn through the investigations along with the recommendation for future aspects of particulate filled metal alloy composites.

******

Chapter 7

Summary, Conclusions and Scope for Future Work

CHAPTER 7

SUMMARY AND FUTURE SCOPE

Introduction

The inquisition of research in this thesis for particulates filled metal alloy composites has accompanied into two parts:

- The first part of the thesis contains description about the experimental analysis for physical, mechanical, thermal and fracture analysis of particulate filled metal alloy composites
- The later or second part of the thesis has been reported about the effect of different particulates on the sliding wear behaviour of metal alloy composite materials by analysing micro-examination through Field emission scanning electron microscopic (FE-SEM), Atomic force microscopic (AFM), Energy dispersive X-ray analysis (EDAX) in order to understand the wear mechanism and morphology behaviour of the composites.

7.1. Summary of research findings

Invention of anything is often born of the need; desire to invent something or to improve. The physical, mechanical, fracture, thermo-mechanical or wear behaviour of any materials describes about the response or outcomes of the materials to apply mechanical loads or deformation. This response of materials can be understood in respect of the primary effect of mechanical loading on different induced defects or atomic motion. The rolling element bearings are widely used in numerous rotating machines for structural applications which get failure due to malfunctions and misalignment. Therefore, to overcome with these problems this work has been studied systematically keeping in view for bearing application. The failure of bearings is majorly caused by different factors such as misalignment, overloading, dirt and rust, manufacturing error and improper material selection or fabrication.

Such information about selecting parameters like proper materials, compositions, different materials properties are very essential for the fabrication of successful composite materials for any required applications. To this end, this thesis work is reported for the performance of new class of composite materials with the combination of Marble dust (Industrial iste) and Quicklime (CaO) particulates in base matrix materials. The filler particulates have been functionally efficient that enhances

the materials properties that are needed for the particular applications. A rich amount of data for two different particulates for two different metal alloy composite materials has been generated in this research work for bearing material applications. Such materials properties have been evaluated by performing determined by physical, mechanical, fracture, thermo-mechanical tests and sliding wear tests under controlled laboratory conditions.

As the filler particulates have hardened in nature, stirred in matrix and improved the load bearing capacity of (Compressive strength) and shock absorbing capacity (Impact strength) of the fabricated composite materials. The reason for the improvement of materials strength can be embitterment effect, through which reinforced particles block the movement in matrix due to which the local stress concentration locations get decreased. The improvement of materials compressive and impact strength is fount up to 7.5wt.-% of particulates but beyond it till 10 wt.-% of filler particulates composite shows the decreasing effect which may be due to the distributions of reinforced particles in composites are strongly dependent upon the response of materials so this inhomogeneous mixing of reinforced particles for larger amount can be the reason of diminishing compressive strength.

The magnitude of stress intensity factor shows the increasing trend for the particulates filled metal alloy composites with the increasing value of crack lengths. The fracture occurs due to the presence of void nucleation growth and coalescence in unreinforced materials as well as composite materials both. This phenomenon can be prevented by the grain refinement for composite materials which helps to prevent the formation of deformation twin which initiate the micro-crack. From the literature it is reported that the SIF depends upon the different mechanical properties, crack size, interface between contacting materials and applying loading conditions on materials. The analysis and examination process of any fractured surface for any materials known as the fractographs technique. This technique used routinely for the different failure analysis which occurred at different materials structure and examined by scanning electron microscope.

The resistance measurement of any materials known as hardness is performed indentation process under standards conditions. The hardness property of particulates filled metal alloy composite materials shows the increasing trend with the increasing amount of particulates compositions. The reason for the swell value of micro hardness

can be presence of hard MD particles in SiBr alloy composite materials that also increases the dislocation density of composite materials. After increases dislocation density the interfacial bond in between filler particulates and matrix become stronger which leads or enhances the micro hardness of fabricated composite.

In the present investigation, it is observed that the composite shows the increasing amount of void contents with the increasing composition of fillers in matrix materials. But the unfilled composite shows the higher amount of void contents as compared to particulates filled metal alloy composites except 10 wt.-% of particulates filled composite materials. The presence of such defect shows the inhomogeneous mixing of matrix and reinforced particles due to which it affects the properties of composite during performance. However, void content in most of the cases are found to be observed, it may possible to reduce by obey proper fabrication technique but as unavoidable parameter. The presence of voids diminishes the quality of product by affecting the various materials properties of composite materials and ultimately which affects the end product, so the presence of voids should be as minimum as possible.

The wear rate increases with the increasing amount of applied load while the constant result is found for sliding speed, where wear rate decreases with the increasing in amount of sliding velocity. Therefore, wear can be assumed as a major problem for the enhancement of life span of any component subjected to wear zone. Hence, particulate filled metal alloy composite showed a major alteration in the place of pure alloys especially in dry lubricating conditions. Therefore, the current work is mainly focused on the fabrication of CaO filled copper alloy (silicon bronze) composites for improvement of tribological properties of composite for bearing materials applications.

7.2. Conclusions

The consequences which found by this research work that, proposes of new particulate filled metal alloy composites and their scientific principles are effectively studied for bearing materials. Different summarization of simulation and experimental investigation for particulate filled metal alloy matrix composites has been descripted by the following specific conclusions:

1. Triumphant fabrication of particulates filled metal alloy composites for different wt.-% (0, 2.5, 5, 7.5 and 10) of marble dust (MD) and quicklime (CaO) particulates has been done by the use of stir casting (liquid fabrication

technique) process by using high temperature vacuum casting machine.

2. It has been studied and observed that the void content of the composites are decreased with the increase in filler content into the matrix alloy material up to 7.5wt.% of marble dust and beyond which the void content starts increasing. The experimental and theoretical densities of the unfilled and particulate filled alloy composites are found to be in line with each other. The hardness of the composites is found to be higher than the base alloy this is mainly due to the influence of hardened particulates.
3. Mechanical properties such as compressive strength and impact strength has positive effect (665MPa and 6J respectively) up to 7.5 wt.-% MD filled ZA-27 alloy composites but the flexural strength shows the increasing effect (684.38 MPa) up to 10 wt.-% MD reinforcement.
4. Mechanical properties such as hardness, flexural strength and impact strength has favorable effect (193Hv, 937MPa and 5J respectively) up to 7.5 wt.-% CaO filled ZA-27 alloy composites but the compressive strength shows the increasing effect (723MPa) up to 5 wt.-% CaO reinforcement only.
5. From the results it is found that the mechanical properties of fabricated MD particulates filled SiBr alloy composite materials become consequentially permute by diverging the volume content of MD particulates. It is found the void content become decreases from 0.824% to 0.380 for 0wt.-% to 7.5wt.-% MD particulates filler particles. And the hardness becomes increases from 119.25Hv to 181.5Hv for 0wt.-% to 7.5wt.-% addition of MD particulates in SiBr alloy composite materials, but the value of hardness become decreases by 176.25Hv on further increases filler content up to 10wt.-% of MD particulates filled metal alloy composites materials, So the most exemplary results is found up to 7.5 wt.-% of MD particulates filler particles for mechanical properties.
6. Mechanical properties of cast CaO filled SiBr alloy composite materials significantly altered by varying the weight percentage of CaO particulates. It is found that void content decreases from 0.824% to 0.504% up to 7.5 wt.-% of CaO filler particles. However, the hardness of the filled alloy composites increases up to 7.5 wt.-% of CaO filler particles i.e. 140.8 Hv but on further increased in CaO particulates the hardness is shown reveres in trend.

7. The magnitude of stress intensity factor (SIF) for varying crack length (1, 2, 3 and 4 mm) of MD filled ZA-27 alloy composites increases and the highest value of SIF occurs, 1.899 MPa.m^1/2 for 4mm crack length. This may be due to strong bonding between interface of reinforcement and matrix phases.
8. The stress intensity factor (SIF) values for varying crack length (1, 2, 3 and 4 mm) of CaO filled ZA-27 alloy composites increases and the highest value of SIF occurs, 2.0127 MPa.m^1/2 for 4mm crack length. The reason for the increased value of SIF can be the strong bonding or relationship in between interface of particulate and matrix phases.
9. Fracture surface analysis (Fractography effect) is observed for particulates filled metal alloy composites which show the number of micro examination behavior such as dimples and cracks are observed on fractured surface of composite material which means the formation of voids and coalescence occurs during fracture process.
10. Thermo-mechanical properties such as Thermo-gravimetric analysis (TGA) and Dynamic Mechanical Analysis (DMA) performed for particulates filled metal alloy composites at temperature range of (25-900°C) and (25-250 °C) respectively.
11. TGA plot indicates following diminishing order of thermal stability for CaO filled ZA-27 alloy composites as : 10 wt.-% CaO > 7.5 wt.-% CaO > 5 wt.-% CaO > 2.5 wt.-% CaO > 0 wt.-% CaO respectively up to 850ºC, thereafter degradation rate of the composites accelerate steeply. Henceforth, the investigated alloy composites could successfully be used as bearing material maximum up to 850ºC, thereafter it fails to retain its parent structure.
12. The storage modulus (E') exhibits following diminishing trend order: 7.5% E' > 5% E' > 0% E' > 2.5% E' > 10% E'. This infers that higher filler content (5-7.5 wt.-%) reinforcement boosts storage modulus of the neat alloy within workable temperature range, where as other filler content supposed to have detoriated effect on E'.
13. The loss modulus (E") magnitude increases with temperature irrespective of filler content for all the alloy composites. Within the temperature range of 25-125°C the order of diminishing E" are: 7.5% E" > 10% E" > 5% E" > 2.5% E" > 0% E", where as in temperature range 125-250°C the order of diminishing E"

are: 7.5% E" > 5% E" > 10% E" > 0% E" > 2.5% E". The loss modulus exhibits trend reversal in-relation-to storage modulus. And the damping capacity shows improvement in-comparisons-to neat alloy except for 2.5 wt.-% filler content.

14. The ANSYS simulated results of the proposed alloy composites are good agreement with the Hertzian theoretical results. The contact analysis of this method can easily and intuitively get the stress and strain values as well as their images, which can efficiently understand the parts running information, such as contact penetration, contact stress, contact area respectively.
15. The dry sliding specific wear rate of the composites materials increased with the addition of marble dust in the alloy composites and the maximum wear resistance is found to be for 10 wt.-% of marble dust filled ZA-27 alloy composites as compared to other unfilled and particulate filled alloy composites. SWR observed to have diminishing magnitude with filler content, consequently the order of SWR as 0 wt.-% MD > 2.5 wt.-% MD > 5 wt.-% MD > 7.5 wt.-% MD > 10 wt.-% MD across all sliding velocity. The sequence of decreasing amount of coefficient of friction magnitude with filler content is 7.5 wt.-% MD > 10 wt.-% MD > 5 wt.-% MD > 2.5 wt.-% MD > 0 wt.-% MD irrespective of sliding velocity condition.
16. With the varying normal load (5 to 45 N) for composite materials the steady state SWR concluded that: the SWR shows the decreasing SWR with the increasing wt.-% of filler particulates. The order of decreasing magnitude SWR follows as: 0 wt.-% MD > 2.5 wt.-% MD > 5 wt.-% MD > 7.5 wt.-% MD > 10 wt.-% MD across all normal load. The coefficient of friction of the composites decreases initially up to 2.094 m/s sliding velocity and after that it is observed in an average values till 5.235 m/s sliding velocity. The order of diminishing coefficient of friction magnitude with filler content is 7.5 wt.-% MD > 5 wt.-% MD > 0 wt.-% MD > 2.5 wt.-% MD > 10 wt.-% MD irrespective of normal load condition.
17. Under varying sliding velocities, steady state specific wear rate for CaO filled ZA-27 alloy composites concluded that (i) SWR of the investigated composites shows increasing trend with sliding velocity irrespective of filler content (ii) SWR observed to have diminishing magnitude with filler content, consequently the order of SWR as 0 wt.-% CaO > 2.5 wt.-% CaO > 5 wt.-% CaO > 7.5 wt.-%

CaO > 10 wt.-% CaO across all sliding velocity. It also shows the coefficient of friction magnitude in order of: 0 wt.-% CaO > 2.5 wt.-% CaO > 5 wt.-% CaO > 7.5 wt.-% CaO > 10 wt.-% CaO for sliding velocity condition.

18. Under varying normal load (5 to 45 N) the steady state SWR concluded that (i) The SWR tends to have increasing trend with normal load irrespective of filler content of the investigated composites (ii) the order of diminishing SWR magnitude with filler content is 0 wt.-% CaO > 2.5 wt.-% CaO > 5 wt.-% CaO > 7.5 wt.-% CaO > 10 wt.-% CaO irrespective of normal load condition. (iii) It is also observed that neat specimen tends to shows higher SWR relative to filled composites. Similarly the coefficient of friction for composites shows by the decreasing magnitude order in respect as: 0 wt.-% CaO > 2.5 wt.-% CaO > 5 wt.-% CaO > 7.5 wt.-% CaO > 10 wt.-% CaO irrespective of normal load condition.
19. The steady state condition for varying sliding velocity keeping other parameters constant to calculate SWR for MD filled SiBr alloy composites culminate that (i) The value of SWR of varying sliding velocities shows decreasing order for different wt.-% of MD particulates filled SiBr alloy composite materials. (ii) The SWR for fabricated composite materials observed to have decreasing in magnitude with increases filler content except monolithic alloy, therefor the value order of SWR is 0 wt.-% MD > 5 wt.-% MD > 2.5 wt.-% MD > 10 wt.-% MD > 7.5 wt.-% MD across all sliding velocity. Under same operating conditions the order of coefficient of friction for particulate filled metal alloy composites is 7.5 wt.-% MD > 10 wt.-% MD > 5 wt.-% MD > 2.5 wt.-% MD > 0 wt.- % MD.
20. With the varying normal load condition (from 5 to 45 N) the results in under steady state condition for specific wear rate concluded as (i) The magnitude of SWR shows the decreasing trend with respect to increases range of loading conditions (ii) The decreasing order for specific wear rate magnitude with varying filler content is 0wt.-% MD > 5 wt.-% MD > 7.5 wt.-% MD > 2.5 wt.-% MD > 10 wt.-% MD irrespective of normal load condition.
21. The specific wear rate of the CaO particulate filled SiBr alloy composites is increased with the increased in sliding velocity keeping all other factors remaining constant in steady state conditions. The order of specific wear rate is 0

wt.-% CaO> 10 wt.-% CaO> 2.5 wt.-% CaO> 5 wt.-% CaO> 7.5 wt.-% CaO across all sliding velocity and under similar operating condition of the same sets of composites the coefficients of friction order is 7.5 wt.-% CaO> 10 wt.-% CaO > 5 wt.-% CaO> 2.5 wt.-% CaO>0 wt.- % CaO respectively.

22. With the varying in normal load (from 5 to 45 N) the outcomes under steady state condition the specific wear rate concluded as (i) The specific wear rate tends to have decreasing in trend with the increased in normal load. (ii) The decreasing order for specific wear rate magnitude with varying filler content is 2.5wt.-% CaO> 5 wt.-% CaO> 10 wt.-% CaO > 7.5 wt.-% CaO>0 wt.-% CaO irrespective of normal load condition.
23. The steady state specific wear rate and coefficient of friction are evaluated under different boundary conditions and thereafter L_{25} Taguchi design of experiment methodology is adopted to compute the experimental specific wear rate of the proposed alloy composites and then analysis of variance (ANOVA) is performed to get the most prominent effective factor in comparison to other factors.
24. The surface morphology of the worn and unworn samples is performed using field emission scanning electron microscope (FE-SEM) to understand the wear mechanism prevailed at rubbing surfaces and then Atomic Force Microscopy (AFM) analysis is studied to evaluate the surface profile of the worn sample. At the end, Energy dispersive X-ray analysis (EDAX) analysis is also performed to find out the elemental compositions of the worn alloy composites.
25. Finally the calculation of ranking order for different physical, mechanical, fracture and wear behavior of particulate filled metal alloy composites has been done by using preference selection index (PSI) method. The sequencing of ranking is ZA-5> ZA-0> ZA-6 >ZA-1> ZA-3 >ZA-4 >ZA-2> SiBr-7> ZA-7 SiBr-2> SiBr-6> SiBr-3> SiBr-1> SiBr-5> ZA-8 >SiBr-0> SiBr-8> SiBr-4 for physical and mechanical properties and SiBr-7> ZA-4 >ZA-8> ZA-7 >ZA-3 >SiBr-4 >ZA-6 >ZA-2 >SiBr-3> SiBr-8> SiBr-1> ZA-5> ZA-1> SiBr-0> SiBr-2> ZA-0> SiBr-6> SiBr-5 for wear behavior is found which shows ZA-5 (2.5wt.-% CaO filled ZA-27 metal alloy) has the optimal performance for physical and mechanical properties among all other particulate filled metal alloy composites similarly, SiBr-7 (7.5wt.-% CaO filled SiBr metal alloy) shows

optimal performance for wear behavior among all other particulates filled metal alloy composites considered in this study.

7.3. Recommendations for potential applications

- The fabricated particulate filled metal alloy composite materials in the thesis are investigated to found the potential application for bearing materials specially for ball bearing inner and outer races due to having prominent properties in dry sliding wear environment conditions as well as having excellent physical and mechanical and tribological properties. Such materials having hardened ceramic particulate can also considered for other bearing applications such as, inner and outer race of other bearing, piston rings etc.
- The present study established that the inclusion of marble dust and CaO particulates in ZA-27 and SiBr alloy composites individually, shows the excellent outcomes which can be done in keeping the strength and sliding wear behaviour phenomenon in mind. These materials produced for ball bearing application keeping in mind but with having such adequate properties can be recommended for other applications such as: brushes, axles, pistons components etc.

7.4. Scope for future work

The work thus far in the development of particulate filled metal alloy composites has highlighted certain areas for future research.

- The grain size of particulates, chemical composition, particle shape and other such type parameters plays an important role in the composite materials in order to maximize the different properties. Hence the synthesized filler can be used in future to have the adequate control on such parameters.
- This research is compiled for dry sliding wear behavior for tribological conditions; Lubricating conditions during sliding wear behavior can be used for future aspects.
- This research is conducted for micro scale particle size i.e. 100 μm for particulates as well as for matrix materials. As we know the Nano or macro size of materials can strengthen the different aspects of different materials also having good tribological behaviour can also use for the fabrication of such composite materials.
- The processing operation plays an important role in the fabrication of any composite materials. The present investigation is done by the use of high temperature vacuum casting fabrication technique only. So the other different

casting techniques could be also tried and analysed so that the comparison aspect can be drawn more effectively.

- Cost is a most important factor for the analysis of any materials so the analysis of fabricated composite materials cost can assess the economic viability for different industrial applications.

******

References

REFERENCES

1. Callister W.D. Fundamentals of Materials Science and Engineering. *John Willey & Sons, Inc*. 2001.
2. Encyclopedia of Polymer Science and Technology. *John Wiley & Sons, Composites fabrication*.
3. Kutz M. Handbook of Materials Selection, *John Wiley & Sons, Inc*., New York 2000.
4. Weidenfeller B., Hofer M., Schilling F. R..Thermal conductivity, thermal diffusivity and a specific heat capacity of particle filled polypropylene composites. *Part A: Applied Science and Manufacturing* 2004; 35 (4):423-429.
5. Mishra S.K., Biswas S, Satapathy A. A study on processing, characterization and erosion wear behaviour of silicon carbide particle filled ZA-27 metal matrix composites. *Materials and Design* 2014; 55:958–965.
6. Seah K.H.W., Tucci A, Sharma S.C., Girish B.M., Kamath R. Mechanical properties of cast lead alloy/silicon carbide particulate composites. *Materials & Design* 1995; 16(6): 367-371.
7. Chawla N. and Chawla K.K. Metal matrix composites. *Springer* 2006.
8. Kainer K.U. Basics of Metal Matrix Composites, *Metal Matrix Composites: Custom-made Materials for Automotive and Aerospace Engineering* 2006.
9. Imran T.B. and Jacobson A.S. Quantifying diffused hydrogen in AISI-52100 bearing steel and in silver steel under tribo-mechanical action: Pure rotating bending, sliding–rotating bending, rolling–rotating bending and uni-axial tensile loading. *Wear* 2006; 261: 86–95.
10. Basavarajappa S, Chandramohan G., Davim JP. Application of Taguchi techniques to study dry sliding wear behavior of metal matrix composites. *Materials and Design* 2007; 28(4): 1393–1398.
11. Yan S, Xie J, Liu Z. Influence of Different Al Contents on Microstructure, Tensile and Wear Properties of Zn-based Alloy. *J. Mater. Sci. Technol* 2010; 26(7): 648-652.
12. Mao F., Chen F., Yan G. Effect of strontium addition on silicon phases and mechanical properties of Zn–27Al–3Si alloy. *Journal of Alloys and Compounds* 2015; 622: 871–879.
13. Chunjiang Z., Xiaokai Y., Qingxue H., et al. Analysis on the load characteristics

and coefficient of friction of angular contact ball bearing at high speed. *Tribology International* 2015; 87:50–56.

14. Fernandez L.E., Borrell A., Salvador M.D., Gutierrez-Gonzalez C.F. et al. Sliding wear behavior of WC-Co-Cr_3C_2-VC composite fabricated by conventional and non-conventional techniques. *Wear* 2013; 307(1-2): 60-67.
15. Ejiofo J.U., Okorie B.A., Reddy R.G. Powder pressing and properties of zircon reinforced Al-13.5Si-2.5Mg alloy composites. *Journal of Materials Engineering and Performance* 1997; 6:326-334.
16. Sastrya S., Krishna M. and Uchil J. A study on damping behavior of aluminite particulate reinforced ZA-27 alloy metal matrix composites. *Journal of Alloys and Compounds* 2001; 314(1-2):268–274.
17. Zhang J., Perez R.J., Lavernia E.J. Documentation of damping capacity of metallic, ceramic and metal matrix composite materials. *Journal of Material Science* 1993; 28: 2395-2404.
18. Clyne T.Y. and Withers P.J. An introduction to metal matrix composites. *Cambridge University Press* 1993.
19. Housford W.F. Mechanical behavior of materials. *Cambridge University Press* 2005.
20. Shukla A. Practical fracture mechanics in design. *Marcel Dekker* 2005.
21. Stachowiak G.W. and Batchelor A.W. Engineering Tribology 1988.
22. El-Idriss T. and Jantunen E. A. descriptive model of wear evolution in rolling bearings. *Engineering Failure Analysis*.2014; 45:204–224.
23. Hua L., Song D., Xinghui H. and Song H. Effect of material defects on crack initiation under rolling contact fatigue in a bearing ring. *Tribology International* 2013; 66:315–323.
24. Maeda K. and Nakashima H. NTN Technical Review 1994; 63: 83.
25. Stachowiak G.W. Wear Materials mechanism and properties. *John Wiley & Sons Ltd* 2005.
26. Mamatha T.G., Patnaik A., Biswas S., Satapathy B.K. and Redhewal A.K. Thermo-mechanical and crack position on stress intensity factor in particle-reinforced Zinc–aluminum alloy composites. *Computational Materials Science* 2012; 55:100–112.
27. Zaretsky E. V. and Branzai E.V. Rolling-Bearing Service Life Based on Probable

Cause for Removal – A Tutorial. *STLE Annual Meeting & Exhibition*. Disney's Contemporary Resort, Lake Buena Vista, Florida, USA 2014.

28. Idayana A., Gnanavelbabu A. and Rajkuma K. Influence of Deep Cryogenic Treatment on the Mechanical Properties of AISI 440C Bearing Steel. *Procedia Engineering* 2014; 97: 1683 – 1691.
29. Bobic B., Jelena B., Pavlovic A. Z., Ilija B. and Bore J. Corrosion behavior of thixoformed and heat-treated ZA-27 alloys in NaCl solution. *Trans. Nonferrous Met. Soc. China* 2013; 23: 931-941.
30. Ranganatha G., Sharma S.C. and Krishna M. Dry sliding wear of garnet reinforced zinc/aluminum metal matrix composites. *Wear* 2001; 251:1408–1413.
31. Elomari S., Boukhili R., Skibo M.D., MASOUNAVE J .Dynamic mechanical analysis of prestrained Al_2O_3/Al metal- matrix composites. *Journal of material science* 1995; 30: 3037-3044.
32. Girish B.M., Prakash K.R., Satish B.M., Jain P.K., Prabhakar P. An investigation into the effects of graphite particles on the damping behavior of ZA-27 alloy composite material. *Materials and Design* 2011; 32: 1050–1056.
33. Cast copper alloy sleeve bearings, non-ferrous foundry society. *Copper development association* 1997.
34. Tevfik K. and Kara L. The friction and wear properties of CuZn39Pb3 alloys under atmospheric and vacuum condition. Wear 2014; 309:21–28.
35. Xia L., Jia B., Zeng J., Xu J. Wear and mechanical properties of carbon fiber reinforced copper alloy composites. *Materials Characterization* 2009; 60:363 – 369.
36. Hiraia Y., Satoa T., Fukuia T., Yamadab K., Tanizawab K., Usami H. Effect of surface groove and penetration on friction properties of sulfide containing copper alloy journal bearing in dry condition. *Procedia Engineering* 2013; 68:37 – 42.
37. Copper alloys for bearing applications: part one. *Total Materia* 2009.
38. Nielsen L.F. Composite materials properties as influenced by phase geometry. *Springer*.
39. Soboyejo W. Mechanical properties of engineered materials 2002.
40. Rahmana M.H. and Rashed M.A. Characterization of silicon carbide reinforced aluminum matrix composites. *Procedia Engineering* 2014; 90:103-109.
41. Shorowordi K.M., Laoui T., Haseeb A. S. M.A., Celis J.P., Froyen L.

Microstructure and interface characteristics of B_4C, SiC and Al_2O_3reinforced Al matrix composites: A comparative study. *Journal of Materials Processing Technology*2003; 142: 738-743.

42. Poza P and Llorca J. Mechanical behavior of AL-Li-SiC Composites: Part 1. Microstructure and tensile deformation. *Metallurgical and Materials transactions A* 1999; 30:845; 855.
43. Louis E., Cordovilla C. G., Narciso J. Abrasive wear resistance of aluminum alloy /ceramic particulate Composites. *Wear* 1996; 192:170-177.
44. Tilly G. P. Two Stage Mechanisms of Ductile Erosion. *Wear* 1973; 23:87-96.
45. Sharma S.C., Girish B.M., Kamath R., and Satish B.M. Fractography, Fluidity, and Tensile Properties of Aluminum/Hematite Particulate Composites. *JMEPEG* 1997; 8:309-314.
46. Aldas K. and Mat M.D. Experimental and theoretical analysis of particle distribution in particulate metal matrix composites. *Journal of materials processing technology* 2005; 160:289; 295.
47. Singla M., Dwivedi D.D., Singh L., Chawla V. Development of Aluminium Based Silicon Carbide Particulate Metal Matrix Composite. *Journal of Minerals and Materials Characterization and Engineering* 2009; 8(6): 455 – 467
48. Bobic B., Bajic N., Jovanovic M.T., Ilijabobic Microstructure and mechanical properties of $Zn_{25}Al_3Cu$ based composites with large Al_2O_3 particles at room and elevated temperatures. *Association of Metallurgical Engineers of Serbia* UDC 669.55'71'3'.018.2.
49. Sharma S.C., Girish B.M., Somashekar D.R., Kamath R., Satish B.M. Mechanical properties and fractography of zircon-particle-reinforced ZA-27 alloy composite materials. *Composites Science and Technology* 1999; 59:1805-1812.
50. Sharma S.C. Elastic Properties of Short Glass Fiber-Reinforced ZA-27 Alloy Metal Matrix Composites. *JMEPEG* 2001; 10:468-474.
51. Sharma S.C. and Girish B.M. Fractrography, Fluidity and Tensile properties of aluminum hematite particulate composites. *Journal of Materials Engineering and Performance* 1999;8:309-314
52. Humphreys B.J., Basu H., Djazeb M.R. The microstructure and strength of particulate metal matrix composites. *Proc. of 12thRiso International symposium on metallurgy and material science*. National laboratory, Rosklide, Denmark

1991:51.

53. Stone R.H.V., Cox T.B., Low J.R., Psioda J.A. Micro structural Aspects of Fracture by Dimpled Rupture. *International Metals Reviews* 1985; 30:157-180.
54. Hemanth J. Production and Mechanical properties (Strength, Wear and Fracture Toughness) of chilled Aluminum-Quartz castable Particulate composites. *JMEPEG* 2001; 10:143-152.
55. Poddar P., Mukerjee, K.L. Sahoo. The microstructure and mechanical properties of SiC reinforced Magnesium based composites by rheo-casting. *Journal of Materials Engineering and Performance* 2009; 18:249-255.
56. Xiao-Dong Y.U., Yang-Wei W., Fu-Chi W.Effect of particle size on mechanical properties of SiCp/5210 Al metal matrix composite. *Trans. Nonferrous Met.Soc.china* 2007; 17:276-279.
57. Ceschini L., Minak G., Morri A. Forging of the AA2618/20vol% Al_2O_3 composite: effects on microstructure and tensile properties. *Composite Science and Technology* 2009; 69:1783-1789.
58. Kleis I. and Hussainova I. Investigation of particle-wall impact process. *Wear* 1998; 233–235:168–173.
59. Kevorkijan V.M. The quality of aluminum dross particles and cost effective reinforcement for structural aluminum based composites. *Composites Science and Technology* 1999; 59:1745-1751.
60. Sharma S. C., Seah K.H.W., Girish B.M., Kamath R., Satish B.M. Mechanical properties and fractography of cast lead / quartz particulate composites. *Materials and design* 1997; 18(3):149-153.
61. Ranganath G., Sharma S.C., Krishna M., Murali M.S. A Study of Mechanical Properties and Fractography of ZA-27/Titanium-Dioxide Metal Matrix Composites. *JMEPEG* 2002; 11:408-413.
62. Kok M. Production and mechanical properties of Al_2O_3 particle reinforced 2024 aluminum alloy composites. *Journal of materials processing technology* 2005; 161:381-387.
63. Hamouda A.M.S., Sulaiman S., Vijayaram T.R, Sayuti M., Ahmad M.H.M. Processing and characterization of particulate reinforced aluminum silicon matrix composites *JAMME* 2007.
64. Xiandong S. The Fabrication and Properties of Particle Reinforced Cast Metal

Matrix Composites. *Journal of Materials Processing Technology* 1997; 63:426 -431.

65. Kennedy A.R. The microstructure and mechanical properties of Al-Si-B_4C metal matrix composites. *Journal of Material Science* 2002; 37:317-323.
66. Kennedy A.R. and Wyatt S.M. The effect of processing on the mechanical properties and interfacial strength of aluminum /TiC MMCs. *Composites Science and Technology* 2000; 60:307-314.
67. Abdizadeh H., Ashuri M., Moghadam P. T., Nouribahadory A., Baharvandi H.R. Improvement in physical and mechanical properties of aluminum /zircon composites fabricated by powder metallurgy method. *Materials and Design* 2011; 32: 4417-4423.
68. Ganseh V.V. and Chawla N. Effect of reinforcement particle orientation Anisotropy on the tensile and fatigue behavior of metal matrix composites. *Metallurgical and Materials Transactions A: Physical Metallurgy and Materials Science* 2004; 35 (1):53-61.
69. Tjong S.C. and Mai Y.W. Processing-structure-property aspects of particulate- and whisker-reinforced titanium matrix composites. *Composites Science and Technology* 2008; 68:583–601.
70. Kataiah G.S. and Girish D.P. The mechanical properties and fractography of aluminum 6061-TiO_2 composites. *International Journal of pharmaceutical studies and research* 2010; 1:17-25.
71. Geng K.,Lu W., Zhang D., Sakata T., Mori H.. Tensile properties of in situ synthesized titanium matrix composites reinforced by TiB and Nd_2O_3 at elevated temperature. *Materials and Design* 2003:24409-414.
72. Aqida S. N., Ghazali M. I., Hashim J. Effects of porosity on mechanical properties of metal matrix composites: An overview. *Journal Teknologi* 2004; 17-32.
73. Ramesh A., Prakash J. N., Gowda A. S. S. S., Appaiah S. Comparison of the mechanical properties of AL6061/Albite and AL6061/ Graphite metal matrix composites. *Journal of minerals and materials characterization and engineering* 2009; 8:93-106.
74. Mizuuchi K., Takeuchi T., Fukusumi M., Sugioka M., Nagai H., Inoue K. Microstructure and mechanical properties of Al matrix composites produced by

LCCS process. *J. of the Japan Inst. of Metals* 1998; 62(10):893-898.

75. Sajjadi S.A., Ezatpour H.R., Parizi M.T. Comparison of microstructure and mechanical properties of A356 aluminum alloy/Al_2O_3 composites fabricated by stir and compo-casting processes. *Materials and Design* 2012; 34:106-111.
76. Silva A.A.M.D., Santos J.F.D., Strohaecker T.R. Micro structural and mechanical characterization of a Ti6Al4V/TiC/10p composite processed by the BE-CHIP method. *Composites Science and Technology* 2005; 65:1749-1755.
77. Lee S., Sohn K.S., Park I.M., Cho K.M. Effect of applied pressure on mechanical properties of squeeze cast Mg matrix composites. *Metals and materials* 19951(1):37-46.
78. Ozben T., Kilikap E., Cakir O. Investigation of mechanical and machinability properties of SiC particle reinforced Al-MMC. *Journal of materials processing technology* 2008; 198: 220-225.
79. Chen L. G., Lin S.J., Chang S.Y.Tensile properties and thermal expansion behaviors of continuous molybdenum fiber reinforced aluminum matrix composites. *Composites Science and Technology* 2006; 66:1793-1802.
80. Mahendra K.V. and Radhakrishna K. Fabrication of Al–4.5% Cu alloy with fly ash metal matrix composites and its characterization. *Materials Science Poland* 2007; 25:57-68.
81. Zhongguang W., Zhengming S., Weicheng Y. Fatigue behavior of metal matrix composite. *Chin. J. Met. Sci. Technology* 1992; 8; 235-248.
82. Bekheet N.E., Gadelrab R.M., Salah M.F., Abd El-Azim A. N. The effects of aging on the hardness and fatigue behaviorof 2024Al alloy /SiC Composites. *Materials and Design.*2002; 23:153-159.
83. Milan M.T. and Bowen P. Fatigue crack growth resistance of SiCp reinforced Al alloys: effect of particle size, volume fraction and matrix strength. *Journal of Materials Engineering and Performance* 2004; 13: 612-618.
84. Seah K.W.H., Sharma S.C., Rao P.R., Girish B.M. Mechanical properties of as – cast and heat treated ZA-27/Silicon carbide particulate composites. *Materials and Design* 1995; 16(5):277-281.
85. Sharma S.C. and Ramesh A. Effect of heat treatment on mechanical properties of particulate reinforced Al6061 Composites. *Journal of Materials Engineering and Performance* 2000;9:557-561

86. Pradeep G.R., Sidddesh S., Kumar G.B.V. Case hardening effect on the mechanical properties in graphite reinforced Al6061 MMCs. *International journal of applied research in mechanical engineering* 2011;1(2).
87. Ehsani R. and Reihani S.M.S. Aging behavior and tensile properties of squeeze cast AL 6061/SIC metal matrix composites. *Scientia Iranica* 2004; 11(4), 392-397.
88. Kashyap K T, Ramachandra C, Dutta C, Chatterji B. Role of work hardening characteristics of metal alloys in the strengthening of metal matrix composites. *Bull Mater.sci*. 2000; 23; 47-49.
89. Bauria R. and Surappa M.K. Processing and properties of Al–Li–SiCp composites. *Science and Technology of Advanced Material*s 2007; 8: 494–502.
90. Basavarajappa S., Chandramohan G., Dinesh A. Mechanical properties of MMC's- An Experimental investigation. *International Symposium of Research Students on Materials and Engineering*, Chennai, India 2004.
91. Das S., Behera R., Datta A., Majumdar G., Oraon B., Sutradhar G. Experimental Investigation on the Effect of Reinforcement Particles on the Forgeability and the Mechanical Properties of Aluminum Metal Matrix Composites. *Materials Sciences and Applications* 2010; 1:310-316.
92. Long S., Beffort O., Cayron C., Bonjour C. Microstructure and Mechanical properties of a high volume fraction reinforced SiCp reinforced $AlCu_4MgAg$ Squeeze casting. *Material Science and Eng.*1999:1-23.
93. Deng X. and Chawla N. Modeling effect of particle clustering on mechanical behavior of SiC reinforced Al matrix composites. *Journal of Materials science* 2006; 41: 5731-5134.
94. Poddar P., Mukherjee S., Sahoo K.L. The Microstructure and Mechanical Properties of SiC Reinforced Magnesium Based Composites by Rheocasting Process. *JMEPEG* 2009; 8:849-855.
95. Alawode A.J. Effect of Glass Particle Addition on the Mechanical Properties of Aluminum-Base Particulate Composites. *The Pacific Journal of Science and Technology* 2011; 14:403-412.
96. Park B. G, Crosky A. G., Hellier A. K. Material characterization and mechanical properties of Al_2O_3 Al metal matrix composites. *Journal of Materials Science* 2001; 36:2417-2426.

97. Aashuri H., Razavimanesh A., Kolahi A., Mohiedin M. Impact and tensile behavior of fractional melting processed ZA-27 alloy. *Materials Science and Engineering* 2002; 333:115–122.
98. Run-xia LI, Rong-de LI, Yan-hua BAI, Ying-dong QU, Xiao-guang YUAN, Effect of specific pressure on microstructure and mechanical properties of squeeze casting ZA27 alloy. *Trans nonferrous Met. Soc. China* 2010; 20:59-63.
99. Srivatsan T.S., Soboyejo W.O. Lederich R.J. The cyclic fatigue and fracture behavior of a titanium alloy metal matrix composites. *Engineering Fracture Mechanics* 1995; 52:465-491.
100. Srivatsan T.S. and Vasudevan V.K. Cyclic plastic strain response and fracture behavior of 2080 aluminum alloy metal matrix composites. *Int. J. Fatigue* 1998; 20:187-202.
101. Tjong S.C. and Ma Z.Y. The High Temperature creep behavior of Aluminum – matrix composites reinforced with SiC, Al_2O_3 and TiB_2 Particles. *Composites Science and Technology* 1997; 51; 697-702.
102. Srivatsan T.S. Cyclic strain resistance and fracture behavior of Al_2O_3 particulate reinforced 2014 aluminum alloy metal matrix composites. *Int. J. Fatigue* 1995; 17:183-199.
103. Srivatsan T.S. and Al-Hajri M. The fatigue and final fracture behavior of SiC particle reinforced 7034 aluminum matrix composites. *Composites: Part B* 2002; 33:391–404.
104. Zhu J.H., Liaw P.K., Corum J.M., Mccoy H.E, Jr. High temperature mechanical behavior of Ti-6Al-4V Alloy and TiCp/Ti-6Al-4V Composite. *Metallurgical and materials Transactions A* 1999; 380:1569-1576.
105. Oh K.H., Han K.S. Short-fiber/particle hybrid reinforcement: Effects on fracture toughness and fatigue crack growth of metal matrix composites. *Composites Science and Technology* 2007; 67:1719–1726.
106. Agrawal P. and Sun C.T. Fracture in metal–ceramic composites. *Composites Science and Technology* 2004; 64:1167–1178.
107. Park B.G., Crosky A.G., Hellier A.K. High cycle fatigue behavior of microsphere $Al–Al_2O_3$ particulate metal matrix composites. *Composites: Part B* 2008; 39:1257–1269.
108. Mukherjee S., Ananth C. R., Chandrat N. Effect of residual fracture behavior

stresses on the interfacial of metal-matrix composites. *Composites Science and Technology* 1997; 57:1501-1512.

109. Hua Y., Zhang L., Cheng L., Li Z., Du J. Microstructure and mechanical properties of SiCP/SiC and SiCW/SiC composites by CVI. *J Mater Sci* 2010; 45:392–398.
110. Reddy A.C. and Zitoun E. Strengthening mechanisms and fracture behavior of 7072Al/Al_2O_3 metal matrix composites. *International Journal of Engineering Science and Technology (IJEST)* 2011; 3(7); 6090-6100.
111. Rajesh G., Sinharoy A., Bhagat R. B. A fracture mechanics based numerical analysis for predicting optimum interface properties in a metal matrix composite. *Composites Engineering* 1995; 5(6):583-596.
112. Kolednik O. and Unterweger K. The ductility of metal matrix composites – Relation to local deformation behavior and damage evolution. *Engineering Fracture Mechanics* 2008; 75; 3663–3676.
113. Leggoe J.W., Hu X.Z., Bush M.B. Crack tip damage development and crack growth resistance in particulate reinforced metal matrix composites. *Engineering fracture mechanics* 1996; 53,873-895.
114. Zdemir I.O., Cen U. M. C., Nel K.O. The effect of forging on the properties of particulate-SiC-reinforced aluminum-alloy composites. *Composites Science and Technology* 2000; 60: 411-419.
115. Mazen A.A. and Ahmed A.Y. Mechanical behavior of Al-Al_2O_3MMC manufactured by PM techniques Part I scheme –Process parameters. *Journal of Materials Engineering and Performance* 1998; 7:393-401.
116. Pandey A.B., Mujumdar B.S., Miracle D.B. Deformation and Fracture of a particle reinforced Al alloy composite: Part I Experiments. *Metallurgical and Materials Transactions* 2000; 31; 905-921.
117. Ochiai S., Ikeda S., Iwamoto S., ShaJ. J., Okuda H., Waku Y., Nakagawa N., Mitani A., Sato M., Ishikawa T. Residual stresses in YAG phase of melt growth Al_2O_3/YAG eutectic composite estimated by indentation fracture test and finite element analysis. *Journal of the European Ceramic Society* 2008; 28:2309–2317.
118. Azarmi F. Creep properties of nickel aluminide composite materials reinforced with SiC particulates. *Composites: Part B*, 2011;42:1779–1785
119. Wang S.R., Geng H.R., Wang Y.Z., Zhang J.C. Microstructure and fracture

characteristic of Mg–Al–Zn–Si3N4 composites. *Theoretical and Applied Fracture Mechanics* 2006; 46:57–69.

120. Poza P. and Llorca J.L. Effect of SiC reinforcement on the deformation and fracture micro mechanisms of Al–Li alloys. *Journal of Microscopy* 1999; 196(2):113–123.
121. Konopkaa K., Majb M.C., Cowski K.J.K. Studies of the effect of metal particles on the fracture toughness of ceramic matrix composites. *Materials Characterization* 2003; 51:335– 340.
122. Mihashi H., Leite J.P.D.B., Yamakoshi S., Kawamata A. Controlling fracture toughness of matrix with mica flake inclusions to design pseudo-ductile fibre reinforced cementitious composites. *Engineering Fracture Mechanics* 2007;74:210–222
123. Singh V. and Prasad R.C. Tensile and fracture behavior of 6061 Al-SiCp Metal matrix composites. *International Symposium of Research Students on Materials Science and Engineering.* Chennai, India 2004.
124. Reddy A. C. and Zitoun E. Matrix Al-alloys for silicon carbide particle reinforced metal matrix composites. *Indian Journal of Science and Technology* 2010; 3(12):1184-1187.
125. Kim B.N., Watanabe M., Enoki M., Kishi T. Simulation of fracture behavior in particle-dispersed ceramic composites. *Engineering fracture mechanics* 1998; 59:289-303.
126. Pendola M., Mohamed A., Lemaire M., Hornet P. Combination of finite element and reliability methods in nonlinear fracture mechanics. *Reliability Engineering and System Safety* 2000; 70: 15–27.
127. Gastaldi D., Vena P., Contro R. Hybrid micro structural finite element modeling for intergranular fracture in ceramic composites and coated systems. *Computational Materials Science* 2008; 44:26–31.
128. Pires F.M.A., Neto E.A.D.S., Owen D.R.J. On the finite element prediction of damage growth and fracture initiation in finitely deforming ductile materials. *Comput. Methods Appl. Mech. Engrg.*2004; 193: 5223–5256.
129. Ural A., Zioupos P., Buchanan D., Vashishth D. The effect of strain rate on fracture toughness of human cortical bone: A finite element study. *Journal of the mechanical behavior of biomedical materials* 2011; 4: 1021 – 1032.

130. Warner D.H. and Molinari J.F. Micromechanical finite element modeling of compressive fracture in confined alumina ceramic. *Acta Materialia* 2006; 54: 5135–5145.
131. Irfan M.A. and Prakash V. Dynamic deformation and fracture behavior of novel damage tolerant discontinuously reinforced aluminum composites. *International Journal of Solids and Structures* 2000; 37: 4477-4507.
132. Shaw L.L., Karpur P., Matikas T.E. Fracture strength and damage progression of the fiber/matrix interfaces in titanium based MMCs with different interfacial layers. *Composites Part B 29B* 1998:331-339.
133. Srivatsan T.S., Al-Hajri M., Vasudevan V.K. Cyclic plastic strain response and fracture behavior of 2009 aluminum alloy metal-matrix composite. *International Journal of Fatigue* 2005; 27: 357–371.
134. Shaw M. C. The effects of strength probabilistic on the fracture mode of ceramic/metal multilayer's. *Engineering Fracture Mechanics* 1998;61: 49-74
135. Gonzalez C. and Llorca J. Multiscale modeling of fracture in fiber-reinforced composites. *Acta Materialia* 2006; 54: 4171–4181.
136. Reyes E., Galvez J.C, Casati M.J., D.A. Cendon, J.M. Sancho, J. Planas. An embedded cohesive crack model for finite element analysis of brickwork masonry fracture. *Engineering Fracture Mechanics* 2009; 76: 1930–1944.
137. Smallman R.E. and Bishop R.J. *Modern physical Metallurgy and materials engineering* 1999.
138. Ren S., He X., Qu X., Humail I.S., Li Y. Effect of Mg and Si in the aluminum on the thermo-mechanical properties of pressure less infiltrated SiCp/Al composites. *J. Composites Science and Technology* 2007; 67:2103–2113.
139. Huber T., Degischer H.P., Lefranc G., Schmitt T.Thermal expansion studies on aluminum-matrix composites with different reinforcement architecture of SiC particles. *Composites science and Technology* 2006; 66:2206-2217.
140. Yan Y.W. and Geng A.L. Effects of particle size on the thermal expansion behavior of SiCp/Al composites. *J Mater Sci* 2007; 42:6433–6438.
141. Zhang L., Qu X., Duan B., He X., Ren S., Qin M. Microstructure and thermo-mechanical properties of pressure less infiltrated SiCp/Cu composites. *Composites Science and Technology* 2008; 68: 2731–2738.
142. Elomari S., Skibo M. D., Sundarrajan A., Richards H. Thermal expansion

behavior of particulate metal-matrix composites. *Composites Science and Technology* 1998; 58: 369-376.

143. Yue H. Y., Fei W.D., Wang L.D. Mechanical properties and thermal stability of ZnAl2O4-coated aluminum borate whiskers reinforced 2024Al composite. *J Mater Sci* 2008; 43:6233–6237.
144. Ke C., Chengchang J., Xuebing L., Hui C., Wenjia G. Effect of particle size on the microstructure and thermal conductivity of Al/diamond composites prepared by spark plasma sintering. *Rare Metals* 2009; 28(6):646-650.
145. Karthikeyan B., Ramanathan S., Ramakrishnan V. Thermo physical property measurement of metal-matrix composites. *Materials and Design* 2010; 31:S82–S86.
146. Wang T.C., Fan T.X., Zhang D., Zhang G.D. Fabrication, thermal expansions, and mechanical properties of carbon/aluminum composites based on wood templates. *J Mater S*ci2006; 41:6095–6099.
147. Wua S.Q., Wei Z.S., Tjong S.C. The mechanical and thermal expansion behavior of an Al-Si alloy composite reinforced with potassium titanate whisker. *Journal of Composites Science and Technology* 2000; 60; 2873-2880.
148. Delannay E., Colin C., Marchal Y., Tao L., Boland F., Cobzaru P., Lips B., Dellis M.A. Processing and properties of metal matrix composites reinforced with continuous fibres for the control of thermal expansion, creep resistance and fracture toughness. *Journal de Physique III* 1993; 3:1675-1685.
149. Khalifa T.A. and Mahmoud T.S. Elevated Temperature Mechanical Properties of Al Alloy AA6063/SiCp MMCs. *Proceedings of the World Congress on Engineering: WCE*, London, U.K. 2009; 2: 978-983.
150. Chawla N., Deng X., Schnell D.R.M. Thermal expansion anisotropy in extruded SiC particle reinforced 2080 aluminum alloy matrix composites. *Materials Science and Engineering* 2006; 426: 314–322.
151. Wu Y.W., Wu K., Deng K.K., Nie K.B., Wang X.J., Hu X.S., Zheng M.Y. Damping capacities and tensile properties of magnesium matrix composites reinforced by graphite particles. *Materials Science and Engineering A* 2010;527: 6816–6821
152. Sastry S., Krishna M., Uchil J. Effect of Thermal Stresses on the Thermal Expansion and Damping Behavior of ZA-27/Aluminite Metal Matrix Composites.

Journal of Materials Engineering and Performance 2001; 10:220-224.

153. Zhang H. and Gu M. Internal friction behavior in SiC particulate reinforced aluminum metal matrix composite in thermal cycling. *Journal of Alloys and Compounds* 2006; 426: 247–252.
154. Deng C.F., Wang D.Z., Zhang X.X., Ma Y.X. Damping characteristics of carbon nanotube reinforced aluminum composite. *Materials Letters* 2007; 61:3229–3231.
155. Ning W.J., Hua S.S., Gang H.U.K., Jun X.I.E.W., Liang M.A.M., Mei L.I.G., Sheng H.A.N.F. Influence of macroscopic graphite particulates on the damping properties of Zn-Al eutectoid alloy. *Sci China Ser G-Phys Mech Astron* 2009; 52(1):70-75.
156. El-khaira M.T. A., Lotfya A., Daouda A., El-Sheikh A.M. Microstructure, thermal behavior and mechanical properties of squeeze cast SiC, ZrO_2 or C reinforced ZA27 composites. *Materials Science and Engineering A* 2011; 528:2353–2362.
157. Jiejun W., Chenggong L., Dianbin W., Manchang G. Damping and sound absorption properties of particle reinforced Al matrix composite foams. *Composites Science and Technology* 2003; 63:569–574.
158. Schaller R. Metal matrix composites, a smart choice for high damping materials. *Journal of Alloys and Compounds* 2003; 355:131–135.
159. Chaudhury S K, Singh A K, Sivaramakrishnan C S S., Panigrahi S C. Preparation and thermo mechanical properties of stir cast Al–2Mg–11TiO_2 (rutile) composite. *Bull. Mater. Sci.* 2004; 27: 517–521.
160. Sulaiman S., Sayuti M., Samin R. Mechanical properties of the as-cast quartz particulate reinforced LM6 alloy matrix composites. *Journal of materials processing technology* 2008; 201:731–735.
161. Wu Y.W., Wu K., Deng K.K., Nie K.B., Wang X.J., Zheng M.Y., Hu X.S. Damping capacities and microstructures of magnesium matrix composites reinforced by graphite particles. *Materials and Design* 2010; 31: 4862–4865.
162. Yadollahpour M., Ziaei-Rad S., Karimzadeh F., Eskandari-Jam J. A numerical study on the damping capacity of metal matrix Nano composites. *Simulation Modeling Practice and Theory* 2011; 19: 337–349.
163.. Lu Y.X, Lee C.S., Li R.K.Y., Lai J.K.L. The effect of cold rolling on the dynamic mechanical responses of SiCp: Al composites. *Journal of Materials*

Processing Technology 1999; 91:215–218.

164. Gu J., Zhang X., Qiu Y., Gu M. Damping behaviors of magnesium matrix composites reinforced with Cu-coated and uncoated SiC particulates. *Composites Science and Technology* 2005; 65; 1736–1742.
165. Zhang J., Perez R.J., Lavernia E.J. Effect of SiC and graphite particulate on damping behavior of Metal matrix composites. *Acta Metall. Mater.* 1994; 42(2):395-409.
166. Zhang J., Perez R.J., Lavernia E.J., Gupta M. Damping behavior of particulate filled 2519 metal matrix composites. *Scripta Metallurgicaet Materillia* 1993; 2:91-96.
167. Cao W., Zhang C., Fan T., Zhang D. In situ synthesis and damping capacities of TiC reinforced magnesium matrix composites. *Materials Science and Engineering A* 2008; 496:242–246.
168. Mitra R. and Mahajan Y.R. Interfaces in discontinuously reinforced metal-matrix composites: An overview. *Bull. Mater.Sci.*1995; 18:405-434.
169. Lavernia E.J., Perez R.J., Zhang J. Damping behavior of discontinuously reinforced Al-alloy metal-matrix composites. *Metall. Mater. Trans. A* 1995; 26:2803-2818.
170. Rao V.V., Murthy M.V.K., Nagaraju J. Thermal conductivity and thermal contact conductance studies on Al_2O_3/Al–AlN metal matrix composite. *Composites Science and Technology* 2004; 64:2459–2462.
171. Chan K.C. and Liang J. Thermal expansion and deformation behavior of aluminum-matrix composites in laser forming. *Composites Science and Technology* 2001; 61:1265–1270.
172. Di-qing Wan, Bo-lin He, Guang-yao Xiong, Zhao-xia Chen, Jin-cheng Wang, Gen-cang Yang. High damping capacities of Mg-Cu based alloys. *Trans. Nonferrous Met. Soc. China* 2010; 20: 448-452.
173. Lu H., Wang X., Zhang T., Cheng Z., Fang Q. Design, Fabrication, and Properties of High Damping Metal Matrix Composites A Review. *Materials* 2009; 2:958-977.
174. Shirazi S.A. and Mc Laury B.S. Erosion modeling of elbows in multiphase flow. In: *Proceedings of 2000 ASME fluids engineering summer meeting.* Boston, MA: Paper no. FEDSM 2000-11251, 2000.

175. Gu J., Zhang X., Gu M. Mechanical properties and damping capacity of (SiCp+ $Al_2O_3 \cdot SiO_2$f)/Mg hybrid metal matrix composite. *Journal of Alloys and Compounds* 2004; 385:104–108.
176. Jiejun W., Chenggong L., Dianbin W., Manchang G. Damping and sound absorption properties of particle reinforced Al matrix composite foams. *Composites Science and Technology* 2003; 63:569–574.
177. Zhang L., Qu X., Duan B., He X., Ren S., Qin M. Microstructure and thermo-mechanical properties of pressure less infiltrated SiCp/Cu composites. *Composites Science and Technology* 2008; 68: 2731–2738.
178. Zhou J., Druz˙ A. T., El DZ˙, Duszczyk J. The effect of extrusion parameters on the fretting wear resistance of Al-based composites produced via powder metallurgy. *Journal of Materials Science* 1999; 34:5089 – 5097.
179. Ramesha C.S., Srinivas C.K., Channabasappa B.H. Abrasive wear behavior of laser sintered iron–SiC composites. *Wear* 2009.
180. Sharma S.C., Girish B.M., Somashekar D.R., B.M. Satish, Kamath R. Sliding wear behavior of zircon particles reinforced ZA-27 alloy composite materials. *Wear* 1999; 224:89–94.
181. Ahlatci H., Era T.K., Candanb E., Huseyin C.¸ Imenoglu. Wear behavior of Al/ (Al_2O_3pCSiCp) hybrid composites. *Tribology International* 2006; 39:213–220.
182. Miyajima T. and Iwai Y. Effects of reinforcements on sliding wear behavior of aluminum matrix composites. *Wear* 2003; 255:606–616.
183. Ramachandra M. and Radhakrishna K. Sliding wear, slurry erosive wear, and corrosive wear of aluminum/SiC composite. *Materials Science-Poland* 2006; 24(2/1).
184. Vencl A., Rac A., Bobic I., Miskovic Z. Tribological Properties of Al-Si Alloy A356 Reinforced With Al_2O_3 Particles. *Tribology in industry* 2006; 28(1&2).
185. Wu S. Q., Wang H. Z., Tjong S. C. Mechanical and wear behavior of an al/si alloy metal-matrix composite reinforced with aluminosilicate fiber. *Composites science and technology* 1996;56: 1261-1270
186. Ghosh K., Troczynski T., Chaklader A.C.D. Aluminum-Silicon Carbide Coatings by Plasma Spraying. *Journal of Thermal Spray Technology 1998*; 7(1).
187. Asthana R. Processing effect on the engineering properties of cast metal matrix composites. *Advance performance material* 1998; 5:213-255.

188. Jin Y., Kato K. and Umehara N. Further investigation on the tribological behavior of Al_2O_3–$20Ag_{20}CaF_2$ composite at 650 ° C. *Tribology Letters* 1999; 6: 225–232.

189. Dogan C. P. and Hawk J. A. Influence of whisker toughening and microstructure on the wear behavior of Si_3N_4- and Al_2O_3-matrix composites reinforced with SiC. *Journal of Materials Science* 2000; 35: 5793 – 5807.

190. *Daoud A., El-Bitar T., Azim A.A.E.* Tensile and Wear Properties of Rolled Al_5Mg-Al_2O_3or C Particulate Composites. *JMEPEG* 2003; 12:390-397.

191. Das S. Development of aluminum alloy composites for engineering applications. *Trans. Indian Inst. Met.*2004;57(4): 325-334

192. Dinesh. A, Basavarajappa S., Chandramohan G. Dry sliding wear studies on hybrid mmc's – A Taguchi technique. *International Symposium of Research Students on Materials Science and Engineering* 2004.

193. Roya D., Basub B., Mallick A.B. Tribological properties of Ti-aluminide reinforced Al-based in situ metal matrix composite. *Intermetallics* 2005; 13:733–740.

194. Ipek R. Adhesive wear behavior of B_4C and SiC reinforced 4147 Al matrix composites (Al/B_4C–Al/SiC). *Journal of Materials Processing Technology* 2005; 162–163:71–75.

195. Basavarajappa S. and Chandramohan G. Dry Sliding Wear Behavior of Metal Matrix Composites: A Statistical Approach. *JMEPEG* 2006;15:656-660

196. Bonollo E, Ceschini L., Garagnani G.L., Palombarini G., Tangerinie I., Zambon A. Early stages of sliding wear behavior of $A1_2O_3$ and Sic reinforced aluminum. *Journal De Physique IV* 1993; 3.

197. Mahendra K.V. and Radhakrishna K. Fabrication of Al–4.5% Cu alloy with fly ash metal matrix composites and its characterization. *Materials Science-Poland* 2007; 25(1).

198. Kumar M.P., Sadashivappa K., Prabhukumar G.P., Basavarajappa S. Dry Sliding Wear Behavior of Garnet Particles Reinforced Zinc-Aluminum Alloy Metal Matrix Composites. *ISSN 1392–1320 Materials Science (Medziagotyra).*2006; 12(3).

199. Shyu R.F. and Ho C.T. In situ reacted titanium carbide-reinforced aluminum alloys composite. *Journal of Materials Processing Technology* 2006; 171:411–416.

200. KlckapE., Akır O. C, Aksoy M., ˙Inan A. Study of tool wear and surface roughness in machining of homogenized SiC-p reinforced aluminum metal matrix composite. *Journal of Materials Processing Technology* 2005;164–165:862–867
201. Pardo A., Merino M. C., Lo´pez M. D., Escalera M. D., Viejo F. Influence of Reinforcement Content and Matrix Composition on the Oxidation Resistance of Aluminum-Matrix Composites (A3xx.x/SiCp). *Oxidation of Metals* 2003; 59(1/2).
202. Lindsley B.A. and Marder A.R. Solid Particle Erosion of a Fe-Fe_3C Metal Matrix Composite. *Metallurgical and Materials Transactions A*: 1998; 29:1071.
203. DAS S., Mondal D.P., Sawla S. Solid Particle Erosion of Al Alloy and Al-Alloy Composites: Effect of Heat Treatment and Angle of Impingement. *Metallurgical and Materials Transactions A* 2004; 35:1369.
204. Miyajima T. and Iwai Y. Effects of reinforcements on sliding wear behavior of aluminum matrix composites. *Wear* 2003; 255:606–616.
205. Ahlatci H., Kocer T., Candanb E., Cimenoglu H. Wear behavior of Al/(Al_2O_3pCSiCp) hybrid composites. *Triblogy International* 2009; 44(5):213-220.
206. Lee A.H.I, Chen W.C., Chang C.J. A fuzzy AHP and BSC approach for evaluating performance of IT department in the manufacturing industry in Taiwan. *Expert Systems with Applications* 2008; 34: 96–107.
207. Gungor Z., Serhadlıoglu G., Kesen S.E. A fuzzy AHP approach to personnel selection problem. *Applied Soft Computing* 2009; 9: 641–646.
208. Awasthi A., Chauhan S.S., Goyal S.K. A fuzzy multicriteria approach for evaluating environmental performance of suppliers. *Int. J. Production Economics* 2010; 126: 370–378.
209. Kelemenis A. and Askounis D. A new TOPSIS-based multi-criteria approach to personnel selection. *Expert Systems with Applications* 2010; 37: 4999–5008.
210. Liao C.N. and Kao H.P. An integrated fuzzy TOPSIS and MCGP approach to supplier selection in supply chain management. *Expert Systems with Applications* 2011; 381; 10803–10811.
211. Buyukozkan G. and Cifci G. A combined fuzzy AHP and fuzzy TOPSIS based strategic analysis of electronic service quality in healthcare industry. *Expert Systems with Applications* 2012; 39: 2341–2354.

212. Paksoy T., Pehlivan N.Y., Kahraman C. Organizational strategy development in distribution channel management using fuzzy AHP and hierarchical fuzzy TOPSIS. *Expert Systems with Applications* 2012; 39: 2822–2841.
213. Patnaik A., Satapathy A., Mahapatra S.S., Dash R.R. Tribo-performance of polyester hybrid composites: Damage assessment and parameter optimization using Taguchi design. *Materials and Design* 2009; 30: 57–67.
214. Zmitrowicz A. Wear patterns and laws of wear: A Review. *Journal of Theoretical and Applied Mechanics*2006; 44(2):219-253.
215. Wu J., Graham L.J.W., Lester D., Wong C.Y., Kilpatrick T., Smith S., Nguyen B. An effective modeling tool for studying erosion. *Wear* 2011; 270: 598–605.
216. Chen Q. and Li D.Y. Computer simulation of solid particle erosion. *Wear* 2003; 254:203–210.
217. Fernandez E., Rocio J.M.D., Fernandez M., Diaz R. V., Navarro R. T.Abrasive Wear Analysis using Factorial Experiment Design. *Wear* 2003; 255: 38–43.
218. Spuzic S., Zee S.M., Abhay K., Ghomasch R., Reid I. Fractional Design of Experiments Applied to a Wear Simulation. *Wear* 1997; 212: 131–139.
219. Prasad B.K. Abrasive Wear Characteristics of a Zinc-based Alloy and Zinc-alloy/SiC Composite. *Wear* 2002; 252(3–4):250–263.
220. Deuis R.L. Three-body Abrasive Wear of Composite Coatings in Dry and Wet Environments. *Wear* 1998; 214: 112–130.
221. Banerjee A., Prasad S.V., Surappa M. K., P.K. Rohatgi. Abrasive Wear of Cast Aluminum Alloy/Zircon Particle Composites. *Wear* 1982; 82: 141–151.
222. Mondal D.P., Das S., Jha A.K., Yegnesswaran A.H. Abrasive Wear of Al alloy–Al_2O_3 Particle Composite: A Study on the Combined Effect of Load and Size of Abrasive. *Wear* 1998; 223:131– 138.
223. Taguchi G. and Konishi S. Taguchi Methods: Orthogonal Arrays and Linear Graphs; Tools for Quality Engineering. *American Supplier Institute Inc., Dearborn, MI* 1987.
224. Taguchi G. Introduction to Quality Engineering, *Asian Productivity Organization*. Tokyo 1990.
225. Phadke M.S. Quality Engineering Using Robost Design. *Prentice-Hall. Englewood Cliffs NJ* 1989.
226. Wu Y. and Moore W.H. Quality Engineering: Product & Process Design

Optimization. *American Supplier Institute Inc., Dearborn, MI* 1986.

227. Basavarajappa S., Chandramohan G. Wear studies on metal matrix composites: A Taguchi method. *Journal of Materials science Technology* 2005; 21(6).
228. Patnaik A. and Mahapatra S.S. Optimization of Wire Electrical Discharge Machining (WEDM) Process Parameters using Taguchi Method. *International Journal for Manufacturing Science & Technology* 2008; 9(2):129-144.
229. Joshi R., Banwet D.K., Ravishankar. A Delphi-AHP-TOPSIS based benchmarking framework for performance improvement of a cold chain. *Expert systems with applications* 2011; 38(8):10170-10182.
230. Kelemenis A. and Askounis D. A new TOPSIS-based multi criteria approach to personnel selection. *Expert systems with applications* 2010; 37:4999-5008.
231. Rao R.V. A decision making methodology for material selection using an improved compromise ranking method. *Materials and Design* 2008; 29:1949-1954.
232. Jahan A., Ismail M.Y., Sapuan S.M., Mustapha F. Material selection based on Ordinal data. *Materials and Design* 2010; 31:3180-3187.
233. Annual book of ASTM standards, ASTM International.
234. www.zorhat.com
235. www.nbmmetals.com
236. www.concast.com
237. Topcu I.B., Bilir T., Lu T.U. Effect of waste marble dust content as filler on properties of self-compacting concrete. *Construction and Building Materials* 2009; 23: 1947–1953.
238. Pigment K. Material safety data sheet 1999.
239. www.vietnamlime.com
240. Lide D.R. CRC Handbook of Chemistry and Physics. 79th Edition. *CRC Press. Boca Raton FL* 1998.
241. Ergun E., Aslantas K., S. Tasgetiren. Effect of crack position on stress intensity factor in particle-reinforced metal-matrix composites. *Mech. Res. Commun. 2008;* 35 (4):209-218.
242. Singh S., Kopke U.G., Howard C.Q., Petersen D. Analyses of contact forces and vibration response for a defective rolling element bearing using an explicit dynamics finite element model. *Journal of Sound and Vibration* 2014; 333:5356–

5377.

243. Ghanati M. F. and Madoliat R. Theoretical and experimental study of spindle ball bearing nonlinear stiffness. *Akademeia* 2013.3(1), 1923-1504.

244. Malviya D., Sharma P.K., Shivankar R. Determine static transmission errors of involute spur gear bodies in mesh appropriate models of contact and bending stresses using finite element analysis. *International Journal of Engineering Sciences & Management* 2014; 4(4):22-32.

245. Neill H.O. Hardness measurements of Metals & Alloys. *Chapman & Hall, London* 1967.

246. Agarwal B.D. and Broutman L.J. Analysis and performance of fiber composites. 2nd edition. *Jhonwieley and SonsNew York* 1990.

247. Kumar SS, Devaiah M, SeshuBai V, Rajasekharan T. Mechanical properties of SiCp/Al_2O_3 ceramic matrix composites prepared by directed oxidation of an aluminium alloy. *Ceramic International* 2012; 38:1139-1147.

248. Siddhartha V, Patnaik A, Bhatt AD. Mechanical and dry sliding wear characterization of epoxy–TiO_2 particulate filled functionally graded composites materials using Taguchi design of experiment. *Material and design* 2011; 32:615-627.

249. Espinosa F. L, Borrell A, Salvador MD, Gutiérrez-González CF. Sliding wear behavior of WC-Co-Cr_3C_2-VC composite fabricated by conventional and non-conventional techniques .*Wear* 2013; 307(1-2):60-67.

250. Singh T., Patnaik A., Gangil B., Chauhan R. Optimization of tribo performance of brake friction materials: Effect of nano filler. *Wear* 2015;324-325:10-16

251. Wolfgang W. R., Lars A., Nils R. Process for production of reinforced composite materials and products thereof , *US 5256183 A.*

252. Kok M. Preparation and Some Properties of SiC Particle Reinforced Al Matrix. Ph.D. Thesis. *The Institute of Science and Technology of Elazig University.* Turkey. 1999.

253. Sug Won Kim, Ui Jong Lee, Sang Won Han, Dong Keun Kim, K. Ogi. Heat treatment and wear characteristics of Al/SiCp composites fabricated by duplex process. *Composites: Part B* 2003; 34:737–745.

254. R.L. Deuis, C. Subramaniun, J.M. Yellup. Abrasive wear of aluminum composites—a review. *Wear* 1996; 201:132–144.

255. Bekheet N.E., Gadelrab R.M., Salah M.F., Abd. ElAzim A.N. The effects of aging on the hardness and fatigue behavior of 2024Al alloy /SiC Composites. *Materials and Design* 2002; 23,153-159.
256. Natarajan N, Vijayarangan S. Rajendran I. Wear behavior of A356/25SiCp aluminum matrix composites sliding against automobile friction materials. *Wear* 2006; 261: 812–822.
257. Akhlaghi F and Zare-Bidaki A. Influence of graphite content on the dry sliding and oil impregnated sliding wear behavior of Al 2024–graphite composites produced by in situ powder metallurgy method. *Wear* 2009; 266: 37–45.
258. Jayalakshmi S., Sahu S., Sankaranarayanan S., Gupta S., Gupta M. Development of novel Mg-Ni60 Nb 40 amorphous particle reinforced composites with enhanced hardness and compressive response. *Materials and Design* 2014; 53:849–855.
259. Agari S. R., Jyothi P. N., Jagath M., Channakeshavalu K. Processing of ZA-27 based MMC reinforced with Al_2O_3 by centrifugal casting. Proc. of the Second Intl. Conf. on Advances In Mechanical and Robotics Engineering- AMRE. *ISBN: 978-1-63248-031-6 D.O.I. 10.15224/ 978-1-63248-031-6-147*. 2014.
260. Somekawa H., Singh A., Osawa Y., Mukai T. High strength and fracture toughness balances in extruded Mg-Zn-RE alloys by dispersion of quasi crystalline phase particles. *Materials Transactions* 2008; 49(9): 1947 – 1952.
261. Dahlberg E.P. Fractography: An Important Tool for Analysing Failures. *Technical Articles from Element experts.*
262. Ibrahim M.F., Samuel E., Samuel A.M., Al-Ahmari A.M.A., Samuel F. H. Impact toughness and fractography of Al-Si-Cu-Mg base alloys. *Materials and Design* 2011; 32:3900–3910.
263. Dong Y.U. X., Wei W. Y., Chi W. F. Effect of particle size on mechanical properties of SiCp/5210Al metal matrix composites. *Trans. Nonferrous Met. Society China* 2007; 17: 276-279.
264. Tahamtan S. and Boostani A F. Evaluation of pitting corrosion of thixoformed A356 alloys using a simulation model. *Transaction of the Non-ferrous Metal Society of China* 2010; 20:1702-1706.
265. Singh P. and Joshi U. K. Fatigue life analysis of thrust ball bearing using ANSYS. *International journal of engineering sciences & research technology* 2014;

3(1):156-162.

266. Hamrock B.J. Fundamentals of fluid film and lubrication. *NASA reference publication* 1991; 1255.

267. M. Emamya, A. Razaghian, H.R. Lashgari, R. Abbasi. The effect of Al–5Ti–1B on the microstructure hardness and tensile properties of Al_2O_3 and SiC-containing metal–matrix composites. *Materials Science and Engineering A* 2008; 485:210–217.

268. Rebbaa B. and Ramanaiah N. Evaluation of Mechanical Properties of Aluminum Alloy (Al-2024) Reinforced with Molybdenum Disulphide (MOS_2) Metal Matrix Composites. *Procedia Materials Science* 2014; 6:1161–1169.

269. El-khaira M.T. A., Lotfya A., Daouda A., El-Sheikh A.M. Microstructure thermal behaviour and mechanical properties of squeeze cast SiC, ZrO_2 or C reinforced ZA27 composites. *Materials Science and Engineering A* 2011; 528:2353–2362.

270. Ramnath B.V., Elanchezhian C., Jaivignesh M., Rajesh S., Parswajinan C., A. Siddique Ahmed Ghias. Evaluation of mechanical properties of aluminum alloy–alumina–boron carbide metal matrix composites. *Materials and Design* 2014;58: 332–338

271. Hassan A.M., Tashtoush G.M., AL-Khalil J.A. Effect of Graphite and/or Silicon Carbide Particles Addition on the Hardness and Surface Roughness of Al-4 wt% Mg Alloy. *Journal of Composite Materials* 2007; 41(4); 453-465.

272. Seah K. H. W., Tucci A., S. C. Sharma, B. M. Girish and R. Kamath. Mechanical properties of cast lead alloy/silicon carbide particulate composites. *Materials & Design*. 1995; 16(6).

273. K. H. W. Seah, S. C. Sharma, B. M. Girish. Mechanical properties of as-cast and heat-treated ZA-27/graphite particulate composites. *Composites A* 1997; 28:251-256.

274. Saravanana S. D. and Kumar M.S. Effect of Mechanical Properties on Rice Husk Ash Reinforced Aluminum alloy ($AlSi_{10}Mg$) Matrix Composites. *Procedia Engineering*, 2013; 64:1505-1513.

275. Xiao-dong Y.U., Yang-wei W., Fu-chi W. Effect of particle size on mechanical properties of SiCp/5210 Al metal matrix composite. *Trans. Nonferrous Met. Society China* 2007; 17:276-279.

276. Li J., Liu Q., Shi R., Wen Y., Yin Y. Preparation and mechanical properties of

Fe3Al(Ti)/TiC composites, *Journal of Materials Processing Technology* 2008;208:105–110.

277. Soboyejo W. *Mechanical properties of engineered materials*. Marcel Dekker 2003.
278. Alaneme K.K. and Aluko A.O. Fracture toughness (K1C) and tensile properties of as-cast and age-hardened aluminum (6063)–silicon carbide particulate composites. *Scientia Iranica A* 2012; 19 (4):992–996.
279. Forn A., Baile M.T., Ruperez E. Spinel effect on the mechanical properties of metal matrix composite AA6061/ (Al_2O_3)p. *J Mater Process Technol* 2003;143–144:58–61.
280. Vedani M. and Gariboldi E. Damage and ductility of particulate and short-fibre Al–Al_2O_3 composites. *Acta Mater* 1996; 44(8): 3077–88.
281. Srivatsan T.S. and Prakash A. The quasi-static fracture behavior of an aluminum alloy metal-matrix composite. *Compos Sci Technol* 1995; 54(3):307–15.
282. Wang Z.G., Li S., Sun L. Fatigue and fracture behaviors of discontinuously reinforced aluminum matrix composites. *Key Eng Mater* 1995; 104–107:729–48.
283. Zhao D., Tuler F.R., Lloyd D.J. Fracture at elevated temperatures in a particle reinforced composite. *Acta Metallet Mater* 1994; 42(7):2525–33.
284. Ibrahim M.F., Alkahtani S.A., AbuhaselKh. A., Samuel F.H. Effect of intermetallic on the microstructure and tensile properties of aluminum based alloys: Role of Sr, Mg and Be addition. *Materials and design* 2015; 86; 30-40.
285. Sajjadi S.A., Torabi Parizi M., Ezatpour H.R., Sedghi A. Fabrication of A356 composite reinforced with micro and nano Al2O3 particles by a developed compo casting method and study of its properties. *J Alloys Compd* 2012; 511: 226–231.
286. Ravi K.R., Pillai R.M., Amaranathan K.R., et al. Fluidity of aluminum alloys and composites: A review. *J Alloys Compd* 2008; 456: 201–210.
287. Mummery P.M. and Derby B. The influence of microstructure on the fracture behavior of particulate metal matrix composites. *Mater. Sci. Eng. A* 1991; 131:221-24.
288. Divecha A.P., Fishman S.G., Karmakar S.D. Silicon carbide reinforced aluminum –a formable composite. *J. Met* 1981; 12:12-7.
289. Nguyen QB and Gupta M. Enhancing compressive response of AZ31B using nano-Al_2O_3 and copper additions. *J Alloys Compd* 2010; 490: 382–387.

290. Mondal DP, Ganesh NV, Muneshwar VS, et al. Effect of SiC concentration and strain rate on the compressive deformation behavior of 2014 Al-SiC composite. *Mater Sci Eng A* 2006; 433: 18–31.
291. V. Hariharan, V. Mohankumar, P. Gnaneswaran. A Review on Tribological And Mechanical Behaviors of Aluminum Metal Matrix Composites. *International Journal on Mechanical Engineering and Robotics (IJMER) ISSN (Print)* 2014; 2(6):2321-5747.
292. Z. Balaka, M.Zakeri, M.R.Rahimipur, E.Salahi, H.Nasiri, Effect of open porosity on flexural strength and hardness of ZrB_2-based composites, *Ceramics International* 2015; 41:8312–8319.
293. Abdullah M., Ahmad J., Mehmood M. Influence ofAl_2O_3 whisker concentration on flexural strength of Al_2O_3 (w)–ZrO_2 (TZ-3Y) composite. *Ceramics International* 2012; 38:6517–6523.
294. Haque S, Bharti P.K., Ansari A.H. Mechanical and Machining Properties Analysis of Al6061-Cu-Reinforced SiCP Metal Matrix Composite. *Journal of Minerals and Materials Characterization and Engineering* 2014; 2:54-60.
295. Lokesh G. N., Ramachandra M., Mahendra K. V., Sreenith T. Characterization of Al-Cu alloy reinforced fly ash metal matrix composites by squeeze casting method, *International Journal of Engineering Science and Technology* 2013;5(4):71-79.
296. Ayhan A.O. Mixed mode stress intensity factors for deflected and inclined surface cracks in finite-thickness plates *Engineering Fracture Mechanics* 2004; 71:1059–1079.
297. Dahlberg E.P. Fractography: An Important Tool for Analyzing Failures Technical Articles from Element experts, Element. 222 Cavalcade Street. *Huston TX 77009-3213 U.S.*
298. Aravindan S., Rao P.V., Ponappa K. Evaluation of physical and mechanical properties of AZ91D/SiC composites by two step stir casting process. *Journal of Magnesium and Alloys* 2015; 3:52-62.
299. Hayrettin A, Tolga K, Ercan C, Huseyin C. Wear behaviour of Al/(Al_2O_{3p}+SiC_p) hybrid composites. *Tribology International* 2006; 39:213–220.

300. Aqida SN, Ghazali MI, Hashim J. Effect of Porosity on Mechanical Properties of Metal Matrix Composite: An Overview. *Jurnal Teknolog,* 2004; 40: 17–32.
301. Balasubramanian I and Maheswaran R. Effect of inclusion of SiC particulates on the mechanical resistance behaviour of stir-cast AA6063/SiC composites. *Materials and Design* 2015; 65:511–520.
302. Sathiskumar R, Murugan N, Dinaharan I, Vijay SJ. Characterization of boron carbide particulate reinforced in situ copper surface composites synthesized using friction stir processing *Materials Characterization* 2013; 84:16-27.
303. Shabani M, Paydar MH, Zamiri R, Goodarzi M, Moshksar MM. Micro structural and sliding wear behaviour of SiC-particle reinforced copper matrix composites fabricated by sintering and sinter-forging processes. *Journal of material research and technology* 2015; 4(2):109-228.
304. Swamy A. R. K., Ramesha A., Kumar G.B. V., Prakash J. N. Effect of Particulate Reinforcements on the Mechanical Properties ofAl6061-WC and Al6061-Gr MMCs, *Journal of Minerals & Materials Characterization & Engineering* 2011;10(12):1141-1152.
305. Zhang Q., Zhang H., Gu M., Jin Y. Studies on the fracture and flexural strength of Al/Sip composite. *Materials Letters* 2004; 58: 3545– 3550.
306. Puneeth H M, Girish K B, Vasudevamurthy B H. Experimental investigation and mechanical behavior of A356.1 aluminum alloy matrix composite reinforced with silicon carbide. *International Research Journal of Engineering and Technology (IRJET)* 2015; 2(3).
307. Hassan M.A., Ofor T.C., Usman A.M., Godi N.Y. Development of Aluminum Metal Matrix Composite Using Stir Casting Method. *The International Journal of Engineering and Science (IJES)* 2014; 3 (8):36-39.
308. Gonzalez C.R. and Mason J.J. Mixed mode dynamic stress intensity factor due to applied point loads. *Computers and Structures* 2000; 76: 237-245.
309. Fett T. Stress intensity factors and t-stress inedge-cracked rectangular plates under mixed boundary conditions. *Engineering Fracture Mechanics* 1998*;* 60(5-6):625-630.
310. Udomphol T. Fractography. *Mechanical Metallurgy Laboratory* 431303.
311. Samer N., Andrieux J., Gardiola B. , Karnatak N. , Martin O., Kurita H. , Chaffron L., Gourdet S., Lay S., Dezellus O. Microstructure and mechanical

properties of an Al–TiC metal matrix composite obtained by reactive synthesis. *Composites: Part A* 2015; 72:50–57.

312. Sahraeinejad S., Izadi H., Haghshenasa M., Gerlich A.P. Fabrication of metal matrix composites by friction stir processing with different Particles and processing parameters. *Materials Science & Engineering A* 2015; 626:505–513.
313. Feng G.H., Yang Y.Q., Luo X., Li J., Huang B., Chen Y. Fatigue properties and fracture analysis of a SiC fiber-reinforced titanium matrix composite. *Composites* 2015; 68:336–342.
314. Youn B. D., Choi K.K., Park Y.H. Hybrid Analysis Method for Reliability-Based Design Optimization. *Journal of Mechanical Design* 2003; 125.
315. Chatterjee P., Athawale V.M., Chakraborty S. Material's selection using complex proportional assessment and evaluation of mixed data methods. *Materials and Design* 2011; 32: 851–860.
316. Loh N.H., Tor S.B., Khor K.A. Production of metal matrix composite part by powder injection moulding. *Journal of Materials Processing Technology* 2001; 108:398-407.
317. Czujko T., Varin R.A., Chiu C., Wronski Z. Investigation of the hydrogen desorption properties of Mg+ 10 wt. %X (X =V, Y, Zr) submicron crystalline composites. *Journal of Alloys and Compounds* 2006; 414: 240–247.
318. Das T., Bandyopadhyay S., Blairs S. DSC and DMA studies of particulate reinforced metal matrix composites. *Journal of Material Science* 1994, 29, 5680-5688.
319. Froberg L. Thermal analysis TGA/DTA. Process chemistry centre. *ABO Academi University*.
320. Geng J., Tsakiropoulos P., Shao G. A thermo-gravimetric and micro structural study of the oxidation of Nbss/Nb5Si3-based in situ composites with Sn addition. *Intermetallics* 2007; 15: 270-281.
321. Kwan K.S. Dynamic mechanical analysis. *Chapter 6*, 1998.
322. Xiao F., Fukuda T., Kakeshita T., Jin M., Jin X. Dynamic mechanical analysis of weak first-order martensitic transformation in an iron palladium alloy. *Journal of Alloys and Compounds* 2015; 649: 211-215.
323. Dynamic mechanical analysis A Beginner's guide. *Perkin Elmer*.
324. Ma S.G., Liaw P.K., Gao M.C., Qiao J.W., Wang Z.H., Zhan Y. Damping

behavior of AlxCoCrFeNi high-entropy alloys by a dynamic mechanical analyzer. *Journal of Alloys and Compounds* 2014; 604: 331–339.

325. Kumar R. and Suresh D. A study of sliding wear behavior of Al-7075 alloy and Al 7075 hybrid composite by response surface methodology analysis *Materials and Design* 2013;50:351-359.

326. Devaraju A., Kumar A., Kumara S.A. and Kotiveerachari B. Wear and mechanical properties of 6061-T6 aluminum alloy surface hybrid composites [(SiC+Gr) and (SiC+Al_2O_3) fabricated by friction stir processing *Mater Res Technol*. 2013; 2(4), :362-369.

327. Pei-peng J., Geng C. Li, H. Jinhui W. Dry sliding friction and wear behaviors of $Mg_2B_2O_5$ whisker reinforced 6061Al matrix composites *Trans. Nonferrous Met. Soc. China* 2014; 24:49-57.

328. Rana, F., Dhindaw B.K., Stefanescu D.M. Optimization of SiC particles dispersion in aluminum metal matrix composites *AFS Trans.* 1989; 41:255–264.

329. Rana, F. and Stefanescu, D.M. Weinberg International symposium on Solidification Process *Metall. Trans. A.* 1989; 20:1564–1566.

330. Prasad S.V., Rohatgi P.K., Kosel T.H. Mechanism of material removal during low stress and high stress abrasion of aluminum alloy–zircon particle composites *Mater. Sci. Eng.* 1986; 80: 213–220.

331. Ranganath G., Sharma S.C., Krishn M. Dry sliding wear of garnet reinforced zinc/aluminum metal matrix composites *Wear* 2001;25(1): 1408–1413.

332. Mukunda D. Prasanna, K. Kanakuppi S. Gundenahalli, P.P. Satyappa B. Dry Sliding Wear Behaviour of Garnet Particles Reinforced Zinc-Aluminum alloy metal matrix composites *ISSN 1392–1320 Materials Science* 2006; 12 (3).

333. Niranjan K. and Lakshminarayanan P.R. Dry sliding wear behavior of in situ Al–TiB_2 composites *Materials and Design 2013;*47: 167–173.

334. Das S., Mondal D. P., Sawla S., Ramakrishnan, N. Synergic effect of reinforcement and heat treatment on the two body abrasive wear of an Al-Si alloy under varying loads and abrasive sizes *Wear* 2008; 264: 47-59.

335. Hutchings I.M. Tribological properties of metal matrix composites *Mater. Sci. Technol*. 1994; 10:513–517.

336. Corrochanoa J., Walker J.C., Lieblich M., Ibáneza J., Rainforth W.M. Dry sliding wear behavior of powder metallurgy Al–Mg–Si alloy-$MoSi_2$composites

and the relationship with the microstructure *Wear* 2011; 270: 658–665.

337. Ames W. and Alpas A.T. Wear mechanism in hybrid composites of graphite–20% SiC in A-356 Aluminum alloy Al–7% Si–0.3% Mg *Met. Mater. Trans. A.* 1995; 26: 85–98.

338. Kumar B.A., Murugan N., Dinaharan I. Dry sliding wear behavior of stir cast AA6061-T6/AlNp composite *Trans. Nonferrous Met. Soc. China* 2014; 24: 2785−2795.

339. Yu S.Y., Ishii H., Chuang T.H. Corrosive wear of SiC whisker and particulate reinforced 6061 aluminum alloy composites *Met. Mater. Trans.* 1996; 27: 26-53.

340. Sharma S.C. The sliding wear behavior of Al6061– garnet particulate composites *Wear* 2001; 249: 1036–1045.

341. Bauri R. and Surappa M.K. Sliding wear behavior of Al–Li–SiCp composites *Wear* 2008; 265: 1756–1766.

342. Toptan F., Kerti I., Rocha L.A. Reciprocal dry sliding wear behavior of B_4Cp reinforced aluminum alloy matrix composites *Wear* 2012; 290–291: 74–85.

343. Ozsarac U., Findik F., Durman M. The wear behavior investigation of sliding bearings with a designed testing machine *Mater Des* 2007; 28: 345–350.

344. Singh M., Prasad B.K., Mondal D.P., Jha A.K. Dry sliding wear behavior of an aluminum alloy–granite particle composite *Tribol Int* 2001; 34: 557–567.

345. Manohara H.R., Chandrashekharaiah T.M., Venkateswarlu K., Kori S.A. Dry sliding wear response of A413 alloy: Influence of intermetallics and test parameters *Tribol Int* 2012; 51:54–60.

346. Babic M., Slobodan M., Dzunic D., Ilija B., Jeremic B. Tribological Behavior of Composites Based on ZA-27 Alloy Reinforced with Graphite Particles *Tribol Lett* 2010;37:401–410.

347. Sharma S.C. The sliding wear behavior of Al6061–garnet particulate composites *Wear* 2001; 249:1036–1045.

348. Ilangovan S., Jiten S. Dry sliding wear behavior of sand cast cu-11ni-6sn alloy *Int J Res Eng Technol* 2014;3(7):2319– 651 1163.

349. Zhang S. and Wang F. Comparison of friction and wear performances of brake material dry sliding against two aluminum matrix composites reinforced with different SiC particles *J Mater Process Technol* 2007;182:122–127

350. Baskaran S, Anandakrishnan V, Duraiselvam M Investigations on dry sliding

wear behavior of in situ casted AA7075–TiC metal matrix composites by using Taguchi technique *Mater 2014;*654(60):184–192.

351. Xiu K, Wang HY, Sui HL, Wang Y, Xu CL, Wang JG, Jiang QC The sliding wear behavior of TiCp/AZ91 magnesium matrix composites *J Mater Sci* 2006; 41:7052–7058.

352. Prasad B.K. Influence of some material and experimental parameters on the sliding wear behavior of a zinc based alloy, its composite and a bronze *Wear* 2003 254:35–46.

353. Krakhmalev P.V. Influence of Cu Addition on Dry Sliding Wear Behavior of A356 Alloy *Wear 2006;* 260:450–457.

354. Prabhudeva M.S., Auradib V., Venkateswarluc K., Siddalingswamy N.H. Influence of Cu Addition on Dry Sliding Wear Behavior of A356 Alloy *Proced Eng* 2014;97:1361–1367.

355. Mahathanabodee S., alathai T., Raadnui S., Tongsri R., Sombatsom N. Dry sliding wear behavior of SS316L composites containing h-BN and MoS_2 solid lubricants *Wear* 2014;316:37–48.

356. Melgarejo Z.H., Su´arez O.M., Kumar S *Scripta Materialia* 2006; 669 55(1):95–98.

357. Kok M. and Ozdin K. Wear resistance of aluminum alloy and its composites reinforced by Al_2O_3 particles *J Mater Process Technol* 2007;183:301–309.

358. Chung K.H. Wear Characteristics of Atomic Force Microscopy Tips: A Review *Int J Precis Eng Manuf* 2014; 15(10):2219–2230.

359. Bi G., Li Y., Huang X., Chen T., Ma Y., Hao Y. Dry sliding wear behavior of an extruded Mge Dye Zn alloy with long period stacking ordered phase *J Magn Alloys* 2015;675 3:63–69.

360. Manohara H.R., Chandrashekharaiah T.M., Venkateswarlu K., Kori S.A. Dry sliding wear response of A413 alloy: Influence of intermetallics and test parameters *Tribol Int* 2012; 51:54–60.

361. Vencla A., Rajkovic V., Zivic F., Mitrovic S., Alagi I.C., Jovanovic M.T. The effect of processing techniques on micro structural and tribological properties of copper-based alloys *Applied Surface Science* 2013; 280:646– 654.

362. Zhang L., He X.B., Qu X.H., Duan B.H., Lu X., Qin M.L. Dry sliding wear properties of high volume fraction SiCp/Cu composites produced by pressure less

infiltration *Wear* 2008;265:1848–1856.

363. Chen R., Iwabuchi A., Shimizu T., Shin H.S., Mifune H The sliding wear resistance behavior of NiAI and SiC particles reinforced aluminum alloy matrix composites *Wear* 1997; 213:175-184.

364. Dinaharan I., Murugan N., Parameswaran S. Influence of in situ formed ZrB_2 particles on microstructure and mechanical properties of AA6061 metal matrix composites *Materials Science and Engineering A* 2011;528: 5733–5740.

365. Baskaran S., Anandakrishnan V., Muthukannan D. Investigations on dry sliding wear behavior of in situ casted AA7075–TiC metal matrix composites by using Taguchi technique *Materials and Design* 2014; 60:184–192.

366. Qing-ju Q.I. Evaluation of sliding wear behavior of graphite particle-containing magnesium alloy composites *Trans. Nonferrous Met. SOCC China* 2006; 161:135-1140.

367. Onat A. Mechanical and dry sliding wear properties of silicon carbide particulate reinforced aluminum–copper alloy matrix composites produced by direct squeeze casting method *Journal of Alloys and Compounds* 2010; 489:119–124.

368. Winzer J., Weiler L., Pouquet J., Rodel J. Wear behavior of interpenetrating alumina–copper composites *Wear* 2011; 271:2845– 2851.

369. Lin N., Xie F., Yang H., Tian W., Wang H., Tang B. Assessments on friction and wear behaviors of P110 steel and chromizing coating sliding against two counterparts under dry and wet conditions *Applied Surface Science* 2012;258 (11):4960-4970.

370. Kumar B.A., Murugan N., Dinharan I. Dry sliding wear behavior of stir cast AA6061-T6/AlNp composite *Trans. Nonferrous Met. Soc. China* 2014; 24:2785−2795.

371. Baskaran S., Anandakrishnan V., Duraiselvam M. Investigations on dry sliding wear behavior of in situ casted AA7075–TiC metal matrix composites by using Taguchi technique *Materials and Design* 2014; 60:184–192.

372. Mondal A.K. and Kumar S. Dry sliding wear behavior of magnesium alloy based hybrid composites in the longitudinal direction *Wear* 2009; 267:458–466.

373. Karande P. and Chakraborty S. Application of multi-objective optimization on the basis of ratio analysis (MOORA) method for materials selection *Materials and Design* 37 2012;37: 317–324.

374.Nandalal K.D.W. and Simonovic S.P. State of the art report on System analysis methods for resolution of conflicts in water resources management 2003.

Appendices

A-I

List of publications based on the research presented in this thesis

Science Citation Indexed International Journals

(i) **Swati Gangwar**, Amar Patnaik, I.K.Bhat. Tribological and Microstructure Behaviour of Quicklime (CaO) filled Silicon Bronze Alloy for Bearing Material, **Silicon (Springer Journal),** 8(2016)601-616 I.F = 1.069.

(ii) **Swati Gangwar**, Amar Patnaik, I.K.Bhat (2015). Tribological and Thermo-mechanical analysis of CaO (Quicklime) particulates filled ZA-27 Alloy Composites for Bearing Application, **Journal of Materials: Design and Applications DOI: 10.1177/1464420715609196.** I.F = 0.672.

(iii) **Swati Gangwar**, I.K.Bhat, Amar Patnaik (2015). Tribological and Microstructure Examination of Environmental Waste (Marble Dust) filled Silicon Bronze Alloy for Wear Resistant Applications, **Silicon (Springer Journal) DOI: 10.1007/s12633-015-9401-9.** I.F = 1.069.

Book Chapter

(i) Amar Patnaik, I.K.Bhat, **Swati Gangwar** (2015). Manufacturing and Characterization of Quicklime (CaO) Filled ZA-27 Metal Alloy Composites for Single Row Deep Groove Ball Bearing, **Handbook of Composites from Renewable Materials, 2017, 2, 133-158. Wiley Scrivener publisher**.

International/National Conferences

(i) **Swati Gangwar**, Amar Patnaik, I.K.Bhat, A review paper on physical and mechanical properties of metal alloy composites for different applications, 1stInternational conference on innovative advancement in engineering & technology, March 7-8, 2014, Jaipur National University Jaipur, India.

(ii) **Swati Gangwar**, Amar Patnaik, I.K.Bhat, Physical , mechanical and tribological properties of particulate filled metal alloy composites for bearing applications: A Review, International conference on Newest drifts in mechanical engineering, December 20-21 2014, Department of mechanical engineering, Maharishi Markandeshwar University , Mullana, Ambala, Haryana-133207.

(iii) **Swati Gangwar**, Amar Patnaik, I.K.Bhat, Surface Wear Behavior of Marble Dust (Stone waste) Filled ZA-27 Alloy Composites for Bearing Material, International Conference (ICMFA-2015), IIT BHU, Oct.27 – 29, 2015.

(iv) **Swati Gangwar**, Amar Patnaik, I.K.Bhat, Wear performance of Marble Dust filled ZA-27 alloy composites for single row deep groove ball bearing in wind turbine gear box, International conference on Emerging Paradigms and Practices in Global Technology, Management and Business Issues, December 22-24,2014 ,NIT Hamirpur, Himachal Pradesh-177005,India

(v) **Swati Gangwar**, Amar Patnaik, I.K.Bhat, Fracture behavior for Marble Dust filled Copper alloy composite for Single Row Deep Groove Ball bearing in Wind Turbine Gear Box, National Conference on Futuristic Approaches in Civil & Mechanical Engineering (FACME-2015) March, 24th – 25th 2015, Maharishi Arvind Institute of Engineering and Technology Jaipur, Rajasthan-302020, India.

(vi) **Swati Gangwar**, Amar Patnaik, I.K.Bhat, Mechanical and Fracture analysis for Calcium Oxide filled ZA-27 Metal Alloy Composites for Single Row Deep Groove Ball Bearing, International conference on Emerging and Futuristic trends in Engineering & Technology,8-9 May 2015, Maharaja Agrasen University, Solan, HP

Patent filed

(i) **Swati Gangwar,** Prof. I.K Bhat, Dr. Amar Patnaik. Marble dust reinforced copper alloy composite fabrication, Patent application number **1319/DEL/2015 A (Under Examination).**

******

A-II

Brief Bio-data of the Author

The author Swati Gangwar was born on December 10th 1989. She graduated in Mechanical Engineering from Uttar Pradesh Technical University Lucknow, Uttar Pradesh INDIA in the year 2009. After the completion of Engineering she joined National Institute of Technology, Hamirpur for her Postgraduate study in Mechanical Engineering with the specialisation of CAD/CAM and completed successfully in the year 2012. After that she joined MNIT Jaipur on January 2013 in Mechanical Engineering department for the degree of Philosophy of Doctorate.

She has published three research papers in Science Citation Journals, filed one patent, authored one book chapter, and presented five research papers in International and one in National conferences to her credit. Since January 2013, she has been engaged in her doctoral research in the area of Development and characterization of metal alloy composite materials for wear resistant applications at M.N.I.T., Jaipur under the Institute Research Fellowship scheme by Ministry of Human Resource Development, Government of India.

At present she is working as an Assistant Professor in the Department of Mechanical Engineering, Madan Mohan Malaviya University Of Technology Gorkhpur, Autonomous Government University, Uttar Pradesh, INDIA.

******